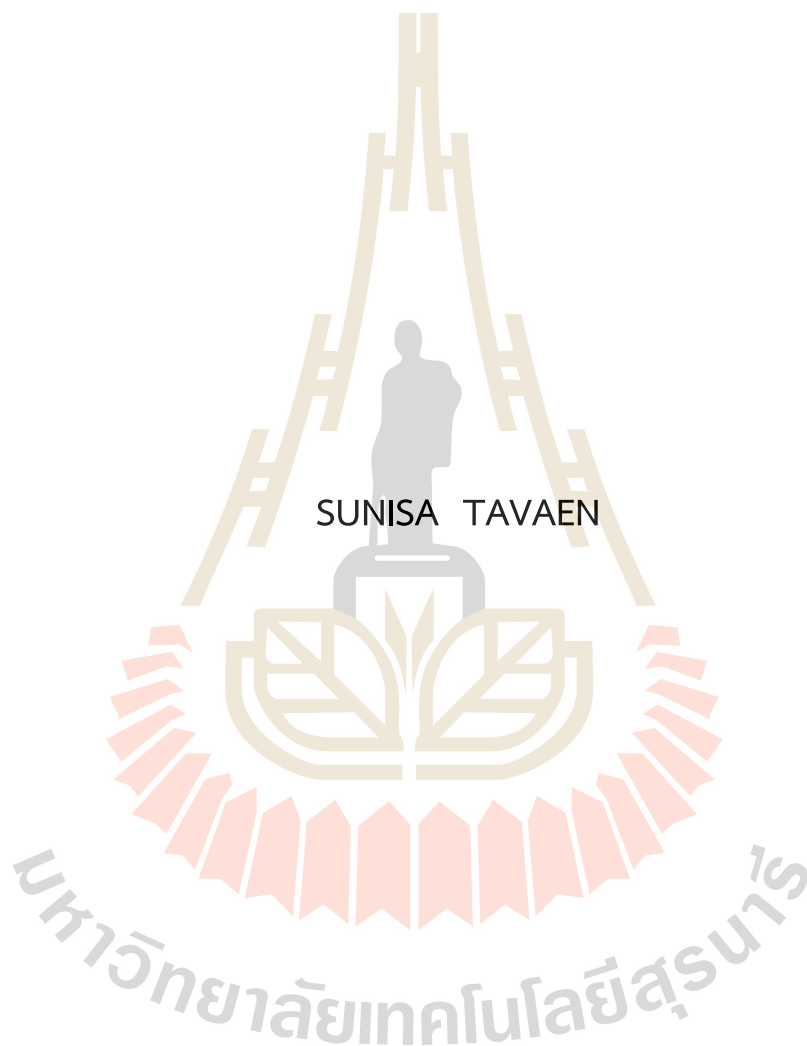


PERFORMANCES OF SHAPEFREE RBF-NEURAL NETWORKS
IN PATTERN RECOGNITION APPLICATION WITH
LARGE SCATTERED DATA SETS



A Thesis Submitted in Partial Fulfillment of the Requirements for the
Degree of Master of Science in Applied Mathematics
Suranaree University of Technology
Academic Year 2021

สมรรถนะของโครงข่ายประสาทเทียมด้วยฟังก์ชันรัศมีฐานหลักด้วย
พารามิเตอร์ที่ปราศจากพจน์ปรับค่า สำหรับประยุกต์ในการจดจำ
แบบแผนของข้อมูลขนาดใหญ่ที่กระจัดกระจาย



นางสาวสุนิสา ตาแว่น

วิทยานิพนธ์นี้เป็นส่วนหนึ่งของการศึกษาตามหลักสูตรปริญญาวิทยาศาสตรมหาบัณฑิต
สาขาวิชาคณิตศาสตร์ประยุกต์
มหาวิทยาลัยเทคโนโลยีสุรนารี
ปีการศึกษา 2564

PERFORMANCES OF SHAPEFREE RBF-NEURAL NETWORKS IN PATTERN
RECOGNITION APPLICATION WITH LARGE SCATTERED DATA SETS

Suranaree University of Technology has approved this thesis submitted in
partial fulfillment of the requirements for a Master's Degree.

Thesis Examining Committee



(Asst. Prof. Dr. Benjawan Rodjanadid)

Chairperson



(Assoc. Prof. Dr. Sayan Kaennakham)

Member (Thesis Advisor)



(Assoc. Prof. Dr. Ratchada Viriyapong)

Member



(Asst. Prof. Dr. Panu Yimmuang)

Member



(Asst. Prof. Dr. Poj Lertchoosakul)

Member



(Assoc. Prof. Dr. Chatchai Jothityangkoon)

Vice Rector for Academic Affairs
and Quality Assurance



(Prof. Dr. Santi Maensiri)

Dean of Institute of Science

สุนิสา ตาแว่น : สมรรถนะของโครงข่ายประสาทเทียมด้วยฟังก์ชันรัศมีฐานหลักด้วยพารามิเตอร์ที่ปราศจากพจน์ปรับค่า สำหรับประยุกต์ในการจดจำแบบแผนของข้อมูลขนาดใหญ่ที่กระจัดกระจาย (PERFORMANCES OF SHAPEFREE RBF-NEURAL NETWORKS IN PATTERN RECOGNITION APPLICATION WITH LARGE SCATTERED DATA SETS)
อาจารย์ที่ปรึกษา : รองศาสตราจารย์ ดร.สาयนต์ แก่นนาคำ, 181 หน้า.

คำสำคัญ : โครงข่ายประสาทเทียม/ฟังก์ชันรัศมีฐานหลัก/การจดจำแบบแผน/ข้อมูลที่กระจัดกระจาย

งานวิจัยนี้มีวัตถุประสงค์หลัก คือ การศึกษาเชิงเปรียบเทียบสมรรถนะของฟังก์ชันรัศมีฐานหลักประเภทที่ไม่มีตัวปรับค่า โดยได้มีการรวบรวมฟังก์ชันรัศมีฐานหลักในลักษณะนี้มาทั้งสิ้น 16 แบบ เพื่อนำมาประยุกต์ใช้ผ่านโครงข่ายประสาทเทียมและความสามารถในการเป็นตัวแทน (ซึ่งถือเป็นเครื่องมือหนึ่งในการลดมิติของข้อมูลในระบบบววิเคราะห์) ปัญหาที่สนใจได้แก่ ปัญหาการจดจำแบบแผนโดยได้ทดสอบกับขนาดข้อมูลที่มีขนาดใหญ่และมีการกระจัดกระจายในรูปแบบที่แตกต่างกัน ข้อมูลเริ่มต้นได้มีการถูกรบกวนด้วยสัญญาณรบกวนและแบ่งออกเป็น 2 ชุดสำหรับ ‘ชุดข้อมูลฝึกฝน/ชุดข้อมูลทดสอบ’ ในการทดลองเชิงตัวเลขทั้งหมดในการวิจัยนี้ ผลการทดลองที่ได้จากการใช้ฟังก์ชันแต่ละรูป ถูกตัดสินประสิทธิภาพโดยใช้เกณฑ์หลายประการ ได้แก่ ความแม่นยำ ตัวเลขเงื่อนไข (ของเมทริกซ์การประมาณค่า) เวลาที่ซีพียูใช้ดำเนินการ หน่วยเก็บข้อมูลที่ซีพียูใช้ ลักษณะโมเดลที่จำเพาะมากเกินไปและโมเดลที่จำเพาะน้อยเกินไป และจำนวนจุดศูนย์กลางที่ถูกสร้างขึ้น และนอกจากนี้ เพื่อเป็นการเปรียบเทียบกับฟังก์ชันรัศมีฐานหลักประเภทปกติ (คือประเภทที่มีตัวปรับค่า) การทดลองยังได้ศึกษาฟังก์ชันประเภทมัลติควอดริกไปด้วย และผลการทดลองที่ได้ในแต่ละกรณีได้มีการนำผลมาเปรียบเทียบกันอย่างระมัดระวัง ผลการทดลองโดยรวมทั้งหมดที่ได้จากงานวิจัยนี้ บ่งชี้อย่างชัดเจนว่าฟังก์ชันรัศมีฐานหลักบางรูปสามารถให้ค่าความแม่นยำที่สูงและมีประสิทธิภาพที่จะรับมือกับปัญหาในรูปแบบของการจดจำแบบแผนได้เทียบเท่า (หรือดีกว่า) ฟังก์ชันประเภทดั้งเดิม การค้นพบนี้เป็นประโยชน์อย่างยิ่งต่อการใช้งานของฟังก์ชันรัศมีฐานหลัก ที่จะไม่ต้องประสบกับปัญหาการหาค่าพารามิเตอร์อีกต่อไป

สาขาวิชาคณิตศาสตร์

ปีการศึกษา 2564

ลายมือชื่อนักศึกษา สุนิสา ตาแว่น

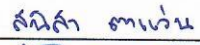

ลายมือชื่ออาจารย์ที่ปรึกษา S. Sanyat

SUNISA TAVAEN : PERFORMANCES OF SHAPEFREE RBF-NEURAL NETWORKS IN
PATTERN RECOGNITION APPLICATION WITH LARGE SCATTERED DATA SETS :
THESIS ADVISOR : ASSOCIATE PROFESSOR SAYAN KAENNAKHAM, Ph.D. 181 PP.

Keyword : NEURAL NETWORKS/RADIAL BASIS FUNCTIONS/PATTERN RECOGNITION/
SCATTERED DATA SETS

This work focuses on radial basis functions containing no parameters. The main objective is to comparatively explore more of their effectiveness. For this, a total of sixteen forms of shapeless radial basis functions are gathered and investigated under the context of the pattern recognition problem through the structure of radial basis function neural networks, with the use of a dimensionality reduction algorithm namely the Representational Capability (RC) algorithm. Different sizes of datasets are disturbed with noise before being imported into the algorithm as 'training/testing' datasets. Each shapeless radial basis function is monitored carefully with effectiveness criteria including accuracy, condition number (of the interpolation matrix), CPU time, CPU-storage requirement, underfitting and overfitting aspects, and the number of centres being generated. For the sake of comparison, the well-known Multiquadric-radial basis function (MQ-RBF) is included as a representative of shape-contained radial basis functions. The numerical results have revealed that some forms of shapeless radial basis functions show good potential and are even better than Multiquadric itself indicating strongly that the future use of radial basis function may no longer face the pain of choosing a proper shape when shapeless forms may be equally (or even better) effective.

School of Mathematics
Academic Year 2021

Student's Signature 
Advisor's Signature 

ACKNOWLEDGEMENT

First and foremost, I would like to acknowledge all the kind support and understanding I have been receiving from my parents and family. I would also like to express my deepest gratitude to my advisor Associate Professor Dr. Sayan Kaennakham for giving me the motivation to do the research, encouragement, continuous support, caring and patience for doing this thesis.

Additionally, I would like to give a million thanks to Assistant Professor Dr. Benjawan Rodjanadid, Assistant Professor Dr. Panu Yimmuang, Assistant Professor Dr. Poj Lertchoosakul, and Assistant Professor Dr. Ratchada Viriyapong for their kindness and useful comments and suggestions. Moreover, many thanks to the School of Mathematics, Institute of Science, Suranaree University of Technology (SUT) and all of my friends at SUT for their support.

Finally, I would like to thank the Development and Promotion of Science and Technology Talents Project (DPST) for all of the financial support.

Sunisa Tavaen

มหาวิทยาลัยเทคโนโลยีสุรนารี

CONTENTS

	Page
ABSTRACT IN THAI.....	I
ABSTRACT IN ENGLISH.....	II
ACKNOWLEDGEMENTS	III
CONTENTS	IV
LIST OF TABLES	VII
LIST OF FIGURES.....	IX
 CHAPTER	
I INTRODUCTION	1
1.1 Neural Networks (NNs).....	1
1.2 Radial Basis Functions (RBFs)	2
1.2.1 Globally-Supported RBFs	4
1.2.2 Compactly-Supported RBFs.....	9
1.3 Radial Basis Function Neural Networks (RBF-NNs).....	9
1.4 Shape Parameter of Radial Basis Function	11
1.4.1 Hardy Method.....	11
1.4.2 Franke Method	11
1.4.3 Carlson Method.....	11
1.4.4 Shape Parameter Strategy	12
1.5 Pattern Recognition.....	12
1.6 Interpolation.....	14
1.7 Research Objective	15
1.8 Scope and Limitations.....	16
1.9 Research Procedure	16
1.10 Expected Results.....	19
II MATHEMATICAL BACKGROUND	20

CONTENTS (Continued)

	Page
2.1 Singular Value Decomposition (SVD).....	20
2.2 The Pseudoinverse (or Moore-Penrose Inverse) of a Matrix	21
2.3 Interpolation by RBF-NNs.....	21
2.4 Shapeless Parameter of Radial Basis Function.....	22
2.5 The Representational Capability (RC).....	24
2.6 Additive White Gaussian Noise (AWGN)	25
III COMPUTATIONAL COMPONENTS.....	27
3.1 The Main Algorithm	27
3.2 Node Distribution Manner	28
3.2.1 The Training Datasets.....	28
3.2.2 The Testing Datasets.....	30
3.3 Performance Criteria	30
IV PRELIMINARY EXPERIMENTS.....	32
4.1 Experiment 1 : A Numerical Study of a Compactly-Supported Radial Basis Function Applied with a Collocation Meshfree Scheme for Solving PDEs	32
4.1.1 The Project Objective	32
4.1.2 Globally-Supported RBFs	32
4.1.3 Compactly-Supported RBFs.....	33
4.1.4 Test Case 1: Interpolation Problem.....	33
4.1.5 Test Case 2: Poisson Problem with Non-rectangular domain	38
4.1.6 Test Case 3: Nonlinear Problem.....	40
4.1.7 Main Conclusion.....	43
4.2 Experiment 2: Performances of Non-Parameterised Radial Basis Functions in Pattern Recognition Applications.....	44
4.2.1 The Project Objective	44
4.2.2 The Non-Parameterised Radial Basis Functions	44
4.2.3 Test Case 1: Linear interpolation.....	44

CONTENTS (Continued)

	Page
4.2.4 Test Case 2: Parabola function	50
4.2.5 Test Case 3: Sine interpolation	55
4.2.6 Main Conclusions	60
4.3 Experiment 3: A Comparison Study on Shape Parameter Selection in Pattern Recognition by Radial Basis Function Neural Networks	60
4.3.1 The Project Objective	60
4.3.2 RBFs and Their Shape Parameter's Selection Strategy	60
4.3.3 Test Case 1: The Sine Function	62
4.3.4 Test Case 2: The Famous Franke's Function	65
4.3.5 Main Conclusion	72
4.4 Experiment 4: Generalized-Multiquadric Radial Basis Function Neural Networks (RBFNs) with Variable Shape Parameters for Function Recovery	72
4.4.1 The Project Objective	72
4.4.2 Variable Shape Parameters	72
4.4.3 Test Case 1: One-Dimensional Case	75
4.4.4 Test Case 2: Two-Dimensional Case	76
4.4.5 Main Conclusions	80
V THE MAIN NUMERICAL EXPERIMENT	81
5.1 The Project Objective	81
5.2 Numerical Experiments and General Discussion	86
5.2.1 Experiment 1: Franke's function	86
5.2.2 Experiment 2: F7	92
5.3 Main Conclusions	98
VI CONCLUSIONS	100
REFERENCES	101
APPENDICES	

CONTENTS (Continued)

	Page
APPENDIX A MAIN CODES	107
A.1 Main Code 1: Experiment.....	108
A.2 Main Code 2: Experiment 3 Selected Main Codes	148
A.3 Main Code 3: The Main Numerical Experiment.....	153
APPENDIX B PUBLICATIONS (SCOPUS-INDEXED)	176
B.1 Experiment 1.....	177
B.2 Experiment 2.....	178
B.3 Experiment 3.....	179
B.4 Experiment 4.....	180
CURRICULUM VITAE	181



LIST OF TABLES

Table	Page
1.1 Type of Globally-Supported Radial Basis Function.....	5
2.1 The popular Wendland’s CS-RBFs.....	23
2.2 The popular Wu’s CS-RBFs.....	24
2.3 The popular Buhmann’s CS-RBFs.....	24
3.1 Error Norms adopted in this work.....	30
4.1 L_{Abs} measured at different locations over the computational domain with 15×15 interpolation nodes/centres.....	36
4.2 Errors produced by each RBF when using different levels of nodes density.....	39
4.3 Numerical solutions comparison with the exacts.....	41
4.4 The locations over the computational domain with 100 points for linear trend case.....	45
4.5 Training and validation errors for candidate models for linear trend case.....	47
4.6 Results comparison when using different numbers of centres and RBFs for linear trend case.....	48
4.7 Listing of basis function centres for linear trend case.....	48
4.8 The locations over the computational domain with 100 points for parabola trend case.....	50
4.9 Training and validation errors for candidate models for parabolas trend case.....	52
4.10 Results comparison when using different numbers of centres and RBFs for parabolas trend case.....	53
4.11 Listing of basis function centres for parabolas trend case.....	53
4.12 The locations over the computational domain with 100 points for sine trend case.....	55
4.13 Training and validation errors for candidate models for sine trend case.....	57

LIST OF TABLES (Continued)

Table	Page
4.14 Results comparison when using different numbers of centres and RBFs for sine trend case	58
4.15 Listing of basis function centres for sine trend case.....	58
4.16 Error comparison for some chosen different <i>TVN</i> cases for sine function	63
4.17 Error comparison for some chosen different <i>TVN</i> cases for Frank's function	68
4.18 Mean absolute errors measured for approximation of the function and its derivative for all forms of generalized MQ when using different variable shape forms.....	76
5.1 Type of radial basis function.....	82
5.2 Training and testing errors measured for Franke's function at $SNR=30$	88
5.3 Training and testing errors measured for Franke's function at $SNR=15$	90
5.4 The number of basis functions (m) and the condition number ($Cond_{\infty}(\cdot)$) of all radial basis function candidates for the Franke's function test case	91
5.5 Training and testing errors measured for F7 at $SNR=30$	94
5.6 Training and testing errors measured for F7 at $SNR=15$	96
5.7 The number of basis functions (m) and the condition number ($Cond_{\infty}(\cdot)$) of all radial basis function candidates for the F7 test case.	97

LIST OF FIGURES

Figure	Page
1.1 The mapping of typical neural networks structure.....	1
1.2 The mapping of a typical radial basis function structure	3
1.3 Two dimensional curves for Multiquadric RBFs under this investigation at $c = 10.00$	5
1.4 Two dimensional curves for Inverse Multiquadric RBFs under this investigation at $c = 10.00$	6
1.5 Two dimensional curves for Gaussian RBFs under this investigation at $c = 10.00$	6
1.6 Two dimensional curves for Thin Plate Splines RBFs.	7
1.7 One dimensional curve for type of Multiquadric RBFs with different shape values.....	7
1.8 One dimensional curve for type of Inverse Multiquadric RBFs with different shape values.....	8
1.9 Radial basis function (RBF) neural networks structure.	10
1.10 Examples of handwritten digits	13
3.1 (x, y) –Node uniformly distribution manner for training datasets using 50×50 nodes.....	29
3.2 (x, y) –Node non-uniformly distribution manner for training datasets using 50×50 nodes.....	29
4.1 L_{RMS} measured at different values of shape parameters with 10×10 interpolation nodes/centres.....	34
4.2 L_{RMS} measured at different values of shape parameters with 30×30 interpolation nodes/centres.....	34
4.3 Solution approximation at selected locations obtained from each RBF type, compared again the exact solution.	37
4.4 Solution profile comparison between that produced by CS1-RBF and that of the exact one	37

LIST OF FIGURES (Continued)

Figure	Page
4.5 Density distribution at 64 nodes.....	39
4.6 Density distribution at 100 nodes	40
4.7 Node solution comparison between that of CS-RBF and the exact one.	40
4.8 Node being uniformly-distributed over the computational domain, together with supported nodes needed for nonlinear computing process.....	41
4.9 Solution comparisons by using MQ-RBF	42
4.10 Solution comparisons by using GA-RBF.....	42
4.11 Solution comparisons by using CS-RBF.....	43
4.12 Data with 100 points for linear trend case.....	47
4.13 Predicted training trend produced by using 4 centres for linear trend case	49
4.14 Predicted validation trend produced by using 4 centres for linear trend case.....	49
4.15 Data with 100 points for parabolas trend case.....	52
4.16 Predicted training trend produced by using 4 centres for parabolas trend case.....	54
4.17 Predicted validation trend produced by using 4 centres for parabolas trend case	54
4.18 Data with 100 points for sine trend case.....	57
4.19 Predicted training trend produced by using 4 centres for sine trend case	59
4.20 Predicted validation trend produced by using 4 centres for sine trend case.....	59
4.21 Pattern reconstruction obtained from using Gaussian RBF with all three choices of shape parameter compared with that produced by the shapeless CS1-RBF where training phase, calculated using $TVN = (100:900)$	65

LIST OF FIGURES (Continued)

Figure	Page
4.22 Pattern reconstruction obtained from using Gaussian RBF with all three choices of shape parameter compared with that produced by the shapeless CS1-RBF where validation phase, calculated using $TVN = (100:900)$	65
4.23 Node-distribution, projected on xy -plane, in the case with 121 training data points (depicted with blue dots) and 3600 validation data points depicted with black dots).....	66
4.24 Surface plot of $f(x, y)$	67
4.25 Pattern reconstruction yielded by using GA-CS with the training phase (Note that: the ‘Exact’ means $f_1(x, y)$ and represented in red).....	69
4.26 Pattern reconstruction yielded by using GA-CS for the validation phase (Note that: the ‘Exact’ means $f_1(x, y)$ and represented in red).....	69
4.27 Pattern reconstruction yielded by using MQ-CS with the training phase (Note that: the ‘Exact’ means $f_1(x, y)$ and represented in red).....	70
4.28 Pattern reconstruction yielded by using MQ-CS for the validation phase (Note that: the ‘Exact’ means $f_1(x, y)$ and represented in red).....	70
4.29 Pattern reconstruction yielded by using CS1 with the training phase (Note that: the ‘Exact’ means $f_1(x, y)$ and represented in red).....	71
4.30 Pattern reconstruction yielded by using CS1 for the validation phase (Note that: the ‘Exact’ means $f_1(x, y)$ and represented in red).....	71
4.31 Generalized MQ with six values of β 's.....	73
4.32 Generalized distribution of centres test function.....	73
4.33 Generalized two-dimensional test function.....	73
4.34 Multiquadrics’ shape determining Stg-1 by using $c_{\min} = 1/\sqrt{N}$, $c_{\max} = 3/\sqrt{N}$, and $N = 30$	74
4.35 Multiquadrics’ shape determining Stg-2 by using $c_{\min} = 1/\sqrt{N}$, $c_{\max} = 3/\sqrt{N}$, and $N = 30$	75

LIST OF FIGURES (Continued)

Figure	Page
4.36 Mean absolute errors measured at different numbers of centres for approximation of $f(x, y)$ by using <i>Stg-1</i>	77
4.37 Mean absolute errors measured at different numbers of centres for approximation of $f(x, y)$ by using <i>Stg-2</i>	77
4.38 Mean absolute errors measured at different numbers of centres for approximation of $\partial f / \partial x$ by using <i>Stg-1</i>	78
4.39 Mean absolute errors measured at different numbers of centres for approximation of $\partial f / \partial x$ by using <i>Stg-2</i>	78
4.40 Mean absolute errors measured at different numbers of centres for approximation of $\partial f / \partial y$ by using <i>Stg-1</i>	79
4.41 Mean absolute errors measured at different numbers of centres for approximation of $\partial f / \partial y$ by using <i>Stg-2</i>	79
5.1 One-dimensional curve for some type of RBFs under this investigation of those containing no shapes (or shapeless) and $2 \leq \phi r \leq 16$	84
5.2 One-dimensional curve for some type of RBFs under this investigation of those containing no shapes (or shapeless) and $0.2 \leq \phi r \leq 2$	84
5.3 One-dimensional curve for some types of RBFs under this investigation of those containing no shapes (or shapefree) and $0 \leq \phi r \leq 0.2$	85
5.4 One-dimensional curve for the famous MQ with different shape values under this investigation.	85
5.5 Noised- $z(x, y)$ training datasets with $SNR = 30$ based on uniformly distribution of $\{(x, y)\}$	87
5.6 Noised- $z(x, y)$ training datasets with $SNR = 30$ based on non-uniformly (randomly) distribution of $\{(x, y)\}$	87
5.7 CPU-storage measurement observed at three different sizes of testing datasets with uniform nodes distribution using $SNR = 30$	88
5.8 CPU-time measurement observed at three different sizes of testing datasets as uniform nodes distribution using $SNR = 30$	89

LIST OF FIGURES (Continued)

Figure	Page
5.9 Noised- $z(x, y)$ training datasets with $SNR = 15$ based on uniformly distribution of $\{(x, y)\}$	89
5.10 Noised- $z(x, y)$ training datasets with $SNR = 15$ based on non-uniformly (randomly) distribution of $\{(x, y)\}$	90
5.11 CPU-storage measurement observed at three different sizes of testing datasets with random nodes distribution using $SNR = 15$	91
5.12 CPU-time measurement observed at three different sizes of testing datasets with random nodes distribution using $SNR = 15$	91
5.13 Noised- $z(x, y)$ training datasets based on non-uniformly (randomly) distribution of $\{(x, y)\}$	93
5.14 Noised- $z(x, y)$ training datasets based on non-uniformly (randomly) distribution of $\{(x, y)\}$	93
5.15 CPU-storage measurement observed at three different sizes of testing datasets with uniform nodes distribution using $SNR = 30$	94
5.16 CPU-time measurement observed at three different sizes of testing datasets with uniform nodes distribution using $SNR = 30$	95
5.17 Noised- $z(x, y)$ training datasets based on uniformly distribution of $\{(x, y)\}$	95
5.18 Noised- $z(x, y)$ training datasets based non-uniformly (randomly) distribution of $\{(x, y)\}$	96
B.1 A Numerical Study of a Compactly-Supported Radial Basis Function Applied with a Collocation Meshfree Scheme for Solving PDEs.	177
B.2 Performances of Non-Parameterised Radial Basis Functions in Pattern Recognition Applications.	178
B.3 A Comparison Study on Shape Parameter Selection in Pattern Recognition by Radial Basis Function Neural Networks.	179
B.4 Generalized-Multiquadric Radial Basis Function Neural Networks (RBFNs) with Variable Shape Parameters for Function Recovery.	180

CHAPTER I

INTRODUCTION

1.1 Neural Networks (NNs)

Neural networks are widely interesting in the computer science and technology industry. In current years, neural networks have been applied to search for the best solution to many problems, for instance, image recognition, facial recognition, voice recognition, speech recognition, optical character recognition (OCR) and natural language processing (NLP), etc. The basic definition of neural networks emulates the brain computational unit, which is a "neuron". The function of the brain is connected with neurons and then multiple connected neurons become neural networks.

The machine mimics the work of the brain, the basic unit of computation in neural networks, or the neuron and connected cell of the brain or in this is called a node or unit. This means that machines can learn and process data in the same way humans do. A typical architecture of a neural network contains three layers which are input layer, hidden layer and output layer as shown Figure 1.1.

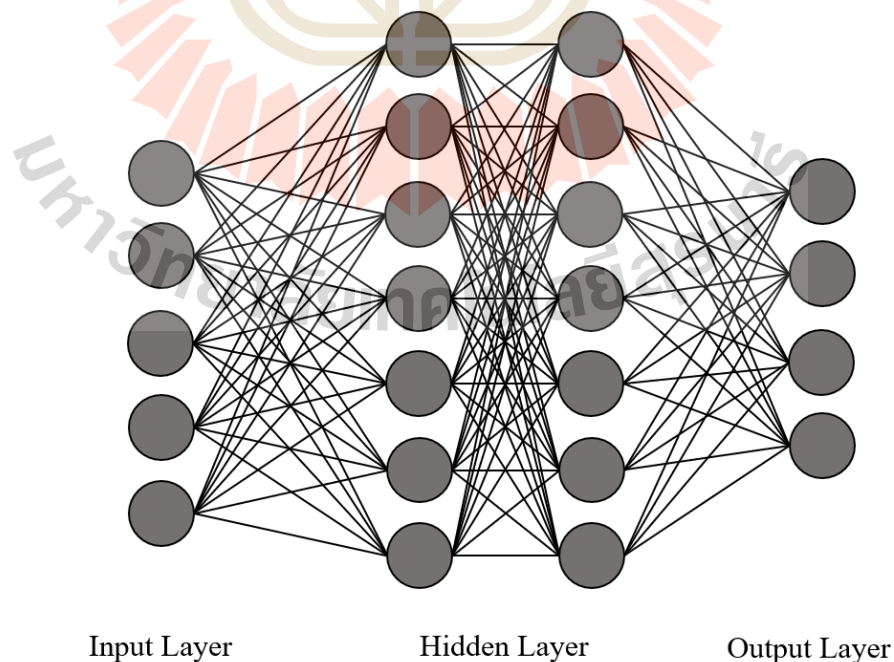


Figure 1.1 The mapping of typical neural networks structure.

In these layers, there will always be input and output layers and it has zero or more hidden layers. The entire learning process of the neural networks is done with layers.

Input Layer: The input layer is the very beginning of the workflow for the neural network which contains input nodes. There are no calculations in this layer. In other words, this layer only passes input data from some external sources to the next layer. Each of the input data has to be numerical and if it is non-numerical, find a way to make it numerical first. The process of manipulating data before inputting it into the neural network is called data processing and oftentimes will be the most time-consuming part of making machine learning models.

Hidden Layer: The hidden layers are composed of most of the neurons in the neural network as superior to machine learning algorithms and are the heart of manipulating the data to get the desired output. They perform computations and transfer information from the input nodes to the output nodes. Then data will pass through the hidden layers and be manipulated by many weights and biases. It is called the “hidden” layer because developers of neural networks will not directly work with these layers, as opposed to input and output layers. There should be zero or more than zero hidden layers in the neural networks. For the large majority of problems one hidden layer is sufficient. In general, the more hidden layers in the neural network, the longer it takes to process for the output. Complex problems can be solved in the hidden layers of the neural network.

Output Layer: The output layer is the final product of manipulating the data in the neural network and can represent different things. There must be always an output layer in the neural networks. The output layer takes the inputs which are passed in from the layers before and performs the calculations through its neurons and then the output is computed. And the output layer has one node per one class label of our model.

1.2 Radial Basis Functions (RBFs)

In the recent years, the application of radial basis functions has been greatly increasing in terms of classification and prediction tasks for examples of interesting contexts included in daily life (Chen, Li, Wang and Deng, 2019; Wang, Li and Miao, 2020; Dawson, 2020), agriculture (Hemageetha and Nasir, 2013; Shastri, Sanjay and Deexith,

2017), finance (Rashedi, Ismail, Hamadneh, Wadi, Jaber and Tahir, 2021), and medicine (Fragopoulos, Pouliakis, Meristoudis, Mastorakis and Margari, 2020).

Radial Basis Functions are commonly found as multivariate functions whose values are dependent only on the distance from the centre, i.e. $\phi(\mathbf{x}) = \phi(r) \in \mathbb{R}$, $\mathbf{x} \in \mathbb{R}^d$ and $r \in \mathbb{R}$ or on the distance from centres point at j -location, $\mathbf{x}_j \in \mathbb{R}^d$ as $\phi(\mathbf{x} - \mathbf{x}_j) = \phi(r_j) \in \mathbb{R}$. The input vector $\mathbf{x}_i = x_1, x_2, \dots, x_d \in \mathbb{R}^d$ of matrix \mathbf{X} are input data and any function $\phi(\mathbf{x}) = \phi(\|\mathbf{x}\|_2)$ is the Euclidean distance. And then radial basis functions are completely described by specifying the number of basis functions, basis function parameters and the weights of the basis function outputs to produce the output data.

From a modeling perspective, it can be viewed as generating a sequence of two mappings. The first is a nonlinear mapping between input data and the basis function and the second is a linear mapping between the basis function and weight was generated from the model outputs.

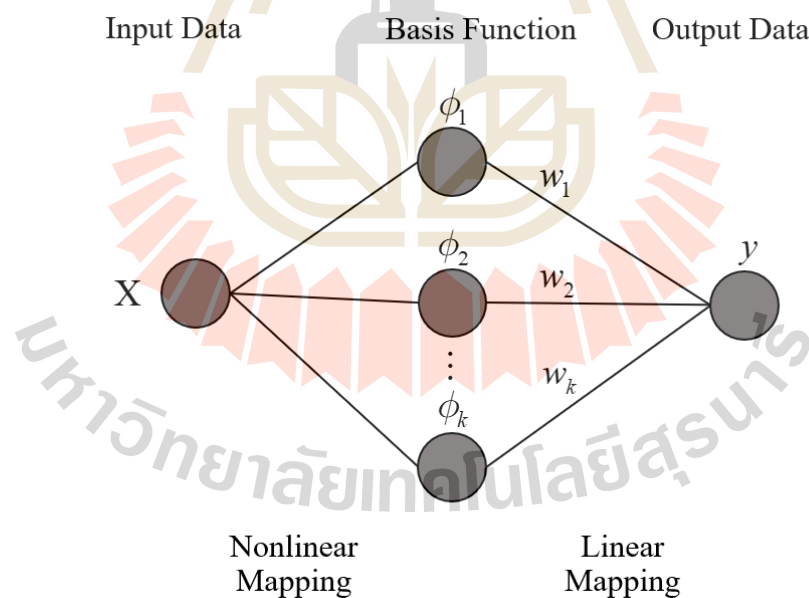


Figure 1.2 The mapping of a typical radial basis function structure.

A typical RBF structure is illustrated in Figure 1.2 that shows the connectivity mapping of input data, basis function and output data. It is clear to understand that an input vector in d -dimensional space is transformed by the basis function into a k -dimensional vector. From the input vector $\mathbf{x} = x_1, x_2, \dots, x_d$ pass the k basis

functions and becomes the basis function output $\phi = \phi_1 \mathbf{x}, \phi_2 \mathbf{x}, \dots, \phi_k \mathbf{x}$ where $\phi_j \cdot$ is the output from the j -th basis function. The output y corresponding to the input vector \mathbf{x} is obtained by the summation of the weighted basis function outputs, which are

$$y = \sum_{j=1}^k w_j \phi_j \mathbf{x} \quad (1.1)$$

Formally, for a mapping $f: \mathbb{R}^d \rightarrow \mathbb{R}$ the radial basis function can be described mathematically as

$$f \mathbf{x} = \sum_{j=1}^k w_j \phi_j \mathbf{x} = \sum_{j=1}^k w_j \phi \left(\frac{\|\mathbf{x} - \boldsymbol{\mu}_j\|_2}{\sigma_j} \right), k \leq N \quad (1.2)$$

where $\mathbf{x} \in \mathbb{R}^d$ is the input vector, $\boldsymbol{\mu}_j \in \mathbb{R}^d$ is the j -th basis function centres, $\phi \cdot$ is the basis function that is the nonlinear function from \mathbb{R} to \mathbb{R} and w_j is the weight associated with the j -th basis function output. Also, σ_j is the parameter to control the receptive field width of the j -th basis function.

The basis functions $\phi \cdot$ in RBF networks play the role of transfer functions in traditional neural networks. However, the basis functions have the unique feature that their responses to the input vectors are not only radially symmetric but also monotonically decreasing or increasing with distance r from the center $\boldsymbol{\mu}_j$. When $r = \|\mathbf{x} - \boldsymbol{\mu}\|/\sigma$, several forms of these functions ϕr can be used.

1.2.1 Globally-Supported RBFs

The interest of this study is the RBF interpolation of a continuous multivariate function, $f \mathbf{x} = \mathbf{x} \in \Omega \subset \mathbb{R}^d$, Ω is a bounded domain. Given N basis functions of output values y_i , $i=1, \dots, N$, when $y_i \in \mathbb{R}$ at data location \mathbf{x}_i , $i=1, \dots, N$. Then the traditional RBFs is Globally-Supported RBFs that defined with N -th unknown basis functions, which related

$$f \mathbf{x} \approx \sum_{j=1}^N w_j \phi_j \|\mathbf{x} - \mathbf{x}_j\|_2 \quad (1.3)$$

where w_j , $j=1, \dots, N$ are the unknown coefficients to be determined.

Some popular choices and their expression are given in Table 1.1, where c is a positive constant (Powell, 1987). Amongst these, the Gaussian is probably the most popular basis function for two reasons that it has attractive mathematical properties and its hill-like shape is easy to control with a parameter σ (Winston, 1993).

The basis functions are radially symmetric with distance r from each input vector \mathbf{x}_j when $r_j = \|\mathbf{x} - \mathbf{x}_j\|_2$.

Table 1.1 Type of Globally-Supported Radial Basis Function.

RBFs	ϕr
Polynomial Spline (PS)	$\begin{cases} r^{2k-1}, k \in \mathbb{N} \\ r^{2k} \ln r, k \in \mathbb{N} \end{cases}$
Thin Plate Splines (TPS)	$r^2 \ln r$
Multiquadric (MQ)	$r^2 + c^{2\beta}, \beta \in \mathbb{R} \text{ such } \beta > 0$
Inverse Multiquadric	$r^2 + c^{2-\beta}, \beta \in \mathbb{R} \text{ such } \beta > 0$
Gaussian	$\exp - cr^2$

Figure 1.3 – Figure 1.6 illustrate their surface profiles of at $c = 10.00$. Differences in the curve profiles for each parameter value can be seen and noticed in Figure 1.7 and Figure 1.8.

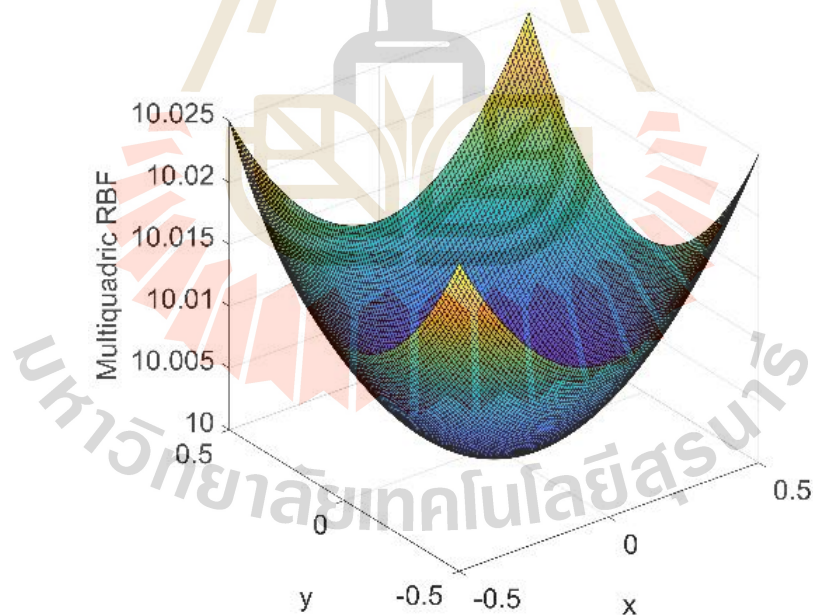


Figure 1.3 Two dimensional curves for Multiquadric RBFs under this investigation at $c = 10.00$.

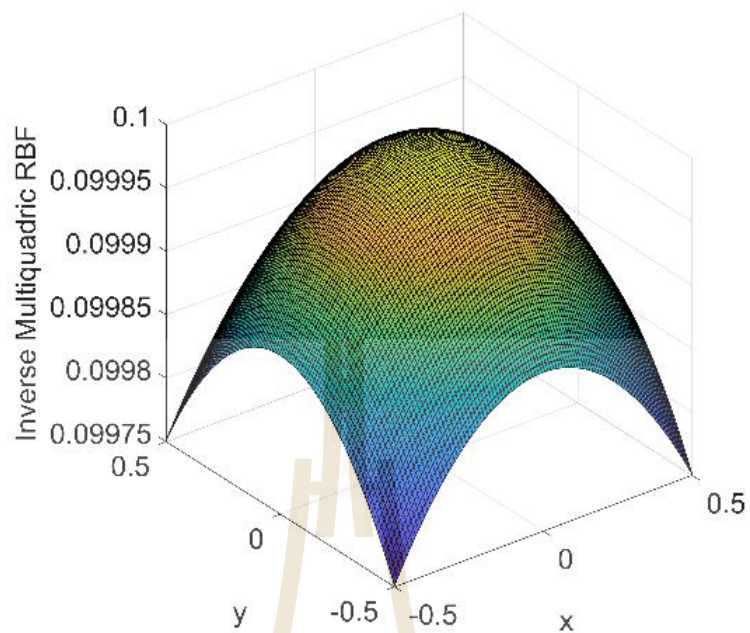


Figure 1.4 Two dimensional curves for Inverse Multiquadric RBFs under this investigation at $c = 10.00$.

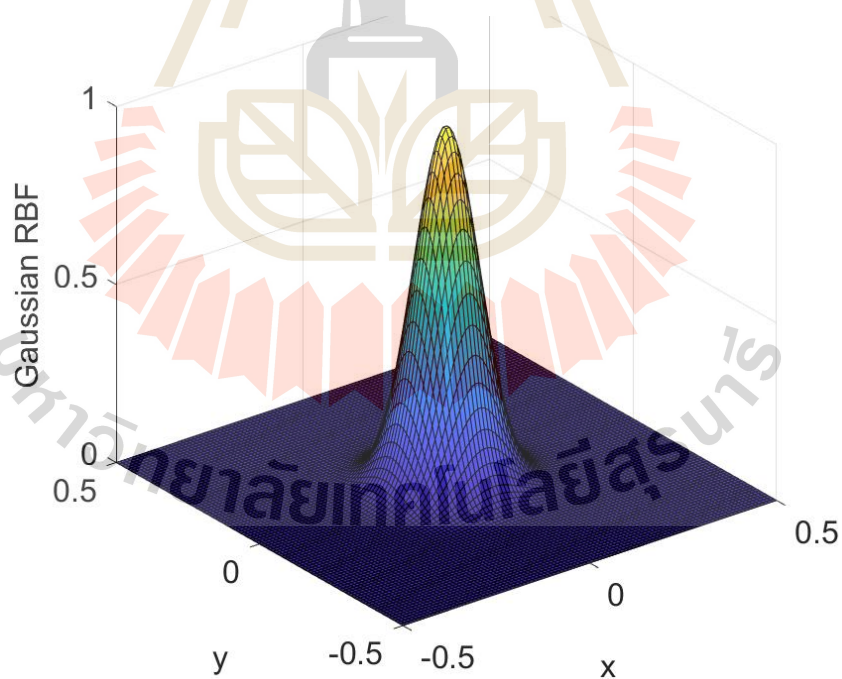


Figure 1.5 Two dimensional curves for Gaussian RBFs under this investigation at $c = 10.00$.

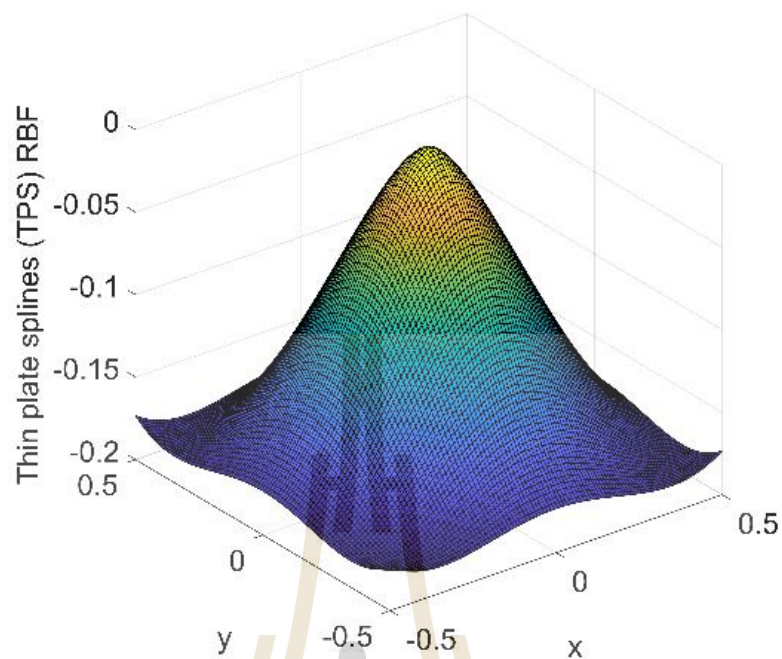


Figure 1.6 Two dimensional curves for Thin Plate Splines RBFs.

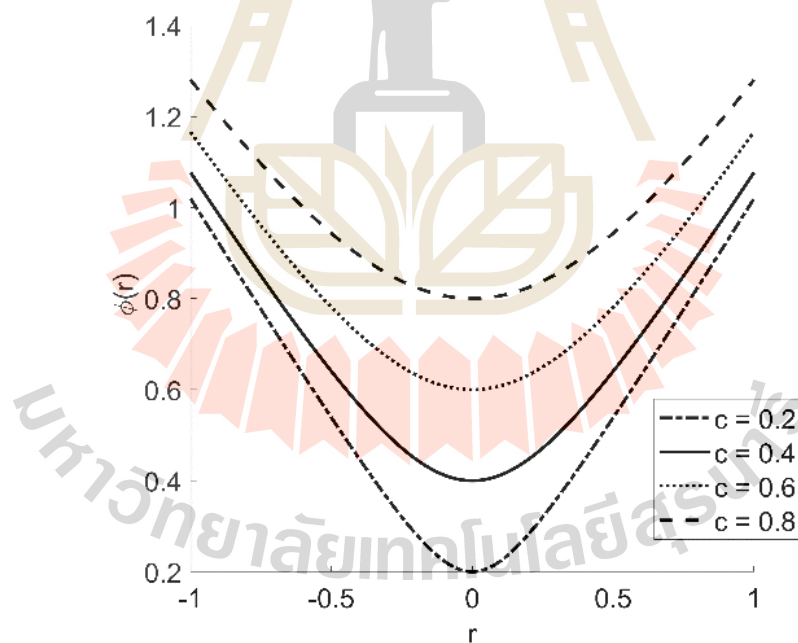


Figure 1.7 One dimensional curve for type of Multiquadric RBFs with different shape values.

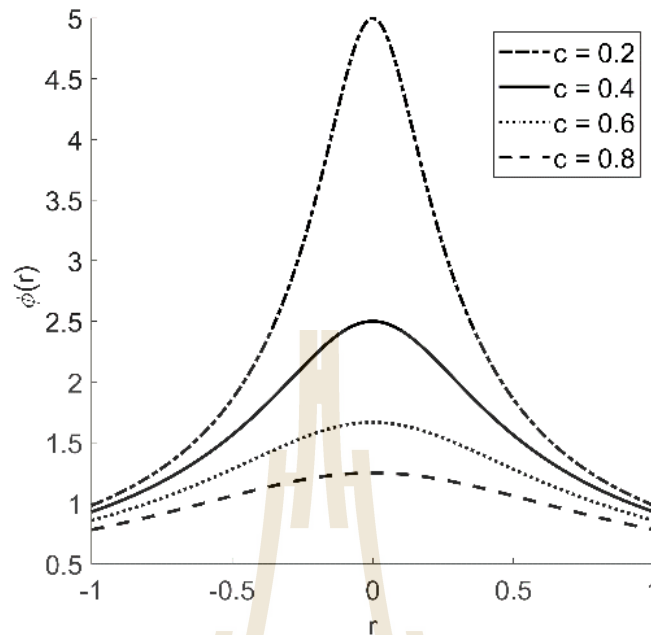


Figure 1.8 One dimensional curve for type of Inverse Multiquadric RBFs with different shape values.

From linear combination equation (1.3), we have

$$y_i = f(\mathbf{x}_i) = \sum_{j=1}^N w_j \phi(\|\mathbf{x}_i - \mathbf{x}_j\|_2), \quad i=1,2,\dots,N. \quad (1.4)$$

The linear system of equations can be rewritten in the following matrix form,

$$\mathbf{A}\mathbf{w} = \mathbf{b}, \quad (1.5)$$

in which $\mathbf{w} = [w_1, w_2, \dots, w_N]^T$ is an unknown coefficient vector to be determined,

$\mathbf{b} = [y_1, y_2, \dots, y_N]^T$ is the right-hand side vector, and the RBF matrix is given by

$$\mathbf{A} = [\phi_{ij}] = \begin{bmatrix} \phi_{11} & \phi_{12} & \phi_{13} & \cdots & \phi_{1j} \\ \phi_{21} & \phi_{22} & \phi_{23} & \cdots & \phi_{2j} \\ \phi_{31} & \phi_{32} & \phi_{33} & \cdots & \phi_{3j} \\ \vdots & \vdots & \vdots & \ddots & \vdots \\ \phi_{i1} & \phi_{i2} & \phi_{i3} & \cdots & \phi_{ij} \end{bmatrix} \quad (1.6)$$

where $\phi_{ij} = \phi(\|\mathbf{x}_i - \mathbf{x}_j\|_2)$, $i, j = 1, 2, \dots, N$.

In recent years, the optimal parameter c is witnessed by the continued efforts of many to establish the theory of evaluating. Since the condition number of the interpolation matrix dramatical grows as the parameter c increases, the optimal parameter c is the largest value at which it can be utilized before the instability of matrix calculation occurs due to the machine precision.

1.2.2 Compactly-Supported RBFs

The Globally-Supported RBFs took a lot of computing space and time, so Wu and Wendland have introduced a new method that has been adjusted to be more local. Therefore, defined as compactly supported positive definite RBFs (CS-RBFs). From the linear combination equation (1.4) which are;

$$y_i = f(\mathbf{x}_i) = \sum_{j=1}^N w_j \phi(r_{ij}) \quad , i=1,2,\dots,N \quad (1.7)$$

where $r_{ij} = \|\mathbf{x}_i - \mathbf{x}_j\|_2$ or written in general form as $\phi(r)$. For constructed radial basis function with compact support are of the form

$$\phi(r) = \begin{cases} p(r) & , 0 \leq r \leq 1 \\ 0 & , otherwise. \end{cases} \quad (1.8)$$

with a univariate polynomial p .

Therefore, the equations can be rewritten in the following matrix form,

$$y_i = f(\mathbf{x}_i) = \begin{cases} \sum_{j=1}^N w_j \phi_j(r) & , 0 \leq r \leq 1 \\ 0 & , otherwise \end{cases} \quad (1.9)$$

1.3 Radial Basis Function Neural Networks (RBF-NNs)

In this section, first of all is introduced the basic neural networks structure of RBF model with some basis function $\phi(r)$ and give expression for the mappings which converts the input data vectors to model inputs that divided into three layers as shown in Figure 1. and can be described as follow:

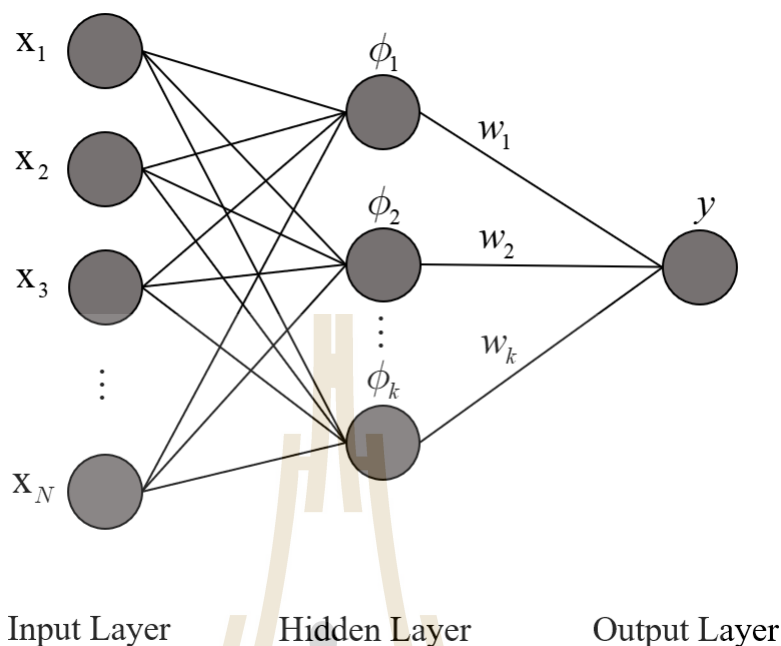


Figure 1.9 Radial basis function (RBF) neural networks structure.

Input Layer: The input layer forwards the data to the hidden layer. The number of neurons in the input layer should be equal to the dimensions of the data. In the input layer, there are no calculations the same as a standard neural network. The input neuron is completely connected to the hidden neuron.

Hidden Layer: The hidden layer takes the input layer to the radial basis function which might not be a linear function and transform it into a new space that is a more linear function. The computations in the hidden layers are based on comparisons with prototype vectors of radial basis function which is a vectors from the training set.

Output Layer: The output layer is a linear function for both classification or prediction tasks. The computations in the output layer are performed in a linear combination between the input vector and the weight vector with calculated in hidden layer by the radial basis function.

1.4 Shape Parameter of Radial Basis Function

In the Globally-Supported RBFs contains shape parameter that is very important problem. Nowadays, the optimal shape parameter is a challenging problem. This research introduces some popular methods how to choose the shape parameter.

1.4.1 Hardy Method

The first method introduced by Hardy (Hardy, 1971), The Hardy method was originally used with the Multiquadric basis function and (Hardy, 1977) indicating the best value for

$$\varepsilon = 0.815d \quad (1.10)$$

where $d = \frac{1}{N} \sum_{i=1}^N d_i$ (the mean distance of each data point to its nearest neighbor) and d_i is the distance from each data point x_i, y_i to the nearest neighbor.

1.4.2 Franke Method

The method was first proposed by Franke (Franke, 1979) which is developed from Hardy's method and changed nominal values. Nevertheless, this method considers the boundary cycle of the data set that it is diameter D and defined as:

$$\varepsilon = \frac{1.25D}{\sqrt{N}} \quad (1.11)$$

where D is the diameter of the smallest circle containing all data points and N is the number of data point. The beginning used for quadratic basis function.

1.4.3 Carlson Method

This method was invested by Carlson (Carlson and Foley, 1991). The second method previously computed only domain however Carlson's method includes range to compute. Start with calculating the minimum and maximum values of the data points x_i, y_i, z_i and next compute the least squares bivariate quadratic polynomial fit to the data $\bar{x}_i, \bar{y}_i, \bar{z}_i$. Defined as:

$$\bar{x}_i = \frac{x_i - x_{\min}}{x_{\max} - x_{\min}}, \quad (1.12)$$

$$\bar{y}_i = \frac{y_i - y_{\min}}{y_{\max} - y_{\min}}, \quad (1.13)$$

$$\bar{z}_i = \frac{z_i - z_{\min}}{z_{\max} - z_{\min}}. \quad (1.14)$$

Next, denoting this quadratic by $q \bar{x}, \bar{y}$ and compute

$$V = \sum_{i=1}^N \frac{\bar{z}_i - q \bar{x}_i, \bar{y}_i^2}{N}. \quad (1.15)$$

Finally, find form of shape parameter as

$$\varepsilon = \frac{1}{1+120V}. \quad (1.16)$$

And the next variables of shape parameter are two nonlinear-variable shape strategies following.

1.4.4 Shape Parameter Strategy

This method was introduced by Nojavan (Nojavan, Abbasbandy and Allahviranloo, 2017). The variable shape parameter strategy which is based on a variably scaled radial kernel that can be defined as:

$$K_c \mathbf{x} - \mathbf{x}_j = \phi \left(\frac{r_j}{c_j} \right)^2, r_j = \|\mathbf{x} - \mathbf{x}_j\|_2, j = 1, 2, \dots, N \quad (1.17)$$

where c_j is the shape parameter corresponding to the j -th center.

In this paper, we have proposed some strategies to choose, defined as

$$\varepsilon_j = c_{\min} + c_{\max} - c_{\min} \exp -j^{-1}, j = 1, 2, \dots, N \quad (1.18)$$

and

$$\varepsilon_j = c_{\min} + c_{\max} - c_{\min} \sin j, j = 1, 2, \dots, N \quad (1.19)$$

where $c_{\max} = 1.3/\sqrt{N}$, and $c_{\min} = 1.1/\sqrt{N}$, are positive parameters.

1.5 Pattern Recognition

Pattern recognition has a long history of being used which has originated in engineering, whereas in the recent year that was used in machine learning and grew out of computer science. Human ability is the recognition and classification from observation. Pattern recognition is the science of recognizing patterns by machines. Nowadays, this is a big wide research area in Artificial Intelligence Science (Parasher, Sharma, Sharma and Gupta, 2011). There are several useful areas, such as biomedical and biology, social medial intelligence (SMI), video surveillance, intelligent retail environment, and digital cultural heritage (Paolanti and Frontoni, 2020).

The task of pattern recognition is to construct a model that captures an unknown input-output mapping on the basis of limited evidence about the nature of this mapping, called training. The evidence available is a set of labelled training data, also called training samples. The goal, however, is not to learn an exact representation of

the training data itself but to build a model that captures the underlying relationship in the training data, so that it can be used to predict the unknown output at some future observations of the input. In the literature, this latter ability is called generalization capability, a term borrowed from psychology.

The process of pattern recognition is successful to adapt and learn from examples which are underlying idea for generating system the predictive learning. The problem of pattern recognition is searching for patterns in the data. For instance, recognizing handwritten digits from the MNIST data set [<http://yann.lecun.com/exdb/mnist/>] illustrated in Figure 1.10, each digit contains a 28x28 pixel image.



Figure 1.10 Examples of handwritten digits.

The goal of this problem is to build a produce of machine system to identify of the digit 0,1,...,9 as the output from the \mathbf{x} vectors input. That is the nonminor problem due to the fact that specific characteristic of handwriting that can be tackled by handcrafted rules or behavior analysis the digits based on the shapes or format of the strokes.

Pattern recognition is the process of differentiating and dividing the data according to certain criteria or by general components, which are performed by special

algorithms. The task of pattern recognition is to construct the model with unknown input-output mapping pattern. In other words, it is to construct the best model, if any, from the train data with some mapping functions and expect this model to best represent the rest of the data, called ‘training data’. Both sets of the data can be of the following form;

$$D = \{(\mathbf{x}_i, y_i) \mid \mathbf{x}_i \in \mathbb{R}^d, y_i \in \mathbb{R}, i = 1, 2, \dots, N\} \quad (1.20)$$

where \mathbf{x}_i are inputs with the corresponding y_i are outputs. The main task is to find a mapping D from the d -dimensional input space to 1-dimensional output space.

Model structure of a typical radial basis function network is depicted in Figure 1., when a data set $D = \{(\mathbf{x}_i, y_i) \mid i = 1, \dots, N\}$ is given and the model searches for the corresponding output estimate \hat{y} for input vector \mathbf{x} , represented by functional form:

$$\hat{y} = f(\mathbf{x}) = \sum_{j=1}^m w_j \phi_j(\mathbf{x}) = \sum_{j=1}^m w_j \phi_j(\|\mathbf{x} - \mathbf{a}_j\|_2 / \sigma) \quad (1.21)$$

where $\|\cdot\|_2$ is the Euclidean distance norm, $\phi(\cdot)$ is a basis function and m is the number of centres, σ is the parameter to control the receptive field width of the j -th basis functions, \mathbf{a}_j are the centres of j -th basis functions, and w_j are the weight associated with the j -th basis functions (note that $m \ll n$). Thus, the RBF model is fully determined by $P = \{m, \mathbf{a}, \sigma, \mathbf{w}\}$.

1.6 Interpolation

Interpolation is a subset of statistical methods to estimate an unknown function by using other established values located by a given discrete data set that the function passes through the provided data points. This work focuses on the radial basis function that the original raised to be used for the interpolation problem. The RBF maps input data vectors \mathbf{x} in \mathbb{R}^d to output value y in \mathbb{R} . Then the domain of the RBF is \mathbb{R}^d and the range is \mathbb{R} . Suppose that given a set of N input-output data points $\{\mathbf{x}_i, y_i\}_{i=1}^N$ is obtained, in which $\mathbf{x}_i \in \mathbb{R}^d$, $y_i \in \mathbb{R}$ and all data vectors are distinct. Therefore, the functional relationship between input vectors \mathbf{x}_i and output vector y_i is

$$y_i = h(\mathbf{x}_i), \quad i = 1, 2, \dots, N. \quad (1.22)$$

where y_i are the exact output and the interpolation problem is to find the RBF $h(\mathbf{x}_i)$ that estimate at the vectors $\mathbf{x}_i, i = 1, 2, \dots, N$. The radial basis function model is contained with N basis function and N is the number of data vectors and all distinct. When used for interpolation, the number of centres equals the number of data points,

i.e., $k=N$. On the other hand, when the RBF model is employed for function approximation, usually the number of centres is much smaller than N . The interpolation matrix which is related to the interpolation problem is analyzed at some length.

It should be noted that in general, the output could consist of several variables y^1, y^2, \dots, y^p . Though this generalization is straight forward, we discuss only the one output variable case in this work.

Then the RBF model can be written in the form

$$y_i = f(\mathbf{x}_i) = \sum_{j=1}^N w_j \phi(\|\mathbf{x}_i - \mathbf{x}_j\|_2), i=1,2,\dots,N \quad (1.23)$$

where the number of centres is equal to the number of data vectors which are $k=N$. Let us denote the new matrix by \mathbf{G} and its columns by $\mathbf{g}_1, \mathbf{g}_2, \dots, \mathbf{g}_N$ for the Gaussian radial basis functions and their shape parameter are $\varepsilon_1, \varepsilon_2, \dots, \varepsilon_N$ respectively, therefore the interpolation matrix is

$$\mathbf{G} = [\mathbf{g}_1 \quad \mathbf{g}_2 \quad \dots \quad \mathbf{g}_j \quad \dots \quad \mathbf{g}_N] \quad (1.24)$$

where $\mathbf{g}_j = \exp\left(-\frac{\|\mathbf{x} - \mathbf{x}_j\|^2}{2\varepsilon_j^2}\right)$. We get the interpolation matrix \mathbf{G} is a square matrix of size $N \times N$.

Moreover, the N basis functions have the centres at $\mathbf{x}_1, \mathbf{x}_2, \dots$, and \mathbf{x}_N and the output of the RBF mapping given in the form of the interpolation matrix as

$$f(\mathbf{x}) = \sum_{j=1}^N w_j \exp\left(-\frac{\|\mathbf{x} - \mathbf{x}_j\|^2}{2\varepsilon_j^2}\right). \quad (1.25)$$

Furthermore, we can be written in matrix form based on the interpolation matrix as following

$$\mathbf{G}\mathbf{w} = \mathbf{y}. \quad (1.26)$$

1.7 Research Objective

The main purpose of this study is to investigate how well radial basis functions containing no shape parameters can perform when being utilized in pattern recognition applications under the structure of neural networks. Its ability is tested with large scattered data sets where the performances are carefully monitored and assessed via several criteria; accuracy, sensitivity to parameters, CPU-time, storage requirement, and ease of implementation.

1.8 Scope and Limitations

Below are scope and limitations of this study.

1. Shapeless radial basis functions being considered are only those stated in Section 2.4

2. Input data is mainly in 2-dimension format.

3. Programming language used is mainly MATLAB.

4. For result validation, the mean square error norms (MSE) are employed and it is of the following form;

$$MSE = \frac{1}{N} \sum_{i=1}^N (y_i - \hat{y}_i)^2, \quad (1.27)$$

with N being the number of data points involved in each case, y_i , \hat{y}_i are respectively the actual and approximated value of the output at a node i^{th} .

5. All computational processes are executed in serial computation manner, one task will be done after another, with the following information;

- Model: Swift SF514-54GT
- Processor: Intel(R) Core(TM) i7-1065G7 CPU @ 1.30GHz 1.50 GHz
- Installed memory(RAM): 16.0 GB(15.8 GB usable)
- System type: 64-bit Operating System, x64-based processor.

1.9 Research Procedure

Before reaching the main experiment of the thesis, five investigations have successfully been carried out, all of which have already been published in a Scopus-indexed journal, as details listed below (See also the APPENDICES).

Project-1:

Title: A Numerical Study of a Compactly-Supported Radial Basis Function Applied with a Collocation Meshfree Scheme for Solving PDEs.

Abstract: It is known that all Radial Basis Function-based meshfree methods suffer from a lack of reliable judgement on the choice of shape parameter, appearing in most of the RBFs. While the popularity of meshfree/meshless numerical methods is growing fast over the past decade, the great challenge is still to find an optimal RBF form with its optimal shape parameter. In this work, the main focus is on one type of RBF namely 'Compactly Supported (CS-RBF)' that contains no parameter, and yet has

not been explored numerically as much in the past, particularly under the context of data interpolation/approximation and solving partial differential equations (PDEs). To compare the potential advantages of CS-RBF, two most popular choices of RBF widely used; Multiquadric (MQ), and Gaussian (GA) were studied parallelly. The information gathered and presented in this work shall be useful for the future users in making decision on RBF.

Publication status: IOP Conf. Series: Journal of Physics: Conf. Series **1489** (2020) 012020. (Scopus)

Project-2 :

Title: Performances of non-parameterised radial basis functions in pattern recognition applications.

Abstract: Pattern recognition appears in many applications with most popular scheme are those involved the so-called ‘Radial Basis Function (RBF)’. It is known that the shape parameter contained in some RBFs used has great influence on the final quality of prediction. This study focusses on RBFs which contains no parameters where three data patterns are used for performance validation. With a good choice of number of centres, it is clearly possible to obtain satisfactory results with no burden on choosing the suitable or optimal shape. This can well shed more light into applications with more complexity with less user’s judgment and be more automatic in the process.

Publication status: IOP Conf. Series: Journal of Physics: Conf. Series **1706** (2020) 012165. (Scopus)

Project-3:

Title: A Comparison Study on Shape Parameter Selection in Pattern Recognition by Radial Basis Function Neural Networks.

Abstract: This study investigates three choices of shape parameter selection when the so-called Radial Basis Function (RBF) is used. Under the problem of pattern recognition via RBF-Neural Network using RC-algorithm, three RBFs are focussed on; Gaussian (GA), Multiquadric (MQ), and Compactly-Supported (CS1). Two pattern recognition cases are tested and the best choice of shape parameter is validated using Model-Selection Criteria (MSC).

Publication status: IOP Conf. Series: Journal of Physics: Conf. Series (SCOPUS)

Project-4 :

Title: Generalized-Multiquadric Radial Basis Function Neural Networks (RBFNs) with Variable Shape Parameters for Function Recovery.

Abstract: After being introduced to approximate two-dimensional geographical surfaces in 1971, the multivariate radial basis functions (RBFs) have been receiving a great amount of attention from scientists and engineers. In 1987 the idea was extended into the construction of neural networks corresponding to the beginning of the era of artificial intelligence, forming what is now called ‘Radial Basis Function Neural Networks (RBFNs)’. Ever since, RBFNs have been developed and applied to a wide variety of problems; approximation, interpolation, classification, prediction, in nowadays science, engineering, and medicine. This also includes numerically solving partial differential equations (PDEs), another essential branch of RBFNs under the name of the ‘Meshfree/Meshless’ method. Amongst many, the so-called ‘Multiquadric (MQ)’ is known as one of the mostly-used forms of RBFs and yet only a couple of its versions have been extensively studied. This study aims to extend the idea toward more general forms of MQ. At the same time, the key factor playing a very crucial role for MQ called ‘shape parameter’ (where selecting a reliable one remains an open problem until now) is also under investigation. The scheme was applied to tackle the problem of function recovery as well as an approximation of its derivatives using six forms of MQ with two choices of the variable shape parameter. The numerical results obtained in this study shall provide useful information on selecting both a suitable form of MQ and a reliable choice of MQ-shape for further applications in general.

Publication status: IOS Press Ebooks: Fuzzy Systems and Data Mining VII Series: Frontiers in Artificial Intelligence and Applications (SCOPUS)

Project-5 :

Title: A modified local distance-weighted (MLD) method of interpolation and its numerical performances for scattered large datasets.

Abstract: The purpose of this study is to propose an interpolation scheme that is designed to remedy shortcomings encountered in two popular interpolation

methods; the triangle-based blending (TBB) and the inverse distance weighed (IDW). At the same time, the proposed method combines their derisible aspects; the local nature and free of quadratic surface construction, making it comparatively less time-consuming and more independent of the global effect. For these properties, it is named as ‘Modified Local Distance-weighted (MLD)’ method and is being tested in detail with different sizes of datasets. Datasets involved in this investigation are both synthetic datasets and real datasets (from some public datasets available) using both uniform and non-uniform node distributions. The performances are being carefully monitored and assessed via several criteria; accuracy, sensitivity to parameters, CPU-time, storage requirement, and ease of implementation. For comparative purposes, three alternative methods are also involved; TBB, IDW, and Radial Basis Function-based (RBF) method. The anticipated outcome is an effective mathematical tool for interpolating data in large scales with acceptable accuracy while requiring less computational efforts. The findings would definitely be useful for a wide range of applications; industry, economy, education, healthcare, environment, and many more.

Publication status: Current Applied Science and Technology Via. the 25th Annual Meeting in Mathematics 2021 (AMM 2021).

Further steps of investigation shall involve more forms of shapefree radial basis functions which will be mentioned in Section 2.4 and larger data sets (both synthetic datasets and real datasets) in scattered manner shall be considered.

1.10 Expected Results

Some insights of performances of some meshfree RBFs are discovered in terms of accuracy, sensitivity to parameters, CPU-time, storage requirement, and ease of implementation. This shall lead to alternative choices for practical applications in many areas; engineering, industry, economy, education, healthcare, environment, and many more.

CHAPTER II

MATHEMATICAL BACKGROUND

2.1 Singular Value Decomposition (SVD)

This is a one of widely technique used to factorization matrix into three matrices that often used to find the rank of matrix. In this work is an important technique used by theorem.

Theorem 2.1 (Singular Value Decomposition) If \mathbf{G} is a real $N \times N$ interpolation

$$\mathbf{G} = \mathbf{U} \mathbf{\Sigma} \mathbf{V}^T \quad (2.1)$$

matrix, then there decompose into the product of three matrices which are:

where \mathbf{U} and \mathbf{V} are an orthogonal $N \times N$ matrices with the property that $\mathbf{U} \mathbf{U}^T = \mathbf{I}$ and $\mathbf{V} \mathbf{V}^T = \mathbf{I}$, and $\mathbf{\Sigma}$ is a diagonal matrix with positive numbers s_1, s_2, \dots, s_N on the diagonal.

Therefore, the orthogonal matrices $\mathbf{U} = \mathbf{u}_1, \mathbf{u}_2, \dots, \mathbf{u}_N \in \mathbb{R}^{N \times N}$ and $\mathbf{V} = \mathbf{v}_1, \mathbf{v}_2, \dots, \mathbf{v}_N \in \mathbb{R}^{N \times N}$ such that $\mathbf{\Sigma} = \text{diag } s_1, s_2, \dots, s_N \in \mathbb{R}^{N \times N}$ where $s_1 \geq s_2 \geq \dots \geq s_N \geq 0$. The s_i are called i -th singular values of matrix \mathbf{G} and the column vectors \mathbf{u}_i and \mathbf{v}_i are called i -th left singular vector and i -th right singular vector, respectively.

The importance of this section to interest in rank of the matrix that the rank of \mathbf{G} is defined as the number of non-zero singular values defined as r by

$$s_1 \geq s_2 \geq \dots \geq s_r > s_{r+1} = \dots = s_N = 0, \quad (2.2)$$

Then

$$\text{rank}(\mathbf{G}) = r, \quad (2.3)$$

And from the rank of matrix which is important to show related matrices to vectors.

2.2 The Pseudoinverse (or Moore-Penrose Inverse) of a Matrix

The pseudoinverse or Moore-Penrose Inverse defined as:

$$\text{pinv } \phi = \phi^T \phi^{-1} \phi^T \quad (2.4)$$

for a system of linear equations $\phi \mathbf{w} = \mathbf{y}$ where ϕ is the interpolation matrix of the basis function where ϕ is an $N \times m$ matrix that can be explained the least squares solution to any system of linear equations.

2.3 Interpolation by RBF-NNs

From radial basis function model is a function which maps input data vectors $\mathbf{x} \in \mathbb{R}^d$ to output values $y \in \mathbb{R}$. Considered, the domain of RBF model \mathbb{R}^d and the range is \mathbb{R} . Additionally, the RBF models was used for interpolation problem. In truth, in the past few years, this model is used in neural networks that are very famous computing systems today. Therefore, the interpolation is carried out according to the structure of the neural networks as follows:

Input Layer: This layer consists the input data $\mathbf{x}_i = x_1, x_2, \dots, x_d \in \mathbb{R}^d$ of matrix \mathbf{X} , i.e.,

$$\mathbf{X} = \mathbf{x}_1 \quad \mathbf{x}_2 \quad \dots \quad \mathbf{x}_N^T \in \mathbb{R}^{N \times d} \quad (2.5)$$

where \mathbf{x}_i are d -dimensional input data vectors, i.e., features of input data and N is the number of input vectors, i.e., size of input data.

Hidden Layer: Suppose that the hidden layer consists of k basis function $\phi_j \cdot j=1, 2, \dots, k$. These functions $\phi_j \mathbf{x} = \phi \|\mathbf{x} - \boldsymbol{\mu}_j\|_2 / \sigma_j$, $j=1, 2, \dots, k$ transform the input data matrix via linear and nonlinear mapping based on the Euclidean distance between the input vector \mathbf{x} and prototype vector $\boldsymbol{\mu}_j$. The $N \times d$ input matrix is transformed by the k basis function into the following $N \times k$ matrix ϕ whose j -th column represents the outputs from the j -th basis function, $j=1, 2, \dots, k$.

$$\phi = \begin{bmatrix} \phi_1 & \dots & \phi_j & \dots & \phi_k \\ \phi_1 \mathbf{x}_1 & \dots & \phi_j \mathbf{x}_1 & \dots & \phi_k \mathbf{x}_1 \\ \phi_1 \mathbf{x}_2 & \dots & \phi_j \mathbf{x}_2 & \dots & \phi_k \mathbf{x}_2 \\ \vdots & \vdots & \vdots & \vdots & \vdots \\ \phi_1 \mathbf{x}_N & \dots & \phi_j \mathbf{x}_N & \dots & \phi_k \mathbf{x}_N \end{bmatrix}_{N \times k} \quad (2.6)$$

For ϕ is the basis function from Section 1.2. As the Gaussian RBF, we have $\phi r = \exp -r^2/2$ so that the expression for the j -th function mapping can be explicitly written as

$$\phi_j \mathbf{x} = \exp\left(-\frac{\|\mathbf{x} - \boldsymbol{\mu}_j\|^2}{2\sigma_j^2}\right), \quad (2.8)$$

where $\boldsymbol{\mu}_j$ is the center and σ_j is the width of the j -th basis function. On substituting for $\phi_j \cdot$ in Equation (2.7), we get the following expression for ϕ .

$$\phi = \begin{bmatrix} \exp\left(-\frac{\|\mathbf{x}_1 - \boldsymbol{\mu}_1\|^2}{2\sigma_1^2}\right) & \dots & \exp\left(-\frac{\|\mathbf{x}_1 - \boldsymbol{\mu}_j\|^2}{2\sigma_j^2}\right) & \dots & \exp\left(-\frac{\|\mathbf{x}_1 - \boldsymbol{\mu}_k\|^2}{2\sigma_k^2}\right) \\ \exp\left(-\frac{\|\mathbf{x}_2 - \boldsymbol{\mu}_1\|^2}{2\sigma_1^2}\right) & \dots & \exp\left(-\frac{\|\mathbf{x}_2 - \boldsymbol{\mu}_j\|^2}{2\sigma_j^2}\right) & \dots & \exp\left(-\frac{\|\mathbf{x}_2 - \boldsymbol{\mu}_k\|^2}{2\sigma_k^2}\right) \\ \vdots & \vdots & \vdots & \vdots & \vdots \\ \exp\left(-\frac{\|\mathbf{x}_n - \boldsymbol{\mu}_1\|^2}{2\sigma_1^2}\right) & \dots & \exp\left(-\frac{\|\mathbf{x}_n - \boldsymbol{\mu}_j\|^2}{2\sigma_j^2}\right) & \dots & \exp\left(-\frac{\|\mathbf{x}_n - \boldsymbol{\mu}_k\|^2}{2\sigma_k^2}\right) \end{bmatrix} \quad (2.9)$$

Output Layer: From mapping of the input data was produced by k basis function in the hidden layer. Imports in this matrix are combined linearly according to weights w_1, w_2, \dots, w_k associated with the k basis functions $\phi_1 \cdot, \phi_2 \cdot, \dots, \phi_k \cdot$, respectively. The output values are given by

$$f \mathbf{x} = \sum_{j=1}^k w_j \phi_j \mathbf{x} \quad (2.10)$$

where $f \mathbf{x}$ represents the RBF output for input vector \mathbf{x} . Therefore, the output layer of the N input vectors $\mathbf{x}_1, \mathbf{x}_2, \dots, \mathbf{x}_N^T$ are generated by estimated output vector $\hat{\mathbf{y}}$ that corresponding with

$$\hat{\mathbf{y}} = \hat{y}_1, \hat{y}_2, \dots, \hat{y}_N^T = f \mathbf{x}_1, f \mathbf{x}_2, \dots, f \mathbf{x}_N^T \quad (2.11)$$

2.4 Shapeless Parameter of Radial Basis Function

As in the previous, the most popular of the RBFs containing shape parameters, which caused the selection problem and have an effect on the accuracy of the model is not good accuracy or not comparable to other methods.

Following the compactly supported radial basis function, the first introduction of this type by Wendland's CS-RBFs (Wendland, 1995). The usual basis function still some problems exist, caused by a large number of centres N That has an effect on methods

of computation and evaluation which was developed to remedy this defect. These problems could be avoided if the radial basis function is compactly supported. If the radial basis function has compact support the interpolation matrices are sparse and for evaluation of the interpolants, only few terms have to be considered. Wendland's CS-RBFs are listed in the Table 2.1.

Table 1.1 The popular Wendland's CS-RBFs.

RBFs	$\phi(r)$
Wendland's	$1 - r_+^3$
	$1 - r_+^3 (3r + 1)$
	$1 - r_+^5 (8r^2 + 5r + 1)$
	$1 - r_+^2$
	$1 - r_+^4 (4r + 1)$
	$1 - r_+^6 (35r^2 + 18r + 3)$
	$1 - r_+^8 (32r^3 + 25r^2 + 8r + 1)$

Note that the cut-off function, r_+ is defined to be r if $0 < r < 1$ and to be zero elsewhere.

Wu considered interpolation matrices generally to have large matrices. Therefore, to improve importantly if the radial basis function of compact support is implemented, Wu provided a criterion that produces a series of compactly supported radial basis functions (Wu, 1995). Wu employs convolution to construct another kind of CS-RBFs as shown in Table 2.2. Wu's function can be derived by the following formula

$$\phi_{k,s} = D^k \phi_s, \quad d \leq 2k + 1, \quad (2.1)$$

where d is the dimension of input space, \mathbb{R}^d and the differential operator D is defined as

$$D_\varphi r = -\phi' r / r, r \geq 0. \quad (2.2)$$

Table 2.2 The popular Wu's CS-RBFs.

RBFs	ϕ_r
Wu	$1 - r + \frac{7}{5}r^6 + 35r^5 + 101r^4 + 147r^3 + 101r^2 + 35r + 5$ $1 - r + \frac{6}{6}r^5 + 30r^4 + 72r^3 + 82r^2 + 36r + 6$ $1 - r + \frac{5}{5}r^4 + 25r^3 + 48r^2 + 40r + 8$ $1 - r + \frac{4}{5}r^3 + 20r^2 + 29r + 16$

Another class of CS-RBFs constructed by Buhmann (Buhmann, 1998) is reminiscent of the popular thin plate splines. Buhmann was interested in studying approximation spaces generated by a novel type of compactly supported radial basis functions as opposed to most previously reviewed globally supported functions. Buhmann has appreciated the advantage of compact support for radial function methods that the linear systems resulting from interpolation from these spaces are easy to solve and on the other hand, that the resulting interpolants can be evaluated very fast. The popular of these CS-RBFs are given in Table 2.3.

Table 2.3 The popular Buhmann's CS-RBFs.

RBFs	ϕ_r
Buhmann	$\left(2r^4 \log r - \frac{7r^4}{2} + \frac{16r^3}{3} - 2r^2 + \frac{1}{6} \right)_+, x \in \mathbb{R}^3$ $\left(\frac{112r^{\frac{9}{2}}}{45} + \frac{16r^{\frac{7}{2}}}{3} - 7r^4 - \frac{14r^2}{15} + \frac{1}{9} \right)_+, x \in \mathbb{R}^2$ $\left(\frac{1}{18} - r^2 + \frac{4r^3}{9} + \frac{r^4}{2} - \frac{4r^3 \log r}{3} \right)_+, x \in \mathbb{R}^2$

2.5 The Representational Capability (RC)

A matrix consists of a set of column vectors and spans a subspace based on these column vectors. Particularly, if a matrix $\mathbf{G} \in \mathbb{R}^{l \times k}$ and its column partitioning is $\mathbf{g}_1 \mathbf{g}_2 \dots \mathbf{g}_k$ then this matrix spans a subspace based on its k vectors in an l dimensional space. For our focus to the matrix $\mathbf{G} \in \mathbb{R}^{N \times N}$, we recall that \mathbf{G} has N columns which are $\mathbf{g}_1 \mathbf{g}_2 \dots \mathbf{g}_N$ and \mathbf{G} spans a subspace of \mathbb{R}^N . Also, the dimensionality of this subspace is equal to the rank of \mathbf{G} . Therefore, the minimum

number of column vectors for representing an interpolation matrix equals its rank. Now we introduce a matrix which we recall *Representational Capability (RC)*.

Definition 2.1 (Representational Capability of \mathbf{G}_m)

Let \mathbf{G} be an $N \times N$ interpolation matrix and the SVD of \mathbf{G}_m be given by Theorem 2.1. If $m \leq N$ and \mathbf{G}_m is

$$\mathbf{G}_m = \sum_{i=1}^m s_i \mathbf{u}_i \mathbf{v}_i^T \quad (2.3)$$

Then RC of \mathbf{G}_m is defined as

$$RC \mathbf{G}_m = 1 - \frac{\|\mathbf{G} - \mathbf{G}_m\|_2}{\|\mathbf{G}\|_2} \quad (2.4)$$

From Corollary 2.2 (Shin, 1998) defined equation (2.14) for $m < N$ as

$$RC \mathbf{G}_m = 1 - \frac{s_{m+1}}{s_m} \quad (2.5)$$

To determination of the number of centres is typically less than the number of input vectors and set centers which provide the best representation of the input space. Note that the interpolation matrix based on N -centres has overfitting problem. Then, the reduction of interpolation based on a number of centres as m with $m \leq N$ and m should not be so small because of leads to under fitting problem.

Since rank of matrix reveals important information about structure of an interpolation matrix. In addition, association of RC-Algorithm with interpolation matrix is its rank which is assumed to be a specific number.

2.6 Additive White Gaussian Noise (AWGN)

The model of noise is the simple and powerful model as Additive White Gaussian Noise (AWGN) from the name have meaning itself:

Additive means the sum of two components which are input term x_k , output term y_k and noise term w_k at the k – th position. We can write

$$y_k = x_k + w_k$$

White from a property of the frequency of the spectra in the signal in which white has a frequency of light that is stabilized by the arrangement. Therefore, the white symbol is taken to represent the constant frequency or in other words is zero-mean.

Gaussian from the noise term w_k is random by a Gaussian random variable. The reason Gaussian distribution is suitable because interference results from a combination of different and independent random variables. Therefore, it is considered a good estimation. Since output term y_k have a noise term w_k obtained from *probability density function* especially at Gaussian distribution:

$$F_w = \frac{1}{\sqrt{2\pi\sigma^2}} e^{-\frac{w-\mu^2}{2\sigma^2}} \quad (2.6)$$

This equation is dependent on mean μ and variance σ^2 . From zero-mean Gaussian noise and the standard deviation may be seen as an expected measurement tool for the amplitude of the noise, which it associates with the power of noise.

From the AWGN is usually use in signal then the power of noise is importance. Such the power of noise dependent with signal to noise ratio (*SNR*). Defined as

$$SNR_w = \frac{\text{input}}{\text{noise}} \quad (2.7)$$

where *input* is input term x_k and *noise* is noise term w_k , this easier to understand *SNR* is inversely proportional to noise.

CHAPTER III

COMPUTATIONAL COMPONENTS

3.1 The Main Algorithm

RC algorithm as proposed by Shin and Park (2000) (Shin and Park, 2000) is a method to drag out information of interpolation matrix when RBF is in use. For given input data $\{\mathbf{x}_i, y_i\}_{i=1}^N$, the algorithm contains the following steps.

Step 1: Select a value to control the receptive field width of the basis function (or the shape parameter) (ε) and effect of noise (δ) which δ is usually taken to be 0.1% to 1.0% and construct the interpolation matrix \mathbf{G} . For example, if Gaussian basis function is used, so that

$$\mathbf{G} = \begin{bmatrix} g_{11} & g_{12} & \cdots & g_{1N} \\ g_{21} & g_{22} & \cdots & g_{2N} \\ \vdots & \vdots & \ddots & \vdots \\ g_{N1} & g_{N2} & \cdots & g_{NN} \end{bmatrix} \quad (3.1)$$

where $g_{ij} = \exp\left(-\|\mathbf{x}_i - \mathbf{x}_j\|^2 / 2\varepsilon^2\right)$ for $i, j = 1, 2, \dots, N$.

Step 2: Determine the number of centres (m) by applying singular value decomposition of the interpolation matrix \mathbf{G} . This yields a diagonal matrix of singular values $s_1 \geq s_2 \geq \cdots \geq s_N \geq 0$. From these, m can be determined from the following:

$$m = \max_{0 \leq i \leq N} \left\{ i \mid s_{i+1} \leq s_1 \times \frac{\delta}{100} \right\}. \quad (3.2)$$

Step 3: Determine the centres of basis function ($\boldsymbol{\mu}$). Partition matrix \mathbf{V} from singular value decomposition of the interpolation matrix \mathbf{G} as:

$$\mathbf{V} = \begin{bmatrix} v_{11} & v_{12} & \cdots & m \\ v_{21} & v_{22} & \cdots & N-m \\ m & N-m & \cdots & \end{bmatrix} \quad (3.3)$$

Next, generate matrix $V' = [v_{11}^T \ v_{21}^T]$ and apply QR factorization with column pivoting of matrix V' . And then compute $X^T P$ and choose the first m elements in $X^T P$ be the centres of basis function which are:

$$\boldsymbol{\mu} = \{\mu_j\}_{j=1}^m. \quad (3.4)$$

Step 4: Compute the weight parameters from the basis function (w). Consider,

$$\phi = \begin{bmatrix} \phi_{11} & \phi_{12} & \cdots & \phi_{1m} \\ \phi_{21} & \phi_{22} & \cdots & \phi_{2m} \\ \vdots & \vdots & \ddots & \vdots \\ \phi_{N1} & \phi_{N2} & \cdots & \phi_{Nm} \end{bmatrix} \quad (3.5)$$

For $i=1,2,\dots,N$ and $j=1,2,\dots,m$. Compute the m weights with

$$w = \phi^+ y \quad (3.6)$$

where ϕ^+ denoted the pseudo inverse of ϕ .

3.2 Node Distribution Manner

For data-partitioning process, suggestion provided by Damiana Lazzaro and Laura B. Montefusco (2002) (Lazzaro and Montefusco, 2002) is followed here with the information described as follows.

3.2.1 The Training Datasets

Two datasets with the size of 50×50 nodes are generated within a $[0,1] \times [0,1]$ domain; uniformly and randomly, shown in Figure 3.1 and Figure 3.2, respectively. These sets of data are to be used as 'Training Dataset' for all numerical experiments in this study.

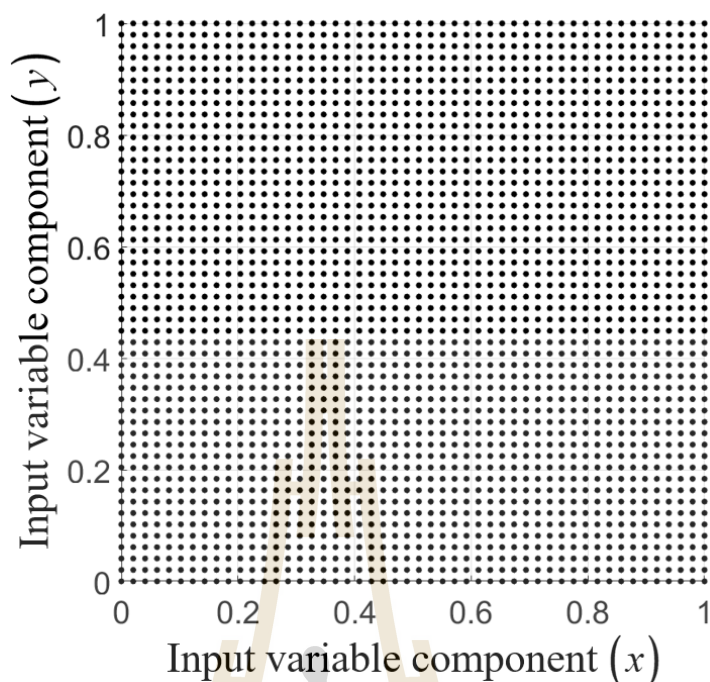


Figure 3.1 (x, y) –Node uniformly distribution manner for training datasets using 50x50 nodes.

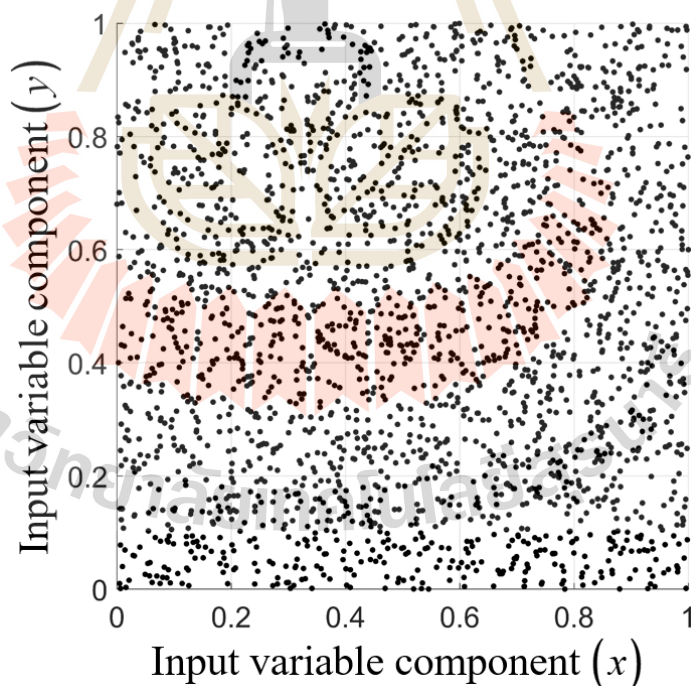


Figure 3.2 (x, y) –Node non-uniformly distribution manner for training datasets using 50x50 nodes.

3.2.2 The Testing Datasets

To monitor and record the effectiveness of each RBF type, three large datasets are generated within the same domain as the training ones in both manners; uniformly (Ufm.) and randomly (Rdm.), and they contain 10000, 20164 and 30276 nodes (Lazzaro and Montefusco, 2002).

3.3 Performance Criteria

As previously mentioned, all fifteen shapeless RBFs are comparatively investigated. Therefore, proper and all-around effectiveness criteria are required and they are listed below.

- *Accuracy*: This process is carried out using the following three error norms;

Table 3.1 Error Norms adopted in this work.

Error Norm	Symbol Defined	Mathematical Formula
Maximum	L_{∞}	$\max_{1 \leq i \leq N} u^{ext.}(\mathbf{x}_i) - u^{appx.}(\mathbf{x}_i) $
Root-Mean-Square	L_{RMS}	$\left(\frac{1}{N} \sum_{j=1}^N (u^{ext.}(\mathbf{x}_i) - u^{appx.}(\mathbf{x}_i))^2 \right)^{1/2}$
Absolute	L_{Abs}	$ u^{ext.}(\mathbf{x}_i) - u^{appx.}(\mathbf{x}_i) $

- *Condition number*: The system can be solvable if the collocation matrix, $\boldsymbol{\Phi}$, has an inverse and this can be indicated by the means of its condition number ($Cond_{\delta}(\cdot)$) expressed as;

$$Cond_{\delta}(\boldsymbol{\Phi}) = \|\boldsymbol{\Phi}\|_{\delta} \|\boldsymbol{\Phi}^{-1}\|_{\delta}. \quad (3.7)$$

The trending behaviour of this number is also recorded throughout this experiment, providing information on the solvability, (Lazzaro and Montefusco, 2002), of the collocation matrix for future uses.

- *CPU-time*: With less amount of time required for the computational process, a method would be more desirable. The ‘tic-toc’ command in MATLAB is employed for this task.

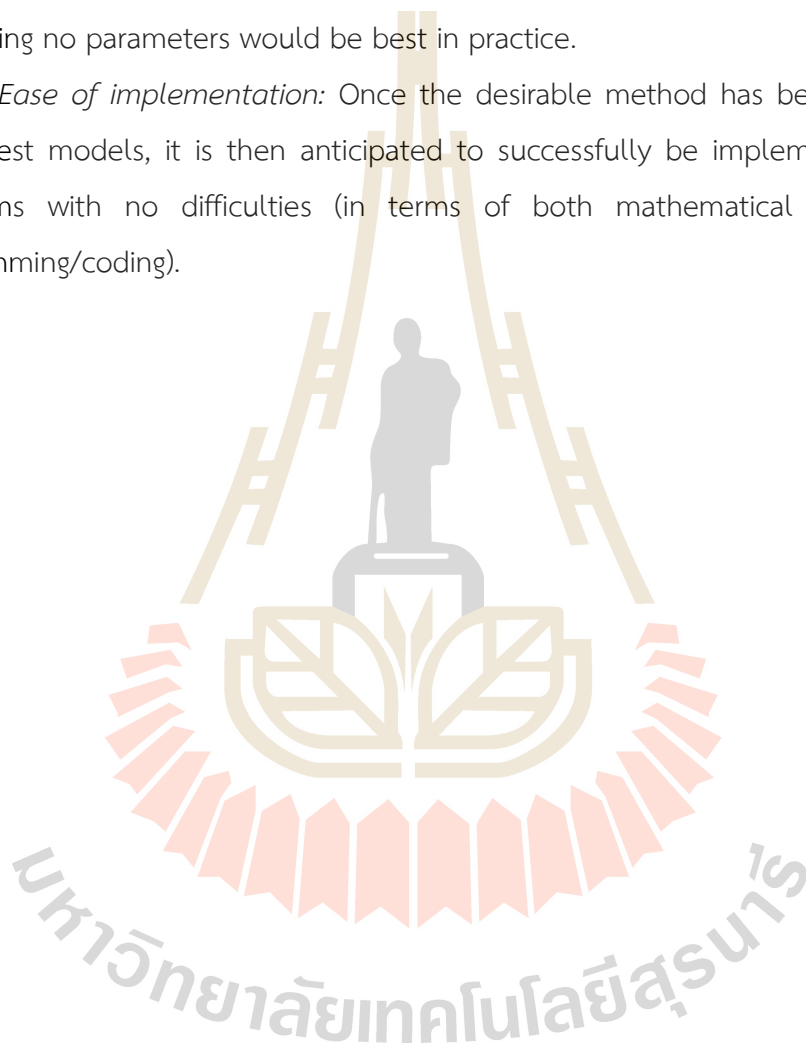
- *Storage requirement*: Each computation step involved in the algorithm should ideally take as least amount of storage space as possible. For the sake of fairness, all experiments are carried out on the same computer; Intel(R) Core(TM) i7-1065G7 CPU

@ 1.30GHz 1.50 GHz with RAM 16.00 GB and 64-bit Operating System.

- *User's Interference*: A good algorithm should be able to process entirely by itself, no human interruption or judgments should be involved. This is all for future practical uses.

- *Sensitivity to parameters*: A small change in parameters embedded in the process should have as little effect as possible on the overall performance. Methods containing no parameters would be best in practice.

- *Ease of implementation*: Once the desirable method has been proven with small test models, it is then anticipated to successfully be implemented to larger problems with no difficulties (in terms of both mathematical structures and programming/coding).



CHAPTER IV

PRELIMINARY EXPERIMENTS

4.1 Experiment 1: A Numerical Study of a Compactly-Supported Radial Basis Function Applied with a Collocation Meshfree Scheme for Solving PDEs

4.1.1 The Project Objective

The main focus is on one type of RBF, 'Compactly-Supported (CS-RBF)', which contains no parameter and has not been explored numerically as much in the past, particularly under the context of data interpolation/approximation and solving partial differential equations (PDEs). To compare the potential advantages of CS-RBF, the two most popular choices of RBF widely used; Multiquadric (MQ), and Gaussian (GA) were studied parallelly.

4.1.2 Globally-Supported RBFs

For the method of collocation meshfree, there are several forms of well-known radial basis function and some are listed below, (Kaennakham and Chuathong, 2017);

- Gaussian (GS), defined as;

$$\phi(r) = e^{-\varepsilon r^2}$$

- Inverse Multiquadric (IMQ), defined as;

$$\phi(r) = 1/\sqrt{1 + \varepsilon r^2}$$

- Multiquadric (MQ), defined as;

$$\phi(r) = \sqrt{1 + \varepsilon r^2}$$

- Inverse quadratic (IQ), defined as;

$$\phi(r) = 1/1 + \varepsilon r^2$$

Here, ε is called shape parameter, determined by the user and this exactly remains the open topic for researchers to investigate the possible optimal choice. A lot of attempts have been made to alleviate this problem but by far no universal

choice has been found (Hardy, 1977; Franke, 1979; Carlson and Foley, 1991). The attempt to get rid of this burden by turning attention away from these groups of RBFs to those containing no parameter is now being made.

4.1.3 Compactly-Supported RBFs

For this purpose, this work focusses on a compactly-supported form of RBF proposed by Buhmann (Buhmann, 1998) and the effectiveness one can obtained when applied this type of RBF with the collocation-based method.

- Noted as CS1 and defined as;

$$\phi(r) = 119r^{9/2}/45 + 16r^{7/2}/3 - 7r^4 - 14r^2/15 + 1/9 \quad +$$

- Noted as CS2 and defined as;

$$\phi(r) = -4r^3 \log(r)/3 + r^4/2 + 4r^3/9 - r^2 + 1/18 \quad +$$

- Noted as CS3 and defined as;

$$\phi(r) = 2r^4 \log(r) - 7r^4/2 + 16r^3/3 - 2r^2 + 1/6 \quad +$$

when + indicates the cut-off function which is defined to be r , when $0 \leq r \leq 1$ and zero elsewhere.

4.1.4 Test Case 1: Interpolation Problem

The interpolation problem starts with a set of discrete data $\mathbf{X} = \{\mathbf{x}_i\}_{i=1}^N$, $\mathbf{x}_i \in \mathbb{R}^d$ where for each \mathbf{x}_i there is its corresponding real value $y_i \in \mathbb{R}$, then the task is to construct a continuous function $\phi(\mathbf{x}): \mathbb{R}^d \rightarrow \mathbb{R}$ such that;

$$\phi(\mathbf{x}_i) = y_i. \quad (4.1)$$

For all $i=1,2,\dots,N$. The first validation of the scheme proposed in this work is done using a benchmark function defined on a square-domain, $[0,4\pi] \times [0,4\pi]$, as follows:

$$f(x, y) = \sin(x)\cos(y). \quad (4.2)$$

As regarded as one of the most influential factors, the shape parameter is firstly investigated. For this purpose simulations using the Multiquadric (MQ) and Gaussian (GA) were under the investigation. Figure 4.1 and Figure 4.2 clearly show the strong effects the shape parameter has for both RBFs. When using different numbers of nodes, it also can be seen that the errors norms can be affected as well.

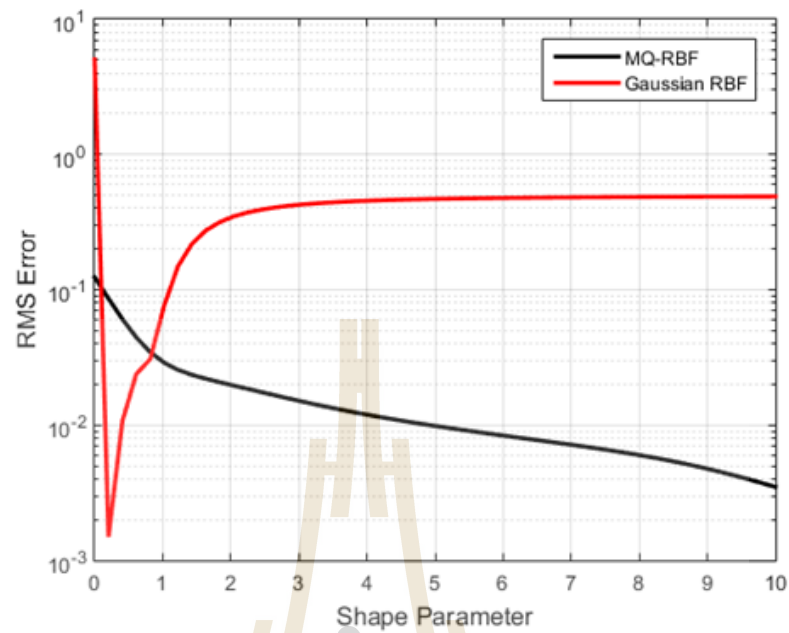


Figure 4.1 L_{RMS} measured at different values of shape parameters with 10×10 interpolation nodes/centres.

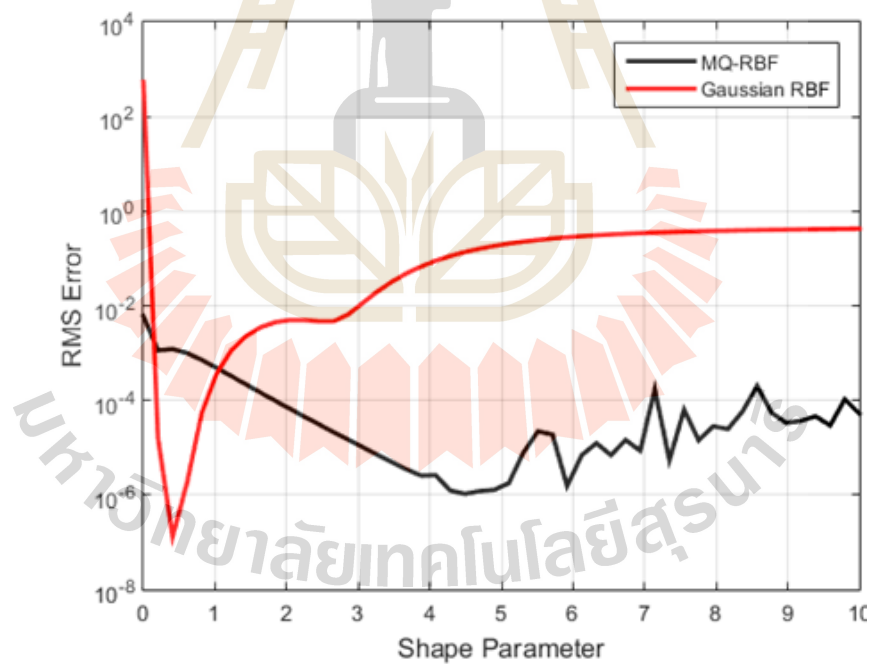


Figure 4.2 L_{RMS} measured at different values of shape parameters with 30×30 interpolation nodes/centres.

At the node density of 15×15 , Table 4.1 provides the absolute errors measured at different locations all over the domain. The information contained in this table shows significant accuracy obtained from all types of RBFs. Nevertheless, for MQ and GA, a caution has been previously taken on fining the optimal shape values and they were found to be in (4,6.5) for MQ, (0.1-0.8) and for GA. It must be noted that no extra treatment was needed for the cases of using compactly-supported RBFs. Solutions produced by all the cases were plotted against one another as shown in Figure 4.3 and Figure 4.4.



Table 4.1 L_{Abs} measured at different locations over the computational domain with 15×15 interpolation nodes/centres.

x	y	MQ ($\varepsilon = 5.00$)	GA ($\varepsilon = 0.50$)	CS1	CS2	CS3
0.000	0.000	8.59E-10	1.57E-12	1.46E-11	3.55E-11	1.46E-11
0.000	1.396	1.87E-06	2.73E-12	4.17E-04	1.09E-02	5.42E-04
0.000	12.566	1.32E-09	3.64E-13	5.46E-11	7.84E-12	6.37E-12
1.396	0.000	7.06E-06	1.60E-05	6.66E-04	7.37E-05	3.86E-03
2.793	0.000	2.56E-06	5.86E-06	3.49E-04	1.41E-03	1.07E-02
2.793	1.396	7.73E-06	1.13E-05	8.23E-04	5.66E-03	9.36E-04
2.793	12.566	2.55E-06	5.86E-06	3.49E-04	1.41E-03	1.07E-02
4.189	0.000	1.12E-06	2.43E-06	5.30E-04	1.21E-02	1.55E-02
4.189	12.566	1.12E-06	2.43E-06	5.30E-04	1.21E-02	1.55E-02
5.585	12.566	3.32E-07	6.88E-07	3.51E-04	6.51E-03	1.64E-02
6.981	0.000	3.32E-07	6.88E-07	3.51E-04	6.51E-03	1.64E-02
6.981	12.566	3.32E-07	6.88E-07	3.51E-04	6.51E-03	1.64E-02
8.378	0.000	1.12E-06	2.43E-06	5.30E-04	1.21E-02	1.55E-02
8.378	12.566	1.12E-06	2.43E-06	5.30E-04	1.21E-02	1.55E-02
9.774	0.000	2.55E-06	5.86E-06	3.49E-04	1.41E-03	1.07E-02
9.774	11.170	7.73E-06	1.13E-05	8.23E-04	5.66E-03	9.36E-04
9.774	12.566	2.56E-06	5.86E-06	3.49E-04	1.41E-03	1.07E-02
11.170	0.000	7.07E-06	1.60E-05	6.66E-04	7.37E-05	3.86E-03
11.170	12.566	7.06E-06	1.60E-05	6.66E-04	7.37E-05	3.86E-03
12.566	0.000	1.09E-09	3.76E-13	1.20E-10	6.24E-11	2.64E-11
12.566	12.566	2.26E-09	9.46E-13	5.91E-13	5.34E-11	4.06E-11

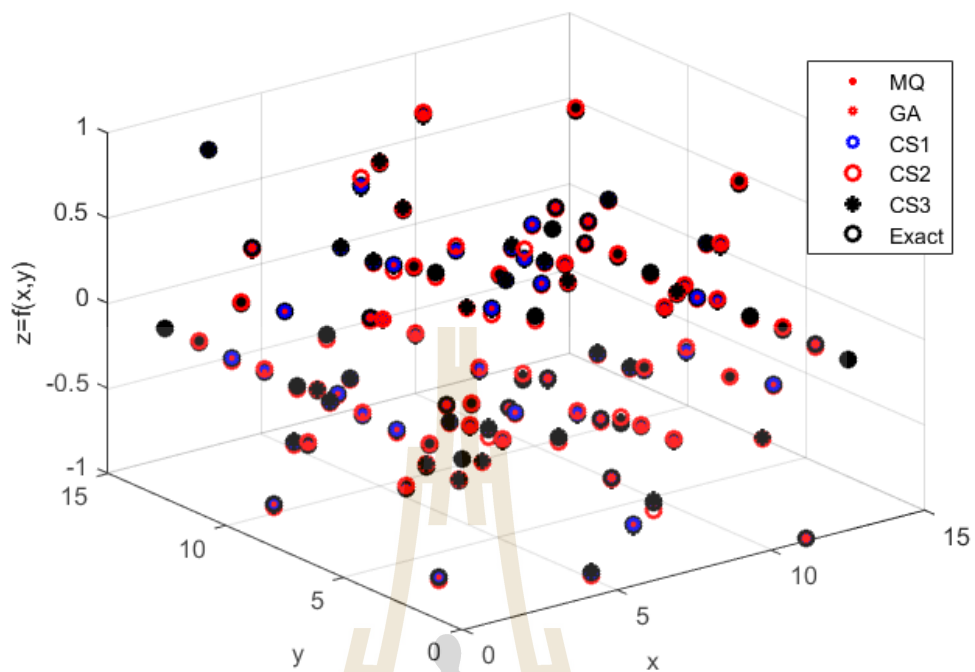


Figure 4.3 Solution approximation at selected locations obtained from each RBF type, compared to against the exact solution.

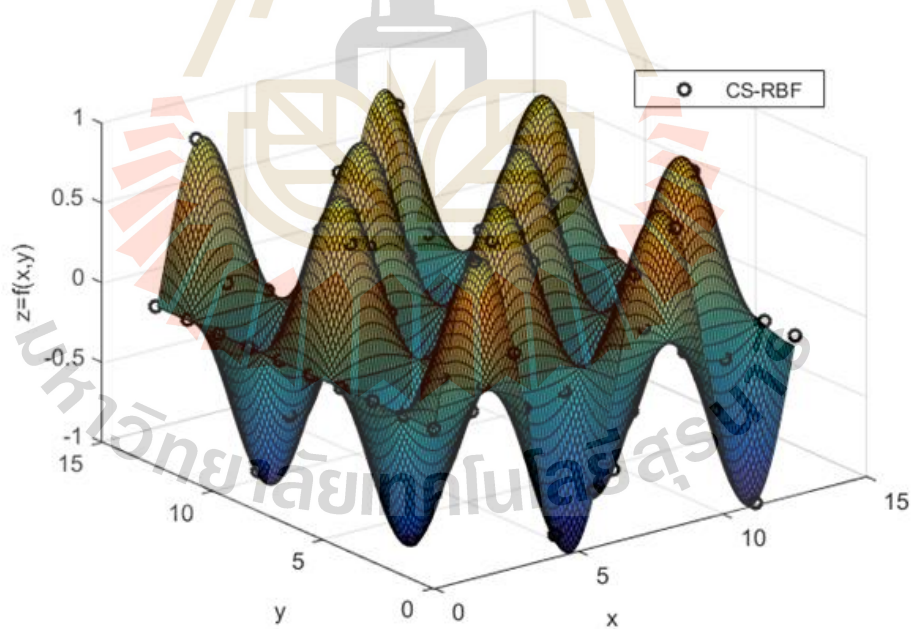


Figure 4.4 Solution profile comparison between that produced by CS1-RBF and that of the exact one.

4.1.5 Test Case 2: Poisson Problem with Non-rectangular domain

In this second test case, the Poisson equation shown below is numerically solved by the collocation meshfree method.

$$\nabla^2 u = \left(\frac{\partial^2}{\partial x^2} + \frac{\partial^2}{\partial y^2} \right) u = -x^2.$$

This is defined on the domain with an elliptical boundary expressed as $(x^2/4) + y^2 = 1$. Where the boundary condition is taken directly from the exact solution which is expressed as follows;

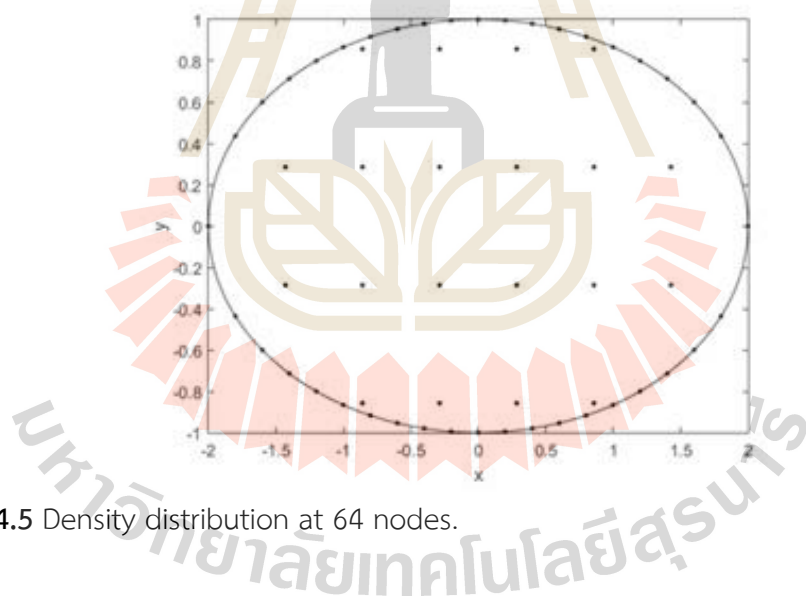
$$u(x, y) = -\frac{1}{246} (50x^2 - 8y^2 + 33.6) \left(\frac{x^4}{4} + y^2 - 1 \right). \quad (4.3)$$

Based on the promising results obtained from the previous example, only CS1 is now presented here and it is marked as 'CS' from hereon.

For this example, L_{∞} and L_{RMS} were utilized to measure the accuracy at different node density of 64, 144, 225, and 400. Table 4.2 clearly shows that the accuracy obtained from using MQ and GA is greatly influenced by the number of nodes involved in the system. This figure is more obvious when using 225 nodes with GA-RBF where a strong fluctuation of L_{RMS} occurs. This is not, however, the case when using CS where the solutions were found to remain almost intact with the change of node density. Figure 4.5, Figure 4.6, and Figure 4.7 depicts the node distributions and the corresponding solution profile. It should also be remarked here that the optimal values of shape parameters shown in the Table 4.2 were obtained from a series of simulations taking place beforehand.

Table 4.2 Errors produced by each RBF when using different levels of nodes density.

Number of Computational Nodes	Error Norms	MQ ($\varepsilon = 0.1$)	GA ($\varepsilon = 0.1$)	CS
64	L_{∞}	8.6331e-04	9.4614e-04	0.0157
	L_{RMS}	3.8422e-04	3.5081e-04	0.0063
144	L_{∞}	5.7818e-04	0.0036	0.0077
	L_{RMS}	2.0858e-04	0.0014	0.0039
225	L_{∞}	0.0057	0.0028	0.0048
	L_{RMS}	0.0024	9.4496e-04	0.0027
400	L_{∞}	0.0034	0.0039	0.0032
	L_{RMS}	0.0012	0.0014	0.0015

**Figure 4.5** Density distribution at 64 nodes.

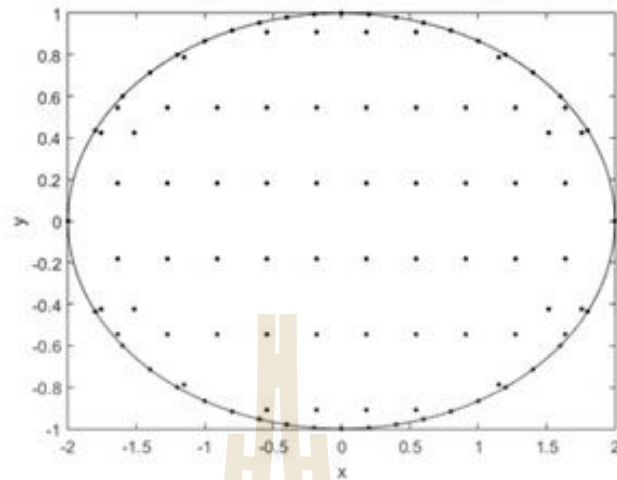


Figure 4.6 Density distribution at 144 nodes.

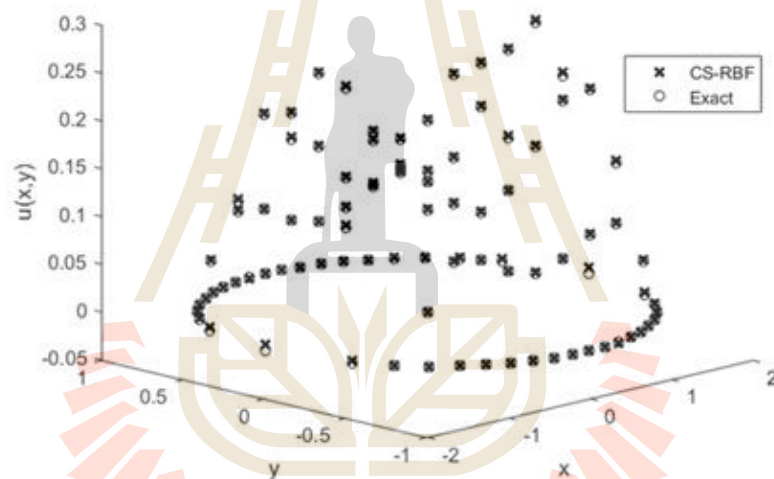


Figure 4.7 Node solution comparison between that of CS-RBF and the exact one.

4.1.6 Test Case 3: Nonlinear Problem

The nonlinear PDE as given in GE. Fasshauer⁵ on a square domain $0 < x < 1$, $0 < y < 1$ is taken a look at. The governing equation is as follows;

$$-\varepsilon^2 \nabla^2 u - u + u^3 = f \quad (4.4)$$

with the boundary condition $u = 0$ on $\partial\Omega$ and the right-hand side of the equation is chosen from the analytical solution of form;

$$u(x, y) = \psi(x)\psi(y) \quad (4.5)$$

with $\psi(t) = 1 + e^{-t/\varepsilon} - e^{-t/\varepsilon} - e^{(t-1)/\varepsilon}$, and (x, y) denotes the Cartesian coordinate of $\mathbf{x} \in \mathbb{R}^2$.

The computational domain for this example is shown in Figure 4.8 where

some extra nodes are required for the computing algorithm for nonlinear case. Table 4.3 provide strong evidence confirming that the solution quality produced by CS can be as good as those obtained from the two popular choices of RBFs. Solution profiles are plotted against the exact ones and shown in Figure 4.9, Figure 4.10 and Figure 4.11.

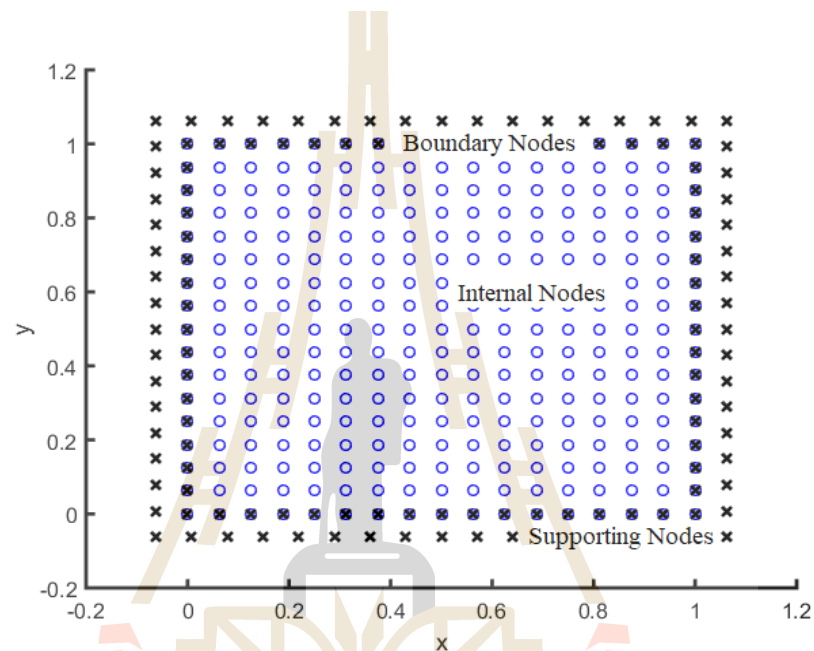


Figure 4.8 Node being uniformly-distributed over the computational domain, together with supported nodes needed for nonlinear computing process.

Table 4.3 Numerical solutions comparison with the exacts.

Points	MQ	GA	CS	Exact
(0.2,0.2)	0.750708	0.751436	0.753032	0.747144
(0.2,0.4)	0.848307	0.849172	0.849450	0.846440
(0.2,0.6)	0.848307	0.849172	0.849450	0.846440
(0.4,0.2)	0.848307	0.849172	0.849450	0.846440
(0.4,0.4)	0.959267	0.960383	0.959399	0.958933
(0.4,0.6)	0.959267	0.960383	0.959399	0.958933
(0.6,0.2)	0.848307	0.849172	0.849450	0.846440
(0.6,0.4)	0.959267	0.960383	0.959399	0.958933
(0.6,0.6)	0.959267	0.960383	0.959399	0.958933
(0.6,0.8)	0.848307	0.849172	0.849450	0.846440
(0.8,0.2)	0.750708	0.751436	0.753032	0.747144
(0.8,0.4)	0.848307	0.849172	0.849450	0.846440
(0.8,0.6)	0.750708	0.751436	0.753032	0.846440

(0.8,0.8)	0.750708	0.751436	0.753032	0.747144
-----------	----------	----------	----------	----------

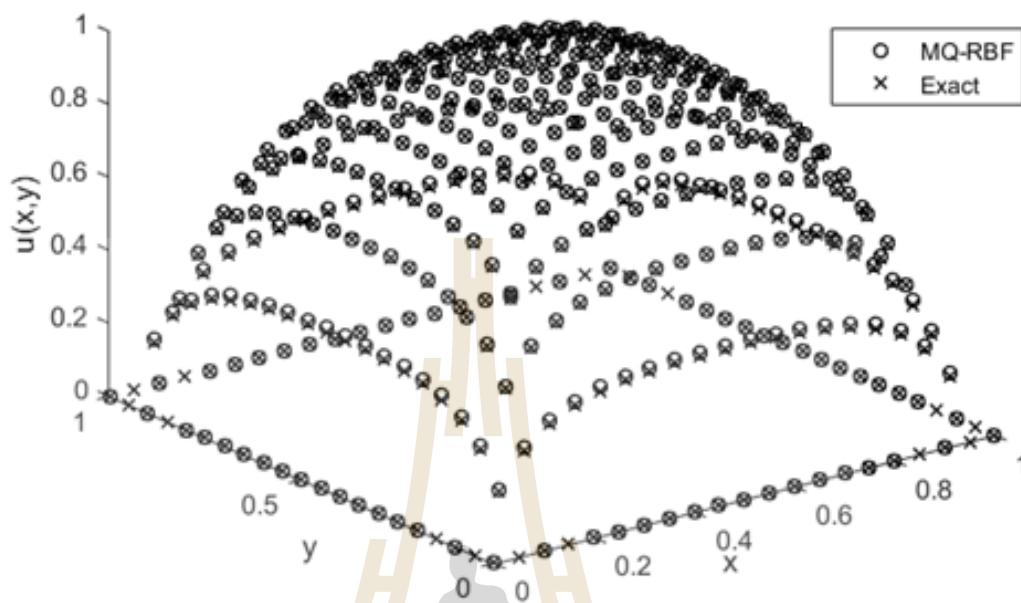


Figure 4.9 Solution comparisons by using MQ-RBF.

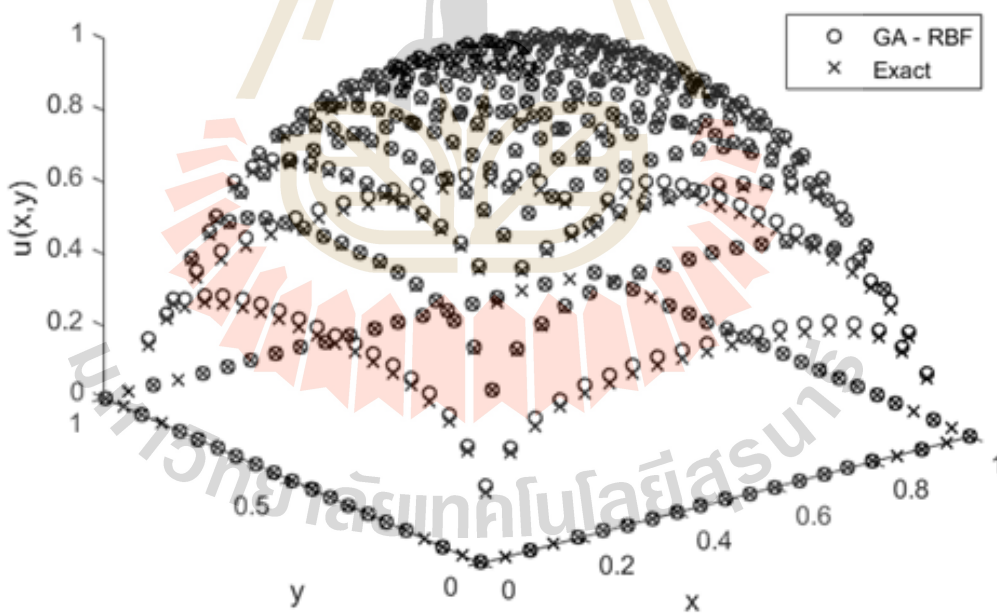


Figure 4.10 Solution comparisons by using GA-RBF.

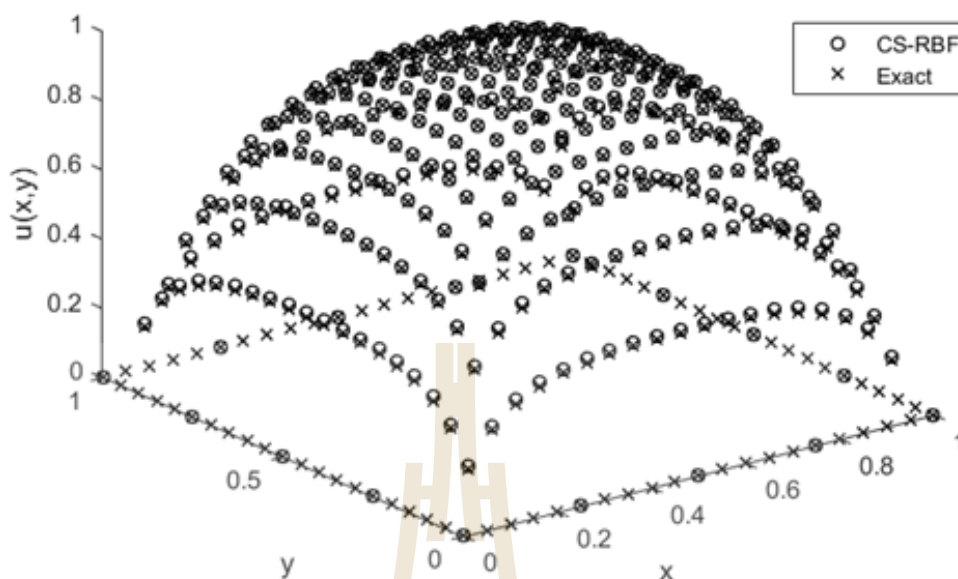


Figure 4.11 Solution comparisons by using CS-RBF.

4.1.7 Main Conclusion

The main objective is to numerically study the effectiveness of one type of radial basis functions that has not been explored as much and it is called ‘compact-supported, CS-RBF’. This is done under the context of a numerical method that requires no mesh or grid so it is called ‘meshfree/meshless’ with collocation on computational nodes. The CS-RBF is applied to several benchmark test cases and its potential uses have been monitored. The main findings obtained from all the experiments are as follows;

1. When compared to the use of two popular RBFs; Multiquadric (MQ) and Gaussian (GA), the burden of finding an optimal shape parameter normally encountered in MQ and GA is completely omitted while the solutions produced are still in a good agreement.

2. The numerical solutions are found to be significantly affected by the distance between centres in the domain. This is not the case for all the shape-parameter-based RBFs such as MQ and GA.

3. The mathematical structure of CS-RBF is much less complex and much simpler when it comes to finding its first and second order of derivatives for solving PDEs.

This all indicates its promising future for further applications in more complex problems and it remains as our future investigation.

4.2 Experiment 2: Performances of Non-Parameterised Radial Basis Functions in Pattern Recognition Applications

4.2.1 The Project Objective

This study focuses on RBFs which contain no parameters where three data patterns (Linear interpolation, Parabola function and Sine interpolation) are used for performance validation and comparison with the popular radial basis function which are Gaussian RBF that contains the large problem is finding the optimal shape parameter. Additionally, by studying the RBF by using RC-Algorithm for interpolation for Pattern Recognition problem and studying the behavior of the numbers of centres with a good choice of the number of centres, it is clearly possible to obtain satisfactory results with no burden on choosing the suitable or optimal shape.

4.2.2 The Non-Parameterised Radial Basis Functions

With the non-straight forward way to pinpoint the optimal choice for Gaussian RBF uses, the main attention has now turned to alternative forms of RBF. In this work, it focuses on non-parameter form of radial basis functions and with this purpose, those proposed by Buhmann are to be explored and they are;

- Noted as ‘CS-RBF1’ and defined as: $\phi(r) = \frac{1}{3} + r^2 - \frac{4}{3}r^3 + 2r^2 \log(r)$.
- Noted as ‘CS1’ and defined as: $\phi(r) = \frac{112}{45}r^{\frac{9}{2}} + \frac{16}{3}r^{\frac{7}{2}} - 7r^4 - \frac{14}{15}r^2 + \frac{1}{9}$.
- Noted as ‘CS2’ and defined as: $\phi(r) = \frac{1}{18} - r^2 + \frac{4}{9}r^3 + \frac{1}{2}r^4 - \frac{4}{3}r^3 \log(r)$.

What appears to be interesting about these forms is that they do not depend on any user’s input information making it more convenient when in use.

4.2.3 Test Case 1: Linear interpolation

In this section, a linear case is studied and the simple line expressed as followed is considered:

$$y = 2x + 1 \quad (4.6)$$

The total number of 100 data points from above function with x in $[0, 2\pi]$ are generated. The data points are generated by $x_i = 2\pi\left(\frac{i-1}{100}\right), i=1, 2, \dots, 100$ with node distribution are shown in Table 4.4 and its plot are in Figure 4.12.

Table 4.4 The locations over the computational domain with 100 points for linear trend case.

i	x_i	y_i	i	x_i	y_i
1	0	0.655842	51	3.141593	5.600409
2	0.062832	2.114886	52	3.204425	7.73681
3	0.125664	1.913245	53	3.267256	5.122997
4	0.188496	3.177257	54	3.330088	8.606219
5	0.251327	0.689014	55	3.39292	8.462995
6	0.314159	1.668217	56	3.455752	9.174039
7	0.376991	-1.3465	57	3.518584	7.321504
8	0.439823	1.61845	58	3.581416	6.916049
9	0.502655	1.532319	59	3.644247	9.373074
10	0.565487	2.71808	60	3.707079	11.14124
11	0.628319	2.020064	61	3.769911	9.624707
12	0.69115	1.312449	62	3.832743	8.687917
13	0.753982	2.001953	63	3.895575	9.33649
14	0.816814	3.82832	64	3.958407	7.912225
15	0.879646	1.935325	65	4.021239	9.111349
16	0.942478	3.008351	66	4.08407	7.770642
17	1.00531	3.669298	67	4.146902	8.799503
18	1.068142	4.632178	68	4.209734	12.25011
19	1.130973	5.154288	69	4.272566	11.29631
20	1.193805	3.174726	70	4.335398	10.34536
21	1.256637	6.069671	71	4.39823	8.374006
22	1.319469	3.162803	72	4.461062	13.23273
23	1.382301	2.696466	73	4.523893	10.0354
24	1.445133	3.421394	74	4.586725	10.7539

Table 4.4 (continued).

i	x_i	y_i	i	x_i	y_i
25	1.507964	0.350422	75	4.649557	11.40374
26	1.570796	2.981907	76	4.712389	9.190378
27	1.633628	2.666889	77	4.775221	12.15359
28	1.69646	1.362263	78	4.838053	9.736684
29	1.759292	7.036787	79	4.900885	12.20263
30	1.822124	4.011233	80	4.963716	12.78446
31	1.884956	4.989338	81	5.026548	10.79367
32	1.947787	5.14384	82	5.08938	12.00101
33	2.010619	7.63181	83	5.152212	7.833796
34	2.073451	4.510752	84	5.215044	9.437101
35	2.136283	4.955316	85	5.277876	8.841867
36	2.199115	6.488184	86	5.340708	8.713244
37	2.261947	5.255902	87	5.403539	13.24431
38	2.324779	7.085093	88	5.466371	13.87933
39	2.38761	5.16598	89	5.529203	11.30799
40	2.450442	3.295977	90	5.592035	9.982219
41	2.513274	5.019097	91	5.654867	11.53432
42	2.576106	8.208935	92	5.717699	12.28004
43	2.638938	7.915806	93	5.78053	12.51945
44	2.70177	3.932963	94	5.843362	15.95529
45	2.764602	6.406319	95	5.906194	12.41553
46	2.827433	3.74281	96	5.969026	12.26261
47	2.890265	5.261321	97	6.031858	14.35
48	2.953097	8.177601	98	6.09469	11.41828
49	3.015929	6.559347	99	6.157522	11.73805
50	3.078761	7.892402	100	6.220353	12.72404

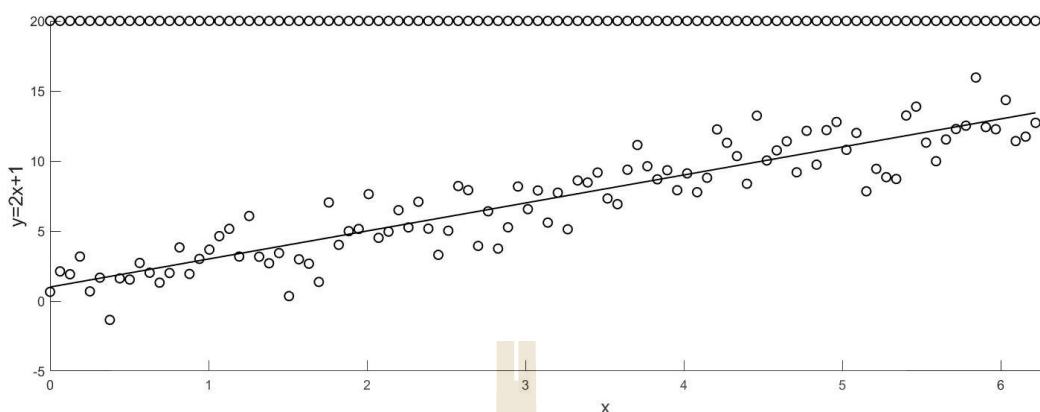


Figure 4.12 Data with 100 points for linear trend case.

With using RC Algorithm, the parameters σ and m are optioned for both training and validation cases are shown in Table 4.5.

Table 4.5 Training and validation errors for candidate models for linear trend case.

RBF	σ	m	MSE	
			Training	Validation
CS-RBF1	-	29	1.6659	3.1688
CS1	-	13	1.9633	2.849
CS2	-	22	1.853	3.0211
Gaussian I	0.2	9	2.2658	2.4408
Gaussian II	0.3	7	2.2941	2.4161
Gaussian III	0.4	5	2.3514	2.3643
Gaussian IV	0.5	5	2.3458	2.3603
Gaussian V	0.6	4	2.3444	2.3585
Gaussian VI	0.7	4	2.3438	2.3574

Thus, based on RC Algorithm, Gaussian III with $\sigma=0.4$ and $m=5$ for this data set can be a good model. When using the same numbers of centres, Table 4.6 and Table 4.7 provide the main results of this case. Figure 4.13 and Figure 4.14 illustrate the predicted training trend and predicted validation trend, respectively.

Table 4.6 Results comparison when using different numbers of centres and RBFs for linear trend case.

RBF	$m=9, \sigma=0.2$		$m=7, \sigma=0.3$		$m=5, \sigma=0.4$		$m=4, \sigma=0.7$	
	Training	Validation	Training	Validation	Training	Validation	Training	Validation
	Error	Error	Error	Error	Error	Error	Error	Error
CS-RBF1	2.1988	2.5176	2.1796	2.4946	2.2539	2.6201	2.4811	2.5307
CS1	2.2469	2.4538	2.2802	2.4502	2.6874	2.6801	2.3129	2.5212
CS2	2.2698	2.4799	2.3149	2.4290	2.6218	2.6326	2.6478	2.8352
Gaussian	2.2658	2.4408	2.2941	2.4161	2.3514	2.3643	2.3438	2.3574

Table 4.7 Listing of basis function centres for linear trend case.

m	RBF	Weights								
		μ_1	μ_2	μ_3	μ_4	μ_5	μ_6	μ_7	μ_8	μ_9
9	CS-RBF1	0.6768	0.9697	0.0303	0.1818	0.9293	0.8586	0.6465	0.2525	0.8990
	CS1	0.0707	0.6667	0.5859	0.9293	0.8485	0.2424	1.0000	0	0.4141
	CS2	0.7172	0.1919	0.2323	0.0404	0.6667	1.0000	0.9091	0.7677	0.1414
	Gaussian	0	1.0000	0.0808	0.9192	0.2121	0.7879	0.3535	0.6465	0.5051
7	CS-RBF1	0.2828	0.9697	0.5051	0.7475	0.9293	0.1818	0.8990		
	CS1	0.2424	0.4141	0.9293	0	0.3333	1.0000	0.5859		
	CS2	0.7172	0.5253	0.1919	0.6162	1.0000	0.0404	0.2828		
	Gaussian	0	1.0000	0.1010	0.8889	0.7071	0.2929	0.4949		
5	CS-RBF1	0.8586	0.4646	0.8182	0.9293	0.3939				
	CS1	0.5051	0.4141	0.5859	0.8485	0.2424				
	CS2	0.2828	0.9091	0.1919	0.7677	0.3333				
	Gaussian	1.0000	0	0.8081	0.2020	0.5051				
4	CS-RBF1	0.7172	0.9293	0.3535	0.1818					
	CS1	0.7576	0.8485	1.0000	0.0707					
	CS2	0.4242	0.5758	1.0000	0.7677					
	Gaussian	1.0000	0	0.2727	0.7071					

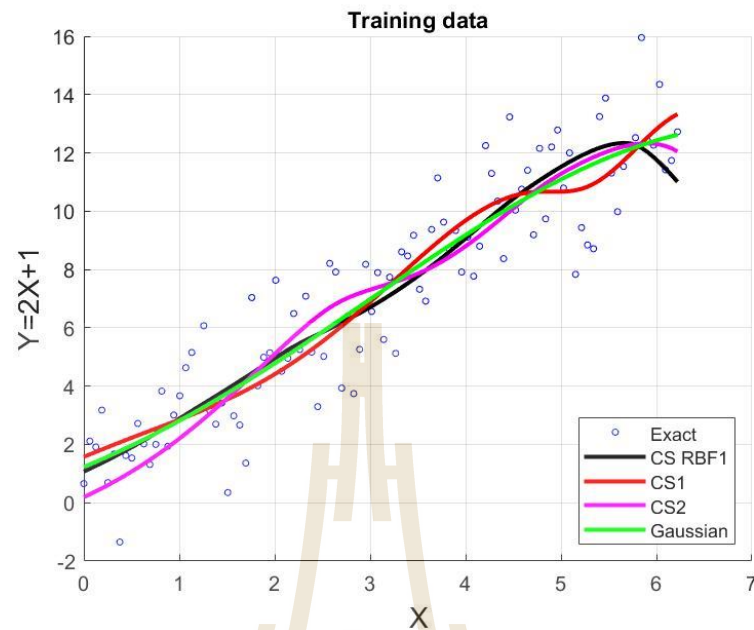


Figure 4.13 Predicted training trend produced by using 4 centres for linear trend case.

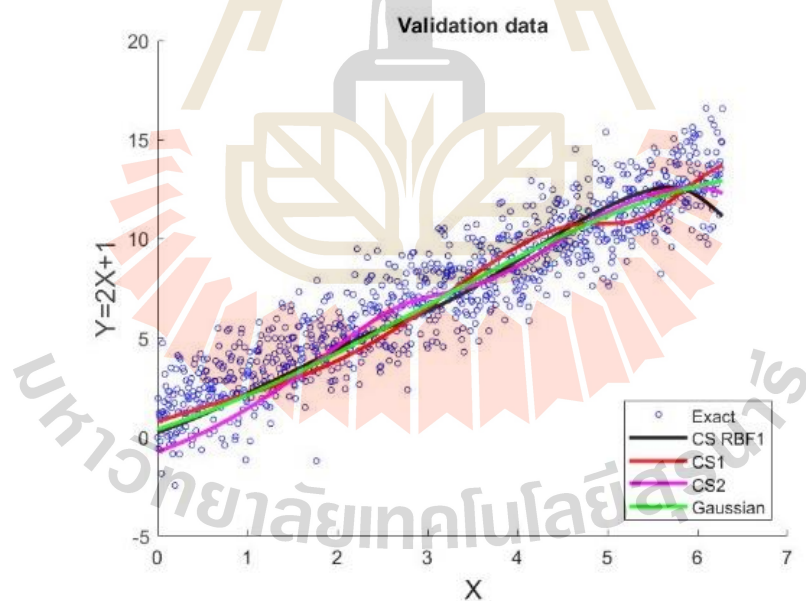


Figure 4.14 Predicted validation trend produced by using 4 centres for linear trend case.

4.2.4 Test Case 2: Parabola function

The second case to investigate is a parabola described as the following equation;

$$y = \frac{x^2}{6} - x + 4. \quad (4.7)$$

The data points are generated similarly to the previous example show in Table 4.8 and Figure 4.15 depicts the plot with nodes.

Table 4.8 The locations over the computational domain with 100 points for parabola trend case.

i	x_i	y_i	i	x_i	y_i
1	0	4.24814	51	3.141593	3.604046
2	0.062832	3.704129	52	3.204425	2.579202
3	0.125664	4.169598	53	3.267256	1.807343
4	0.188496	3.80927	54	3.330088	2.351547
5	0.251327	3.737286	55	3.39292	3.171114
6	0.314159	4.194421	56	3.455752	3.909455
7	0.376991	3.873224	57	3.518584	2.434338
8	0.439823	3.131685	58	3.581416	2.215887
9	0.502655	3.585788	59	3.644247	2.640374
10	0.565487	2.777425	60	3.707079	2.329124
11	0.628319	3.018628	61	3.769911	2.689632
12	0.69115	3.94122	62	3.832743	2.383895
13	0.753982	2.924287	63	3.895575	1.91565
14	0.816814	4.103699	64	3.958407	2.733152
15	0.879646	3.121798	65	4.021239	2.613712
16	0.942478	3.667874	66	4.08407	1.75167
17	1.00531	3.087243	67	4.146902	2.591541
18	1.068142	3.556016	68	4.209734	3.31661
19	1.130973	3.212318	69	4.272566	2.065257
20	1.193805	2.839454	70	4.335398	2.945395
21	1.256637	2.198888	71	4.39823	3.153849

Table 4.8 (continued).

i	x_i	y_i	i	x_i	y_i
22	1.319469	2.854652	72	4.461062	3.36909
23	1.382301	1.320843	73	4.523893	3.693778
24	1.445133	2.485727	74	4.586725	3.221386
25	1.507964	2.629543	75	4.649557	2.778476
26	1.570796	2.603496	76	4.712389	3.352436
27	1.633628	3.497001	77	4.775221	3.480584
28	1.69646	3.166593	78	4.838053	3.345557
29	1.759292	2.94798	79	4.900885	2.639394
30	1.822124	2.863549	80	4.963716	3.038108
31	1.884956	1.377919	81	5.026548	3.265107
32	1.947787	3.41562	82	5.08938	3.36192
33	2.010619	2.518353	83	5.152212	3.401107
34	2.073451	2.415294	84	5.215044	2.460658
35	2.136283	2.273644	85	5.277876	3.513121
36	2.199115	3.257021	86	5.340708	3.020274
37	2.261947	2.406498	87	5.403539	3.86994
38	2.324779	3.192788	88	5.466371	3.490127
39	2.38761	2.733065	89	5.529203	2.096448
40	2.450442	2.78557	90	5.592035	3.480605
41	2.513274	2.50616	91	5.654867	3.053712
42	2.576106	2.203222	92	5.717699	3.385007
43	2.638938	2.669624	93	5.78053	4.334289
44	2.70177	2.295242	94	5.843362	4.214735
45	2.764602	2.688145	95	5.906194	4.293023
46	2.827433	2.931139	96	5.969026	4.202053
47	2.890265	2.774863	97	6.031858	4.068915
48	2.953097	2.429877	98	6.09469	4.440242
49	3.015929	1.973173	99	6.157522	3.394129
50	3.078761	2.430819	100	6.220353	3.690945

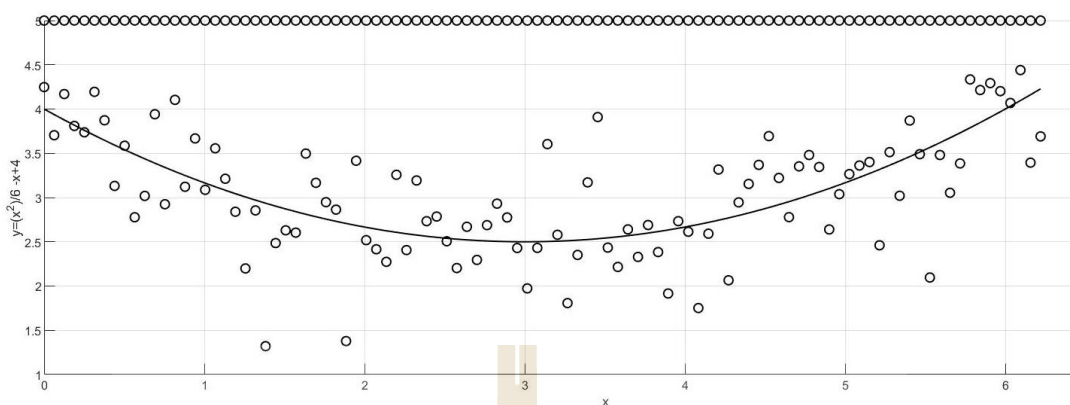


Figure 4.15 Data with 100 points for parabolas trend case.

With using RC Algorithm, the parameters σ and m are optioned for both training and validation cases are shown in Table 4.9.

Table 4.9 Training and validation errors for candidate models for parabolas trend case.

RBF	σ	m	MSE	
			Training	Validation
CS-RBF1	-	29	0.17637	0.52294
CS1	-	13	0.22069	0.44781
CS2	-	22	0.18575	0.51042
Gaussian I	0.2	9	0.24256	0.3985
Gaussian II	0.3	7	0.24649	0.3960
Gaussian III	0.4	5	0.24742	0.39345
Gaussian IV	0.5	5	0.24736	0.39365
Gaussian V	0.6	4	0.25371	0.39465
Gaussian VI	0.7	4	0.25203	0.39386

Thus, based on RC Algorithm, Gaussian V with $\sigma = 0.6$ and $m = 4$ for this data set can be a good model. When using the same numbers of centres, Table 4.10 and Table 4.11 provide the main results of this case. Figure 4.16 and 4.17 illustrates the predicted trend with all the testing data points.

Table 4.10 Results comparison when using different numbers of centres and RBFs for parabolas trend case.

RBF	$m=9, \sigma=0.2$		$m=7, \sigma=0.3$		$m=5, \sigma=0.5$		$m=4, \sigma=0.6$	
	Training	Validation	Training	Validation	Training	Validation	Training	Validation
	Error	Error	Error	Error	Error	Error	Error	Error
CS-RBF1	0.2432	0.41758	0.24342	0.40239	0.26359	0.3919	0.25937	0.39388
CS1	0.22953	0.43281	0.24674	0.39482	0.26100	0.3992	0.25813	0.40699
CS2	0.24407	0.40677	0.25483	0.40454	0.25456	0.39304	0.24952	0.40052
Gaussian	0.24256	0.3985	0.24649	0.3960	0.24742	0.39345	0.25371	0.39465

Table 4.11 Listing of basis function centres for parabolas trend case.

m	RBF	Weights								
		μ_1	μ_2	μ_3	μ_4	μ_5	μ_6	μ_7	μ_8	μ_9
9	CS-RBF1	0	0.9293	0.8182	0.1414	0.2525	0.5354	0.7172	0.0707	0.3232
	CS1	0.5051	0.1616	0.0707	0.8485	0.9293	0.7576	0.4141	0.6667	1.0000
	CS2	0.4747	1.0000	0.4242	0.5253	0.2323	0.6162	0.0909	0.7677	0.9596
	Gaussian	0	1.0000	0.0808	0.9192	0.2121	0.7879	0.3535	0.6465	0.5051
7	CS-RBF1	0	1.0000	0.4646	0.5354	0.1010	0.8586	0.7172		
	CS1	0.8485	0.2424	0.6667	1.0000	0	0.1616	0.9293		
	CS2	0	0.9091	0.5253	0.2828	0.8081	0.7172	0.0404		
	Gaussian	0	1.0000	0.1010	0.8889	0.7071	0.2929	0.4949		
5	CS-RBF1	0.4646	1.0000	0.7172	0.0303	0.9697				
	CS1	0	0.7576	0.0707	0.6667	0.8485				
	CS2	0	0.7172	1.0000	0.3838	0.4747				
	Gaussian	1.0000	0	0.8081	0.2020	0.5051				
4	CS-RBF1	0.9697	0.7879	0.6465	0					
	CS1	0.1616	0	1.0000	0.4141					
	CS2	1.0000	0.4747	0.0404	0					
	Gaussian	1.0000	0	0.7172	0.3030					

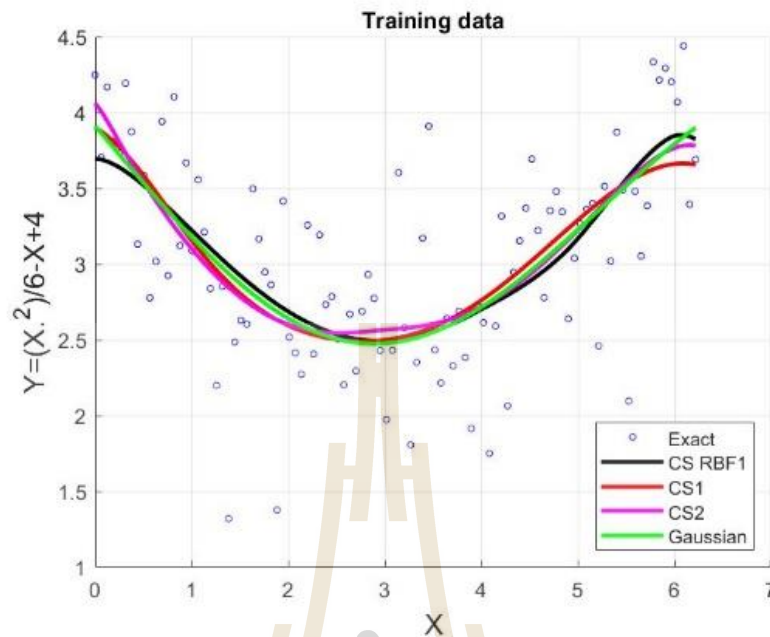


Figure 4.16 Predicted training trend produced by using 4 centres for parabolias trend case.

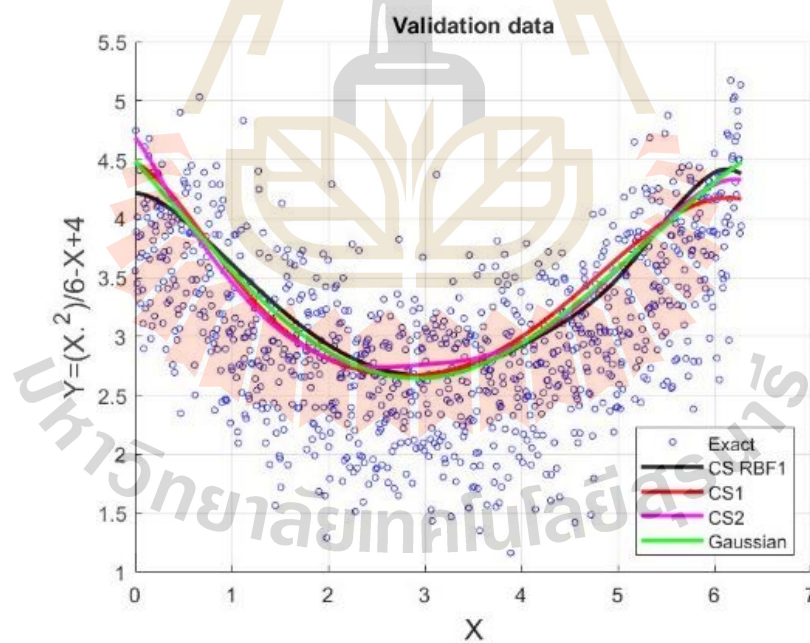


Figure 4.17 Predicted validation trend produced by using 4 centres for parabolias trend case.

4.2.5 Test Case 3: Sine interpolation

In the final case study, a non-linear sine function expressed below is studied;

$$y = \sin(x) + \varepsilon. \quad (4.8)$$

A set of 100 data on $[0, 2\pi]$ is generated and the noise is set to be a Gaussian distribution with mean zero and standard deviation 0.5, as depicted in Figure 4.18 and Table 4.12.

Table 4.12 The locations over the computational domain with 100 points for sine trend case.

i	x_i	y_i	i	x_i	y_i
1	0	0.358921	51	3.141593	-0.57653
2	0.062832	1.287004	52	3.204425	-0.01115
3	0.125664	-1.38256	53	3.267256	-0.93582
4	0.188496	0.762927	54	3.330088	-0.9307
5	0.251327	0.461482	55	3.39292	-0.25326
6	0.314159	-0.56393	56	3.455752	0.714093
7	0.376991	0.078679	57	3.518584	-0.88192
8	0.439823	0.654499	58	3.581416	-0.17786
9	0.502655	2.870519	59	3.644247	-0.63234
10	0.565487	2.38457	60	3.707079	0.210066
11	0.628319	-0.31333	61	3.769911	-1.31479
12	0.69115	2.663393	62	3.832743	-0.61569
13	0.753982	1.168792	63	3.895575	-0.31571
14	0.816814	0.686876	64	3.958407	0.005746
15	0.879646	1.247641	65	4.021239	0.260328
16	0.942478	0.672192	66	4.08407	-0.75165
17	1.00531	0.761455	67	4.146902	-1.84004
18	1.068142	1.870757	68	4.209734	-1.37183
19	1.130973	1.845431	69	4.272566	-1.61349
20	1.193805	1.875826	70	4.335398	0.639276
21	1.256637	1.399316	71	4.39823	-1.362
22	1.319469	0.162523	72	4.461062	-0.4692

Table 4.12 (continued).

i	x_i	y_i	i	x_i	y_i
23	1.382301	1.461081	73	4.523893	-1.11074
24	1.445133	2.080381	74	4.586725	-0.39892
25	1.507964	1.324389	75	4.649557	-1.5086
26	1.570796	1.690711	76	4.712389	-1.93609
27	1.633628	1.48326	77	4.775221	-1.94754
28	1.69646	0.789552	78	4.838053	-0.66622
29	1.759292	1.178462	79	4.900885	-1.10069
30	1.822124	0.443031	80	4.963716	-1.09946
31	1.884956	1.544107	81	5.026548	-0.00359
32	1.947787	0.164048	82	5.08938	-0.73513
33	2.010619	0.191301	83	5.152212	-0.77278
34	2.073451	0.335924	84	5.215044	0.183565
35	2.136283	-1.12113	85	5.277876	-1.38135
36	2.199115	1.76921	86	5.340708	-0.34398
37	2.261947	0.987595	87	5.403539	-0.21305
38	2.324779	0.225015	88	5.466371	-0.89166
39	2.38761	1.599292	89	5.529203	-0.54058
40	2.450442	-0.5051	90	5.592035	-1.41569
41	2.513274	0.519533	91	5.654867	-1.3541
42	2.576106	0.374648	92	5.717699	-0.46582
43	2.638938	0.694841	93	5.78053	0.000388
44	2.70177	0.634629	94	5.843362	1.30017
45	2.764602	-0.20923	95	5.906194	-0.81331
46	2.827433	0.288956	96	5.969026	-0.18396
47	2.890265	0.138625	97	6.031858	-0.30376
48	2.953097	0.606408	98	6.09469	-1.47777
49	3.015929	0.855145	99	6.157522	-0.41837
50	3.078761	0.803288	100	6.220353	-1.26083

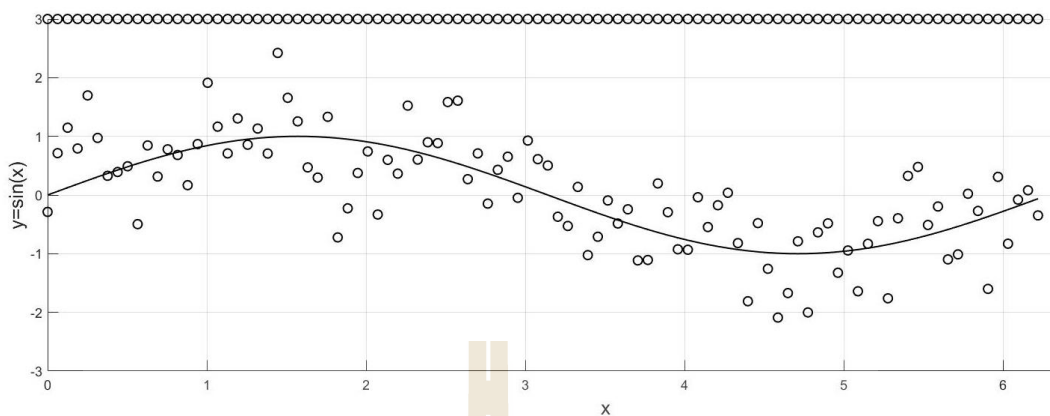


Figure 4.18 Data with 100 points for sine trend case.

With using RC Algorithm, the parameters σ and m are optioned for both training and validation cases are shown in Table 4.13.

Table 4.13 Training and validation errors for candidate models for sine trend case.

RBF	σ	m	MSE	
			Training	Validation
CS-RBF1	-	29	0.22723	0.78921
CS1	-	13	0.30183	0.64521
CS2	-	22	0.24992	0.73249
Gaussian I	0.2	9	0.36463	0.53588
Gaussian II	0.3	7	0.36596	0.53268
Gaussian III	0.4	5	0.37101	0.52852
Gaussian IV	0.5	5	0.37275	0.52933
Gaussian V	0.6	4	0.37927	0.52375
Gaussian VI	0.7	4	0.37985	0.52492

Thus, based on RC Algorithm, Gaussian V with $\sigma=0.6$ and $m=4$ for this data set can be a good model. When using the same numbers of centres, Table 4.14 and Table 4.15 provide the main results of this case. Figure 4.19 and Figure 4.20 illustrates the predicted trend with all the testing data points.

Table 4.14 Results comparison when using different numbers of centres and RBFs for sine trend case.

RBF	$m=9, \sigma=0.2$		$m=7, \sigma=0.3$		$m=5, \sigma=0.5$		$m=4, \sigma=0.6$	
	Training	Validation	Training	Validation	Training	Validation	Training	Validation
	Error	Error	Error	Error	Error	Error	Error	Error
CS-RBF1	0.34868	0.55688	0.37794	0.53255	0.45835	0.66754	0.46907	0.63571
CS1	0.35783	0.54659	0.34087	0.57013	0.47041	0.66921	0.38884	0.53472
CS2	0.33763	0.58504	0.36135	0.56636	0.41765	0.55269	0.52803	0.80572
Gaussian	0.36463	0.53588	0.36596	0.53268	0.37275	0.52933	0.37927	0.52375

Table 4.15 Listing of basis function centres for sine trend case.

m	RBF	Weights								
		μ_1	μ_2	μ_3	μ_4	μ_5	μ_6	μ_7	μ_8	μ_9
9	CS-RBF1	0	0.4646	0.8182	0.8586	0.0707	0.5758	0.1414	0.7475	0.2525
	CS1	0.1616	0.5051	0.5859	0.7576	0.0707	0.4141	0	1.0000	0.6667
	CS2	0	0.9091	0.7172	0.5253	0.6162	0.0404	0.2323	0.6667	0.3333
	Gaussian	0	1.0000	0.0808	0.9192	0.2121	0.7879	0.3535	0.6465	0.5051
7	CS-RBF1	0.8586	0.0303	1.0000	0.1414	0	0.2828	0.5051		
	CS1	0.3333	0.5051	0.2424	0.7576	0.8485	0.6667	0.5859		
	CS2	0.5253	0.1919	0.2828	0.7172	0.3838	0.5758	0.8586		
	Gaussian	0	1.0000	0.1010	0.8889	0.7071	0.2929	0.4949		
5	CS-RBF1	0.6768	0.2828	0.7172	0.4242	0				
	CS1	0.7576	0.4141	0.2424	0.1616	0				
	CS2	0.6162	0.2323	0.2828	0.9091	0.1919				
	Gaussian	1.0000	0	0.1818	0.8081	0.4949				
4	CS-RBF1	0.7475	0.4242	0.6768	0.2121					
	CS1	0.7576	0	0.3333	0.8485					
	CS2	0.7172	0.1919	0.4747	0.0404					
	Gaussian	1.0000	0	0.7172	0.3030					

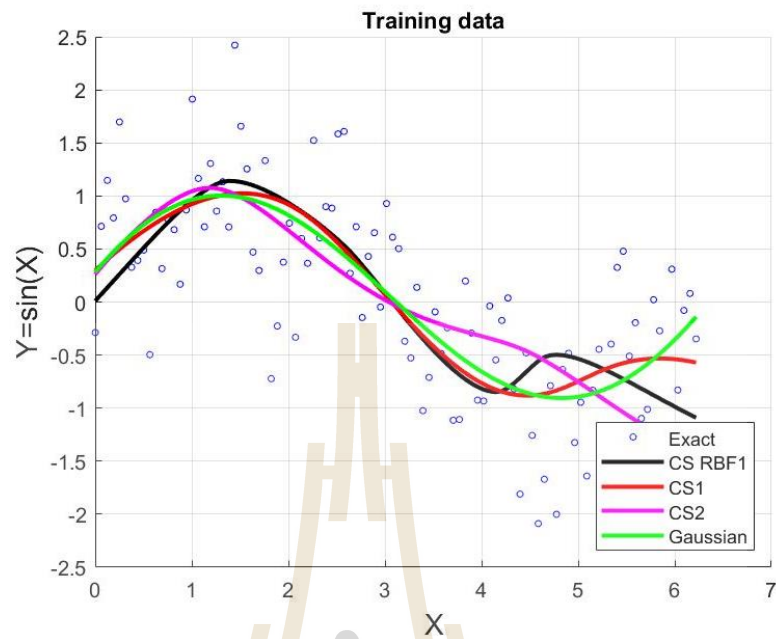


Figure 4.19 Predicted training trend produced by using 4 centres for sine trend case.

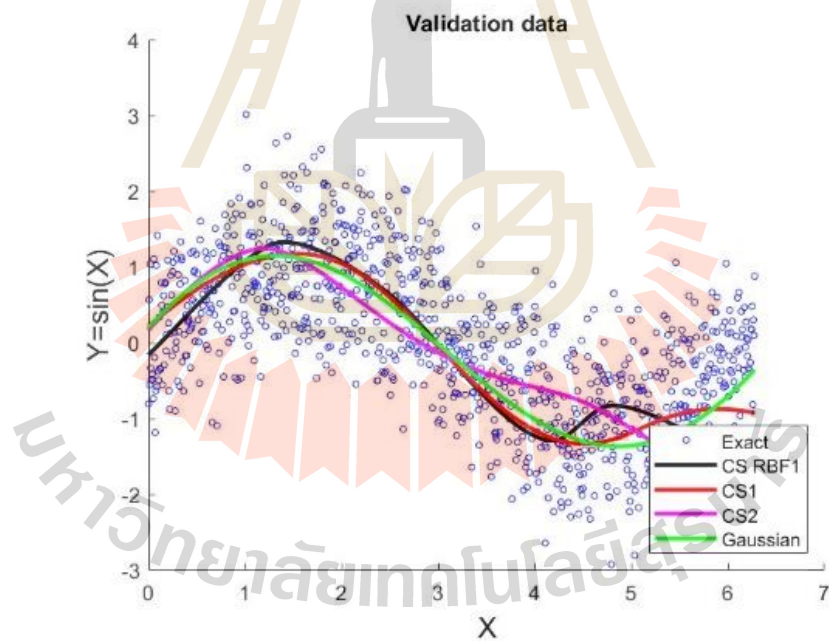


Figure 4.20 Predicted validation trend produced by using 4 centres for sine trend case.

4.2.6 Main Conclusions

The investigation begins with the observation that RBF-pattern recognition problem relies highly on the choice of what is called ‘shape parameter’ which requires a user’s pre-judgement. It then comes to attention an alternative way to avoid this difficulty by using RBFs that contain no-parameter. For this, three non-parameterized RBF have been explored numerically. For the comparison purpose, the RC algorithm normally used with Gaussian RBF is utilized for suggestion for the number of suitable centres. Three trends of data patterns are tested with the scheme and the main findings are;

- With RC-algorithm, it is found that CS-RBF1, CS1, and CS2 have appeared to be slightly overfitting. This figure is to be further investigated.
- With appropriate choice of number of centres, these selected non-parameterized RBFs are found to perform equally well when compared to the famous Gaussian.

The next step of this study is to tackle problems in more dimensions and with more complexity.

4.3 Experiment 3: A Comparison Study on Shape Parameter Selection in Pattern Recognition by Radial Basis Function Neural Networks

4.3.1 The Project Objective

This study constructs the model with unknown input-output mapping pattern under the problem of pattern recognition via RBF-Neural Network using RC-algorithm. In this work, we focus on radial basis function and investigate the capability of other RBFs containing no shape parameter by comparison with 3 choices of shape parameters for the same problem of pattern recognition. For the purpose, to introduce three popular shape parameter acquisition algorithms commonly used with Multiquadric RBF are used as a guide for selecting the optimal shape parameter initially.

4.3.2 R B F s a n d T h e i r S h a p e P a r a m e

4.3.2.1 The Selected RBFs

For the purpose of comparison, three forms of radial basis functions are focused on and they are listed as follows;

Gaussian RBF (GA):

$$\phi(r) = \exp - r^2 / 2\varepsilon^2 \quad (4.9)$$

Multiquadric RBF (MQ):

$$\phi(r) = \sqrt{\varepsilon^2 + r^2} \quad (4.10)$$

Compactly-Supported RBF (CS1):

$$\phi(r) = \frac{112}{45} r^{\frac{9}{2}} + \frac{16}{3} r^{\frac{7}{2}} - 7r^4 - \frac{14}{15} r^2 + \frac{1}{9}. \quad (4.11)$$

The first two are known to be popular in many areas of research and are determined by the choice of the so-called ‘shape parameter, ε ’, (Shin, 1998). The third one is included in this study with the main aim to monitor the performance and compare with the other two RBFs driven by ε . It is also discovered in our previous study (Tavaen, Viriyapong and Kaennakham, 2020) that amongst three forms of Compactly-Supported RBFs, CS1 is more simply implemented with no significant differences in final results quality. This is the main reason why it is being further investigated in this work.

4.3.2.2 The Parameter's Choices

In this work, the main attention is paid on the effect of choices of the shape parameter proposed in three well-known numerical researches (under the applications of interpolation) and they are briefly detailed below.

Choice Hardy Shape (HS)

This was proposed by Hardy (Hardy, 1977) and it is of the following form:

$$\varepsilon_{HS} = 0.815d \quad (4.12)$$

where $d = \frac{1}{N} \sum_{i=1}^N d_i$ and d_i is the mean distance from each data point (x_i, y_i) to its nearest neighbor.

Choice Franke Shape (FS)

This was invented by Franke (Franke, 1979) and uses the following formula:

$$\varepsilon_{FS} = \frac{1.25D}{\sqrt{N}} \quad (4.13)$$

where D is the diameter of the smallest circle containing all data points.

Choice Carlson Shape (CS)

It was formed by Carlson (Carlson and Foley, 1991) and it starts by computing the least squares bivariate quadratic polynomial fit to the data $(\bar{x}_i, \bar{y}_i, \bar{z}_i)$

and denoting this quadratic by $q(\bar{x}_i, \bar{y}_i)$, i.e. compute $V = \sum_{i=1}^N \frac{(\bar{z}_i - q(\bar{x}_i, \bar{y}_i))^2}{N}$ by

setting $\bar{x}_i = \frac{(x_i - x_{\min})}{(x_{\max} - x_{\min})}$, $\bar{y}_i = \frac{(y_i - y_{\min})}{(y_{\max} - y_{\min})}$ and $\bar{z}_i = \frac{(z_i - z_{\min})}{(z_{\max} - z_{\min})}$. The proposed form of shape parameter is then of the following:

$$\varepsilon_{CS} = \frac{1}{1 + 120V}. \quad (4.14)$$

These three interesting forms of ε are numerically tested with 1D and 2D pattern applications and the results are discussed in the following section.

4.3.2.3 Additional Criteria

The following are experiment's ingredients used in this study.

1. The whole dataset for each case is split into two parts namely 'training dataset (TD)' and 'validation dataset (VD)', and they are fixed throughout the investigation.

2. $TD \cap VD = \{ \} = \text{empty set}$.

3. Define TVN represents the ratio of " $TD:VD$ "

4. Defining 'The Model Selection Criteria', the best model is ideally the one with the following properties;

4.1. produces small validation error.

4.2. requires small number of centres, i.e. small m in RC-algorithm.

4.3. the number of centres, m , should be as less affected by TD as possible.

(This is all to compromise the problem of over- and under-fitting scenarios.)

4.3.3 Test Case 1: The Sine Function

In the first case study, a sine function expressed below is investigated.

$$y = \sin(x) + \omega \quad (4.15)$$

A set of 100 data on $[0, 2\pi]$ is generated and the noise ω is set to be a Gaussian distribution with mean zero and standard deviation 0.5. The data points are generated uniformly over the domain with 1,000 points.

The experiments are conducted covering a wide range of TVN from 100:900 to 900:100 (only some are shown here, however). Table 4.16 provides information concerned in each case and it is clearly seen that the number of centres is significantly increasing with more training data being involved in the case of HS or

both GA ($29 \leq m \leq 135$) and MQ ($22 \leq m \leq 49$). On the other hand, FS and CS lead to a much narrow range of m over the same interval of TD for both GA and MQ, indicating that FS and CS are comparatively less affected by TD . For all cases, it should be noted that the shapeless CS1 is not being at all affected by the increase in training dataset TD .

In terms of validation error trends, at every ratio of TVN , it can be seen from the Table 4.16 that HS produces the comparatively highest error for both GA and MQ. On the other hand, FS and CS are found to generate small error and stay very close to each other for all TVN shown. It is also found that errors produced by CS1 is smaller than that obtained from HS but higher than that of FS and CS. For the case of GA only, pattern simulations obtained from all the shape choices are illustrated in Figure 4.21 and in Figure 4.22.

To sum up for this sine-function experiment, as long as the MSE is concerned, the shape parameter choice proposed by Franke (Franke, 1979) can be considered as the best.

Table 4.16 Error comparison for some chosen different TVN cases for sine function.

TVN	RBF	Type of			MSE	
		ϵ	ϵ	m	Training	Validation
100:900	GA	HS	0.0512	29	0.3721	0.9191
		FS	0.7775	4	0.4709	0.7535
		CS	0.2403	8	0.4362	0.8176
	MQ	HS	0.0512	22	0.3926	0.8906
		FS	0.7775	4	0.4701	0.7526
		CS	0.2403	9	0.4383	0.8132
	CS1	-	-	13	0.4259	0.8352
200:800	GA	HS	0.1322	12	0.4534	0.6915
		FS	0.5526	4	0.4677	0.6662
		CS	0.2403	8	0.4362	0.8176

Table 4.16 (continued).

TVN	RBF	Type of ϵ	ϵ	m	MSE	
					Training	Validation
100:900	MQ	HS	0.0512	22	0.3926	0.8906
		FS	0.7775	4	0.4701	0.7526
		CS	0.2403	9	0.4383	0.8132
	CS1	-	-	13	0.4259	0.8352
200:800	GA	HS	0.1322	12	0.4534	0.6915
		FS	0.5526	4	0.4677	0.6662
		CS	0.2401	8	0.4582	0.6806
	MQ	HS	0.1322	13	0.4504	0.6981
		FS	0.5526	5	0.4644	0.6632
		CS	0.2401	9	0.4581	0.6800
	CS1	-	-	13	0.4519	0.6949
	250:750	GA	HS	0.0205	69	0.3449
FS			0.4947	5	0.4587	0.6316
CS			0.3326	6	0.4577	0.6340
MQ		HS	0.0205	36	0.4093	0.6919
		FS	0.4947	5	0.4590	0.6328
		CS	0.3326	7	0.4579	0.6340
CS1		-	-	13	0.4498	0.6428
500:500		GA	HS	0.0102	135	0.3415
	FS		0.3505	6	0.4759	0.5014
	CS		0.3552	6	0.4758	0.5014
	MQ	HS	0.0102	49	0.4271	0.5533
		FS	0.3505	7	0.4740	0.5020
		CS	0.3552	7	0.4740	0.5020
CS1	-	-	13	0.4720	0.5044	

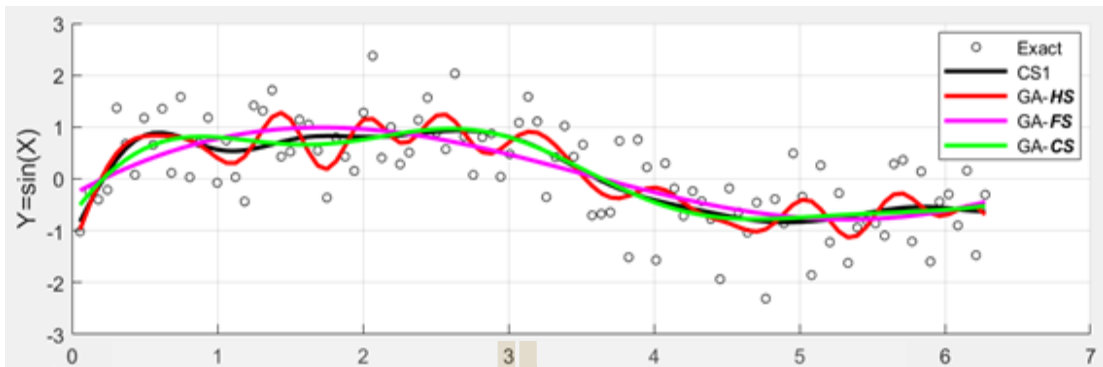


Figure 4.21 Pattern reconstruction obtained from using Gaussian RBF with all three choices of shape parameter compared with that produced by the shapeless CS1-RBF where training phase, calculated using $TVN = (100:900)$.

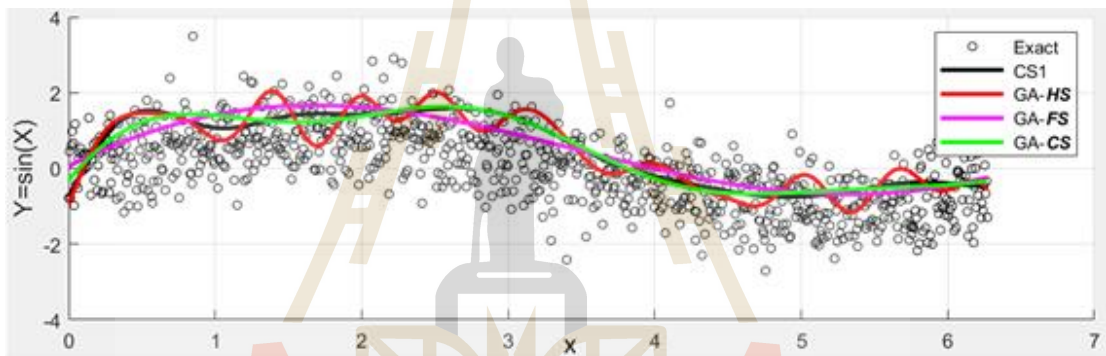


Figure 4.22 Pattern reconstruction obtained from using Gaussian RBF with all three choices of shape parameter compared with that produced by the shapeless CS1-RBF where validation phase, calculated using $TVN = (100:900)$.

4.3.4 Test Case 2: The Famous Franke's Function

This experiment is concerned with one of the most well-known testing functions invented by Franke (Franke, 1982). The complication of the function's surface makes it a good test for validating any interpolation-based methods proposed over the past two decades. The expression of the function is as followed.

$$f(x, y) = 0.75 \exp\left(-\frac{(9x-2)^2 + (9y-2)^2}{4}\right) + 0.75 \exp\left(-\frac{(9x+1)^2}{49} - \frac{9y+1}{10}\right) \quad (4.16)$$

$$+ 0.5 \exp\left(-\frac{(9x-7)^2 + (9y-3)^2}{4}\right) - 0.2 \exp(-(9x-4)^2 - (9y-7)^2).$$

Like done in the previous experiment, this function is disturbed with Gaussian distribution with mean zero and standard deviation 15.0 and for simplicity the following function is denoted.

$$f_1(x, y) = f(x, y) + \omega. \quad (4.17)$$

Several ratios of training to validation data points have been carried out. The data points are generated uniformly over the domain with 61×61 points. Figure 4.23 shows the node distribution in the case of using TVN(121:3600) and Figure 4.24 shows the corresponding exact surface (without noise).

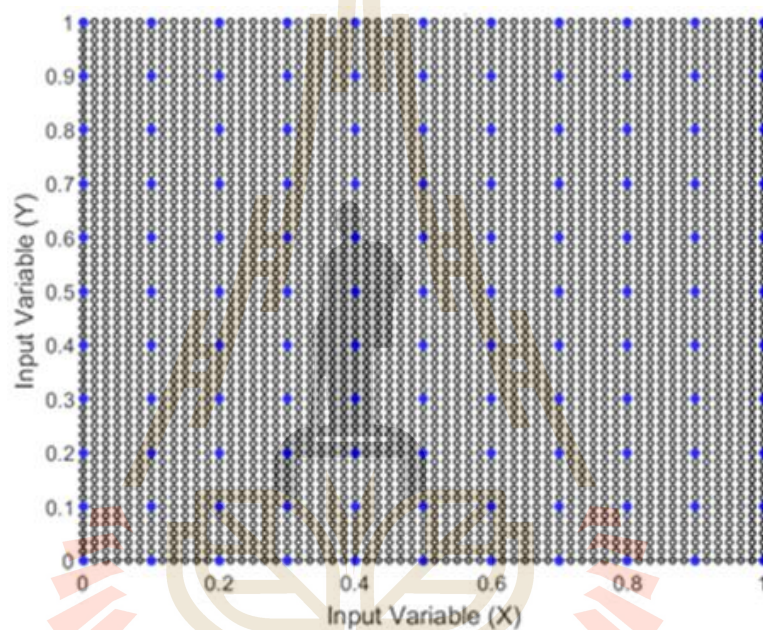


Figure 4.23 Node-distribution, projected on xy -plane, in the case with 121 training data points (depicted with blue dots) and 3600 validation data points (depicted with black dots).

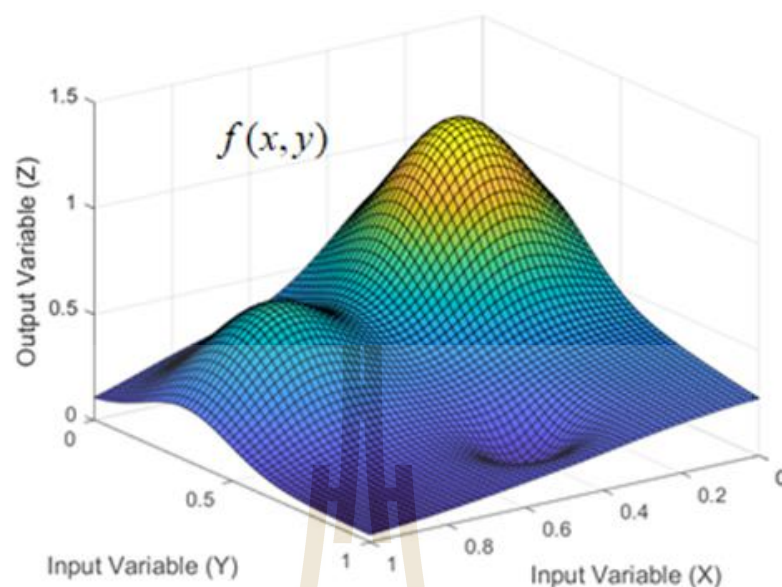


Figure 4.24 Surface plot of $f(x, y)$.

Similar to the previous case of sine function, a number of experiments are conducted and some discovery is provided in Table 4.17. From the Table, the mostly noticeable figure is the training error produced by using HS_n both GA and MQ. This over-fitting phenomenon is directly resulted from the fact that it uses the whole set of TD as its centres, i.e. it simply reflects itself for all TV . Even though it yields small validation errors, it cannot be crowned as the great model. On the other hand, FS and CS are seen to produce even smaller value of validation errors while the training errors still look reasonable. In both GA and MQ, it is found that CS leads to slightly better validation error than FS where the significant figure is revealed in terms of the number of centres required, i.e. m . Not only CS is capable of producing good results with small value of m , it is also seen to be mostly independent of the increase in training data. Even though CS_1 is not being affected by TD , the smallest m is still seen in the case of using CS (with GA in particular). For all these reasons, it is concluded in this experiment that CS shape parameter is the best choice for both GA-RBF and MQ-RBF. Solution distributions approximated using GA- CS , MQ- CS and CS_1 are illustrated in Figure 4.25 - Figure 4.30.

Table 4.17 Error comparison for some chosen different TVN cases for the Franke's function.

TVN	RBF	Type of ε	ε	m	MSE		
					Training	Validation	
121:3600	GA	HS	0.0815	121	1.5864e-30	0.0133	
		FS	0.1607	83	0.0023	0.0119	
		CS	0.4060	24	0.0063	0.0100	
	MQ	HS	0.0815	106	8.4055e-04	0.0123	
		FS	0.1607	53	0.0048	0.0098	
		CS	0.4060	24	0.0061	0.0097	
	CS1	-	-	66	0.0037	0.0106	
	441:3280	GA	HS	0.0408	441	3.2124e-30	0.0137
			FS	0.0842	257	0.0033	0.0114
CS			0.4264	19	0.0087	0.0097	
MQ		HS	0.0408	135	0.0052	0.0097	
		FS	0.0842	89	0.0059	0.0091	
		CS	0.4264	20	0.0079	0.0089	
CS1		-	-	66	0.0064	0.0086	
961:2760		GA	HS	0.0272	961	5.0043e-30	0.0137
			FS	0.0570	526	0.0035	0.0117
	CS		0.4103	19	0.0093	0.0091	
	MQ	HS	0.0272	155	0.0067	0.0086	
		FS	0.0570	113	0.0070	0.0085	
		CS	0.4103	21	0.0086	0.0085	
	CS1	-	-	66	0.0074	0.0081	

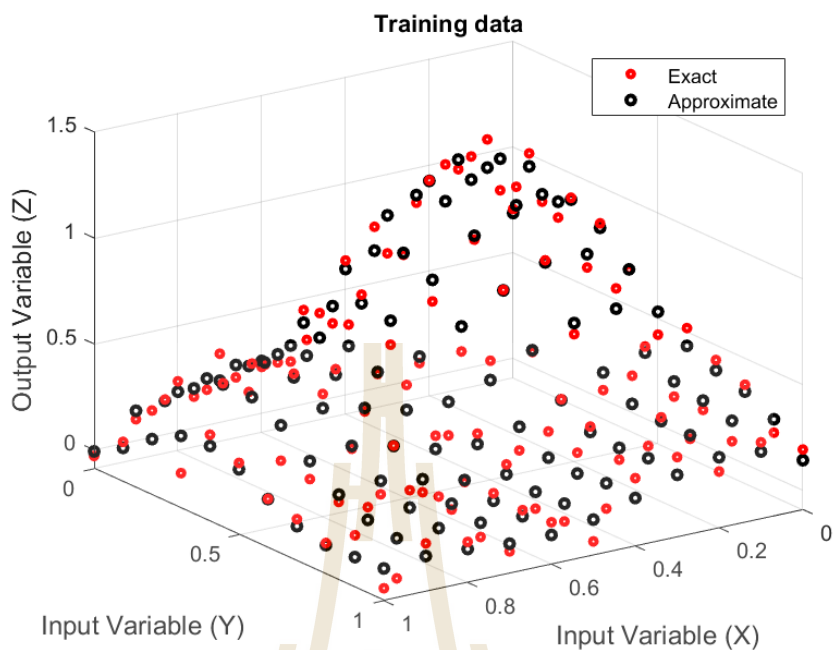


Figure 4.25 Pattern reconstruction yielded by using GA-CS with the training phase (Note that: the 'Exact' means $f_1(x, y)$ and represented in red).

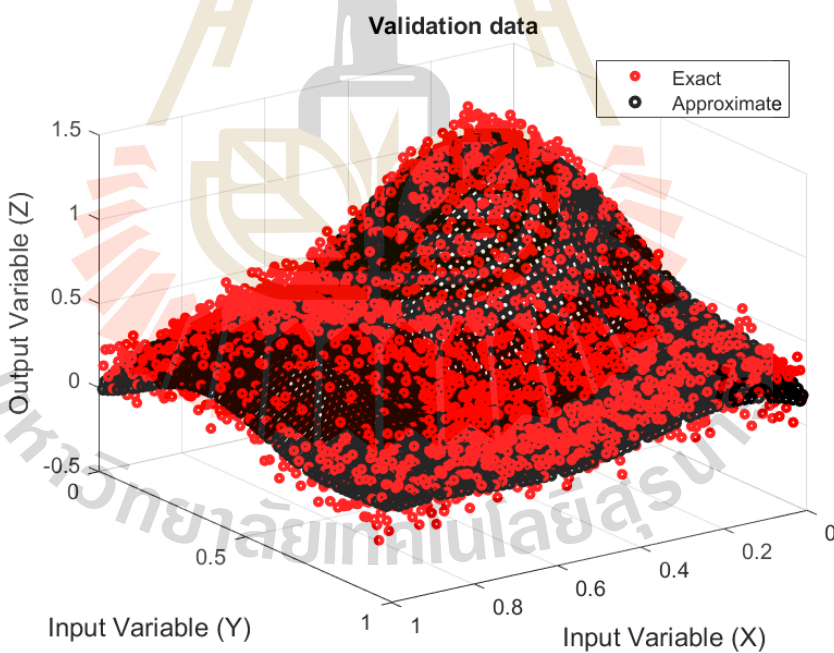


Figure 4.26 Pattern reconstruction yielded by using GA-CS for the validation phase (Note that: the 'Exact' means $f_1(x, y)$ and represented in red).

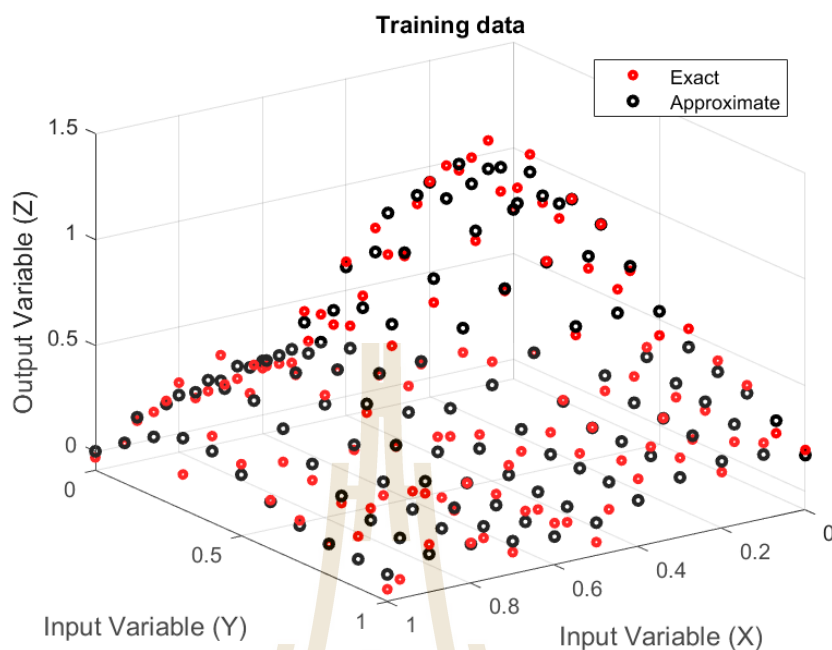


Figure 4.27 Pattern reconstruction yielded by using MQ-CS with the training phase (Note that: the 'Exact' means $f_1(x, y)$ and represented in red).

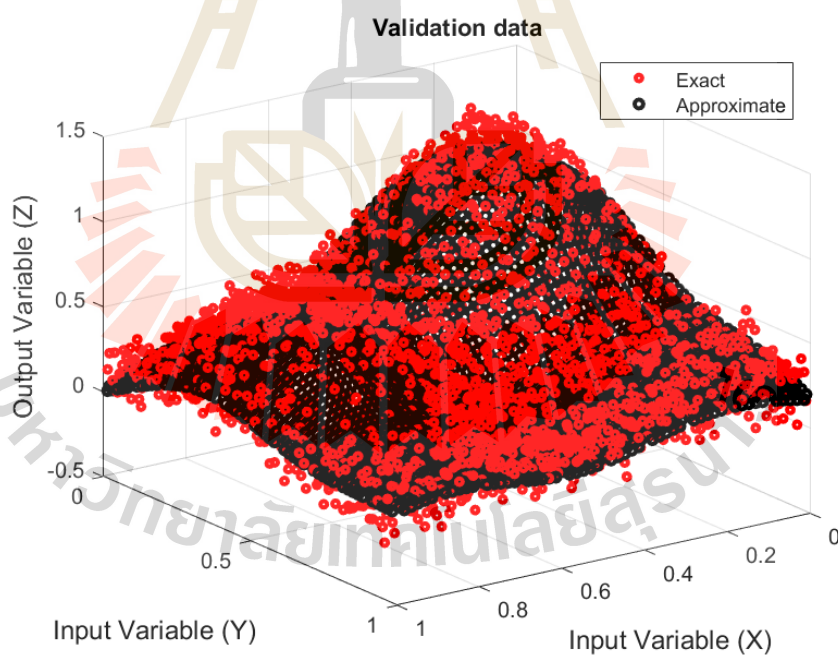


Figure 4.28 Pattern reconstruction yielded by using MQ-CS for the validation phase (Note that: the 'Exact' means $f_1(x, y)$ and represented in red).

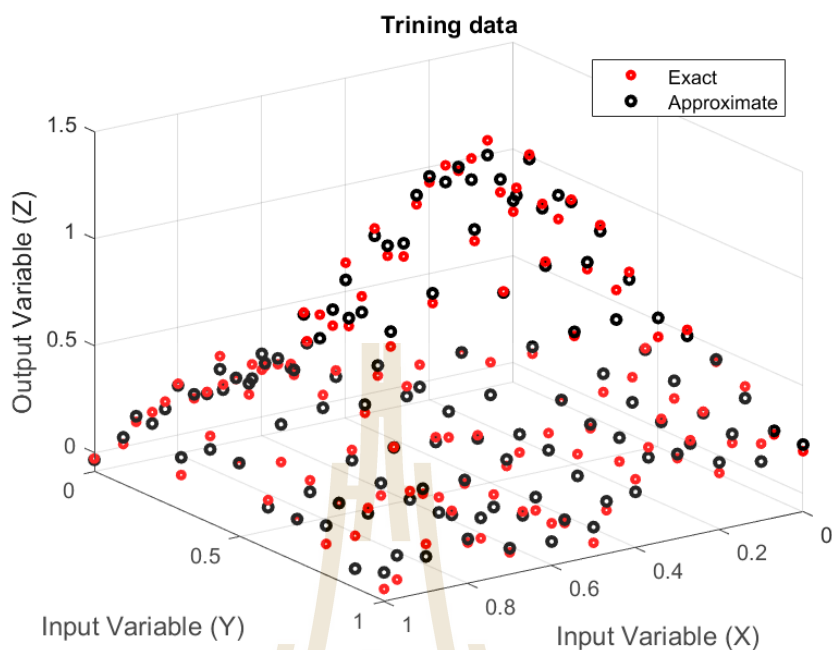


Figure 4.29 Pattern reconstruction yielded by using CS₁ with the training phase (Note that: the 'Exact' means $f_1(x, y)$ and represented in red).

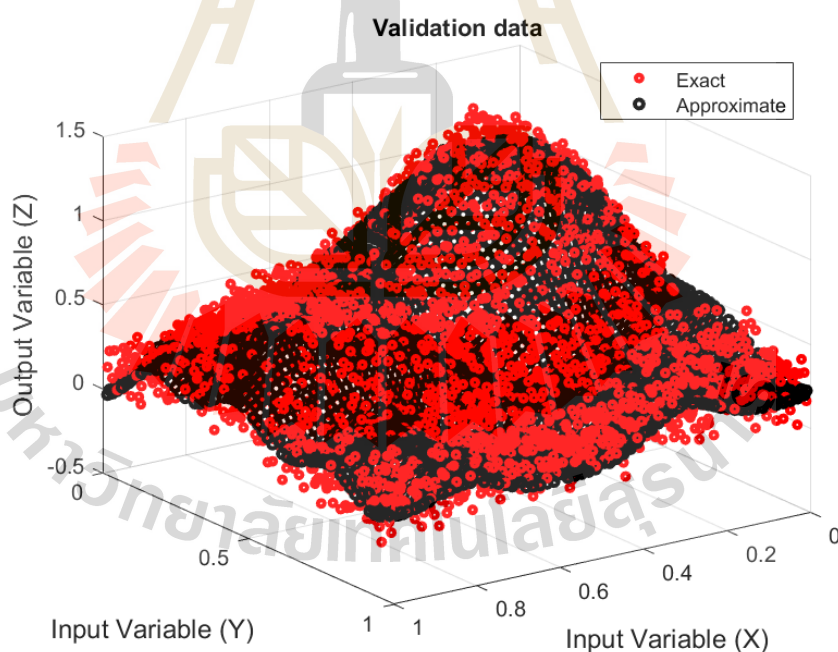


Figure 4.30 Pattern reconstruction yielded by using CS₁ for the validation phase (Note that: the 'Exact' means $f_1(x, y)$ and represented in red).

4.3.5 Main Conclusion

Under the pattern recognition problem, it can be observed that RBFs involve normally require a suitable shape in order to produce reliable results. The trends observed from the 2 experiments represented in 1D and 2D were as follows:

- With HS for both GA and MQ, the number of centres is significantly increasing with more training data being involved. On the other hand, FS and CS are comparatively less affected. For all cases, it should be noted that the shapefree CS1 is not being at all affected by the increase in training dataset.

- With appropriate choice of validation error, these selected CS are found to perform equally well when compared to the famous GA and MQ.

4.4 Experiment 4: Generalized-Multiquadric Radial Basis Function Neural Networks (RBFNs) with Variable Shape Parameters for Function Recovery

4.4.1 The Project Objective

The scheme was applied to tackle the problem of approximation of its derivatives using six forms of MQ with two choices of the variable shape parameter. The numerical results obtained in this study shall provide useful information on selecting both a suitable form of MQ and a reliable choice of MQ shape for further applications in general.

4.4.2 Variable Shape Parameters

The main focus of this work is on one of the popular form of basis function known as ‘multiquadric (MQ)’ in its generalized form defined as follows;

$$\phi_j(x, y) = \varepsilon^2 + r_j^{2\beta} = \varepsilon^2 + (x - x_j)^2 + (y - y_j)^2^\beta \quad (4.18)$$

where $\beta = \dots, -3/2, -1/2, 1/2, 3/2, \dots$. These values give direct effect on the singularity of the interpolation matrix and, unavoidably, the effectiveness of the methods’ performance. Different values yield different shape curves depicted in Figure 4.31.

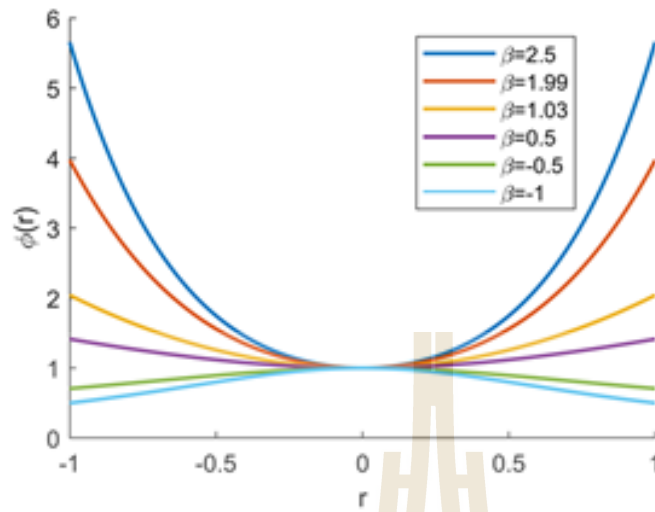


Figure 4.31 Generalized MQ with six values of β 's .

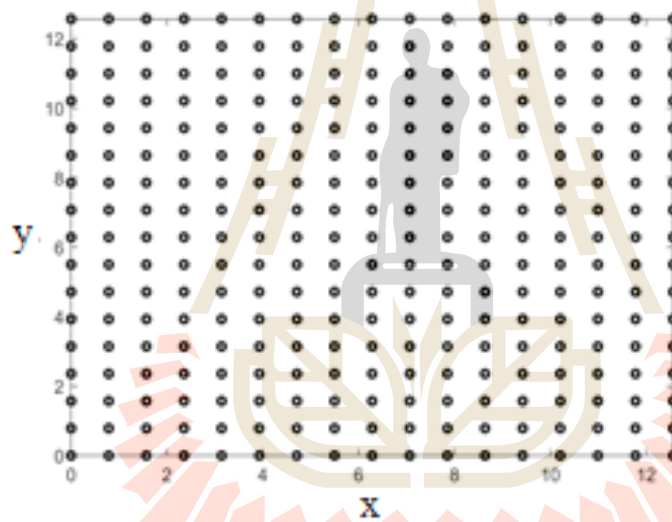


Figure 4.32 Generalized distribution of centres test function.

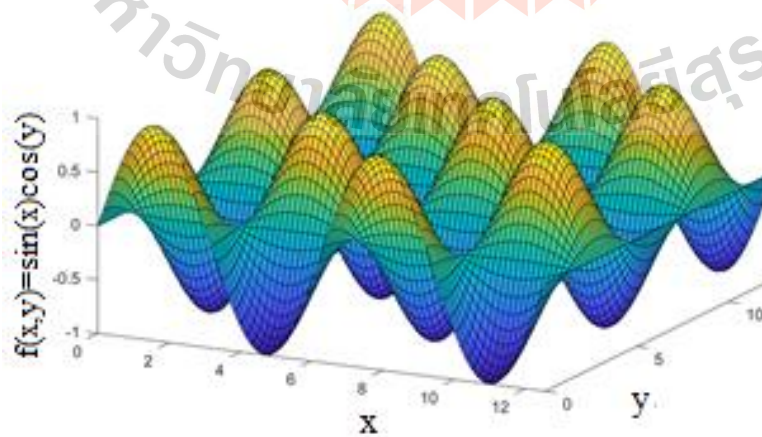


Figure 4.33 Generalized two-dimensional test function.

One crucial factor affecting the method's performance is the shape parameter. Choices available in literature can be categorized into three forms; constant/fixed, variable, and iterative-based. This work focuses on two nonlinear-variable shape strategies (illustrated in Figure 4.34- 4.35)

- Strategy-1 (St₁): by Nojavan (Nojavan, Abbasbandy and Allahviranloo, 2017), defined as;

$$\varepsilon_j = (c_{\min} + (c_{\max} - c_{\min}) \exp(-j))^{-1} \quad (4.19)$$

- Strategy-2 (St₂): by Xiang et.al. (2012) (Xiang, Wang, Ai, Sha and Shi, 2012), defined as;

$$\varepsilon_j = c_{\min} + (c_{\max} - c_{\min}) \sin(j) \quad (4.20)$$

with $j = 1, 2, \dots, N$. Apart from these chosen forms of shape selection strategies, those nicely documented in (Cheng, 2012) and (Chen, Hong and Lin, 2018) are also highly recommended for interested readers.

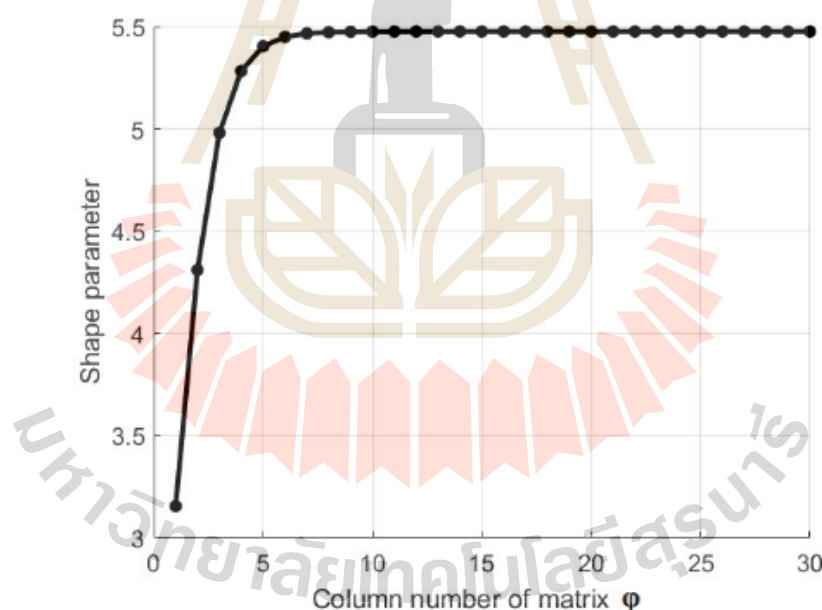


Figure 4.34 Multiquadrics' shape determining St₁ by using $c_{\min} = 1/\sqrt{N}$, $c_{\max} = 3/\sqrt{N}$, and $N = 30$.

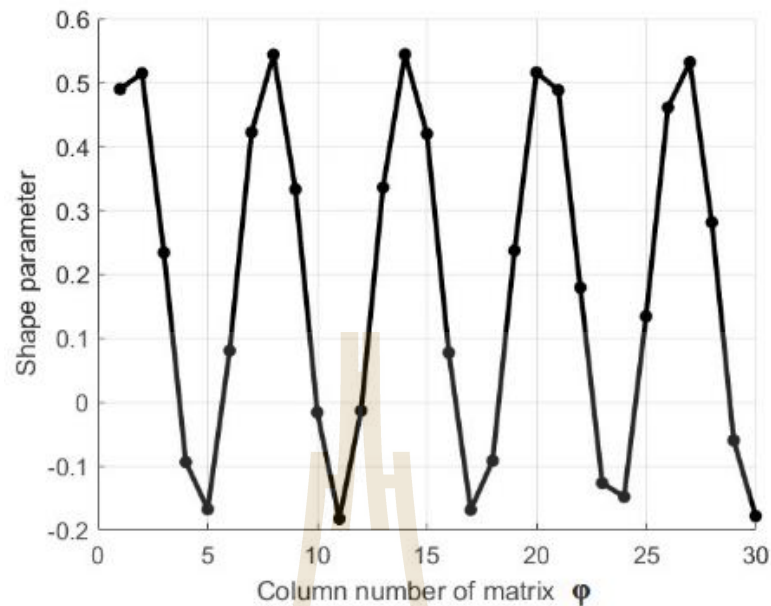


Figure 4.35 Multiquadrics' shape determining St_2 by using $c_{\min} = 1/\sqrt{N}$, $c_{\max} = 3/\sqrt{N}$, and $N = 30$.

4.4.3 Test Case 1: One-Dimensional Case

The first case deals with the approximation of a function in one dimension expressed below.

$$f(x) = e^{-x^3} + \cos(2x) \quad (4.21)$$

To compare the overall accuracy, those shape values stated in the work of Maggie (Chenoweth and Sarra, 2009) were also tested. The total of 25 nodes uniformly distributed over a $-1 \leq x \leq 1$ domain was considered where the function's values at 17 equally-spaced nodes were numerically approximated. The results were obtained from all six forms of MQ with two variable shapes (St_1 and St_2) together with fixed values are presented in Table 4.18. It can be shown in the table that all cases performed reasonably well with not much of a significant difference. One interesting finding worth mentioning is that those values obtained by using a fixed value were found the best ones. This might be attributed to the fact that Maggie (Chenoweth and Sarra, 2009) had actually performed a tremendous amount of experiments to find the best value of shape before utilizing that value for the actual experiment.

Table 4.18 Mean absolute errors measured for approximation of the function and its derivative for all forms of generalized MQ when using different variable shape forms (compared with a fixed form from literature).

Type	Shape	$\beta = 2.50$	$\beta = 1.99$	$\beta = 1.03$	$\beta = 0.50$	$\beta = -0.50$	$\beta = -1.00$
$f(x)$	St ₁	28.70E-05	12.00E-04	71.60E-05	27.00E-04	11.66E-05	40.57E-05
	St ₂	61.07E-07	15.18E-06	42.77E-06	48.52E-06	42.48E-05	16.00E-04
	Maggie	16.00E-04	16.00E-04	59.44E-05	89.55E-06	74.68E-07	54.15E-07
$f'(x)$	St ₁	22.00E-04	70.00E-04	35.00E-04	81.00E-04	12.00E-04	30.00E-04
	St ₂	29.36E-05	71.61E-05	20.00E-04	23.00E-04	17.80E-03	66.00E-03
	Maggie	33.00E-04	86.00E-04	20.00E-04	21.20E-05	10.05E-05	91.73E-06

4.4.4 Test Case 2: Two-Dimensional Case

A more complex problem is now visited and a two-dimensional function is addressed, defined as follows:

$$f(x, y) = \cos(y) \cdot \sin(x) \quad (4.22)$$

This is defined on a $[0, 4\pi] \times [0, 4\pi]$ domain where the corresponding centres distribution is depicted in Figure 4.32, and its surface is being visualized in Figure 4.33. To focus on the two main variable shape strategies. Five densities of centres were tested for each strategy to observe the overall behavior of the variable when dealing with larger sizes of datasets. The set of 17×17 equally-spaced is used for the target locations for approximation. As depicted in Figures 4.36 - Figures 4.41, all three forms; the function itself, its x -direction derivative, and its y -direction derivative, reveal the same trends of accuracy. Those functions' approximation produced by shape strategy 1 (or St₁) is found to be highly sensitive to the increase in centres (N) while St₂ is not. This could be attributed to the fact that St₁ is in an exponential curve where it can easily be affected by the pre-judged values of c_{\min} and c_{\max} , whose values depend on N . The best accuracy is found for St₁ when $\beta = -0.50$ and $N = 225$ are used where the comparatively worst results are revealed when $\beta = 2.50$ and $N = 625$ are used, see Figures 4.36, Figures 4.38 and Figures 4.40. The opposite scenario is found in the use of St₂ where $\beta = 2.50$ is clearly seen to outperform the rest for all three targeted function forms, see Figures 4.37, Figures 4.39 and Figures 4.41. As can be anticipated,

St_2 produces better solutions, for all values of β 's, when more supporting centres are involved, indicating the benefits one can achieve when deploying the strategy for larger datasets. It can also be seen from these same figures that the fastest reduction in error is obtained from $\beta = 2.50$ whereas the slowest one is from $\beta = -1.00$.

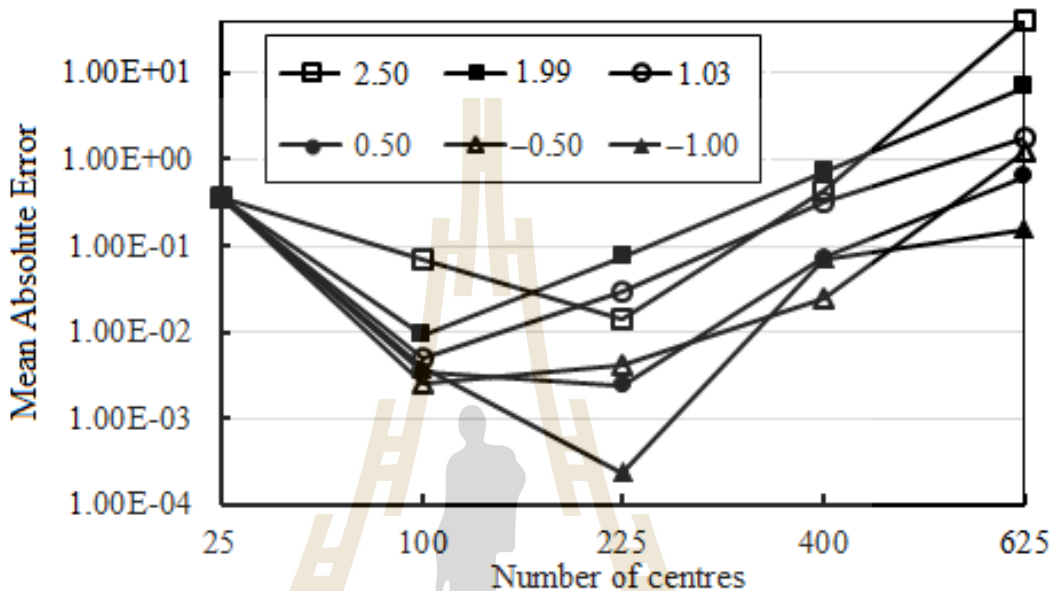


Figure 4.36 Mean absolute errors measured at different numbers of centres for approximation of $f(x,y)$ by using St_1 .

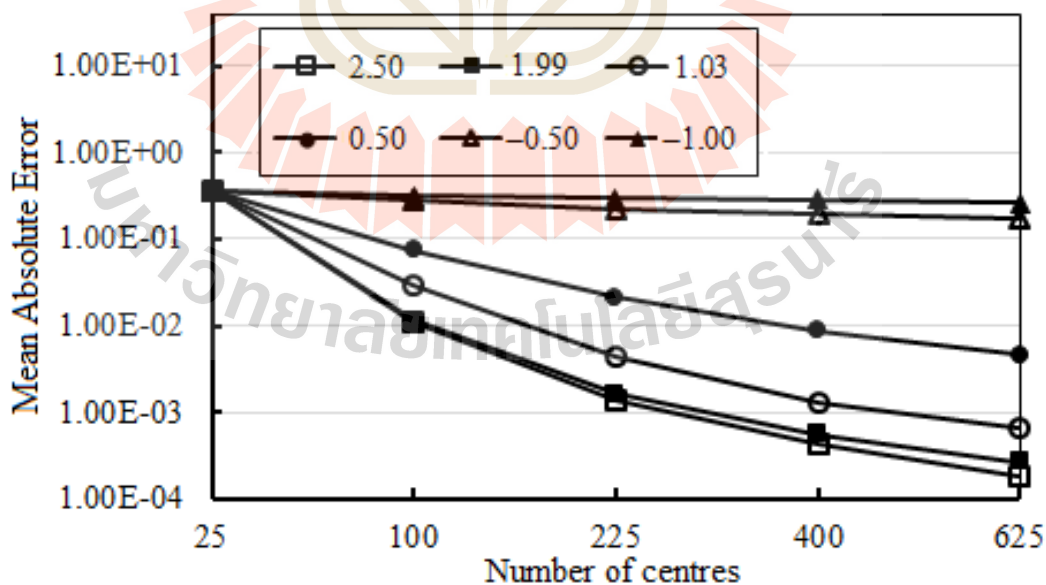


Figure 4.37 Mean absolute errors measured at different numbers of centres for approximation of $f(x,y)$ by using St_2 .

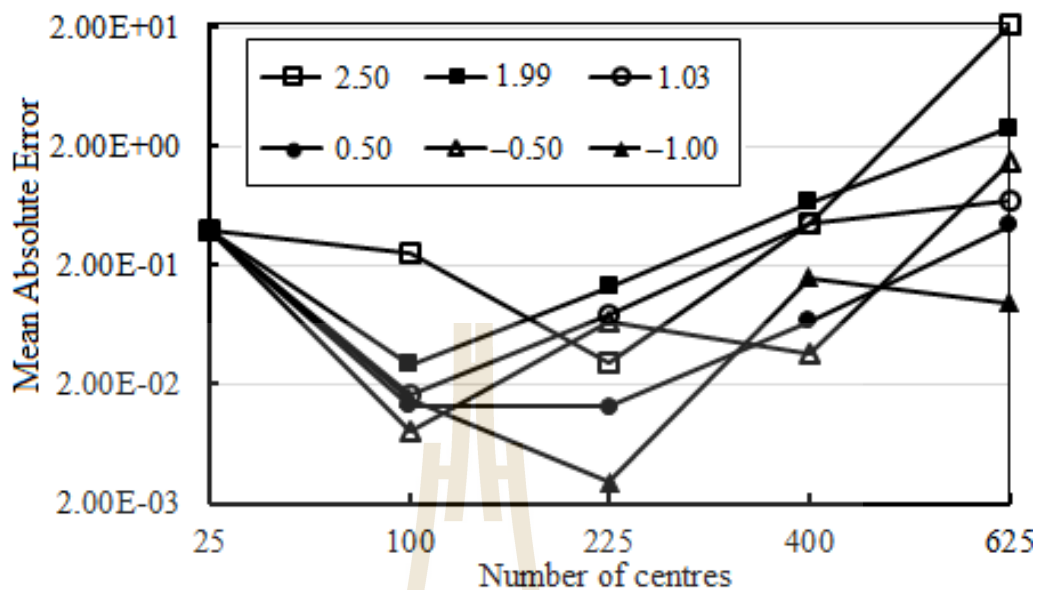


Figure 4.38 Mean absolute errors measured at different numbers of centres for approximation of $\partial f / \partial x$ by using $St\phi$.

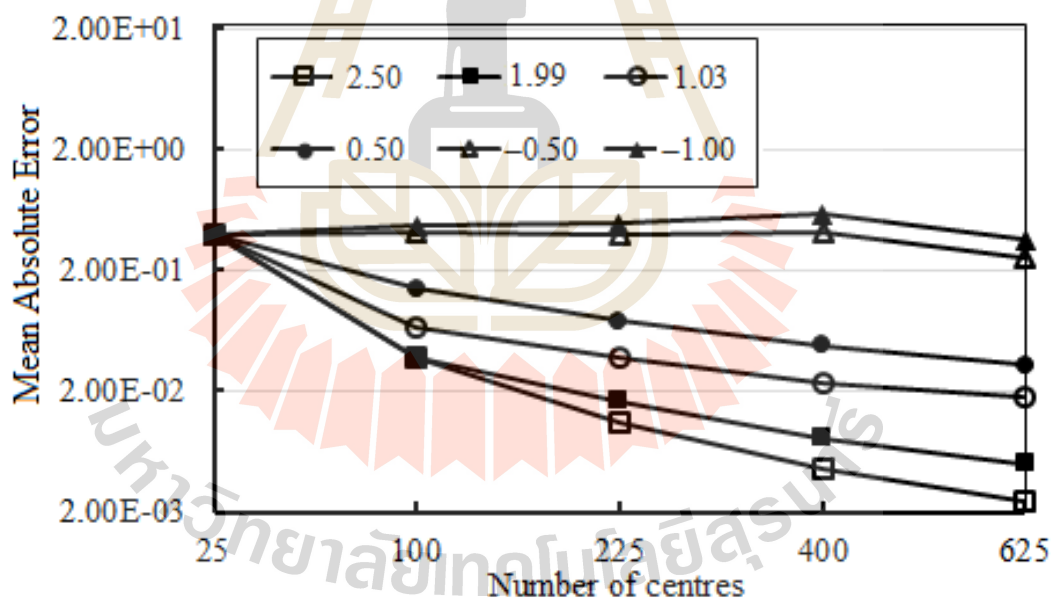


Figure 4.39 Mean absolute errors measured at different numbers of centres for approximation of $\partial f / \partial x$ by using $St\phi$.

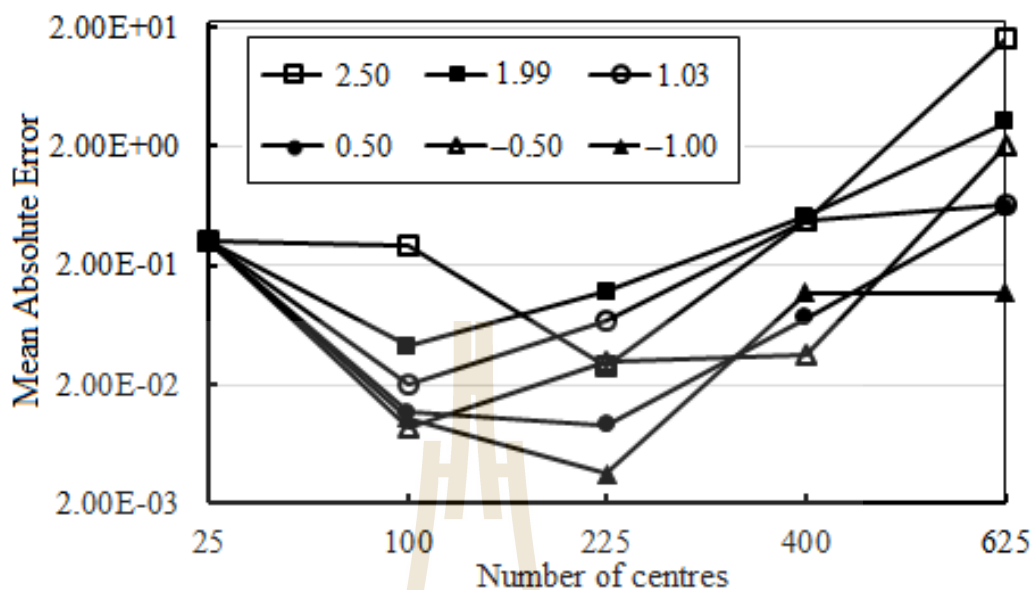


Figure 4.40 Mean absolute errors measured at different numbers of centres for approximation of $\partial f / \partial y$ by using Stq .

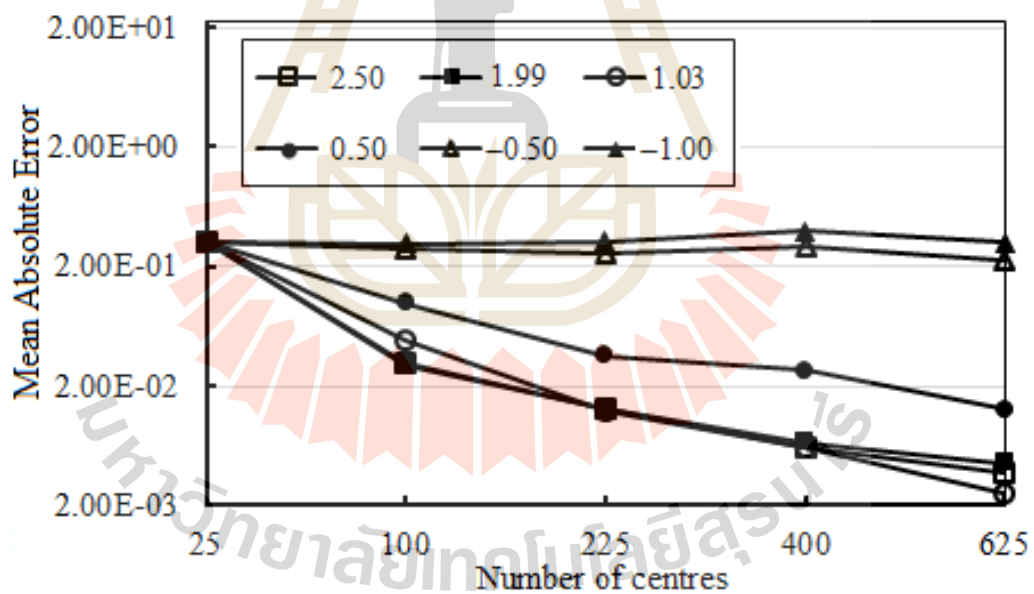
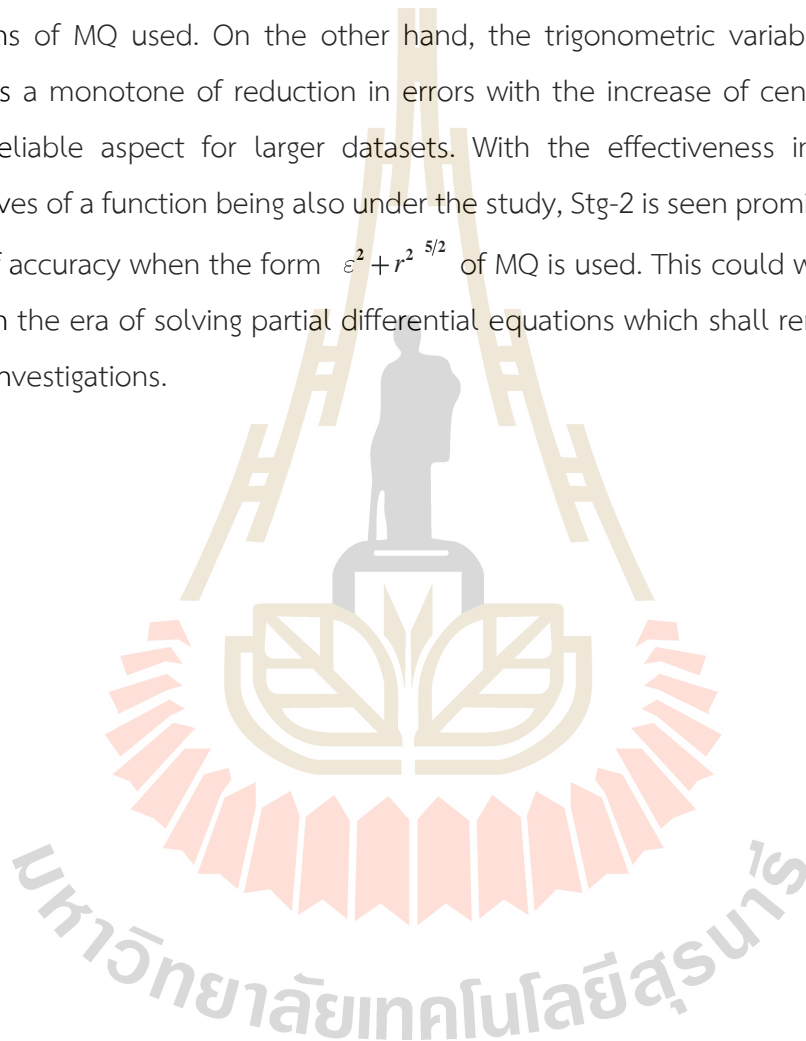


Figure 4.41 Mean absolute errors measured at different numbers of centres for approximation of $\partial f / \partial y$ by using Stq .

4.4.5 Main Conclusions

Emerging as an alternative numerical tool for approximating and recovering functions and their derivatives, multiquadric radial basis function neural networks (MQ-RBFNs) are under investigation in this work. Six generalized forms of MQ were numerically applied using two popular choices of shape parameters. It was found that the exponential variable shape (Stg-1) is highly sensitive to the number of centres for all forms of MQ used. On the other hand, the trigonometric variable shape (Stg-2) provides a monotone of reduction in errors with the increase of centres indicating a more reliable aspect for larger datasets. With the effectiveness in approximating derivatives of a function being also under the study, Stg-2 is seen promising with a great level of accuracy when the form $e^{-2} + r^{2.5/2}$ of MQ is used. This could well have a great effect in the era of solving partial differential equations which shall remain one of our future investigations.



CHAPTER V

THE MAIN NUMERICAL EXPERIMENT

5.1 The Project Objective

In this work, therefore, the main focus is paid on numerical investigation of the effectiveness of some of the most shapeless RBFs. The challenge is carried out under the context of pattern recognition through the structure of Radial Basis Function Neural Networks (RBF-NNs) where the effectiveness is validated using several criteria; accuracy, condition number, CUP-time and storage, user's interference, and the sensitivity to other factors.

Sixteen forms of shapeless RBFs, all of which have been receiving great attention over the past decade, are paid attention in this work and they are listed in Table 5.1. For the sake of comparison, the well-known shape-contained RBF namely 'Multiquadric, MQ' is also parallelly studied where the shape choosing scheme proposed by Carlson, 1991 (Carlson and Foley, 1991) is used. Differences in the curve profiles for each RBF can clearly be seen and noticed in Figure 5.1 – Figure 5.4.

Table 5.1 Type of Radial Basis Function.

No.	Name of RBF	Abbreviation	Definition
1	Multiquadric	MQ	$\sqrt{r^2 + \varepsilon^2}$
2	Polyharmonic spline	PS	$\begin{cases} r^{2k-1}, k \in \mathbb{N} \\ r^{2k} \ln r, k \in \mathbb{N} \end{cases}$
3	Thin plate splines	TPS	$r^2 \log r$
4	Wu's CS-RBFs (Wu, 1995)	WU1	$1 - r + \frac{7}{5} 5r^6 + 35r^5 + 101r^4 + 147r^3 + 101r^2 + 35r + 5$
5	Wu's CS-RBFs (Wu, 1995)	WU2	$1 - r + \frac{6}{6} 6r^5 + 30r^4 + 72r^3 + 82r^2 + 36r + 6$
6	Wu's CS-RBFs (Wu, 1995)	WU3	$1 - r + \frac{5}{5} 5r^4 + 25r^3 + 48r^2 + 40r + 8$
7	Wu's CS-RBFs (Wu, 1995)	WU4	$1 - r + \frac{4}{4} 5r^3 + 20r^2 + 29r + 16$
8	Wendland's CS-RBFs (Wendland, 1995)	WL1	$1 - r + \frac{1}{6} (1 - r)^3 (3r + 1)$
9	Wendland's CS-RBFs (Wendland, 1995)	WL2	$1 - r + \frac{3}{6} (1 - r)^3 (3r + 1)$
10	Wendland's CS-RBFs (Wendland, 1995)	WL3	$1 - r + \frac{5}{6} (1 - r)^3 (8r^2 + 5r + 1)$

Table 5.1 (continued).

No.	Name of RBF	Abbreviation	Definition
11	Wendland's CS-RBFs (Wendland, 1995)	WL4	$1 - r^2_+$
12	Wendland's CS-RBFs (Wendland, 1995)	WL5	$1 - r^4_+ 4r + 1$
13	Wendland's CS-RBFs (Wendland, 1995)	WL6	$1 - r^6_+ 35r^2 + 18r + 3$
14	Wendland's CS-RBFs (Wendland, 1995)	WL7	$1 - r^8_+ 32r^3 + 25r^2 + 8r + 1$
15	Buhmann (Buhmann, 1998)	BUH1	$\left(2r^4 \log r - \frac{7r^4}{2} + \frac{16r^3}{3} - 2r^2 + \frac{1}{6} \right)_+$
16	Buhmann (Buhmann, 1998)	BUH2	$\left(\frac{112r^9}{45} + \frac{16r^7}{3} - 7r^4 - \frac{14r^2}{15} + \frac{1}{9} \right)_+$
17	Buhmann (Buhmann, 1998)	BUH3	$\left(\frac{1}{18} - r^2 + \frac{4r^3}{9} + \frac{r^4}{2} - \frac{4r^3 \log r}{3} \right)_+$

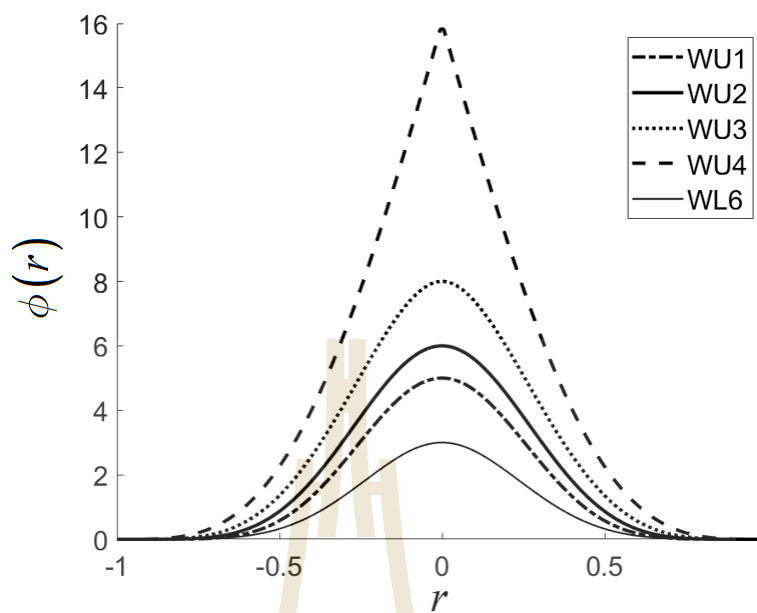


Figure 5.1 One-dimensional curve for some types of RBFs under this investigation of those containing no shapes (or shapefree) and $2 \leq \phi r \leq 16$.

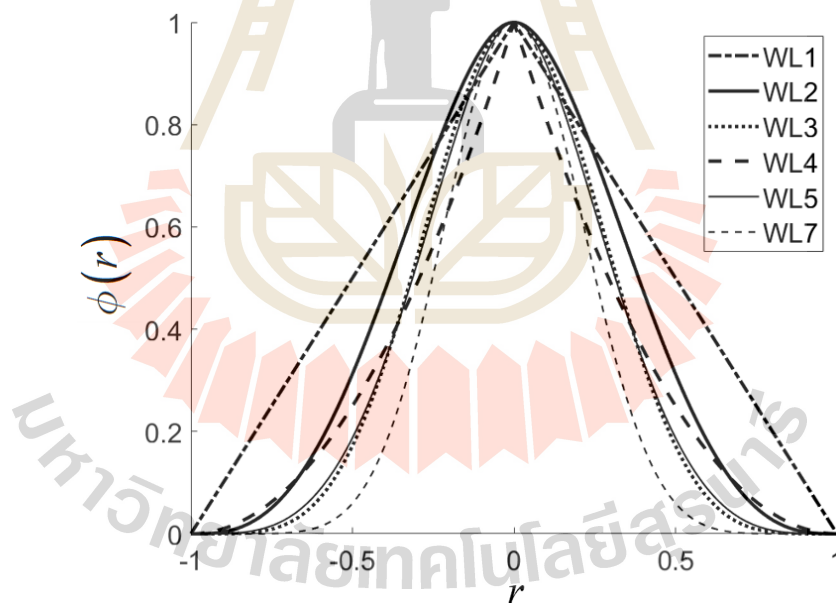


Figure 5.2 One-dimensional curve for some types of RBFs under this investigation of those containing no shapes (or shapefree) and $0.2 \leq \phi r \leq 2$.

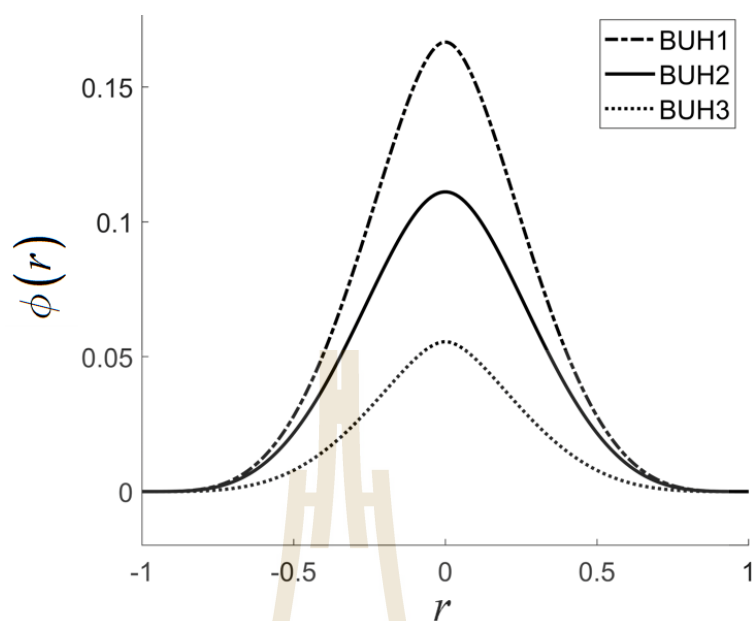


Figure 5.3 One-dimensional curve for some types of RBFs under this investigation of those containing no shapes (or shapefree) and $0 \leq \phi r \leq 0.2$.

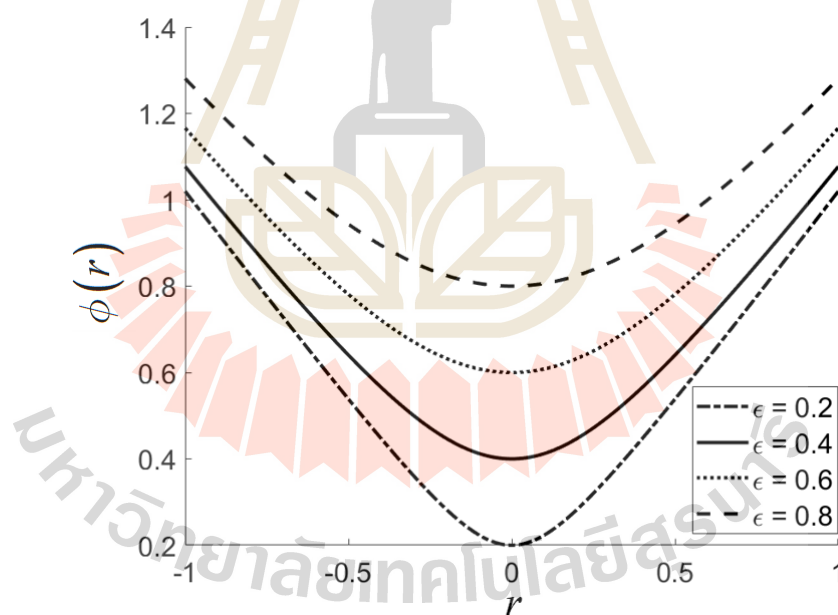


Figure 5.4 One-dimensional curve for the famous MQ with different shape values under this investigation.

5.2 Numerical Experiments and General Discussion

In this section, two well-known benchmarking test cases are numerically experimented using all the RBF forms studied in this work. Nevertheless, with the limitation of the space, only those significant and relevant results are being illustrated and discussed.

5.2.1 Experiment 1: Franke's function

This first experiment is concerned with one of the most well-known testing functions invented by Franke (Franke, 1982), and to be referred to as 'Franke's function' hereafter. The expression of the function is as follows:

$$z = f(x, y) = 0.75 \exp\left(-\frac{(9x-2)^2 + (9y-2)^2}{4}\right) + 0.75 \exp\left(-\frac{(9x+1)^2}{49} - \frac{9y+1}{10}\right) + 0.5 \exp\left(-\frac{(9x-7)^2 + (9y-3)^2}{4}\right) - 0.2 \exp(-(9x-4)^2 - (9y-7)^2). \quad (5.1)$$

The results validation for all RBFs for this first case is to be numerically investigated at two different noise levels (SNR); $SNR=15$ and 30 , as illustrated in Figure 5.5, Figure 5.6, Figure 5.9, and Figure 5.10.

As can be seen in Figure 5.5, Figure 5.6, Figure 5.9, and Figure 5.10 that the accuracy, measured by both L_∞ and L_{RMS} from both cases of node distribution manners, slightly decreases with the increase of noise variance. This is not surprising as the pattern becomes more complicated with data being more disturbed with noise.

In terms of the number of centres (m) generated by the RC-algorithm, at $SNR=30$ and with comparatively low values of L_∞ , L_{RMS} , and condition numbers, it is found that $m=87$, $m=100$ and $m=83$ are reproduced for WU3, WL5, and BUH2, respectively. This figure can be seen as a good success of these RBFs, taking 2,500 original into consideration, while good accuracy is still achievable (see Table 5.2 and Table 5.4). Table 5.3 also shows the similar figure of these RBFs $SNR=30$ confirming their positive potential for further uses. The ability to preserve the data's pattern while using small number of nodes is desirable for any kind of RBF in practical applications. Small number in m also strongly affects both CPU-time and storage required for each computation process as clearly seen in Figure 5.7 and Figure 5.8 for $SNR=30$ and Figure 5.11 and Figure 5.12 for $SNR=15$.

5.2.1.1 Performance at $SNR = 30$

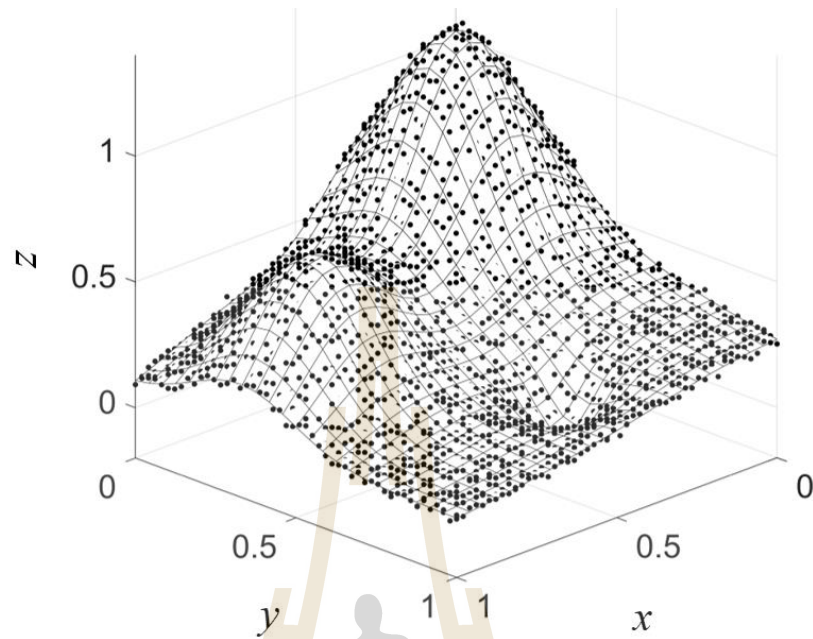


Figure 5.5 Noised- $z(x, y)$ training datasets with $SNR = 30$ based on uniformly distribution of $\{(x, y)\}$.

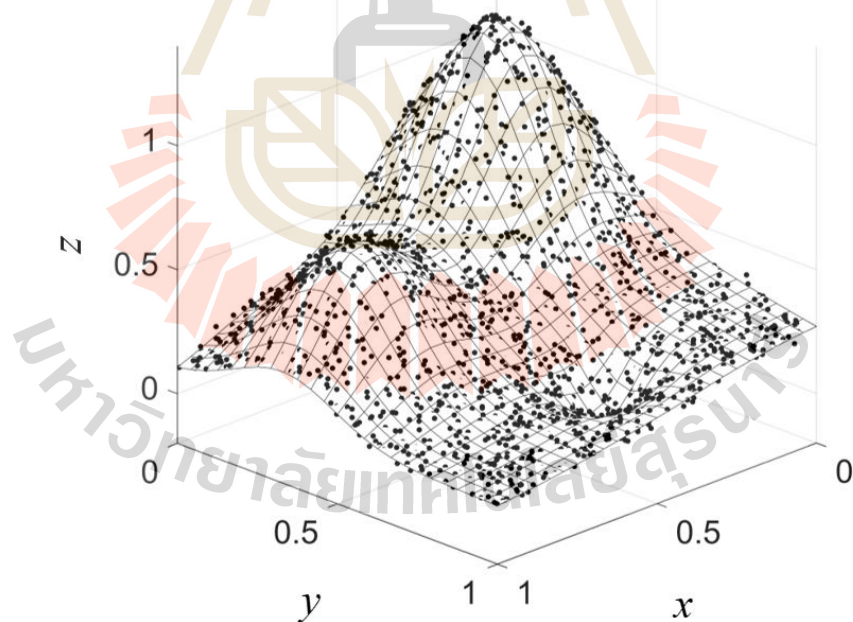
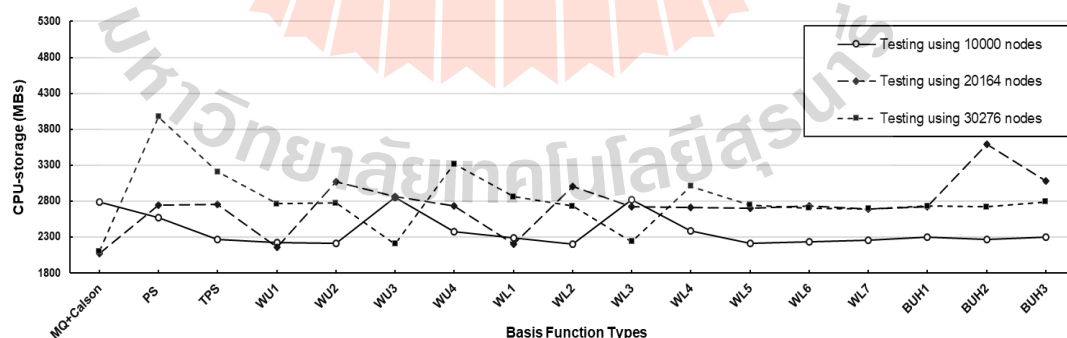


Figure 5.6 Noised- $z(x, y)$ training datasets with $SNR = 30$ based on non-uniformly (randomly) distribution of $\{(x, y)\}$.

Table 5.2 Training and testing errors measured for Franke's function at $SNR = 30$.

Types of RBF	Uniform nodes distribution				Random nodes distribution			
	L_{∞}		L_{RMSE}		L_{∞}		L_{RMSE}	
	Training	Testing	Training	Testing	Training	Testing	Training	Testing
MQ+	1.77E-01	1.55E-01	3.57E-02	3.18E-02	1.99E-01	2.19E-01	3.78E-02	3.58E-02
Carlson								
PS	5.50E-02	7.60E-01	1.15E-02	8.39E-02	5.75E-02	2.60E+00	1.24E-02	1.20E-01
TPS	5.48E-02	3.54E-02	1.51E-02	6.50E-03	5.73E-02	1.52E-01	1.49E-02	7.60E-03
WU1	1.07E-01	8.19E-02	2.04E-02	1.33E-02	9.10E-02	8.66E-02	2.08E-02	1.45E-02
WU2	8.03E-02	5.80E-02	1.84E-02	1.00E-02	6.03E-02	5.00E-02	1.72E-02	8.20E-03
WU3	5.80E-02	2.58E-02	1.57E-02	3.90E-03	5.75E-02	2.26E-02	1.54E-02	3.80E-03
WU4	5.65E-02	3.07E-02	1.34E-02	7.10E-03	4.63E-02	3.08E-02	1.31E-02	7.10E-03
WL1	6.26E-02	5.13E-02	1.53E-02	6.00E-03	6.72E-02	7.88E-02	1.53E-02	6.60E-03
WL2	6.19E-02	3.72E-02	1.65E-02	6.20E-03	5.84E-02	3.09E-02	1.58E-02	4.90E-03
WL3	6.84E-02	4.64E-02	1.70E-02	7.50E-03	5.92E-02	3.61E-02	1.62E-02	5.40E-03
WL4	5.93E-02	2.98E-02	1.38E-02	6.70E-03	5.70E-02	3.90E-02	1.37E-02	6.30E-03
WL5	5.64E-02	1.76E-02	1.55E-02	3.70E-03	5.74E-02	2.01E-02	1.54E-02	3.90E-03
WL6	5.83E-02	2.45E-02	1.59E-02	4.40E-03	6.09E-02	3.71E-02	1.60E-02	5.70E-03
WL7	6.14E-02	3.72E-02	1.63E-02	5.80E-03	6.12E-02	3.74E-02	1.60E-02	5.60E-03
BUH1	5.74E-02	2.00E-02	1.55E-02	4.00E-03	5.56E-02	2.78E-02	1.52E-02	3.70E-03
BUH2	5.66E-02	1.95E-02	1.56E-02	3.60E-03	5.74E-02	2.39E-02	1.54E-02	3.50E-03
BUH3	5.68E-02	1.45E-02	1.51E-02	4.10E-03	5.63E-02	1.80E-02	1.50E-02	4.30E-03

**Figure 5.7** CPU-storage measurement observed at three different sizes of testing datasets with uniform nodes distribution using $SNR = 30$.

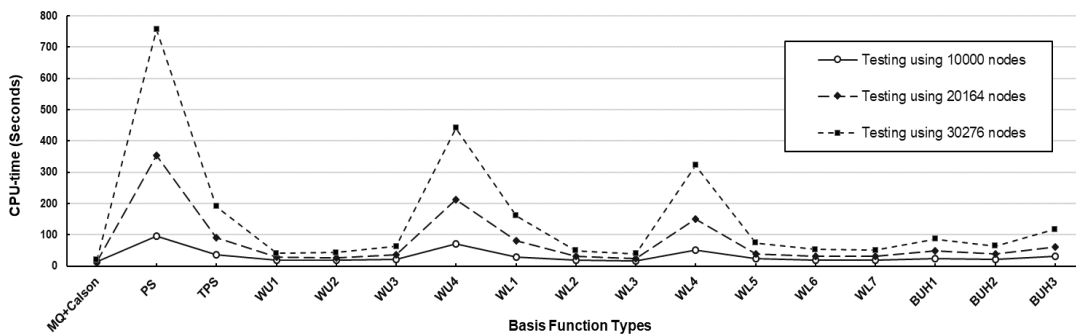


Figure 5.8 CPU-time measurement observed at three different sizes of testing datasets as uniform nodes distribution using $SNR = 30$.

5.2.1.2 Performance at $SNR = 15$

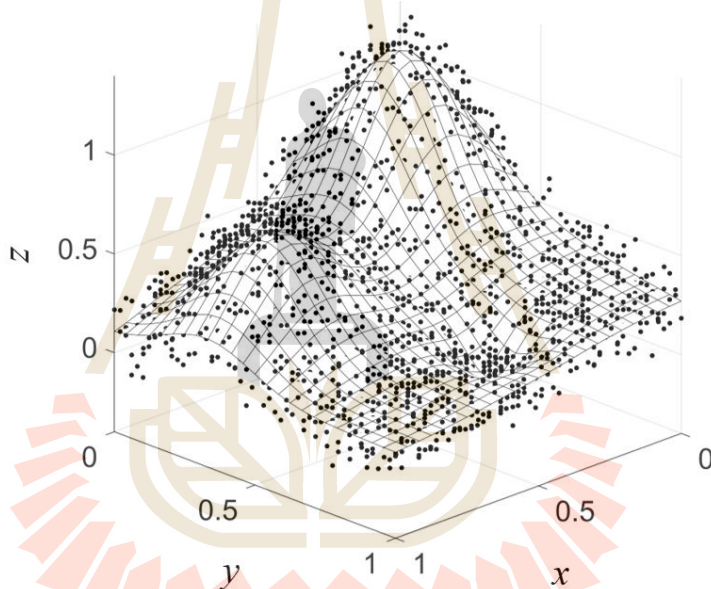


Figure 5.9 Noised- $z(x,y)$ training datasets with $SNR = 15$ based on uniformly distribution of $\{(x,y)\}$.

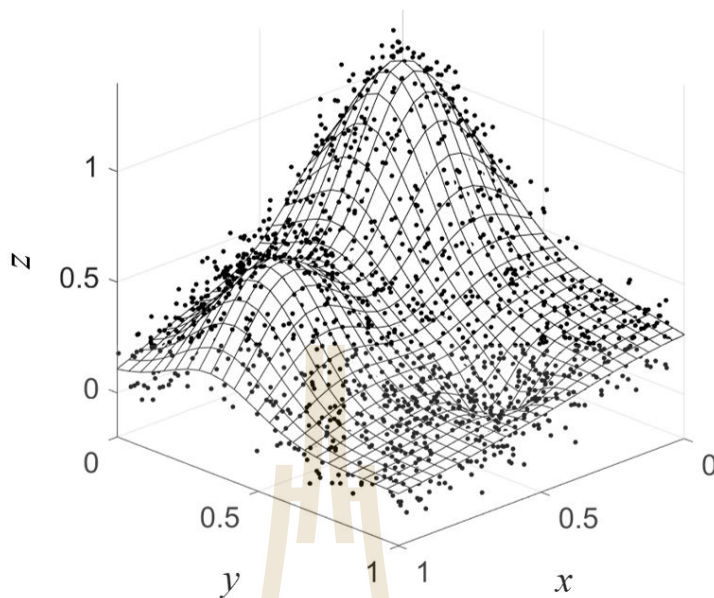


Figure 5.10 Noised- $z(x, y)$ training datasets with $SNR=15$ based on non-uniformly (randomly) distribution of $\{(x, y)\}$.

Table 5.3 Training and testing errors measured for Franke's function at $SNR=15$.

Types of RBF	Uniform nodes distribution				Random nodes distribution			
	L_∞		L_{RMSE}		L_∞		L_{RMSE}	
	Training	Testing	Training	Testing	Training	Testing	Training	Testing
MQ+Carlson	3.50E-01	2.55E-01	9.84E-02	3.88E-02	4.02E-01	2.02E-01	9.30E-02	3.75E-02
PS	2.90E-01	4.27E+00	6.36E-02	3.28E-01	3.02E-01	3.92E+00	6.55E-02	3.34E-01
TPS	2.76E-01	1.56E-01	8.40E-02	3.18E-02	2.90E-01	1.92E-01	8.15E-02	3.19E-02
WU1	3.56E-01	8.46E-02	8.97E-02	1.76E-02	3.09E-01	1.06E-01	8.63E-02	1.91E-02
WU2	3.39E-01	6.11E-02	8.93E-02	1.56E-02	3.00E-01	7.43E-02	8.54E-02	1.55E-02
WU3	3.26E-01	6.36E-02	8.82E-02	1.81E-02	2.75E-01	6.31E-02	8.44E-02	1.82E-02
WU4	3.36E-01	2.02E-01	7.60E-02	4.27E-02	2.62E-01	1.92E-01	7.35E-02	3.82E-02
WL1	3.17E-01	1.03E-01	8.51E-02	2.91E-02	3.02E-01	1.11E-01	8.22E-02	2.53E-02
WL2	3.30E-01	6.13E-02	8.89E-02	1.66E-02	2.99E-01	6.40E-02	8.51E-02	1.57E-02
WL3	3.44E-01	5.93E-02	8.93E-02	1.49E-02	2.91E-01	6.91E-02	8.52E-02	1.52E-02
WL4	3.52E-01	1.68E-01	7.94E-02	3.87E-02	2.70E-01	1.61E-01	7.66E-02	3.42E-02
WL5	3.22E-01	6.49E-02	8.81E-02	1.86E-02	2.72E-01	5.87E-02	8.44E-02	1.83E-02
WL6	3.32E-01	7.15E-02	8.87E-02	1.64E-02	2.77E-01	7.17E-02	8.49E-02	1.73E-02
WL7	3.29E-01	7.20E-02	8.89E-02	1.63E-02	2.83E-01	7.05E-02	8.50E-02	1.68E-02
BUH1	3.25E-01	7.75E-02	8.77E-02	2.04E-02	2.77E-01	8.06E-02	8.39E-02	2.06E-02
BUH2	3.20E-01	8.29E-02	8.83E-02	1.77E-02	2.73E-01	5.88E-02	8.46E-02	1.73E-02
BUH3	3.20E-01	1.03E-01	8.68E-02	2.34E-02	2.85E-01	9.31E-02	8.34E-02	2.25E-02

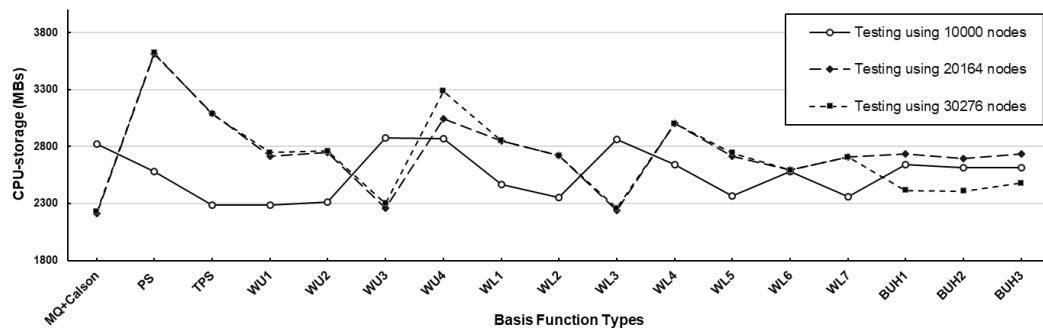


Figure 5.11 CPU-storage measurement observed at three different sizes of testing datasets with random nodes distribution using $SNR = 15$.

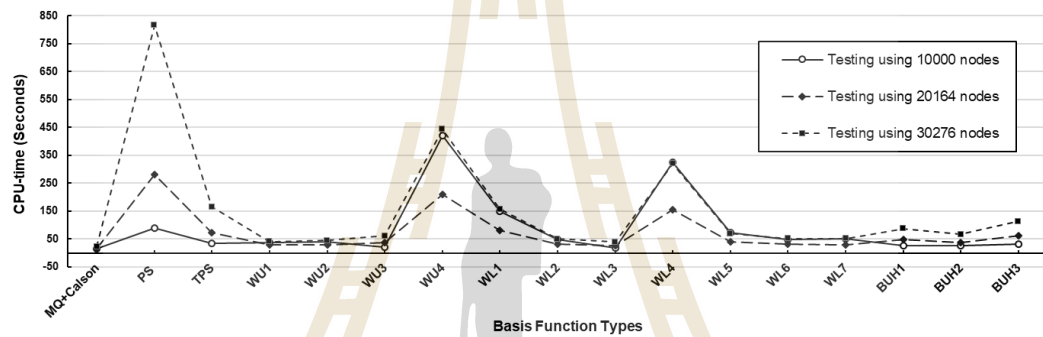


Figure 5.12 CPU-time measurement observed at three different sizes of testing datasets with random nodes distribution using $SNR = 15$.

Table 5.4 The number of centres (m) and the condition number ($Cond_{\infty}(\cdot)$) of all radial basis function candidates for the Franke's function test case.

Types of RBF	$SNR = 30$				$SNR = 15$			
	m		$Cond_{\infty}(\cdot)$		m		$Cond_{\infty}(\cdot)$	
	Ufm.	Rdm.	Ufm.	Rdm.	Ufm.	Rdm.	Ufm.	Rdm.
MQ+Carlson	19	19	5.41E+03	6.44E+03	19	19	5.84E+03	6.02E+03
PS	1239	996	2.92E+04	2.39E+04	1239	996	2.92E+04	2.39E+04
TPS	295	243	1.40E+04	1.32E+04	295	243	1.40E+04	1.32E+04
WU1	41	39	8.26E+03	6.62E+03	41	39	8.26E+03	6.62E+03
WU2	47	47	6.99E+03	9.16E+03	47	47	6.99E+03	9.16E+03
WU3	87	83	9.01E+03	9.35E+03	87	83	9.01E+03	9.35E+03
WU4	689	662	9.29E+03	8.32E+03	689	662	9.29E+03	8.32E+03
WL1	245	234	9.62E+03	9.77E+03	245	234	9.62E+03	9.77E+03
WL2	64	62	9.28E+03	8.53E+03	64	62	9.28E+03	8.53E+03
WL3	51	50	7.02E+03	7.86E+03	51	50	7.02E+03	7.86E+03

Table 5.4 (continued).

Types of RBF	$SNR = 30$				$SNR = 15$			
	m		$Cond_{\infty}(\cdot)$		m		$Cond_{\infty}(\cdot)$	
	Ufm.	Rdm.	Ufm.	Rdm.	Ufm.	Rdm.	Ufm.	Rdm.
WL4	511	504	9.25E+03	7.95E+03	511	504	9.25E+03	7.95E+03
WL5	100	94	1.23E+04	1.01E+04	100	94	1.23E+04	1.01E+04
WL6	69	65	1.07E+04	8.81E+03	69	65	1.07E+04	8.81E+03
WL7	64	62	8.71E+03	8.57E+03	64	62	8.71E+03	8.57E+03
BUH1	117	113	1.13E+04	1.01E+04	117	113	1.13E+04	1.01E+04
BUH2	83	78	1.22E+04	9.22E+03	83	78	1.22E+04	9.22E+03
BUH3	164	154	1.10E+04	1.24E+04	164	154	1.10E+04	1.24E+04

5.2.2 Experiment 2: F7

For the second test case, we study one of the functions called F7 in the investigated nicely carried out by R. J. Renka and R. Brown (Renka and Brown, 1999), (and shall be referred to as ‘F7’ in this work as well). The function is defined as follows.

$$z = f(x, y) = 2\cos(10x)\sin(10y) + \sin(10xy). \quad (5.2)$$

Similarly to the first experiment, two different noise levels (SNR); $SNR=15$ and 30 are under the investigation with their nodes distributions are illustrated in Figure 5.13, Figure 5.14, Figure 5.17 and Figure 5.18, respectively.

With the results obtained in these cases, shown in Table 5.5, Table 5.6, and Table 5.7, together with information provided in Figure 5.15 and Figure 5.16, it has been observed that the overall trends in accuracy (both L_{∞} and L_{RMS}) are similar to those discovered in the first experiment (with F1) where some smaller errors are noticed in the cases of WL6 and WL7. Moreover, the similarity to the first experiment in terms of the number of centres (m) produced by each shapeless RBF after undergoing the RC-algorithm is also noticeable here. This is due to the fact that with no parameter involved this values are dependent only the distance between two nodes. In the case of MQ, nevertheless, with different values of shape parameter generated by Carlson algorithm, the change in the number of centres (m) shall be anticipated.

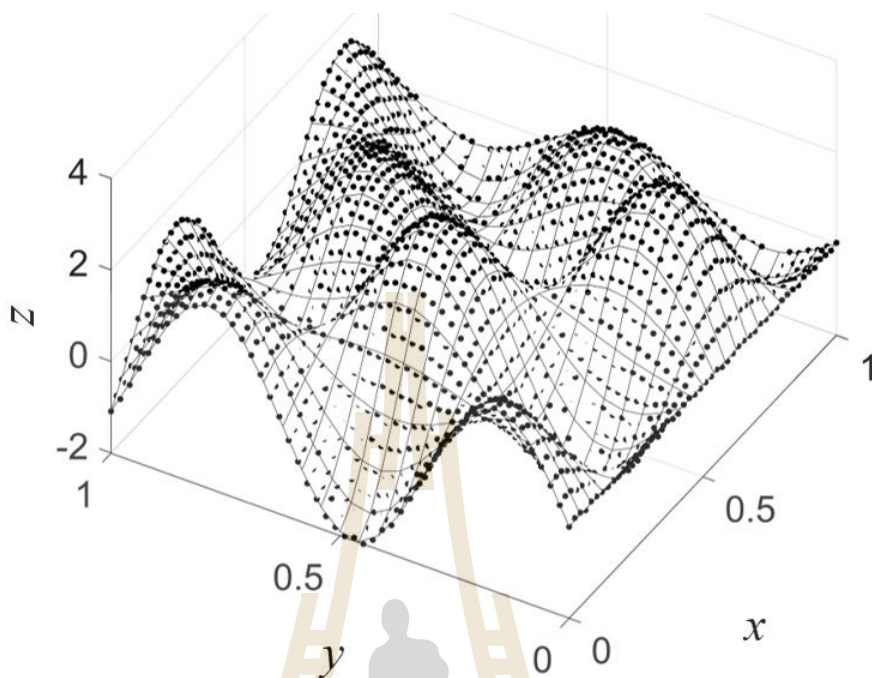
5.2.2.1 Performance at $SNR=30$ 

Figure 5.13 Noised- $z(x,y)$ training datasets based on uniformly distribution of $\{(x,y)\}$.

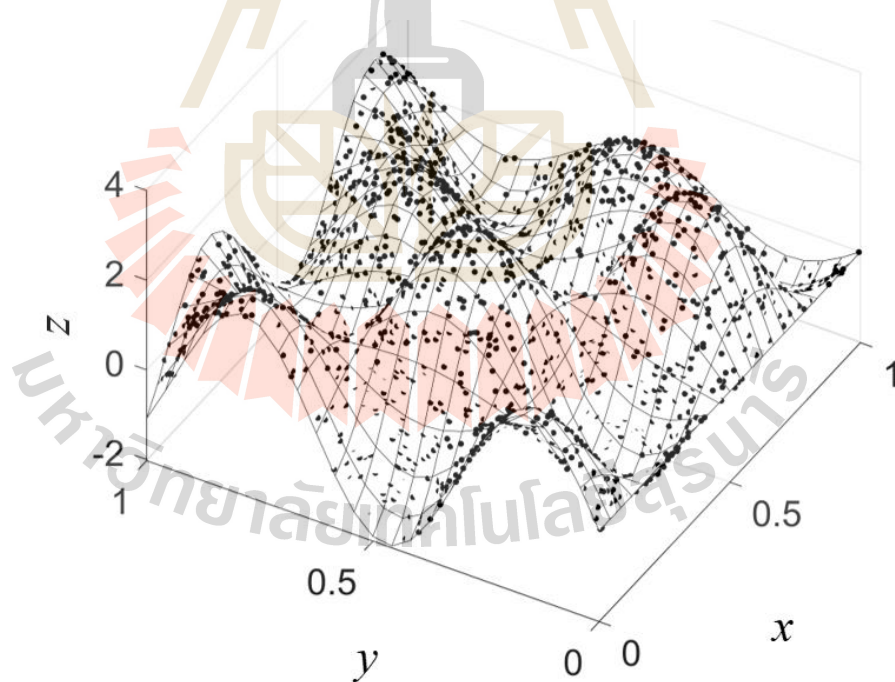
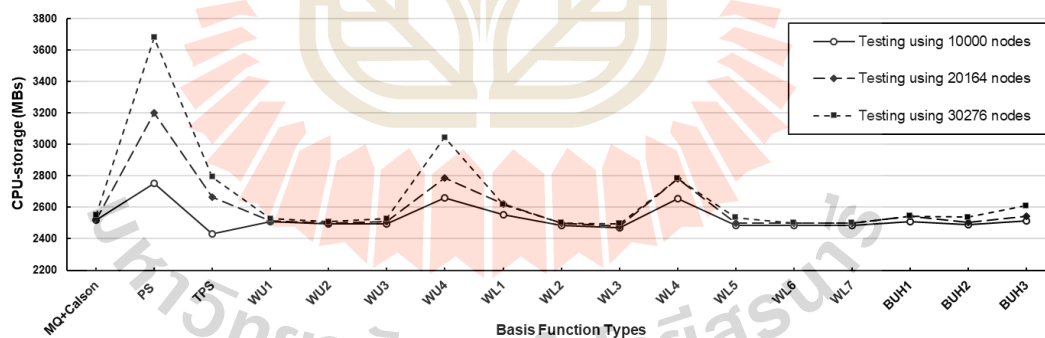


Figure 5.14 Noised- $z(x,y)$ training datasets based on non-uniformly (randomly) distribution of $\{(x,y)\}$.

Table 5.5 Training and testing errors measured for F7 at $SNR = 30$.

Types of RBF	Uniform nodes distribution				Random nodes distribution			
	L_{∞}		L_{RMSE}		L_{∞}		L_{RMSE}	
	Training	Testing	Training	Testing	Training	Testing	Training	Testing
MQ+Carlson	4.93E-01	4.38E-01	1.03E-01	9.38E-02	5.84E-01	6.33E-01	1.06E-01	1.10E-01
PS	2.90E-01	1.26E+01	6.65E-02	1.15E+00	2.33E-01	2.28E+01	4.78E-02	1.18E+00
TPS	3.88E-01	4.48E-01	6.88E-02	5.98E-02	4.55E-01	1.14E+00	6.24E-02	8.27E-02
WU1	7.16E-01	6.96E-01	1.49E-01	1.40E-01	1.12E+00	1.78E+00	1.71E-01	1.83E-01
WU2	4.84E-01	4.74E-01	9.45E-02	8.42E-02	5.00E-01	5.72E-01	8.64E-02	8.66E-02
WU3	1.93E-01	1.94E-01	4.65E-02	3.06E-02	2.14E-01	2.72E-01	4.46E-02	3.50E-02
WU4	1.14E-01	7.67E-02	3.03E-02	1.63E-02	1.39E-01	7.50E-01	2.94E-02	2.67E-02
WL1	1.08E+00	1.08E+00	7.74E-02	6.27E-02	8.93E-01	2.80E+00	7.54E-02	9.60E-02
WL2	3.99E-01	4.03E-01	7.21E-02	6.05E-02	6.38E-01	7.21E-01	7.25E-02	7.09E-02
WL3	4.92E-01	4.77E-01	9.19E-02	8.18E-02	2.31E-01	3.27E-01	5.80E-02	5.27E-02
WL4	1.29E-01	7.42E-02	3.20E-02	1.54E-02	1.69E-01	8.44E-01	3.20E-02	3.03E-02
WL5	1.86E-01	1.43E-01	3.94E-02	2.08E-02	1.98E-01	2.62E-01	4.20E-02	3.20E-02
WL6	2.00E-01	2.17E-01	4.17E-02	2.45E-02	2.18E-01	2.22E-01	4.33E-02	3.14E-02
WL7	1.89E-01	1.72E-01	4.41E-02	2.68E-02	1.95E-01	2.13E-01	4.23E-02	2.99E-02
BUH1	1.27E-01	8.67E-02	3.62E-02	1.60E-02	1.89E-01	5.10E-01	3.85E-02	2.76E-02
BUH2	1.66E-01	1.36E-01	4.10E-02	2.36E-02	2.17E-01	2.37E-01	4.55E-02	3.57E-02
BUH3	1.47E-01	8.09E-02	3.45E-02	1.30E-02	1.23E-01	4.18E-01	3.47E-02	1.88E-02

Figure 5.15 CPU-storage measurement observed at three different sizes of testing datasets with uniform nodes distribution using $SNR = 30$.

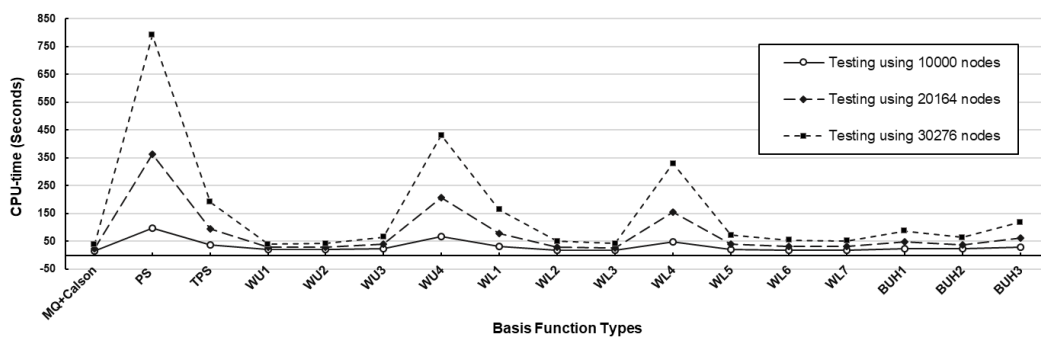


Figure 5.16 CPU-time measurement observed at three different sizes of testing datasets with uniform nodes distribution using $SNR = 30$.

5.2.2.2 Performance at $SNR = 15$

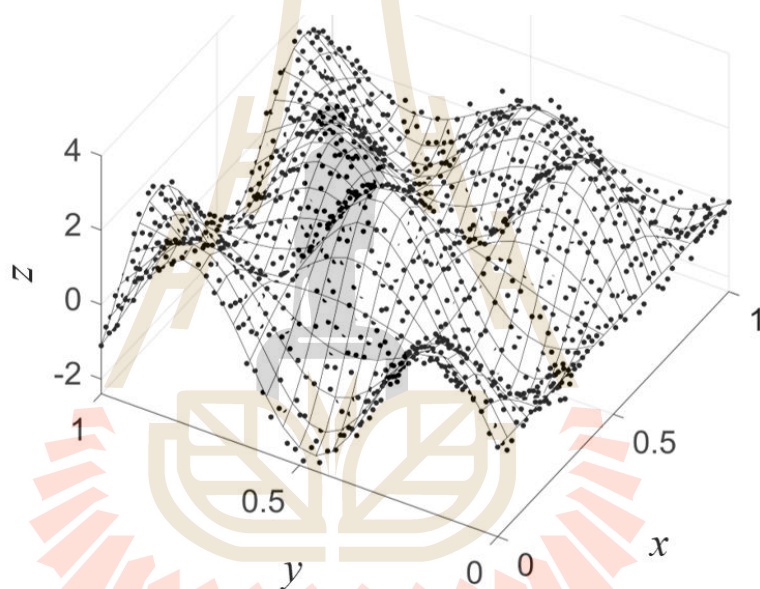


Figure 5.17 Noised- $z(x,y)$ training datasets based on uniformly distribution of $\{(x,y)\}$.

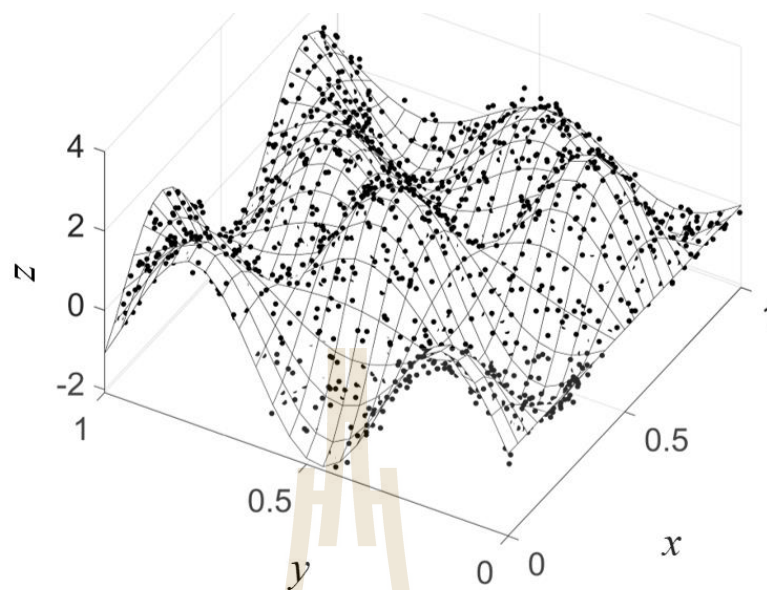


Figure 5.18 Noised- $z(x,y)$ training datasets based non-uniformly (randomly) distribution of $\{(x,y)\}$.

Table 5.6 Training and testing errors measured for F7 at $SNR = 15$.

Types of RBF	Uniform nodes distribution				Random nodes distribution			
	L_∞		L_{RMSE}		L_∞		L_{RMSE}	
	Training	Testing	Training	Testing	Training	Testing	Training	Testing
MQ+Carlson	1.12E+00	7.32E-01	2.37E-01	1.38E-01	9.91E-01	7.55E-01	2.15E-01	1.16E-01
PS	6.88E-01	1.58E+01	1.52E-01	1.35E+00	6.82E-01	2.56E+01	1.50E-01	1.35E+00
TPS	7.51E-01	4.71E-01	1.92E-01	8.70E-02	7.27E-01	1.28E+00	1.88E-01	1.10E-01
WU 1	9.39E-01	7.39E-01	2.40E-01	1.41E-01	1.26E+00	1.96E+00	2.54E-01	1.86E-01
WU 2	8.34E-01	5.10E-01	2.10E-01	8.69E-02	9.69E-01	5.20E-01	2.05E-01	8.92E-02
WU 3	7.31E-01	1.91E-01	1.93E-01	4.60E-02	7.85E-01	2.83E-01	1.90E-01	4.88E-02
WU 4	7.00E-01	4.72E-01	1.65E-01	8.91E-02	6.37E-01	8.65E-01	1.64E-01	8.95E-02
WL 1	1.15E+00	1.13E+00	1.96E-01	8.31E-02	8.27E-01	3.24E+00	1.93E-01	1.15E-01
WL 2	7.43E-01	3.51E-01	2.01E-01	6.72E-02	9.69E-01	6.64E-01	2.02E-01	7.77E-02
WL 3	8.41E-01	4.51E-01	2.10E-01	8.38E-02	9.16E-01	3.31E-01	1.94E-01	5.86E-02
WL 4	7.23E-01	3.70E-01	1.72E-01	8.04E-02	6.43E-01	8.41E-01	1.71E-01	7.98E-02
WL 5	7.08E-01	1.51E-01	1.90E-01	4.33E-02	8.01E-01	2.79E-01	1.89E-01	5.04E-02
WL 6	7.05E-01	1.57E-01	1.92E-01	3.88E-02	7.92E-01	2.69E-01	1.90E-01	4.36E-02
WL 7	7.05E-01	1.89E-01	1.92E-01	3.85E-02	7.88E-01	2.06E-01	1.90E-01	4.24E-02
BUH 1	7.05E-01	1.55E-01	1.89E-01	4.40E-02	7.40E-01	4.54E-01	1.87E-01	4.98E-02
BUH 2	7.14E-01	1.67E-01	1.91E-01	4.16E-02	8.34E-01	2.82E-01	1.91E-01	4.96E-02
BUH 3	7.20E-01	2.23E-01	1.87E-01	5.05E-02	7.82E-01	3.79E-01	1.84E-01	5.21E-02

Table 5.7 The number of centres (m) and the condition number ($Cond_{\infty}(\cdot)$) of all radial basis function candidates for the F7 test case.

Types of RBF	$SNR = 30$				$SNR = 15$			
	m		$Cond_{\infty}(\cdot)$		m		$Cond_{\infty}(\cdot)$	
	Ufm.	Rdm.	Ufm.	Rdm.	Ufm.	Rdm.	Ufm.	Rdm.
MQ+Carlson	49	47	9.93E+03	1.20E+04	43	46	1.06E+04	8.56E+03
PS	1239	996	2.92E+04	2.39E+04	1239	996	2.92E+04	2.39E+04
TPS	295	243	1.40E+04	1.32E+04	295	243	1.40E+04	1.32E+04
WU1	41	39	8.26E+03	6.62E+03	41	39	8.26E+03	6.62E+03
WU2	47	47	6.99E+03	9.16E+03	47	47	6.99E+03	9.16E+03
WU3	87	83	9.01E+03	9.35E+03	87	83	9.01E+03	9.35E+03
WU4	689	662	9.29E+03	8.32E+03	689	662	9.29E+03	8.32E+03
WL1	245	234	9.62E+03	9.77E+03	245	234	9.62E+03	9.77E+03
WL2	64	62	9.28E+03	8.53E+03	64	62	9.28E+03	8.53E+03
WL3	51	50	7.02E+03	7.86E+03	51	50	7.02E+03	7.86E+03
WL4	511	504	9.25E+03	7.95E+03	511	504	9.25E+03	7.95E+03
WL5	100	94	1.23E+04	1.01E+04	100	94	1.23E+04	1.01E+04
WL6	69	65	1.07E+04	8.81E+03	69	65	1.07E+04	8.81E+03
WL7	64	62	8.71E+03	8.57E+03	64	62	8.71E+03	8.57E+03
BUH1	117	113	1.13E+04	1.01E+04	117	113	1.13E+04	1.01E+04
BUH2	83	78	1.22E+04	9.22E+03	83	78	1.22E+04	9.22E+03
BUH3	164	154	1.10E+04	1.24E+04	164	154	1.10E+04	1.24E+04

From all the numerical results obtained so far and in addition to the criteria stated, it has to be acknowledged that ‘overfitting and overfitting’ is another crucial figure to be considered. Regarding all cases, a significant reduction in accuracy, measured by both error norms, produced by PS type of RBF strongly indicates its overfitting nature and shall not be recommended for practical uses. On the other hand, WL5, BUH1, WU3, and BUH2 are seen to be slightly under fitting for both numerical demonstrations. The best types of RBF in terms of this aspect are WU1, WU2, WL1, WL4, and MQ.

5.3 Main Conclusions

This work aims to provide insights of the use of sixteen forms of radial basis function (RBF) containing no shape parameter, so they are referred to as ‘shapeless RBFs’. The challenge under the main experiment is the problem of pattern recognition through neural networks computation process and architecture. The ability to deal with large and noised datasets of each shapeless RBF is measured under several criteria against the well-known shape-containing RBF called multiquadric (MQ). Two testing functions are tackled and important findings observed based on each criterion are listed below.

1. Accuracy (L_∞ and L_{RMSE}): The best three shapeless RBFs are WL6, WL7, and BUH3, whereas PS, WU1, and MQ are found to produce the least accurate results.

2. The condition number ($Cond_\infty(\cdot)$): The best three are WU1, WU2, and WL3 with the comparatively worse ones being PS, TPS, and WL5.

3. In terms of CPU (time and storage) and also the number of centres (m): MQ, WL3 and WL6 are seen to be the most desirable whereas PS, WU4, and WL4 are not so promising under these criteria.

4. User’s Interference: It is obvious that as long as no parameter-turning process is required, there is no need to interfere the algorithm and this is one desirable aspect of using shapeless RBF. This is also the case for the sensitivity-to-parameter criteria.

5. Ease of implementation: It is observed that all shapeless RBF types under this work are as equally simple when it comes to implementing the scheme. For MQ, on the other hand, an additional coding routine may be needed for the process of a reliable shape searching procedure, as is the case in this investigation for Carlson algorithm.

Together with the ‘overfitting and underfitting’ aspect, this work suggests that shapeless RBFs from Wu’s and Wendland’s families are highly promising, whereas the rest forms are still skeptical for practical uses. Apart from this useful piece of information for pattern recognition application, it might be considered a weakness of the work that the figure discovered so far may change when dealing with other kinds of applications such as direct interpolation, function approximation, and recovery, as well as solving different equations (DEs) under the concepts of meshless or meshfree

methods. Furthermore, other kinds of node distribution of sizes may result in different aspects. This is all set as our future research direction and is highly recommended for interested researchers to further explore.



CHAPTER VI

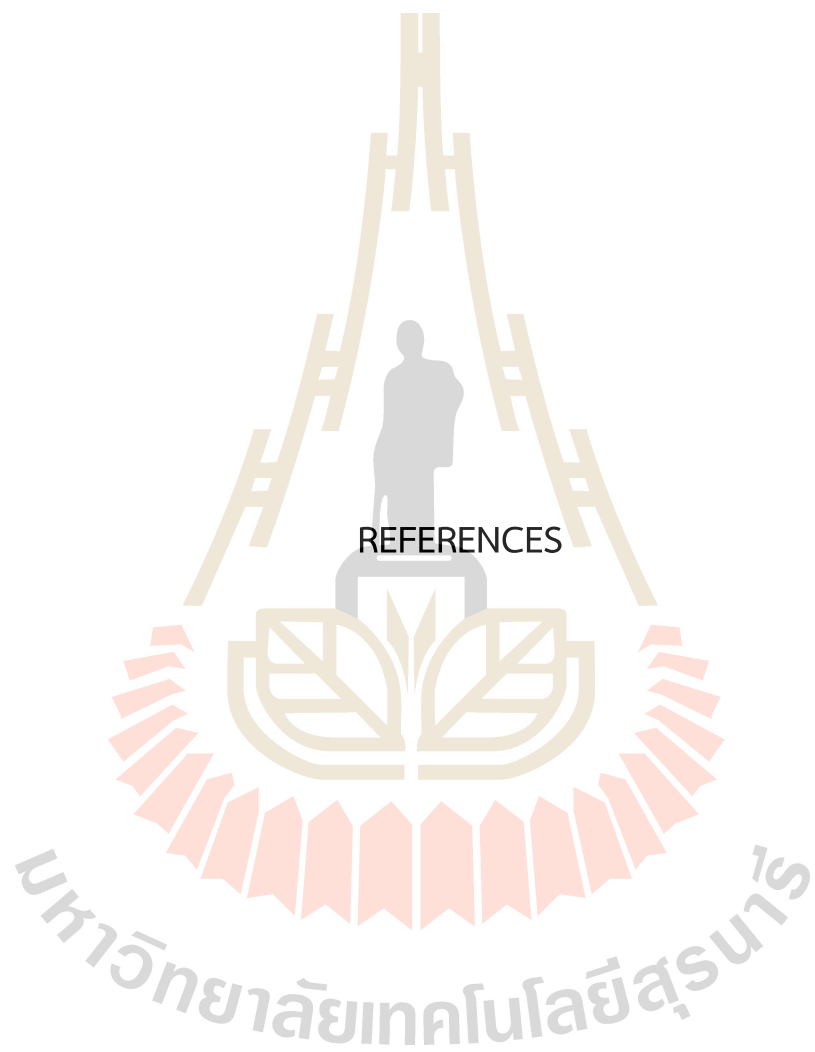
CONCLUSIONS

In this study, the main attention is paid to numerically investigate the overall performances of newly-proposed radial basis functions (RBFs). These RBFs have a special feature where they contain no shape parameter so they are referred to as 'shapeless-RBF'. A structure of neural network under the application of pattern recognition is utilized and a total of sixteen forms of shapeless RBFs have been paid attention to. Before reaching the point where all these RBFs were investigated, there had been five numerical experiments carried out in three main different contexts; pattern recognition, function recovery, and PDEs solution approximation.

Together with all the preliminary results previously obtained, the main and important findings discovered in this work can be listed as follows:

1. As long as a shape-contained RBF is in use, the most challenging task is still the search for an optimal value of the shape, no matter what context it is applied under.
2. Different forms of RBF require different values of shape meaning that there is no such thing as 'optimal shape' for all RBFs.
3. Taking into consideration all the performance criteria stated in this work, shapeless RBFs have been proved to comparatively be promising whereas the pain of searching for a good shape has been eliminated.
4. Amongst the sixteen forms of shapeless RBFs under this investigation, the results have shown that those in Wu's and Wendland's families can well be good alternatives.

It is also recommended in this work that the experiment is extended to more complex problems with higher dimension and/or node distribution manners. Moreover, other applications such as function recovery or solving differential equations are also of interest.



REFERENCES

- Radial basis function artificial neural network for the investigation of Thyroid Cytological Lesions, *Journal of Thyroid Research*, 2020.
- Franke, R. (1979). A critical comparison of some methods for interpolation of scattered data, Naval Postgraduate School, Technical Report NPS-53-79-003.
- Franke, R. (1982) Scattered Data Interpolation: Tests of Some Method, *Mathematics of Computation*, 38(157), 181–200. doi.org/10.2307/2007474
- Hardy, R. L. (1971). Multiquadric equations of topography and other irregular surfaces, *Journal of Geophysical Research*, 76(8), 1905-1915. doi.org/10.1029/JB076i008p01905
- Hardy, R. L. (1977) Least Squares Prediction Photogrammetric, *Engineering and Remote Sensing*, 43(4), 475-492.
- Hemageetha, N., and Nasir, G. M. (2013). Radial basis function model for vegetable price prediction, Proceedings of the 2013 International Conference on Pattern Recognition, Informatics and Mobile Engineering, Salem, India. 424-428. doi: 10.1109/ICPRIME.2013.6496514
- Kaennakham, S., and Chuathong, N. (2017) Solution to a Convection-Diffusion Problem Using a New Variable Inverse-Multiquadric Parameter in a Collocation Meshfree Scheme, *International Journal of Multiphysics*, 4, 359-374, doi.org/10.21152/1750-9548.11.4.359
- Lazzaro, D., and Montefusco, L. B. (2002) Radial basis functions for the multivariate interpolation of large scattered data sets, *Journal of Computational and Applied Mathematics*, 140, 521–536.
- Nojavan, H., Abbasbandy, S., and Allahviranloo, T. (2017) Variable shape parameter strategy in local radial basis functions collocation method for solving the 2D nonlinear coupled Burgers' equations. *Mathematics*, 5(3), 1-21. doi.org/10.3390/math5030038.
- Paolanti, M., and Frontoni, E. (2020) Multidisciplinary pattern recognition applications: a review, *Emanuele Frontoni*, 37. doi: 10.1016/j.cosrev.2020.100276

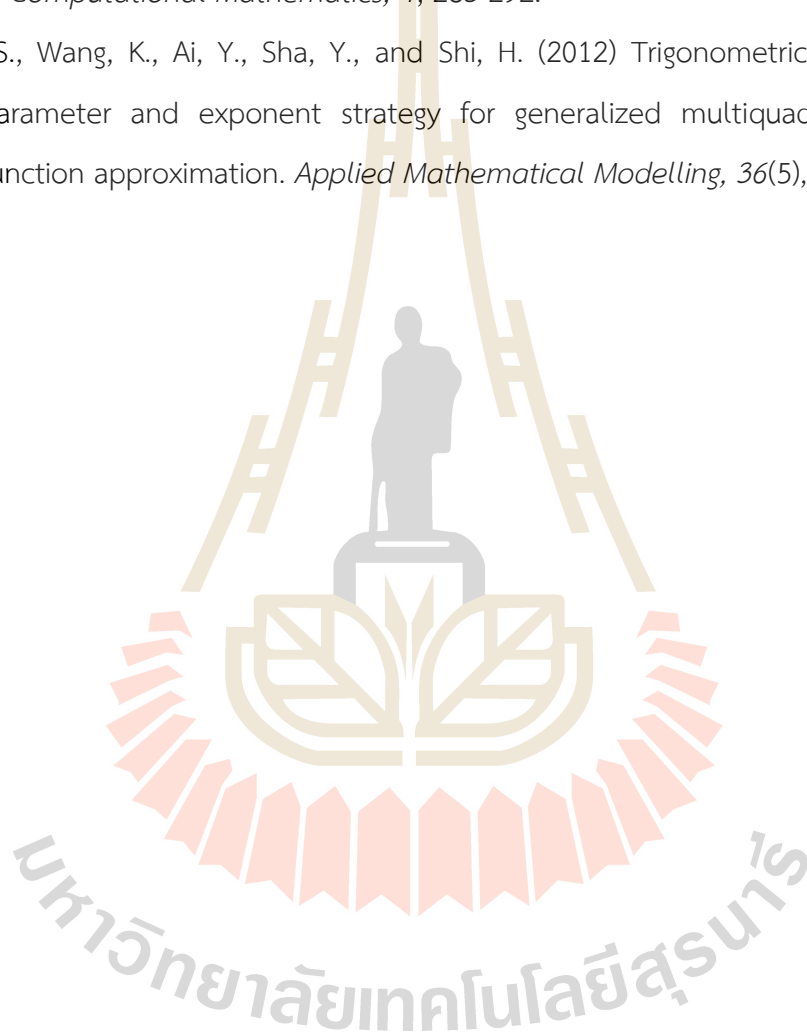
- Parasher, M., Sharma, S., Sharma, A.K., and Gupta, J.P. (2011) Anatomy on pattern recognition, *Indian Journal of Computer Science and Engineering (IJCSE)*, 2(3), 371-378.
- Powell, M. J. D. (1987). Radial basis functions for multivariable interpolation: a review, in *Algorithms for approximation*, Clarendon Press, United States, 143–167.
- Rashedi, K. A., Ismail, M. T., Hamadneh, N. N., Wadi, S. AL, Jaber J. J. and Tahir, M. (2021). Application of radial basis function neural network coupling particle swarm optimization algorithm to classification of Saudi Arabia stock returns, *Journal of Mathematics*, 5, 1-8. doi: <https://doi.org/10.1155/2021/5593705>
- Renka, R. J., and Brown, R. (1999) Algorithm 792: accuracy tests of ACM algorithms for interpolation of scattered data in the plane, *ACM Transactions on Mathematical Software*, 25(1), 78–94. doi.org/10.1145/305658.305745.
- Rippa, S. (1999) An algorithm for selecting a good value for the parameter c in radial basis function interpolation. *Advances in Computational Mathematics*, 11, 193–210. doi.org/10.1023/A:1018975909870
- Shastry, K. A., Sanjay, H. A., and Deexith, G. (2017). Quadratic-radial-basis-function-kernel for classifying multi-class agricultural datasets with continuous attributes, *Applied Soft Computing Journal*, 58, 65-74. <https://doi.org/10.1016/j.asoc.2017.04.049>
- Shin, M. (1998) Design and evaluation of radial basis function model for function approximation. Syracuse University, Syracuse, NY, United States.
- Shin, M., and Park C. (2000) A radial basis function approach to pattern recognition and its applications, *ETRI Journal*, 22(2).
- Tavaen, S., Viriyapong, R., and Kaennakham, S. (2020) Performances of non-parameterised radial basis functions in pattern recognition applications, *Journal of Physics: Conference Series*, 1706(1):012165, doi: 10.1088/1742-6596/1706/1/012165
- Winston, P. H. (1993). *Artificial Intelligence*. Addison-Wesley Publishing Company.
- Wang, R., Li, D., and Miao, K. (2020). Optimized radial basis function neural network based intelligent control algorithm of unmanned surface vehicles. *Journal of*

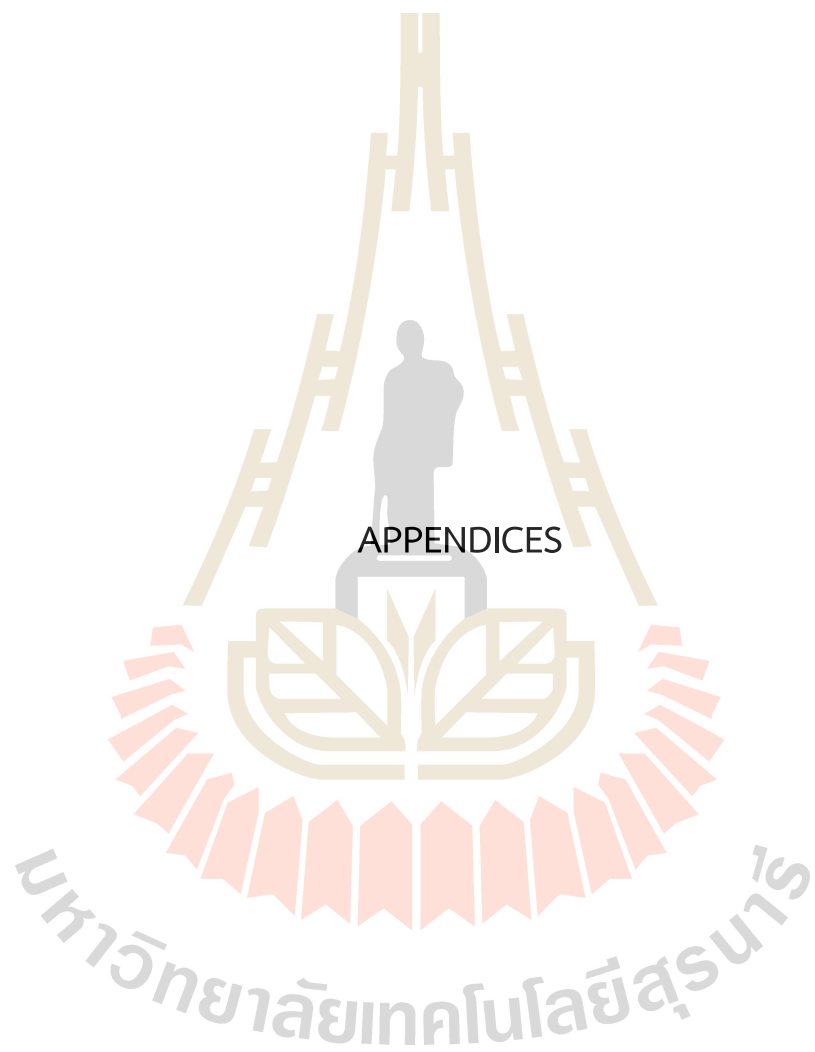
Marine Science and Engineering, 8(3). doi: 10.3390/jmse8030210

Wendland, H. (1995) Piecewise polynomial, positive definite and compactly supported radial functions of minimal degree, *Advances in Computational Mathematics*, 4, 389-396. doi: <https://doi.org/10.1007/BF02123482>.

Wu, Z. (1995) Compactly supported positive definite radial basis functions, *Advances in Computational Mathematics*, 4, 283-292.

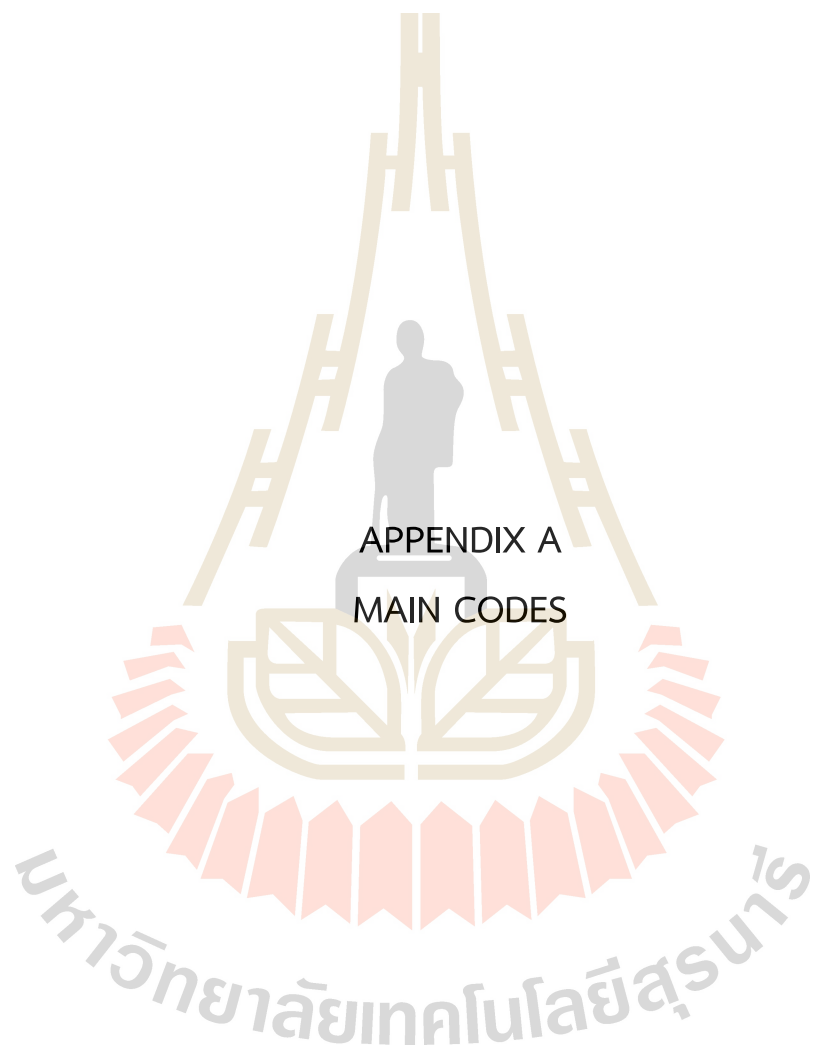
Xiang, S., Wang, K., Ai, Y., Sha, Y., and Shi, H. (2012) Trigonometric variable shape parameter and exponent strategy for generalized multiquadric radial basis function approximation. *Applied Mathematical Modelling*, 36(5), 1931-1931





APPENDICES

มหาวิทยาลัยเทคโนโลยีสุรนารี



APPENDIX A
MAIN CODES

A.1 Main Code 1: Experiment 2

A.1.1 Test Case 1: Linear interpolation

A.1.1.1 Training and validation errors for candidate models for linear interpolation case.

```

1 clc
2 clear all
3 close all
4
5 %*****
6 %----- Step 1:Generate training dataset -----
7 %*****
8 for i=1:100
9 X_trn(i)=2*pi*(i-1)/100;
10 end
11 Y_trn =awgn(2*X_trn +1,15,'measured');%Y_trn with Gaussian noise
12 for i=1:100
13 for j=1:100
14 XY_trn (i,1)=X_trn (i);
15 XY_trn (j,2)=Y_trn (j);
16 end
17 end
18 XY_trn;
19
20 N_tr = length(X_trn);
21
22 %*****
23 %----- Step 2:Normalizing both X_trn and Y_trn -----
24 %*****
25 xlmax = max(X_trn);
26 X_trnN=(X_trn -min(X_trn))/(xlmax); % Normalized X_trn
27 Y_trnN=(Y_trn -min(Y_trn))/(max(Y_trn)-min(Y_trn)); % Normalized Y_trn
28
29 %*****
30 %----- Step 3:Choosing the shape parameter-----
31 %*****
32 shp = input('Enter the shape parameter = ');
33
34 %*****
35 %----- Step 4:Construct the interpolation matrix-----
36 %----- CS_RBF1, CS1, CS2, G-----
37 %*****
38 for i=1:N_tr
39 for j=1:N_tr
40 r(i,j)=abs(X_trnN (1,i)-X_trnN (1,j));
41 CS_RBF1(i,j)=(1/3)+r(i,j).^2-(4/3)*r(i,j).^3+2*r(i,j).^2*log(r(i,j));
42 CS1(i,j)=(112/45)*r(i,j)^(9/2)+(16/3)*r(i,j)^(7/2)-7*r(i,j).^4-(14/15)*r(i,j).^2+(1/9);
43 CS2(i,j)=(1/18)*r(i,j).^2+(4/9)*r(i,j).^3+0.5*r(i,j).^4-(4/3)*r(i,j).^3*log(r(i,j));
44 G(i,j)=exp(-r(i,j)^2/(2*shp^2));
45 if r(i,j)== 0
46 CS_RBF1(i,j)=(1/3)+r(i,j).^2-(4/3)*r(i,j).^3;
47 CS2(i,j)=(1/18)*r(i,j).^2+(4/9)*r(i,j).^3+0.5*r(i,j).^4;
48 end

```

```

49 end
50 end
51
52 %*****
53 %-----Step 5:Using SVD to get the number of centres-----
54 %-----out of matrix CS_RBF1, CS1, CS2, G -----
55 %*****
56 delta = 0.01/100;
57
58 %----- Step 5.1:CS_RBF1 -----
59 [U_CS_RBF1,S_CS_RBF1,V_CS_RBF1]=svd(CS_RBF1);
60 S11_CS_RBF1 = S_CS_RBF1(1,1);
61 %The firsts singular of singular value
62 S1_CS_RBF1 = S11_CS_RBF1*(delta);
63
64 for i=1:N_tr
65 Sii_CS_RBF1 = S_CS_RBF1(i,i);
66 if Sii_CS_RBF1 <= S1_CS_RBF1
67 M_CS_RBF1 = i-1;
68 break
69 end
70 i = i+1 ;
71 end
72
73 %----- Step 5.2:CS1 -----
74 [U_CS1,S_CS1,V_CS1]=svd(CS1);
75 S11_CS1 = S_CS1(1,1);
76 %The firsts singular of singular value
77 S1_CS1 = S11_CS1*(delta);
78 for i=1:N_tr
79 Sii_CS1 = S_CS1(i,i);
80 if Sii_CS1 <= S1_CS1
81 M_CS1 = i-1;
82 break
83 end
84 i = i+1 ;
85 end
86
87 %----- Step 5.3:CS2 -----
88 [U_CS2,S_CS2,V_CS2]=svd(CS2);
89 S11_CS2 = S_CS2(1,1);
90 %The firsts singular of singular value
91 S1_CS2 = S11_CS2*(delta);
92
93 for i=1:N_tr
94 Sii_CS2 = S_CS2(i,i);
95 if Sii_CS2 <= S1_CS2
96 M_CS2 = i-1;
97 break
98 end
99 i = i+1 ;
100 end
101
102 %----- Step 5.4:Gaussian RBF-----
103 [U, S, V]=svd(G);
104 S11 = S(1,1);
105 S1 = S11*(delta);
106

```

```

107 for i=1:N_tr
108 Sii = S(i,i);
109 if Sii <= S1 ;
110 M = i-1 ;
111 break
112 end
113 i = i+1 ;
114 end
115
116 %*****
117 %----- Step 6:Using QR to find the centres of-----
118 %----- basis function and the location of centres -----
119 %*****
120 %----- Step 6.1:CS_RBF1 -----
121 V1_CS_RBF1 = -V_CS_RBF1;
122 V11_CS_RBF1=V1_CS_RBF1(1:M_CS_RBF1,1:M_CS_RBF1);
123 %partition matrix
124 V21_CS_RBF1=V1_CS_RBF1(M_CS_RBF1+1:N_tr,1:M_CS_RBF1);
125 V2_CS_RBF1 = [V11_CS_RBF1' V21_CS_RBF1'];
126
127 [Q_CS_RBF1,R_CS_RBF1,P_CS_RBF1]=qr(V2_CS_RBF1);
128 mu_CS_RBF1 = X_trnN*P_CS_RBF1;
129 Xctr_CS_RBF1 = mu_CS_RBF1(1,1:M_CS_RBF1);
130
131 %----- Step 6.2:CS1 -----
132 V1_CS1 = -V_CS1;
133 V11_CS1=V1_CS1(1:M_CS1,1:M_CS1);
134 %partition matrix V
135 V21_CS1=V1_CS1(M_CS1+1:N_tr,1:M_CS1);
136 V2_CS1 = [V11_CS1' V21_CS1'];
137
138 [Q_CS1,R_CS1,P_CS1]=qr(V2_CS1);
139 mu_CS1 = X_trnN*P_CS1;
140 Xctr_CS1 = mu_CS1(1,1:M_CS1);
141
142 %----- Step 6.3:CS2 -----
143 V1_CS2 = -V_CS2;
144 V11_CS2=V1_CS2(1:M_CS2,1:M_CS2);
145 %partition matrix V
146 V21_CS2=V1_CS2(M_CS2+1:N_tr,1:M_CS2);
147 V2_CS2 = [V11_CS2' V21_CS2'];
148
149 [Q_CS2,R_CS2,P_CS2]=qr(V2_CS2);
150 mu_CS2 = X_trnN*P_CS2;
151 Xctr_CS2 = mu_CS2(1,1:M_CS2);
152
153 %----- Step 6.4:Gaussian RBF-----
154 V1 = -V;
155 V11=V1(1:M,1:M); %partition matrix V
156 V21=V1(M+1:N_tr,1:M);
157 V2 = [V11' V21'];
158 [Q,R,P]=qr(V2);
159 mu = X_trnN*P;
160 Xctr = mu(1,1:M)
161
162 %*****
163 %----- Step 7:Construct the interpolation matrix-----

```

```

164 %*****
165 %----- Step 7.1:CS_RBF1 -----
166 for i=1:N_tr
167 for j=1:M_CS_RBF1
168 r1_CS_RBF1(i,j)=abs(X_trnN(1,i)-Xctr_CS_RBF1(1,j));
169 Phi_CS_RBF1(i,j)=(1/3)+r1_CS_RBF1(i,j).^2-
    (4/3)*r1_CS_RBF1(i,j).^3+2*(r1_CS_RBF1(i,j).^2)*log(r1_CS_RBF1(i,j));
170 if r1_CS_RBF1(i,j)== 0
171 Phi_CS_RBF1(i,j)=(1/3)+r1_CS_RBF1(i,j).^2-(4/3)*r1_CS_RBF1(i,j).^3;
172 end
173 end
174 end
175
176 %----- Step 7.2:CS1 -----
177 for i=1:N_tr
178 for j=1:M_CS1
179 r1_CS1(i,j)=abs(X_trnN (1,i)-Xctr_CS1(1,j));
180 Phi_CS1(i,j)=(112/45)*r1_CS1(i,j)^(9/2)+(16/3)*r1_CS1(i,j)^(7/2)-7*r1_CS1(i,j).^4-
    (14/15)*r1_CS1(i,j).^2+(1/9);
181 end
182 end
183
184 %----- Step 7.3:CS2 -----
185 for i=1:N_tr
186 for j=1:M_CS2
187 r1_CS2(i,j)=abs(X_trnN (1,i)-Xctr_CS2(1,j));
188 Phi_CS2(i,j)=(1/18)*r1_CS2(i,j).^2+(4/9)*r1_CS2(i,j).^3+0.5*r1_CS2(i,j).^4-
    (4/3)*r1_CS2(i,j).^3*log(r1_CS2(i,j));
189 if r1_CS2(i,j)== 0
190 Phi_CS2(i,j)=(1/18)*r1_CS2(i,j).^2+(4/9)*r1_CS2(i,j).^3+0.5*r1_CS2(i,j).^4;
191 end
192 end
193 end
194
195 %----- Step 7.4:Gaussian RBF -----
196 for i=1:N_tr
197 for j=1:M
198 r1(i,j)=abs(X_trnN (1,i)-Xctr(1,j));
199 Phi(i,j)=exp(-(r1(i,j))^2/(2*(shp^2)));
200 end
201 end
202
203 %*****
204 %----- Step 8:Computing the weight 'w' -----
205 %*****
206 %Moore-Penrose Pseudoinverse of matrix
207 w_CS_RBF1 =pinv(Phi_CS_RBF1)*Y_trnN;
208 w_CS1 = pinv(Phi_CS1)*Y_trnN;
209 w_CS2 = pinv(Phi_CS2)*Y_trnN;
210 w=pinv(Phi)*Y_trnN;
211
212 %*****
213 %----- Step 9:Computing the approximation of -----
214 %----- training dataset-----
215 %*****
216 %----- Step 9.1:CS_RBF1 -----
217 YappxN_CS_RBF1=Phi_CS_RBF1*w_CS_RBF1;
218 Yappx_CS_RBF1 = YappxN_CS_RBF1*(max(Y_trn)-min(Y_trn))+min(Y_trn);

```

```

219
220 %----- Step 9.2:CS1 -----
221 YappxN_CS1=Phi_CS1*w_CS1;
222 Yappx_CS1 = YappxN_CS1*(max(Y_trn)-min(Y_trn))+min(Y_trn);
223
224 %----- Step 9.3:CS2 -----
225 YappxN_CS2=Phi_CS2*w_CS2;
226 Yappx_CS2 = YappxN_CS2*(max(Y_trn)-min(Y_trn))+min(Y_trn);
227
228 %----- Step 9.4:Gaussian RBF-----
229 YappxN=Phi*w;
230 Yappx = YappxN*(max(Y_trn)-min(Y_trn))+min(Y_trn);
231
232 %*****
233 %----- Step 10:Computing the training error with MSE-----
234 %*****
235 Err_Trn_CS_RBF1=(1/N_tr)*sum((Y_trn -Yappx_CS_RBF1).^2);
236 Err_Trn_CS1=(1/N_tr)*sum((Y_trn -Yappx_CS1).^2);
237 Err_Trn_CS2=(1/N_tr)*sum((Y_trn -Yappx_CS2).^2);
238 Err_Trn=(1/N_tr)*sum((Y_trn -Yappx).^2);
239
240 T_Trn = table(Err_Trn_CS_RBF1,Err_Trn_CS1,Err_Trn_CS2,Err_Trn)
241
242 %*****
243 %----- Step 11:Generate validation dataset -----
244 %*****
245 %-----////Generate a validation dataset of 1000 data points-----
246 for i=1:1000
247 X_vld(i)=2*pi*(i-1)/1000);
248 End
249
250 Y_vld=awgn(2*X_vld+1,15, 'measured');
251 %Y_vld with Gaussian noise
252
253 for i=1:1000
254 for j=1:1000
255 XY_vld(i,1)=X_vld(i);
256 XY_vld(j,2)=Y_vld(j);
257 end
258 end
259 XY_vld;
260
261 x2max = max(X_vld);
262 X_vldN=(X_vld-min(X_vld))/(x2max);
263
264 %*****
265 %----- Step 12:Construct the interpolation matrix-----
266 %----- from Xvld to Xctr -----
267 %*****
268 %----- Step 12.1:CS_RBF1 -----
269 for i=1:1000
270 for j=1:M_CS_RBF1
271 r2_CS_RBF1(i,j)=abs(X_vldN (1,i)-Xctr_CS_RBF1(1,j));
272 Phi2_CS_RBF1(i,j)=(1/3)+r2_CS_RBF1(i,j).^2-
(4/3)*r2_CS_RBF1(i,j).^3+2*(r2_CS_RBF1(i,j).^2)*log(r2_CS_RBF1(i,j));
273 if r2_CS_RBF1(i,j)== 0
274 Phi2_CS_RBF1(i,j)=(1/3)+r2_CS_RBF1(i,j).^2-(4/3)*r2_CS_RBF1(i,j).^3;
275 end

```



```

276 end
277 end
278
279 %----- Step 12.2:CS1 -----
280 for i=1:1000
281 for j=1:M_CS1
282 r2_CS1(i,j)=abs(X_vldN (1,i)-Xctr_CS1(1,j));
283 Phi2_CS1(i,j)=(112/45)*r2_CS1(i,j)^(9/2)+(16/3)*r2_CS1(i,j)^(7/2)-7*r2_CS1(i,j).^4-
    (14/15)*r2_CS1(i,j).^2+(1/9);
284 end
285 end
286
287 %----- Step 12.3:CS2 -----
288 for i=1:1000
289 for j=1:M_CS2
290 r2_CS2(i,j)=abs(X_vldN (1,i)-Xctr_CS2(1,j));
291 Phi2_CS2(i,j)=(1/18)*r2_CS2(i,j)^2+(4/9)*r2_CS2(i,j)^3+0.5*r2_CS2(i,j)^4-
    (4/3)*r2_CS2(i,j)^3*log(r2_CS2(i,j));
292 if r2_CS2(i,j)== 0
293 Phi2_CS2(i,j)=(1/18)*r2_CS2(i,j)^2+(4/9)*r2_CS2(i,j)^3+0.5*r2_CS2(i,j)^4;
294 end
295 end
296 end
297
298 %----- Step 12.4:Gaussian RBF-----
299 for i=1:1000
300 for j=1:M
301 r2(i,j)=abs(X_vldN (1,i)-Xctr(1,j));
302 Phi2(i,j)=exp(-(r2(i,j))^2)/(2*(shp^2));
303 end
304 end
305
306 %*****
307 %----- Step 13:Construct the YvldapxN from Phi2-----
308 %-----and weight 'w' -----
309 %*****
310 %----- Step 13.1:CS_RBF1 -----
311 YvldapxN_CS_RBF1=Phi2_CS_RBF1*w_CS_RBF1;
312 Yvldapx_CS_RBF1 = YvldapxN_CS_RBF1*(max(Y_vld)-min(Y_vld))+min(Y_vld);
313
314 %----- Step 13.2:CS1 -----
315 YvldapxN_CS1=Phi2_CS1*w_CS1;
316 Yvldapx_CS1 = YvldapxN_CS1*(max(Y_vld)-min(Y_vld))+min(Y_vld);
317
318 %----- Step 13.3:CS2 -----
319 YvldapxN_CS2=Phi2_CS2*w_CS2;
320 Yvldapx_CS2 = YvldapxN_CS2*(max(Y_vld)-min(Y_vld))+min(Y_vld);
321
322 %----- Step 13.4:Gaussian RBF-----
323 YvldapxN=Phi2*w;
324 Yvldapx = YvldapxN*(max(Y_vld)-min(Y_vld))+min(Y_vld);
325
326 %*****
327 %----- Step 14:Computing the validation error with MSE -----
328 %*****
329 Err_vld_CS_RBF1=(1/1000)*sum((Y_vld -Yvldapx_CS_RBF1).^2);
330 Err_vld_CS1=(1/1000)*sum((Y_vld -Yvldapx_CS1).^2);
331 Err_vld_CS2=(1/1000)*sum((Y_vld -Yvldapx_CS2).^2);

```

```

332 Err_Vld =(1/1000)*sum((Y_vld -Yvldapx)^2);
333
334 T_Vld = table(Err_Vld_CS_RBF1,Err_Vld_CS1,Err_Vld_CS2,Err_Vld)
335
336 %*****
337 %----- Step 15:Results Plotting -----
338 %*****
339 figure;
340 hold on
341 plot(X_trn, Y_trn,'ob','markersize',3);
342 xlabel('Input Variable (x)', 'FontSize',14);
343 ylabel('Output Variable (y)', 'FontSize',14);
344 grid on
345
346 figure;
347 hold on
348 plot(X_trn, Y_trn,'ob','markersize',3);
349 plot(X_trn,Yappx_CS_RBF1,'k','LineWidth',2);
350 plot(X_trn,Yappx_CS1,'-r','LineWidth',2);
351 plot(X_trn,Yappx_CS2,'-m','LineWidth',2);
352 plot(X_trn, Yappx,'-g','LineWidth',2);
353 title('Training data')
354 xlabel('X', 'FontSize',14);
355 ylabel('Y=2X+1', 'FontSize',14);
356 legend('Exact', 'CS RBF1', 'CS1', 'CS2', 'Gaussian', 'Location',
        'SouthEast')
357 grid on
358
359 figure;
360 hold on
361 plot(X_vld, Y_vld, 'ob', 'markersize', 3);
362 plot(X_vld, Yvldapx_CS_RBF1, 'k', 'LineWidth', 2);
363 plot(X_vld, Yvldapx_CS1, '-r', 'LineWidth', 2);
364 plot(X_vld, Yvldapx_CS2, '-m', 'LineWidth', 2);
365 plot(X_vld, Yvldapx, '-g', 'LineWidth', 2);
366 title('Validation data')
367 xlabel('X', 'FontSize',14);
368 ylabel('Y=2X+1', 'FontSize',14);
369 legend('Exact', 'CS RBF1', 'CS1', 'CS2', 'Gaussian', 'Location',
        'SouthEast')
370 grid on
371 %----- THIS IS THE END -----

```

A.1.1.2 Using different numbers of centres and RBFs for linear interpolation.

```

1 clc
2 clear all
3 close all
4
5 %*****
6 %----- Step 1:Generate training dataset -----
7 %*****
8 for i=1:100
9 X_trn (i)=2*pi*(i-1)/100;
10 end
11 Y_trn =awgn(2*X_trn +1,15,'measured');
12 %Y_trn with Gaussian
13 for i=1:100
14 for j=1:100

```

```

15 XY_trn (i,1)=X_trn (i);
16 XY_trn (j,2)=Y_trn (j);
17 end
18 end
19
20 XY_trn;
21 N_tr = length(X_trn);
22
23 %*****
24 %----- Step 2:Normalizing both X_trn and Y_trn -----
25 %*****
26 x1max = max(X_trn);
27 X_trnN=(X_trn-min(X_trn))/(x1max);
28 % Normalized X_trn
29 Y_trnN=(Y_trn-min(Y_trn))/(max(Y_trn)-min(Y_trn));
30 % Normalized Y_trn
31
32 %*****
33 %----- Step 3:Choosing the shape parameter-----
34 %*****
35 shp = input('Enter the shape parameter = ');
36
37 %*****
38 %----- Step 4:Construct the interpolation matrix-----
39 %----- CS_RBF1, CS1, CS2, G -----
40 %*****
41 for i=1:N_tr
42 for j=1:N_tr
43 r(i,j)=abs(X_trnN (1,i)-X_trnN (1,j));
44 CS_RBF1(i,j)=(1/3)+r(i,j).^2-(4/3)*r(i,j).^3+2*(r(i,j).^2)*log(r(i,j));
45 CS1(i,j)=(112/45)*r(i,j).^(9/2)+(16/3)*r(i,j).^(7/2)-7*r(i,j).^4-(14/15)*r(i,j).^2+(1/9);
46 CS2(i,j)=(1/18)-r(i,j).^2+(4/9)*r(i,j).^3+0.5*r(i,j).^4-(4/3)*r(i,j).^3.*log(r(i,j));
47 G(i,j)=exp(-(r(i,j).^2)/(2*(shp^2)));
48 if r(i,j)==0
49 CS_RBF1(i,j)=(1/3)+r(i,j).^2-(4/3)*r(i,j).^3;
50 CS2(i,j)=(1/18)-r(i,j).^2+(4/9)*r(i,j).^3+0.5*r(i,j).^4;
51 end
52 end
53 end
54
55 %*****
56 %----- Step 5:Using SVD to get the number of centres-----
57 %----- out of matrix CS_RBF1, CS1, CS2, G -----
58 %*****
59 delta = 0.01/100;
60
61 %----- Step 5.1:CS_RBF1 -----
62 [U_CS_RBF1,S_CS_RBF1,V_CS_RBF1]=svd(CS_RBF1);
63 S11_CS_RBF1 = S_CS_RBF1(1,1);
64 %The firsts singular of singular value
65 S1_CS_RBF1 = S11_CS_RBF1*(delta);
66
67 for i=1:N_tr
68 Sii_CS_RBF1 = S_CS_RBF1(i,i);
69 if Sii_CS_RBF1 <= S1_CS_RBF1
70 M_CS_RBF1 = i-1;
71 break
72 end

```

```

73 i = i+1 ;
74 end
75
76 %----- Step 5.2:CS1 -----
77 [U_CS1,S_CS1,V_CS1]=svd(CS1);
78 S11_CS1 = S_CS1(1,1); %The firsts singular of singular value
79 S1_CS1 = S11_CS1*(delta);
80
81 for i=1:N_tr
82 Sii_CS1 = S_CS1(i,i);
83 if Sii_CS1 <= S1_CS1
84 M_CS1 = i-1;
85 break
86 end
87 i = i+1 ;
88 end
89
90 %----- Step 5.3:CS2 -----
91 [U_CS2,S_CS2,V_CS2]=svd(CS2);
92 S11_CS2 = S_CS2(1,1); %The firsts singular of singular value
93 S1_CS2 = S11_CS2*(delta);
94
95 for i=1:N_tr
96 Sii_CS2 = S_CS2(i,i);
97 if Sii_CS2 <= S1_CS2
98 M_CS2 = i-1;
99 break
100 end
101 i = i+1 ;
102 end
103
104 %----- Step 5.4:Gaussian RBF -----
105 [U,S,V]=svd(G);
106 S11 = S(1,1);
107 S1 = S11*(delta);
108
109 for i=1:N_tr
110 Sii = S(i,i);
111 if Sii <= S1 ;
112 M = i-1
113 break
114 end
115 i = i+1 ;
116 end
117
118 %*****
119 %----- Step 6:Using QR to find the centres of basis function ---
120 %----- and the location of centres -----
121 %*****
122 %----- Step 6.1:CS_RBF1 -----
123 V1_CS_RBF1 = -V_CS_RBF1;
124 V11_CS_RBF1=V1_CS_RBF1(1:M_CS_RBF1,1:M_CS_RBF1);
125 %partition matrix V
126 V21_CS_RBF1=V1_CS_RBF1(M_CS_RBF1+1:N_tr,1:M_CS_RBF1);V2_CS_RBF1 =
[V11_CS_RBF1' V21_CS_RBF1'];
127
128 [Q_CS_RBF1,R_CS_RBF1,P_CS_RBF1]=qr(V2_CS_RBF1);
129 mu_CS_RBF1 = X_trnN*P_CS_RBF1;

```

```

130 Xctr_CS_RBF1_ex = mu_CS_RBF1(1,1:M_CS_RBF1);
131 Xctr_CS_RBF1 = randsample(Xctr_CS_RBF1_ex,M)
132
133 %----- Step 6.2:CS1 -----
134 V1_CS1 = -V_CS1;
135 V11_CS1=V1_CS1(1:M_CS1,1:M_CS1);           %partition matrix V
136 V21_CS1=V1_CS1(M_CS1+1:N_tr,1:M_CS1);
137 V2_CS1 = [V11_CS1' V21_CS1'];
138
139 [Q_CS1,R_CS1,P_CS1]=qr(V2_CS1);
140 mu_CS1 = X_trnN*P_CS1;
141 Xctr_CS1_ex = mu_CS1(1,1:M_CS1);
142
143 Xctr_CS1 = randsample(Xctr_CS1_ex,M)
144
145 %----- Step 6.3:CS2 -----
146 V1_CS2 = -V_CS2;
147 V11_CS2=V1_CS2(1:M_CS2,1:M_CS2);           %partition matrix V
148 V21_CS2=V1_CS2(M_CS2+1:N_tr,1:M_CS2);
149 V2_CS2 = [V11_CS2' V21_CS2'];
150
151 [Q_CS2,R_CS2,P_CS2]=qr(V2_CS2);
152 mu_CS2 = X_trnN*P_CS2;
153 Xctr_CS2_ex = mu_CS2(1,1:M_CS2);
154
155 Xctr_CS2 = randsample(Xctr_CS2_ex,M)
156
157 %----- Step 6.4:Gaussian RBF -----
158 V1 = -V;
159 V11=V1(1:M,1:M);           %partition matrix V
160 V21=V1(M+1:N_tr,1:M);
161 V2 = [V11' V21'];
162
163 [Q,R,P]=qr(V2);
164 mu = X_trnN*P;
165 Xctr = mu(1,1:M)
166
167 %*****
168 %----- Step 7:Construct the interpolation matrix -----
169 %*****
170 %----- Step 7.1:CS_RBF1 -----
171 for i=1:N_tr
172 for j=1:M
173 r1_CS_RBF1(i,j)=abs(X_trnN(1,i)-Xctr_CS_RBF1(1,j));
174 Phi_CS_RBF1(i,j)=(1/3)+r1_CS_RBF1(i,j)^2-
    (4/3)*r1_CS_RBF1(i,j).^3+2*(r1_CS_RBF1(i,j).^2)*log(r1_CS_RBF1(i,j));
175 if r1_CS_RBF1(i,j)==0
176 Phi_CS_RBF1(i,j)=(1/3)+r1_CS_RBF1(i,j).^2-(4/3)*r1_CS_RBF1(i,j).^3;
177 end
178 end
179 end
180
181 %----- Step 7.2:CS1 -----
182 for i=1:N_tr
183 for j=1:M
184 r1_CS1(i,j)=abs(X_trnN(1,i)-Xctr_CS1(1,j));
185 Phi_CS1(i,j)=(112/45)*r1_CS1(i,j)^(9/2)+(16/3)*r1_CS1(i,j)^(7/2)-7*r1_CS1(i,j).^4-
    (14/15)*r1_CS1(i,j).^2+(1/9);

```

```

186 end
187 end
188
189 %----- Step 7.3:CS2 -----
190 for i=1:N_tr
191 for j=1:M
192 r1_CS2(i,j)=abs(X_trnN(1,i)-Xctr_CS2(1,j));
193 Phi_CS2(i,j)=(1/18)-r1_CS2(i,j).^2+(4/9)*r1_CS2(i,j).^3+0.5*r1_CS2(i,j).^4-
    (4/3)*r1_CS2(i,j).^3*log(r1_CS2(i,j));
194 if r1_CS2(i,j)== 0
195 Phi_CS2(i,j)=(1/18)-r1_CS2(i,j).^2+(4/9)*r1_CS2(i,j).^3+0.5*r1_CS2(i,j).^4;
196 end
197 end
198
199 %----- Step 7.4:Gaussian RBF-----
200 for i=1:N_tr
201 for j=1:M
202 r1(i,j)=abs(X_trnN(1,i)-Xctr(1,j));
203 Phi(i,j)=exp(-(r1(i,j)^2)/(2*(shp^2)));
204 end
205 end
206
207 %*****
208 %----- Step 8:Computing the weight 'w' -----
209 %*****
210 %Moore-Penrose Pseudoinverse of matrix
211 w_CS_RBF1 =pinv(Phi_CS_RBF1)*Y_trnN
212 w_CS1 = pinv(Phi_CS1)*Y_trnN
213 w_CS2 = pinv(Phi_CS2)*Y_trnN
214 w=pinv(Phi)*Y_trnN
215
216 %*****
217 %----- Step 9:Computing the approximation of training dataset -
218 %*****
219 %----- Step 9.1:CS_RBF1 -----
220 YappxN_CS_RBF1=Phi_CS_RBF1*w_CS_RBF1;
221 Yappx_CS_RBF1 = YappxN_CS_RBF1*(max(Y_trn)-min(Y_trn))+min(Y_trn);
222
223 %----- Step 9.2:CS1 -----
224 YappxN_CS1=Phi_CS1*w_CS1;
225 Yappx_CS1 = YappxN_CS1*(max(Y_trn)-min(Y_trn))+min(Y_trn);
226
227 %----- Step 9.3:CS2 -----
228 YappxN_CS2=Phi_CS2*w_CS2;
229 Yappx_CS2 = YappxN_CS2*(max(Y_trn)-min(Y_trn))+min(Y_trn);
230
231 %----- Step 9.4:Gassian RBF-----
232 YappxN=Phi*w;
233 Yappx = YappxN*(max(Y_trn)-min(Y_trn))+min(Y_trn);
234
235 %*****
236 %----- Step 10:Computing the training error with MSE-----
237 %*****
238 Err_Trn_CS_RBF1=(1/N_tr)*sum((Y_trn-Yappx_CS_RBF1).^2);
239 Err_Trn_CS1=(1/N_tr)*sum((Y_trn-Yappx_CS1).^2);
240 Err_Trn_CS2=(1/N_tr)*sum((Y_trn-Yappx_CS2).^2);
241 Err_Trn=(1/N_tr)*sum((Y_trn-Yappx).^2);
242

```

```

243 T_Trn = table(Err_Trn_CS_RBF1,Err_Trn_CS1,Err_Trn_CS2,Err_Trn)
244
245 %*****
246 %----- Step 11:Generate validation dataset -----
247 %*****
248 %----//Generate a validation dataset of 1000 data points in ----//-----
249 for i=1:1000
250 X_vld(i)=2*pi*(i-1)/1000);
251 end
252 Y_vld=awgn(2*X_vld+1,15,'measured');
253 %Y_vld with Gaussian noise
254
255 for i=1:1000
256 for j=1:1000
257 XY_vld(i,1)=X_vld(i);
258 XY_vld(j,2)=Y_vld(j);
259 end
260 end
261 XY_vld;
262
263 x2max = max(X_vld);
264 X_vldN=(X_vld-min(X_vld))/(x2max);
265 %*****
266 %----- Step 12:Construct the interpolation matrix-----
267 %-----from X_vld to Xctr -----
268 %*****
269 %----- Step 12.1:CS_RBF1 -----
270 for i=1:1000
271 for j=1:M
272 r2_CS_RBF1(i,j)=abs(X_vldN(1,i)-Xctr_CS_RBF1(1,j));
273 Phi2_CS_RBF1(i,j)=(1/3)+r2_CS_RBF1(i,j)^2-
    (4/3)*r2_CS_RBF1(i,j)^3+2*(r2_CS_RBF1(i,j)^2)*log(r2_CS_RBF1(i,j));
274 if r2_CS_RBF1(i,j)== 0
275 Phi2_CS_RBF1(i,j)=(1/3)+r2_CS_RBF1(i,j)^2+(4/3)*r2_CS_RBF1(i,j)^3;
276 end
277 end
278 end
279
280 %----- Step 12.2:CS1 -----
281 for i=1:1000
282 for j=1:M
283 r2_CS1(i,j)=abs(X_vldN(1,i)-Xctr_CS1(1,j));
284 Phi2_CS1(i,j)=(112/45)*r2_CS1(i,j)^(9/2)+(16/3)*r2_CS1(i,j)^(7/2)-7*r2_CS1(i,j)^4-
    (14/15)*r2_CS1(i,j)^2+(1/9);
285 end
286 end
287
288 %----- Step 12.3:CS2 -----
289 for i=1:1000
290 for j=1:M
291 r2_CS2(i,j)=abs(X_vldN(1,i)-Xctr_CS2(1,j));
292 Phi2_CS2(i,j)=(1/18)*r2_CS2(i,j)^2+(4/9)*r2_CS2(i,j)^3+0.5*r2_CS2(i,j)^4-
    (4/3)*r2_CS2(i,j)^3*log(r2_CS2(i,j));
293 if r2_CS2(i,j)== 0
294 Phi2_CS2(i,j)=(1/18)*r2_CS2(i,j)^2+(4/9)*r2_CS2(i,j)^3+0.5*r2_CS2(i,j)^4;
295 end
296 end
297 end

```

```

298
299 %----- Step 12.4:Gaussian RBF-----
300 for i=1:1000
301 for j=1:M
302 r2(i,j)=abs(X_vldN(1,i)-Xctr(1,j));
303 Phi2(i,j)=exp(-(r2(i,j)^2)/(2*(shp^2)));
304 end
305 end
306
307 %*****
308 %----- Step 13:Construct the Y_vldapxN from Phi2 and weight 'w'
309 %*****
310 %----- Step 13.1:CS_RBF1 -----
311 Y_vldapxN_CS_RBF1=Phi2_CS_RBF1*w_CS_RBF1;
312 Y_vldapx_CS_RBF1 = Y_vldapxN_CS_RBF1.*(max(Y_vld)-min(Y_vld))+min(Y_vld);
313
314 %----- Step 13.2:CS1 -----
315 Y_vldapxN_CS1=Phi2_CS1*w_CS1;
316 Y_vldapx_CS1 = Y_vldapxN_CS1.*(max(Y_vld)-min(Y_vld))+min(Y_vld);
317
318 %----- Step 13.3:CS2 -----
319 Y_vldapxN_CS2=Phi2_CS2*w_CS2;
320 Y_vldapx_CS2 = Y_vldapxN_CS2.*(max(Y_vld)-min(Y_vld))+min(Y_vld);
321
322 %----- Step 13.4:Gaussian RBF-----
323 Y_vldapxN=Phi2*w;
324 Y_vldapx = Y_vldapxN.*(max(Y_vld)-min(Y_vld))+min(Y_vld);
325
326 %*****
327 %----- Step 14:Computing the validation error with MSE -----
328 %*****
329 Err_vld_CS_RBF1=(1/1000)*sum((Y_vld-Y_vldapx_CS_RBF1).^2);
330 Err_vld_CS1=(1/1000)*sum((Y_vld-Y_vldapx_CS1).^2);
331 Err_vld_CS2=(1/1000)*sum((Y_vld-Y_vldapx_CS2).^2);
332 Err_vld =(1/1000)*sum((Y_vld-Y_vldapx).^2);
333
334 T_vld = table(Err_vld_CS_RBF1,Err_vld_CS1,Err_vld_CS2,Err_vld)
335
336 Y1 = 2*X_trn+1;
337
338 for i=1:100
339 Y3(i) = 20;
340 End
341
342 %----- Step 12 : Results Plotting -----
343 figure;
344 hold on
345 plot(X_trn,Y_trn,'ok','LineWidth',1);
346 plot(X_trn,Y3,'ok','LineWidth',1);
347 plot(X_trn,Y1,'k','LineWidth',1);
348 xlabel('x','FontSize',14);
349 ylabel('y=2x+1','FontSize',14);
350 grid on
351
352 figure;
353 hold on
354 plot(X_trn,Y_trn,'ok','markersize',3);
355 plot(X_trn,Yappx_CS_RBF1,'k','LineWidth',2);

```



```

356 plot(X_trn,Yappx_CS1,'r','LineWidth',2);
357 plot(X_trn,Yappx_CS2,'m','LineWidth',2);
358 plot(X_trn,Yappx,'g','LineWidth',2);
359 title('Training data')
360 xlabel('X', 'FontSize',14);
361 ylabel('Y=2X+1', 'FontSize',14);
362 legend('Exact', 'CS RBF1', 'CS1', 'CS2', 'Gaussian', 'Location',
        'SouthEast')
363 grid on
364
365 figure;
366 hold on
367 plot(X_vld,Y_vld,'ok','markersize',3);
368 plot(X_vld,Y_vldapx_CS_RBF1,'k','LineWidth',2);
369 plot(X_vld,Y_vldapx_CS1,'r','LineWidth',2);
370 plot(X_vld,Y_vldapx_CS2,'m','LineWidth',2);
371 plot(X_vld,Y_vldapx,'g','LineWidth',2);
372 title('Validation data')
373 xlabel('X', 'FontSize',14);
374 ylabel('Y=2X+1', 'FontSize',14);
375 legend('Exact', 'CS RBF1', 'CS1', 'CS2', 'Gaussian', 'Location',
        'SouthEast')
%----- THIS IS THE END -----

```

A.1.2 Test Case 2: Parabola function

A.1.2.1 Training and validation errors for candidate models for parabola function case.

```

1 clc
2 clear all
3 close all
4
5 %*****
6 %----- Step 1:Generate training dataset -----
7 %*****
8 for i=1:100
9 X_trn(i)=2*pi*(i-1)/100;
10 end
11 Y_trn =awgn(X_trn.^2/6- X_trn+4,15,'measured');
12 for i=1:100
13 for j=1:100
14 XY_trn (i,1)=X_trn (i);
15 XY_trn (j,2)=Y_trn (j);
16 end
17 end
18 XY_trn;
19
20 N_tr = length(X_trn);
21
22 %*****
23 %----- Step 2:Normalizing both X_trn and Y_trn -----
24 %*****
25 x1max =max(X_trn);
26 X_trnN=(X_trn -min(X_trn))/(x1max);           %Normalized X_trn

```

```

27 Y_trnN=(Y_trn -min(Y_trn))/(max(Y_trn)-min(Y_trn)); %Normalized Y_trn
28
29 %*****
30 %-----Step 3:Choosing the shape parameter-----
31 %*****
32 shp = input('Enter the shape parameter = ');
33
34 %*****
35 %-----Step 4:Construct the interpolation matrix-----
36 %-----CS_RBF1, CS1, CS2, G-----
37 %*****
38 for i=1:N_tr
39 for j=1:N_tr
40 r(i,j)=abs(X_trnN(1,i)-X_trnN(1,j));
41 CS_RBF1(i,j)=(1/3)+r(i,j).^2-(4/3)*r(i,j).^3+2*(r(i,j).^2)*log(r(i,j));
42 CS1(i,j)=(112/45)*r(i,j).^(9/2)+(16/3)*r(i,j).^(7/2)-7*r(i,j).^4-(14/15)*r(i,j).^2+(1/9);
43 CS2(i,j)=(1/18)*r(i,j).^2+(4/9)*r(i,j).^3+0.5*r(i,j).^4-(4/3)*r(i,j).^3*log(r(i,j));
44 G(i,j)=exp(-(r(i,j).^2)/(2*(shp^2)));
45 if r(i,j)==0
46 CS_RBF1(i,j)=(1/3)+r(i,j).^2-(4/3)*r(i,j).^3;
47 CS2(i,j)=(1/18)*r(i,j).^2+(4/9)*r(i,j).^3+0.5*r(i,j).^4;
48 end
49 end
50 end
51
52 %*****
53 %-----Step 5:Using SVD to get the number of centres-----
54 %-----out of matrix CS_RBF1, CS1, CS2, G-----
55 %*****
56 delta = 0.01/100;
57
58 %-----Step 5.1:CS_RBF1-----
59 [U_CS_RBF1,S_CS_RBF1,V_CS_RBF1]=svd(CS_RBF1);
60 S11_CS_RBF1 = S_CS_RBF1(1,1);
61 %The firsts singular of singular value
62 S1_CS_RBF1 = S11_CS_RBF1*(delta);
63
64 for i=1:N_tr
65 Sii_CS_RBF1 = S_CS_RBF1(i,i);
66 if Sii_CS_RBF1 <= S1_CS_RBF1
67 M_CS_RBF1 = i-1;
68 break
69 end
70 i = i+1 ;
71 end
72
73 %-----Step 5.2:CS1-----
74 [U_CS1,S_CS1,V_CS1]=svd(CS1);
75 S11_CS1 = S_CS1(1,1);
76 %The firsts singular of singular value
77 S1_CS1 = S11_CS1*(delta);
78 for i=1:N_tr
79 Sii_CS1 = S_CS1(i,i);
80 if Sii_CS1 <= S1_CS1
81 M_CS1 = i-1;
82 break
83 end
84 i = i+1 ;

```

```

85 end
86
87 %----- Step 5.3:CS2 -----
88 [U_CS2,S_CS2,V_CS2]=svd(CS2);
89 S11_CS2 = S_CS2(1,1);
90 %The firsts singular of singular value
91 S1_CS2 = S11_CS2*(delta);
92
93 for i=1:N_tr
94 Sii_CS2 = S_CS2(i,i);
95 if Sii_CS2 <= S1_CS2
96 M_CS2 = i-1;
97 break
98 end
99 i = i+1 ;
100 end
101 %----- Step 5.4:Gaussian RBF -----
102 [U,S,V]=svd(G);
103 S11 = S(1,1);
104 S1 = S11*(delta);
105
106 for i=1:N_tr
107 Sii = S(i,i);
108 if Sii <= S1 ;
109 M = i-1 ;
110 break
111 end
112 i = i+1 ;
113 end
114
115 %*****
116 %----- Step 6:Using QR to find the centres of -----
117 %----- basis function and the location of centres -----
118 %*****
119 %----- Step 6.1:CS_RBF1 -----
120 V1_CS_RBF1 = -V_CS_RBF1;
121 V11_CS_RBF1=V1_CS_RBF1(1:M_CS_RBF1,1:M_CS_RBF1);
122 %partition matrix
123 V21_CS_RBF1=V1_CS_RBF1(M_CS_RBF1+1:N_tr,1:M_CS_RBF1);
124 V2_CS_RBF1 = [V11_CS_RBF1' V21_CS_RBF1'];
125
126 [Q_CS_RBF1,R_CS_RBF1,P_CS_RBF1]=qr(V2_CS_RBF1);
127 mu_CS_RBF1 = X_trnN*P_CS_RBF1;
128 Xctr_CS_RBF1 =mu_CS_RBF1(1,1:M_CS_RBF1);
129
130 %----- Step 6.2:CS1 -----
131 V1_CS1 = -V_CS1;
132 V11_CS1=V1_CS1(1:M_CS1,1:M_CS1);
133 %partition matrix V
134 V21_CS1=V1_CS1(M_CS1+1:N_tr,1:M_CS1);
135 V2_CS1 = [V11_CS1' V21_CS1'];
136
137 [Q_CS1,R_CS1,P_CS1]=qr(V2_CS1);
138 mu_CS1 = X_trnN*P_CS1;
139 Xctr_CS1 =mu_CS1(1,1:M_CS1);
140
141 %----- Step 6.3:CS2 -----
142 V1_CS2 = -V_CS2;

```

```

143 V11_CS2=V1_CS2(1:M_CS2,1:M_CS2);
144 %partition matrix V
145 V21_CS2=V1_CS2(M_CS2+1:N_tr,1:M_CS2);
146 V2_CS2 = [V11_CS2' V21_CS2'];
147
148 [Q_CS2,R_CS2,P_CS2]=qr(V2_CS2);
149 mu_CS2 = X_trnN*P_CS2;
150 Xctr_CS2 = mu_CS2(1,1:M_CS2);
151
152 %----- Step 6.4:Gaussian RBF-----
153 V1 = -V;
154 V11=V1(1:M,1:M);           %partition matrix V
155 V21=V1(M+1:N_tr,1:M);
156 V2 = [V11' V21'];
157 [Q,R,P]=qr(V2);
158 mu = X_trnN*P;
159 Xctr = mu(1,1:M)
160
161 %*****
162 %----- Step 7:Construct the interpolation matrix -----
163 %*****
164 %----- Step 7.1:CS_RBF1 -----
165 for i=1:N_tr
166 for j=1:M_CS_RBF1
167 r1_CS_RBF1(i,j)=abs(X_trnN(1,i)-Xctr_CS_RBF1(1,j));
168 Phi_CS_RBF1(i,j)=(1/3)+r1_CS_RBF1(i,j).^2-
    (4/3)*r1_CS_RBF1(i,j).^3+2*(r1_CS_RBF1(i,j).^2)*log(r1_CS_RBF1(i,j));
169 if r1_CS_RBF1(i,j)==0
170 Phi_CS_RBF1(i,j)=(1/3)+r1_CS_RBF1(i,j).^2-(4/3)*r1_CS_RBF1(i,j).^3;
171 end
172 end
173 end
174
175 %----- Step 7.2:CS1 -----
176 for i=1:N_tr
177 for j=1:M_CS1
178 r1_CS1(i,j)=abs(X_trnN(1,i)-Xctr_CS1(1,j));
179 Phi_CS1(i,j)=(112/45)*r1_CS1(i,j).^9/2+(16/3)*r1_CS1(i,j).^7/2-7*r1_CS1(i,j).^4-
    (14/15)*r1_CS1(i,j).^2+(1/9);
180 end
181 end
182
183 %----- Step 7.3:CS2 -----
184 for i=1:N_tr
185 for j=1:M_CS2
186 r1_CS2(i,j)=abs(X_trnN(1,i)-Xctr_CS2(1,j));
187 Phi_CS2(i,j)=(1/18)-r1_CS2(i,j).^2+(4/9)*r1_CS2(i,j).^3+0.5*r1_CS2(i,j).^4-
    (4/3)*r1_CS2(i,j).^3*log(r1_CS2(i,j));
188 if r1_CS2(i,j)==0
189 Phi_CS2(i,j)=(1/18)-r1_CS2(i,j).^2+(4/9)*r1_CS2(i,j).^3+0.5*r1_CS2(i,j).^4;
190 end
191 end
192 end
193
194 %----- Step 7.4:Gaussian RBF-----
195 for i=1:N_tr
196 for j=1:M
197 r1(i,j)=abs(X_trnN(1,i)-Xctr(1,j));

```

```

198 Phi(i,j)=exp(-(r1(i,j)^2)/(2*(shp^2)));
199 end
200 end
201
202 %*****
203 %-----Step 8:Computing the weight 'w' -----
204 %*****
205 %Moore-Penrose Pseudoinverse of matrix
206 w_CS_RBF1 =pinv(Phi_CS_RBF1)*Y_trnN;
207 w_CS1 = pinv(Phi_CS1)*Y_trnN;
208 w_CS2 = pinv(Phi_CS2)*Y_trnN;
209 w=pinv(Phi)*Y_trnN;
210
211 %*****
212 %----- Step 9:Computing the approximation of -----
213 %----- training dataset-----
214 %*****
215 %----- Step 9.1:CS_RBF1 -----
216 YappxN_CS_RBF1=Phi_CS_RBF1*w_CS_RBF1;
217 Yappx_CS_RBF1 = YappxN_CS_RBF1*(max(Y_trn)-min(Y_trn))+min(Y_trn);
218
219 %----- Step 9.2:CS1 -----
220 YappxN_CS1=Phi_CS1*w_CS1;
221 Yappx_CS1 = YappxN_CS1*(max(Y_trn)-min(Y_trn))+min(Y_trn);
222
223 %----- Step 9.3:CS2 -----
224 YappxN_CS2=Phi_CS2*w_CS2;
225 Yappx_CS2 = YappxN_CS2*(max(Y_trn)-min(Y_trn))+min(Y_trn);
226
227 %----- Step 9.4:Gaussian RBF -----
228 YappxN=Phi*w;
229 Yappx = YappxN*(max(Y_trn)-min(Y_trn))+min(Y_trn);
230
231 %*****
232 %----- Step 10:Computing the training error with MSE-----
233 %*****
234 Err_Trn_CS_RBF1=(1/N_tr)*sum((Y_trn -Yappx_CS_RBF1).^2);
235 Err_Trn_CS1=(1/N_tr)*sum((Y_trn -Yappx_CS1).^2);
236 Err_Trn_CS2=(1/N_tr)*sum((Y_trn -Yappx_CS2).^2);
237 Err_Trn=(1/N_tr)*sum((Y_trn -Yappx).^2);
238
239 T_Trn = table(Err_Trn_CS_RBF1,Err_Trn_CS1,Err_Trn_CS2,Err_Trn)
240
241 %*****
242 %----- Step 11:Generate validation dataset -----
243 %*****
244 %-----////Generate a validation dataset of 1000 data points
245 for i=1:1000
246 X_vld(i)=2*pi*(i-1)/1000);
247 End
248
249 Y_vld=awgn(X_vld^2)/6-X_vld+4,15, 'measured');
250 %Y_vld with Gaussian noise
251
252 for i=1:1000
253 for j=1:1000
254 XY_vld(i,1)=X_vld(i);
255 XY_vld(j,2)=Y_vld(j);

```

```

256 end
257 end
258 XY_vld;
259
260 x2max =max(X_vld);
261 X_vldN=(X_vld-min(X_vld))/(x2max);
262
263 %*****
264 %----- Step 12:Construct the interpolation matrix-----
265 %----- from Xvld to Xctr -----
266 %*****
267 %----- Step 12.1:CS_RBF1 -----
268 for i=1:1000
269 for j=1:M_CS_RBF1
270 r2_CS_RBF1(i,j)=abs(X_vldN (1,i)-Xctr_CS_RBF1(1,j));
271 Phi2_CS_RBF1(i,j)=(1/3)+r2_CS_RBF1(i,j).^2-
    (4/3)*r2_CS_RBF1(i,j).^3+2*(r2_CS_RBF1(i,j).^2)*log(r2_CS_RBF1(i,j));
272 if r2_CS_RBF1(i,j)== 0
273 Phi2_CS_RBF1(i,j)=(1/3)+r2_CS_RBF1(i,j).^2-(4/3)*r2_CS_RBF1(i,j).^3;
274 end
275 end
276 end
277
278 %----- Step 12.2:CS1 -----
279 for i=1:1000
280 for j=1:M_CS1
281 r2_CS1(i,j)=abs(X_vldN (1,i)-Xctr_CS1(1,j));
282 Phi2_CS1(i,j)=(112/45)*r2_CS1(i,j).^(9/2)+(16/3)*r2_CS1(i,j).^(7/2)-7*r2_CS1(i,j).^4-
    (14/15)*r2_CS1(i,j).^2+(1/9);
283 end
284 end
285
286 %----- Step 12.3:CS2 -----
287 for i=1:1000
288 for j=1:M_CS2
289 r2_CS2(i,j)=abs(X_vldN (1,i)-Xctr_CS2(1,j));
290 Phi2_CS2(i,j)=(1/18)+r2_CS2(i,j).^2+(4/9)*r2_CS2(i,j).^3+0.5*r2_CS2(i,j).^4-
    (4/3)*r2_CS2(i,j).^3*log(r2_CS2(i,j));
291 if r2_CS2(i,j)== 0
292 Phi2_CS2(i,j)=(1/18)+r2_CS2(i,j).^2+(4/9)*r2_CS2(i,j).^3+0.5*r2_CS2(i,j).^4;
293 end
294 end
295 end
296
297 %----- Step 12.4:Gaussian RBF -----
298 for i=1:1000
299 for j=1:M
300 r2(i,j)=abs(X_vldN (1,i)-Xctr(1,j));
301 Phi2(i,j)=exp(-(r2(i,j)^2)/(2*(shp^2)));
302 end
303 end
304
305 %*****
306 %----- Step 13:Construct the YvldapxN from Phi2-----
307 %----- and weight 'w' -----
308 %*****
309 %----- Step 13.1:CS_RBF1 -----
310 YvldapxN_CS_RBF1=Phi2_CS_RBF1*w_CS_RBF1;

```

```

311 Yvldapx_CS_RBF1 = YvldapxN_CS_RBF1*(max(Y_vld)-min(Y_vld))+min(Y_vld);
312
313 %----- Step 13.2:CS1 -----
314 YvldapxN_CS1=Phi2_CS1*w_CS1;
315 Yvldapx_CS1 = YvldapxN_CS1*(max(Y_vld)-min(Y_vld))+min(Y_vld);
316
317 %----- Step 13.3:CS2 -----
318 YvldapxN_CS2=Phi2_CS2*w_CS2;
319 Yvldapx_CS2 = YvldapxN_CS2*(max(Y_vld)-min(Y_vld))+min(Y_vld);
320
321 %----- Step 13.4:Gaussian RBF -----
322 YvldapxN=Phi2*w;
323 Yvldapx = YvldapxN*(max(Y_vld)-min(Y_vld))+min(Y_vld);
324
325 %*****
326 %----- Step 14:Computing the validation error with MSE -----
327 %*****
328 Err_Vld_CS_RBF1=(1/1000)*sum((Y_vld -Yvldapx_CS_RBF1).^2);
329 Err_Vld_CS1=(1/1000)*sum((Y_vld -Yvldapx_CS1).^2);
330 Err_Vld_CS2=(1/1000)*sum((Y_vld -Yvldapx_CS2).^2);
331 Err_Vld =(1/1000)*sum((Y_vld -Yvldapx).^2);
332
333 T_Vld = table(Err_Vld_CS_RBF1,Err_Vld_CS1,Err_Vld_CS2,Err_Vld)
334
335 %*****
336 %----- Step 15:Results Plotting -----
337 %*****
338 figure;
339 hold on
340 plot(X_trn, Y_trn, 'ob', 'markersize', 3);
341 xlabel('Input Variable (x)', 'FontSize', 14);
342 ylabel('Output Variable (y)', 'FontSize', 14);
343 grid on
344
345 figure;
346 hold on
347 plot(X_trn, Y_trn, 'ob', 'markersize', 3);
348 plot(X_trn, Yappx_CS_RBF1, 'k', 'LineWidth', 2);
349 plot(X_trn, Yappx_CS1, 'r', 'LineWidth', 2);
350 plot(X_trn, Yappx_CS2, 'm', 'LineWidth', 2);
351 plot(X_trn, Yappx, 'g', 'LineWidth', 2);
352 title('Training data')
353 xlabel('X', 'FontSize', 14);
354 ylabel('Y=(X.^2)/6-X+4', 'FontSize', 14);
355 legend('Exact', 'CS RBF1', 'CS1', 'CS2', 'Gaussian', 'Location',
        'SouthEast')
356 grid on
357
358 figure;
359 hold on
360 plot(X_vld, Y_vld, 'ob', 'markersize', 3);
361 plot(X_vld, Yvldapx_CS_RBF1, 'k', 'LineWidth', 2);
362 plot(X_vld, Yvldapx_CS1, 'r', 'LineWidth', 2);
363 plot(X_vld, Yvldapx_CS2, 'm', 'LineWidth', 2);
364 plot(X_vld, Yvldapx, 'g', 'LineWidth', 2);
365 title('Validation data')
366 xlabel('X', 'FontSize', 14);
367 ylabel('Y=(X.^2)/6-X+4', 'FontSize', 14);

```

```

368 legend('Exact', 'CS RBF1', 'CS1', 'CS2', 'Gaussian', 'Location',
        'SouthEast')
369 grid on
370
371 %-----THIS IS THE END -----

```

A.1.2.2 Using different numbers of centres and RBFs for parabola function.

```

1 clc
2 clear all
3 close all
4
5 %*****
6 %----- Step 1:Generate training dataset -----
7 %*****
8 for i=1:100
9 X_trn (i)=2*pi*(i-1)/100;
10 end
11 Y_trn =awgn(X_trn.^2)/6- X_trn+4,15, 'measured');
12 %Y_trn with Gaussian
13 for i=1:100
14 for j=1:100
15 XY_trn (i,1)=X_trn (i);
16 XY_trn (j,2)=Y_trn (j);
17 end
18 end
19
20 XY_trn;
21 N_tr = length(X_trn);
22
23 %*****
24 %----- Step 2:Normalizing both X_trn and Y_trn -----
25 %*****
26 x1max =max(X_trn);
27 X_trnN=(X_trn-min(X_trn))/(x1max);
28 %Normalized X_trn
29 Y_trnN=(Y_trn-min(Y_trn))/(max(Y_trn)-min(Y_trn));
30 %Normalized Y_trn
31
32 %*****
33 %----- Step 3:Choosing the shape parameter -----
34 %*****
35 shp = input('Enter the shape parameter = ');
36
37 %*****
38 %----- Step 4:Construct the interpolation matrix-----
39 %-----CS_RBF1, CS1, CS2, G -----
40 %*****
41 for i=1:N_tr
42 for j=1:N_tr
43 r(i,j)=abs(X_trnN (1,i)-X_trnN (1,j));
44 CS_RBF1(i,j)=(1/3)+r(i,j).^2-(4/3)*r(i,j).^3+2*r(i,j).^2.*log(r(i,j));
45 CS1(i,j)=(112/45)*r(i,j).^(9/2)+(16/3)*r(i,j).^(7/2)-7*r(i,j).^4-(14/15)*r(i,j).^2+(1/9);
46 CS2(i,j)=(1/18)*r(i,j).^2+(4/9)*r(i,j).^3+0.5*r(i,j).^4-(4/3)*r(i,j).^3.*log(r(i,j));
47 G(i,j)=exp(-(r(i,j)^2)/(2*shp^2));
48 if r(i,j)== 0

```



```

49 CS_RBF1(i,j)=(1/3)+r(i,j).^2-(4/3)*r(i,j).^3;
50 CS2(i,j)=(1/18)-r(i,j).^2+(4/9)*r(i,j).^3+0.5*r(i,j).^4;
51 end
52 end
53 end
54
55 %*****
56 %-----Step 5:Using SVD to get the number of centres-----
57 %-----out of matrix CS_RBF1, CS1, CS2, G -----
58 %*****
59 delta = 0.01/100;
60
61 %----- Step 5.1:CS_RBF1 -----
62 [U_CS_RBF1,S_CS_RBF1,V_CS_RBF1]=svd(CS_RBF1);
63 S11_CS_RBF1 = S_CS_RBF1(1,1);
64 %The firsts singular of singular value
65 S1_CS_RBF1 = S11_CS_RBF1*(delta);
66
67 for i=1:N_tr
68 Sii_CS_RBF1 = S_CS_RBF1(i,i);
69 if Sii_CS_RBF1 <= S1_CS_RBF1
70 M_CS_RBF1 = i-1;
71 break
72 end
73 i = i+1 ;
74 end
75
76 %----- Step 5.2:CS1 -----
77 [U_CS1,S_CS1,V_CS1]=svd(CS1);
78 S11_CS1 = S_CS1(1,1); %The firsts singular of singular value
79 S1_CS1 = S11_CS1*(delta);
80
81 for i=1:N_tr
82 Sii_CS1 = S_CS1(i,i);
83 if Sii_CS1 <= S1_CS1
84 M_CS1 = i-1;
85 break
86 end
87 i = i+1 ;
88 end
89
90 %----- Step 5.3:CS2 -----
91 [U_CS2,S_CS2,V_CS2]=svd(CS2);
92 S11_CS2 = S_CS2(1,1); %The firsts singular of singular value
93 S1_CS2 = S11_CS2*(delta);
94
95 for i=1:N_tr
96 Sii_CS2 = S_CS2(i,i);
97 if Sii_CS2 <= S1_CS2
98 M_CS2 = i-1;
99 break
100 end
101 i = i+1 ;
102 end
103
104 %----- Step 5.4:Gaussian RBF-----
105 [U, S, V]=svd(G);
106 S11 = S(1,1);

```

```

107 S1 = S11*(delta);
108
109 for i=1:N_tr
110 Sii = S(i,i);
111 if Sii <= S1 ;
112 M = i-1
113 break
114 end
115 i = i+1 ;
116 end
117
118 %*****
119 %-----Step 6:Using QR to find the centres of basis function --
120 %-----and the location of centres -----
121 %*****
122 %----- Step 6.1:CS_RBF1 -----
123 V1_CS_RBF1 = -V_CS_RBF1;
124 V11_CS_RBF1=V1_CS_RBF1(1:M_CS_RBF1,1:M_CS_RBF1);
125 %partition matrix V
126 V21_CS_RBF1=V1_CS_RBF1(M_CS_RBF1+1:N_tr,1:M_CS_RBF1);V2_CS_RBF1 =
    [V11_CS_RBF1' V21_CS_RBF1'];
127
128 [Q_CS_RBF1,R_CS_RBF1,P_CS_RBF1]=qr(V2_CS_RBF1);
129 mu_CS_RBF1 = X_trnN*P_CS_RBF1;
130 Xctr_CS_RBF1_ex = mu_CS_RBF1(1,1:M_CS_RBF1);
131 Xctr_CS_RBF1 = randsample(Xctr_CS_RBF1_ex,M)
132
133 %----- Step 6.2:CS1 -----
134 V1_CS1 = -V_CS1;
135 V11_CS1=V1_CS1(1:M_CS1,1:M_CS1); %partition matrix V
136 V21_CS1=V1_CS1(M_CS1+1:N_tr,1:M_CS1);
137 V2_CS1 = [V11_CS1' V21_CS1'];
138
139 [Q_CS1,R_CS1,P_CS1]=qr(V2_CS1);
140 mu_CS1 = X_trnN*P_CS1;
141 Xctr_CS1_ex = mu_CS1(1,1:M_CS1);
142
143 Xctr_CS1 = randsample(Xctr_CS1_ex,M)
144
145 %----- Step 6.3:CS2 -----
146 V1_CS2 = -V_CS2;
147 V11_CS2=V1_CS2(1:M_CS2,1:M_CS2); %partition matrix V
148 V21_CS2=V1_CS2(M_CS2+1:N_tr,1:M_CS2);
149 V2_CS2 = [V11_CS2' V21_CS2'];
150
151 [Q_CS2,R_CS2,P_CS2]=qr(V2_CS2);
152 mu_CS2 = X_trnN*P_CS2;
153 Xctr_CS2_ex = mu_CS2(1,1:M_CS2);
154
155 Xctr_CS2 = randsample(Xctr_CS2_ex,M)
156
157 %----- Step 6.4:Gaussian RBF-----
158 V1 = -V;
159 V11=V1(1:M,1:M); %partition matrix V
160 V21=V1(M+1:N_tr,1:M);
161 V2 = [V11' V21'];
162
163 [Q, R, P]= qr(V2);

```

```

164 mu = X_trnN*P;
165 Xctr = mu(1,1:M)
166
167 %*****
168 %----- Step 7: Construct the interpolation matrix-----
169 %*****
170 %----- Step 7.1: CS_RBF1 -----
171 for i=1:N_tr
172 for j=1:M
173 r1_CS_RBF1(i,j)=abs(X_trnN(1,i)-Xctr_CS_RBF1(1,j));
174 Phi_CS_RBF1(i,j)=(1/3)+r1_CS_RBF1(i,j).^2-
    (4/3)*r1_CS_RBF1(i,j).^3+2*(r1_CS_RBF1(i,j).^2)*log(r1_CS_RBF1(i,j));
175 if r1_CS_RBF1(i,j)== 0
176 Phi_CS_RBF1(i,j)=(1/3)+r1_CS_RBF1(i,j).^2-(4/3)*r1_CS_RBF1(i,j).^3;
177 end
178 end
179 end
180
181 %----- Step 7.2: CS1 -----
182 for i=1:N_tr
183 for j=1:M
184 r1_CS1(i,j)=abs(X_trnN(1,i)-Xctr_CS1(1,j));
185 Phi_CS1(i,j)=(112/45)*r1_CS1(i,j).^(9/2)+(16/3)*r1_CS1(i,j).^(7/2)-7*r1_CS1(i,j).^4-
    (14/15)*r1_CS1(i,j).^2+(1/9);
186 end
187 end
188
189 %----- Step 7.3: CS2 -----
190 for i=1:N_tr
191 for j=1:M
192 r1_CS2(i,j)=abs(X_trnN(1,i)-Xctr_CS2(1,j));
193 Phi_CS2(i,j)=(1/18)-r1_CS2(i,j).^2+(4/9)*r1_CS2(i,j).^3+0.5*r1_CS2(i,j).^4-
    (4/3)*r1_CS2(i,j).^3*log(r1_CS2(i,j));
194 if r1_CS2(i,j)== 0
195 Phi_CS2(i,j)=(1/18)-r1_CS2(i,j).^2+(4/9)*r1_CS2(i,j).^3+0.5*r1_CS2(i,j).^4;
196 end
197 end
198
199 %----- Step 7.4: Gaussian RBF-----
200 for i=1:N_tr
201 for j=1:M
202 r1(i,j)=abs(X_trnN(1,i)-Xctr(1,j));
203 Phi(i,j)=exp(-(r1(i,j).^2)/(2*(shp^2)));
204 end
205 end
206
207 %*****
208 %----- Step 8: Computing the weight 'w' -----
209 %*****
210 %Moore-Penrose Pseudoinverse of matrix
211 w_CS_RBF1 = pinv(Phi_CS_RBF1)*Y_trnN
212 w_CS1 = pinv(Phi_CS1)*Y_trnN
213 w_CS2 = pinv(Phi_CS2)*Y_trnN
214 w=pinv(Phi)*Y_trnN
215
216 %*****
217 %----- Step 9: Computing the approximation of training dataset ---
218 %*****

```

```

219 %----- Step 9.1:CS_RBF1 -----
220 YappxN_CS_RBF1=Phi_CS_RBF1*w_CS_RBF1;
221 Yappx_CS_RBF1 = YappxN_CS_RBF1*(max(Y_trn)-min(Y_trn))+min(Y_trn);
222
223 %----- Step 9.2:CS1 -----
224 YappxN_CS1=Phi_CS1*w_CS1;
225 Yappx_CS1 = YappxN_CS1*(max(Y_trn)-min(Y_trn))+min(Y_trn);
226
227 %----- Step 9.3:CS2 -----
228 YappxN_CS2=Phi_CS2*w_CS2;
229 Yappx_CS2 = YappxN_CS2*(max(Y_trn)-min(Y_trn))+min(Y_trn);
230
231 %----- Step 9.4:Gaussian RBF -----
232 YappxN=Phi*w;
233 Yappx = YappxN*(max(Y_trn)-min(Y_trn))+min(Y_trn);
234
235 %*****
236 %----- Step 10:Computing the training error with MSE -----
237 %*****
238 Err_Trn_CS_RBF1=(1/N_tr)*sum((Y_trn-Yappx_CS_RBF1).^2);
239 Err_Trn_CS1=(1/N_tr)*sum((Y_trn-Yappx_CS1).^2);
240 Err_Trn_CS2=(1/N_tr)*sum((Y_trn-Yappx_CS2).^2);
241 Err_Trn=(1/N_tr)*sum((Y_trn-Yappx).^2);
242
243 T_Trn = table(Err_Trn_CS_RBF1,Err_Trn_CS1,Err_Trn_CS2,Err_Trn)
244
245 %*****
246 %----- Step 11:Generate validation dataset -----
247 %*****
248 %----//Generate a validation dataset of 1000 data points in ----//
249 for i=1:1000
250 X_vld(i)=2*pi*(i-1)/1000;
251 end
252 Y_vld=awgn(X_vld.^2)/6-X_vld+4,15,'measured');
253 %Y_vld with Gaussian noise
254
255 for i=1:1000
256 for j=1:1000
257 XY_vld(i,1)=X_vld(i);
258 XY_vld(j,2)=Y_vld(j);
259 end
260 end
261 XY_vld;
262
263 x2max = max(X_vld);
264 X_vldN=(X_vld-min(X_vld))/(x2max);
265 %*****
266 %----- Step 12:Construct the interpolation matrix -----
267 %----- from X_vld to Xctr -----
268 %*****
269 %----- Step 12.1:CS_RBF1 -----
270 for i=1:1000
271 for j=1:M
272 r2_CS_RBF1(i,j)=abs(X_vldN(1,i)-Xctr_CS_RBF1(1,j));
273 Phi2_CS_RBF1(i,j)=(1/3)+r2_CS_RBF1(i,j).^2-
(4/3)*r2_CS_RBF1(i,j).^3+2*(r2_CS_RBF1(i,j).^2)*log(r2_CS_RBF1(i,j));
274 if r2_CS_RBF1(i,j)==0

```

```

275 Phi2_CS_RBF1(i,j)=(1/3)+r2_CS_RBF1(i,j).^2-(4/3)*r2_CS_RBF1(i,j).^3;
276 end
277 end
278 end
279
280 %----- Step 12.2:CS1 -----
281 for i=1:1000
282 for j=1:M
283 r2_CS1(i,j)=abs(X_vldN(1,i)-Xctr_CS1(1,j));
284 Phi2_CS1(i,j)=(112/45)*r2_CS1(i,j).^2+(16/3)*r2_CS1(i,j).^3+0.5*r2_CS1(i,j).^4-
(14/15)*r2_CS1(i,j).^2+(1/9);
285 end
286 end
287
288 %----- Step 12.3:CS2 -----
289 for i=1:1000
290 for j=1:M
291 r2_CS2(i,j)=abs(X_vldN(1,i)-Xctr_CS2(1,j));
292 Phi2_CS2(i,j)=(1/18)*r2_CS2(i,j).^2+(4/9)*r2_CS2(i,j).^3+0.5*r2_CS2(i,j).^4-
(4/3)*r2_CS2(i,j).^3*log(r2_CS2(i,j));
293 if r2_CS2(i,j)==0
294 Phi2_CS2(i,j)=(1/18)*r2_CS2(i,j).^2+(4/9)*r2_CS2(i,j).^3+0.5*r2_CS2(i,j).^4;
295 end
296 end
297 end
298
299 %----- Step 12.4:Gaussian RBF -----
300 for i=1:1000
301 for j=1:M
302 r2(i,j)=abs(X_vldN(1,i)-Xctr(1,j));
303 Phi2(i,j)=exp(-(r2(i,j)^2)/(2*(shp^2)));
304 end
305 end
306
307 %*****
308 %----- Step 13:Construct the Y_vldapxN from Phi2 and weight 'w'
309 %*****
310 %----- Step 13.1:CS_RBF1 -----
311 Y_vldapxN_CS_RBF1=Phi2_CS_RBF1*w_CS_RBF1;
312 Y_vldapx_CS_RBF1 = Y_vldapxN_CS_RBF1.*(max(Y_vld)-min(Y_vld))+min(Y_vld);
313
314 %----- Step 13.2:CS1 -----
315 Y_vldapxN_CS1=Phi2_CS1*w_CS1;
316 Y_vldapx_CS1 = Y_vldapxN_CS1.*(max(Y_vld)-min(Y_vld))+min(Y_vld);
317
318 %----- Step 13.3:CS2 -----
319 Y_vldapxN_CS2=Phi2_CS2*w_CS2;
320 Y_vldapx_CS2 = Y_vldapxN_CS2.*(max(Y_vld)-min(Y_vld))+min(Y_vld);
321
322 %----- Step 13.4:Gaussian RBF -----
323 Y_vldapxN=Phi2*w;
324 Y_vldapx = Y_vldapxN.*(max(Y_vld)-min(Y_vld))+min(Y_vld);
325
326 %*****
327 %----- Step 14:Computing the validation error with MSE -----
328 %*****
329 Err_Vld_CS_RBF1=(1/1000)*sum((Y_vld-Y_vldapx_CS_RBF1).^2);
330 Err_Vld_CS1=(1/1000)*sum((Y_vld-Y_vldapx_CS1).^2);

```

```

331 Err_Vld_CS2=(1/1000)*sum((Y_vld-Y_vldapx_CS2).^2);
332 Err_Vld =(1/1000)*sum((Y_vld-Y_vldapx).^2);
333
334 T_Vld = table(Err_Vld_CS_RBF1,Err_Vld_CS1,Err_Vld_CS2,Err_Vld)
335
336 Y1 =(X_trn.^2)/6- X_trn +4;
337
338 for i=1:100
339 Y3(i)= 20;
340 End
341
342 %----- Step 12 : Results Plotting -----
343 figure;
344 hold on
345 plot(X_trn,Y_trn,'ok','LineWidth',1);
346 plot(X_trn,Y3,'ok','LineWidth',1);
347 plot(X_trn,Y1,'k','LineWidth',1);
348 xlabel('x', 'FontSize',14);
349 ylabel('Y=(X.^2)/6-X+4', 'FontSize',14);
350 grid on
351
352 figure;
353 hold on
354 plot(X_trn,Y_trn,'ok','markersize',3);
355 plot(X_trn,Yappx_CS_RBF1,'k','LineWidth',2);
356 plot(X_trn,Yappx_CS1,'-r','LineWidth',2);
357 plot(X_trn,Yappx_CS2,'-m','LineWidth',2);
358 plot(X_trn,Yappx,'-g','LineWidth',2);
359 title('Training data')
360 xlabel('X', 'FontSize',14);
361 ylabel('Y=(X.^2)/6-X+4', 'FontSize',14);
362 legend('Exact', 'CS RBF1', 'CS1', 'CS2', 'Gaussian', 'Location',
        'SouthEast')
363 grid on
364
365 figure;
366 hold on
367 plot(X_vld,Y_vld,'ok','markersize',3);
368 plot(X_vld,Y_vldapx_CS_RBF1,'k','LineWidth',2);
369 plot(X_vld,Y_vldapx_CS1,'-r','LineWidth',2);
370 plot(X_vld,Y_vldapx_CS2,'-m','LineWidth',2);
371 plot(X_vld,Y_vldapx,'-g','LineWidth',2);
372 title('Validation data')
373 xlabel('X', 'FontSize',14);
374 ylabel('Y=(X.^2)/6-X+4', 'FontSize',14);
375 legend('Exact', 'CS RBF1', 'CS1', 'CS2', 'Gaussian', 'Location',
        'SouthEast')
376 %----- THIS IS THE END -----

```

A.1.3 Test Case 3: Sine interpolation

A.1.3.1 Training and validation errors for candidate models for sine interpolation case.

```

1 clc
2 clear all

```

```

3 close all
4
5 %*****
6 %----- Step 1:Generate training dataset -----
7 %*****
8 for i=1:100
9 X_trn(i)=2*pi*(i-1)/100;
10 end
11 Y_trn=awgn(sin(X_trn),0.5,'measured');
12 for i=1:100
13 for j=1:100
14 XY_trn (i,1)=X_trn (i);
15 XY_trn (j,2)=Y_trn (j);
16 end
17 end
18 XY_trn;
19
20 N_tr = length(X_trn);
21
22 %*****
23 %----- Step 2:Normalizing both X_trn and Y_trn -----
24 %*****
25 x1max =max(X_trn);
26 X_trnN=(X_trn -min(X_trn))/(x1max); % Normalized X_trn
27 Y_trnN=(Y_trn -min(Y_trn))/(max(Y_trn)-min(Y_trn)); % Normalized Y_trn
28
29 %*****
30 %----- Step 3:Choosing the shape parameter-----
31 %*****
32 shp = input('Enter the shape parameter = ');
33
34 %*****
35 %----- Step 4:Construct the interpolation matrix-----
36 %----- CS_RBF1, CS1, CS2, G -----
37 %*****
38 for i=1:N_tr
39 for j=1:N_tr
40 r(i,j)=abs(X_trnN (1,i)-X_trnN (1,j));
41 CS_RBF1(i,j)=(1/3)+r(i,j).^2-(4/3)*r(i,j).^3+2*(r(i,j).^2)*log(r(i,j));
42 CS1(i,j)=(112/45)*r(i,j).^(9/2)+(16/3)*r(i,j).^(7/2)-7*r(i,j).^4-(14/15)*r(i,j).^2+(1/9);
43 CS2(i,j)=(1/18)*r(i,j).^2+(4/9)*r(i,j).^3+0.5*r(i,j).^4-(4/3)*r(i,j).^3*log(r(i,j));
44 G(i,j)=exp(-(r(i,j)^2)/(2*(shp^2)));
45 if r(i,j)== 0
46 CS_RBF1(i,j)=(1/3)+r(i,j).^2-(4/3)*r(i,j).^3;
47 CS2(i,j)=(1/18)*r(i,j).^2+(4/9)*r(i,j).^3+0.5*r(i,j).^4;
48 end
49 end
50 end
51
52 %*****
53 %----- Step 5:Using SVD to get the number of centres -----
54 %----- out of matrix CS_RBF1, CS1, CS2, G -----
55 %*****
56 delta = 0.01/100;
57
58 %----- Step 5.1:CS_RBF1 -----
59 [U_CS_RBF1,S_CS_RBF1,V_CS_RBF1]= svd(CS_RBF1);
60 S11_CS_RBF1 = S_CS_RBF1(1,1);

```

```

61 %The firsts singular of singular value
62 S1_CS_RBF1 = S11_CS_RBF1*(delta);
63
64 for i=1:N_tr
65 Sii_CS_RBF1 = S_CS_RBF1(i,i);
66 if Sii_CS_RBF1 <= S1_CS_RBF1
67 M_CS_RBF1 = i-1;
68 break
69 end
70 i = i+1 ;
71 end
72
73 %----- Step 5.2:CS1 -----
74 [U_CS1,S_CS1,V_CS1]=svd(CS1);
75 S11_CS1 = S_CS1(1,1);
76 %The firsts singular of singular value
77 S1_CS1 = S11_CS1*(delta);
78 for i=1:N_tr
79 Sii_CS1 =S_CS1(i,i);
80 if Sii_CS1 <= S1_CS1
81 M_CS1 = i-1;
82 break
83 end
84 i = i+1 ;
85 end
86
87 %----- Step 5.3:CS2 -----
88 [U_CS2,S_CS2,V_CS2]=svd(CS2);
89 S11_CS2 = S_CS2(1,1);
90 %The firsts singular of singular value
91 S1_CS2 = S11_CS2*(delta);
92
93 for i=1:N_tr
94 Sii_CS2 =S_CS2(i,i);
95 if Sii_CS2 <= S1_CS2
96 M_CS2 = i-1;
97 break
98 end
99 i = i+1 ;
100 end
101 %----- Step 5.4:Gaussian RBF -----
102 [U,S,V]=svd(G);
103 S11 = S(1,1);
104 S1 = S11*(delta);
105
106 for i=1:N_tr
107 Sii = S(i,i);
108 if Sii <= S1 ;
109 M = i-1 ;
110 break
111 end
112 i = i+1 ;
113 end
114
115 %*****
116 %-----Step 6:Using QR to find the centres of-----
117 %-----basis function and the location of centres -----
118 %*****

```



```

119 %-----Step 6.1:CS_RBF1 -----
120 V1_CS_RBF1 = -V_CS_RBF1;
121 V11_CS_RBF1=V1_CS_RBF1(1:M_CS_RBF1,1:M_CS_RBF1);
122 %partition matrix
123 V21_CS_RBF1=V1_CS_RBF1(M_CS_RBF1+1:N_tr,1:M_CS_RBF1);
124 V2_CS_RBF1 = [V11_CS_RBF1' V21_CS_RBF1'];
125
126 [Q_CS_RBF1,R_CS_RBF1,P_CS_RBF1]=qr(V2_CS_RBF1);
127 mu_CS_RBF1 = X_trnN*P_CS_RBF1;
128 Xctr_CS_RBF1 = mu_CS_RBF1(1,1:M_CS_RBF1);
129
130 %-----Step 6.2:CS1 -----
131 V1_CS1 = -V_CS1;
132 V11_CS1=V1_CS1(1:M_CS1,1:M_CS1);
133 %partition matrix V
134 V21_CS1=V1_CS1(M_CS1+1:N_tr,1:M_CS1);
135 V2_CS1 = [V11_CS1' V21_CS1'];
136
137 [Q_CS1,R_CS1,P_CS1]=qr(V2_CS1);
138 mu_CS1 = X_trnN*P_CS1;
139 Xctr_CS1 = mu_CS1(1,1:M_CS1);
140
141 %-----Step 6.3:CS2 -----
142 V1_CS2 = -V_CS2;
143 V11_CS2=V1_CS2(1:M_CS2,1:M_CS2);
144 %partition matrix V
145 V21_CS2=V1_CS2(M_CS2+1:N_tr,1:M_CS2);
146 V2_CS2 = [V11_CS2' V21_CS2'];
147
148 [Q_CS2,R_CS2,P_CS2]=qr(V2_CS2);
149 mu_CS2 = X_trnN*P_CS2;
150 Xctr_CS2 = mu_CS2(1,1:M_CS2);
151
152 %-----Step 6.4:Gaussian RBF-----
153 V1 = -V;
154 V11=V1(1:M,1:M); %partition matrix V
155 V21=V1(M+1:N_tr,1:M);
156 V2 = [V11' V21'];
157 [Q,R,P]=qr(V2);
158 mu = X_trnN*P;
159 Xctr = mu(1,1:M)
160
161 %*****
162 %-----Step 7:Construct the interpolation matrix-----
163 %*****
164 %-----Step 7.1:CS_RBF1 -----
165 for i=1:N_tr
166 for j=1:M_CS_RBF1
167 r1_CS_RBF1(i,j)=abs(X_trnN(1,i)-Xctr_CS_RBF1(1,j));
168 Phi_CS_RBF1(i,j)=(1/3)+r1_CS_RBF1(i,j).^2-
(4/3)*r1_CS_RBF1(i,j).^3+2*(r1_CS_RBF1(i,j).^2)*log(r1_CS_RBF1(i,j));
169 if r1_CS_RBF1(i,j)==0
170 Phi_CS_RBF1(i,j)=(1/3)+r1_CS_RBF1(i,j).^2-(4/3)*r1_CS_RBF1(i,j).^3;
171 end
172 end
173 end
174

```

```

175 %----- Step 7.2:CS1 -----
176 for i=1:N_tr
177 for j=1:M_CS1
178 r1_CS1(i,j)=abs(X_trnN (1,i)-Xctr_CS1(1,j));
179 Phi_CS1(i,j)=(112/45)*r1_CS1(i,j)^(9/2)+(16/3)*r1_CS1(i,j)^(7/2)-7*r1_CS1(i,j)^4-
    (14/15)*r1_CS1(i,j)^(2+1/9);
180 end
181 end
182
183 %----- Step 7.3:CS2 -----
184 for i=1:N_tr
185 for j=1:M_CS2
186 r1_CS2(i,j)=abs(X_trnN (1,i)-Xctr_CS2(1,j));
187 Phi_CS2(i,j)=(1/18)*r1_CS2(i,j)^2+(4/9)*r1_CS2(i,j)^3+0.5*r1_CS2(i,j)^4-
    (4/3)*r1_CS2(i,j)^3*log(r1_CS2(i,j));
188 if r1_CS2(i,j)== 0
189 Phi_CS2(i,j)=(1/18)*r1_CS2(i,j)^2+(4/9)*r1_CS2(i,j)^3+0.5*r1_CS2(i,j)^4;
190 end
191 end
192 end
193
194 %----- Step 7.4:Gaussian RBF-----
195 for i=1:N_tr
196 for j=1:M
197 r1(i,j)=abs(X_trnN (1,i)-Xctr(1,j));
198 Phi(i,j)=exp(-(r1(i,j)^2)/(2*(shp^2)));
199 end
200 end
201
202 %*****
203 %----- Step 8:Computing the weight 'w' -----
204 %*****
205 %Moore-Penrose Pseudoinverse of matrix
206 w_CS_RBF1 =pinv(Phi_CS_RBF1)*Y_trnN;
207 w_CS1 =pinv(Phi_CS1)*Y_trnN;
208 w_CS2 =pinv(Phi_CS2)*Y_trnN;
209 w=pinv(Phi)*Y_trnN;
210
211 %*****
212 %----- Step 9:Computing the approximation of -----
213 %----- training dataset-----
214 %*****
215 %----- Step 9.1:CS_RBF1 -----
216 YappxN_CS_RBF1=Phi_CS_RBF1*w_CS_RBF1;
217 Yappx_CS_RBF1 = YappxN_CS_RBF1*(max(Y_trn)-min(Y_trn))+min(Y_trn);
218
219 %----- Step 9.2:CS1 -----
220 YappxN_CS1=Phi_CS1*w_CS1;
221 Yappx_CS1 = YappxN_CS1*(max(Y_trn)-min(Y_trn))+min(Y_trn);
222
223 %----- Step 9.3:CS2 -----
224 YappxN_CS2=Phi_CS2*w_CS2;
225 Yappx_CS2 = YappxN_CS2*(max(Y_trn)-min(Y_trn))+min(Y_trn);
226
227 %----- Step 9.4:Gaussian RBF-----
228 YappxN=Phi*w;
229 Yappx = YappxN*(max(Y_trn)-min(Y_trn))+min(Y_trn);
230

```

```

231 %*****
232 %-----Step 10:Computing the training error with MSE-----
233 %*****
234 Err_Trn_CS_RBF1=(1/N_tr)*sum((Y_trn -Yappx_CS_RBF1).^2);
235 Err_Trn_CS1=(1/N_tr)*sum((Y_trn -Yappx_CS1).^2);
236 Err_Trn_CS2=(1/N_tr)*sum((Y_trn -Yappx_CS2).^2);
237 Err_Trn=(1/N_tr)*sum((Y_trn -Yappx).^2);
238
239 T_Trn = table(Err_Trn_CS_RBF1,Err_Trn_CS1,Err_Trn_CS2,Err_Trn)
240
241 %*****
242 %-----Step 11:Generate validation dataset -----
243 %*****
244 %-----///Generate a validation dataset of 1000 data points ///-----
245 for i=1:1000
246 X_vld(i)=2*pi*(i-1)/1000);
247 End
248
249 Y_vld=awgn(sin(X_vld),15, 'measured');
250 %Y_vld with Gaussian noise
251
252 for i=1:1000
253 for j=1:1000
254 XY_vld(i,1)=X_vld(i);
255 XY_vld(j,2)=Y_vld(j);
256 end
257 end
258 XY_vld;
259
260 x2max = max(X_vld);
261 X_vldN=(X_vld-min(X_vld))/(x2max);
262
263 %*****
264 %-----Step 12:Construct the interpolation matrix-----
265 %-----from Xvld to Xctr-----
266 %*****
267 %-----Step 12.1:CS_RBF1 -----
268 for i=1:1000
269 for j=1:M_CS_RBF1
270 r2_CS_RBF1(i,j)=abs(X_vldN(1,i)-Xctr_CS_RBF1(1,j));
271 Phi2_CS_RBF1(i,j)=(1/3)+r2_CS_RBF1(i,j).^2-
    (4/3)*r2_CS_RBF1(i,j).^3+2*(r2_CS_RBF1(i,j).^2)*log(r2_CS_RBF1(i,j));
272 if r2_CS_RBF1(i,j)==0
273 Phi2_CS_RBF1(i,j)=(1/3)+r2_CS_RBF1(i,j).^2-(4/3)*r2_CS_RBF1(i,j).^3;
274 end
275 end
276 end
277
278 %-----Step 12.2:CS1 -----
279 for i=1:1000
280 for j=1:M_CS1
281 r2_CS1(i,j)=abs(X_vldN(1,i)-Xctr_CS1(1,j));
282 Phi2_CS1(i,j)=(112/45)*r2_CS1(i,j)^(9/2)+(16/3)*r2_CS1(i,j)^(7/2)-7*r2_CS1(i,j)^(4-
    (14/15)*r2_CS1(i,j)^(2+(1/9));
283 end
284 end
285
286 %-----Step 12.3:CS2 -----

```

```

287 for i=1:1000
288 for j=1:M_CS2
289 r2_CS2(i,j)=abs(X_vldN(1,i)-Xctr_CS2(1,j));
290 Phi2_CS2(i,j)=(1/18)*r2_CS2(i,j).^2+(4/9)*r2_CS2(i,j).^3+0.5*r2_CS2(i,j).^4-
    (4/3)*r2_CS2(i,j).^3*log(r2_CS2(i,j));
291 if r2_CS2(i,j)==0
292 Phi2_CS2(i,j)=(1/18)*r2_CS2(i,j).^2+(4/9)*r2_CS2(i,j).^3+0.5*r2_CS2(i,j).^4;
293 end
294 end
295 end
296
297 %----- Step 12.4:Gaussian RBF-----
298 for i=1:1000
299 for j=1:M
300 r2(i,j)=abs(X_vldN(1,i)-Xctr(1,j));
301 Phi2(i,j)=exp(-(r2(i,j))^2/(2*(shp^2)));
302 end
303 end
304
305 %*****
306 %----- Step 13:Construct the YvldapxN from Phi2-----
307 %-----and weight 'w'-----
308 %*****
309 %----- Step 13.1:CS_RBF1-----
310 YvldapxN_CS_RBF1=Phi2_CS_RBF1*w_CS_RBF1;
311 Yvldapx_CS_RBF1 = YvldapxN_CS_RBF1*(max(Y_vld)-min(Y_vld))+min(Y_vld);
312
313 %----- Step 13.2:CS1-----
314 YvldapxN_CS1=Phi2_CS1*w_CS1;
315 Yvldapx_CS1 = YvldapxN_CS1*(max(Y_vld)-min(Y_vld))+min(Y_vld);
316
317 %----- Step 13.3:CS2-----
318 YvldapxN_CS2=Phi2_CS2*w_CS2;
319 Yvldapx_CS2 = YvldapxN_CS2*(max(Y_vld)-min(Y_vld))+min(Y_vld);
320
321 %----- Step 13.4:Gaussian RBF-----
322 YvldapxN=Phi2*w;
323 Yvldapx = YvldapxN*(max(Y_vld)-min(Y_vld))+min(Y_vld);
324
325 %*****
326 %----- Step 14:Computing the validation error with MSE-----
327 %*****
328 Err_Vld_CS_RBF1=(1/1000)*sum((Y_vld -Yvldapx_CS_RBF1).^2);
329 Err_Vld_CS1=(1/1000)*sum((Y_vld -Yvldapx_CS1).^2);
330 Err_Vld_CS2=(1/1000)*sum((Y_vld -Yvldapx_CS2).^2);
331 Err_Vld =(1/1000)*sum((Y_vld -Yvldapx).^2);
332
333 T_Vld = table(Err_Vld_CS_RBF1,Err_Vld_CS1,Err_Vld_CS2,Err_Vld)
334
335 %*****
336 %----- Step 15:Results Plotting-----
337 %*****
338 figure;
339 hold on
340 plot(X_trn, Y_trn,'ob','markersize',3);
341 xlabel('Input Variable (x)', 'FontSize',14);
342 ylabel('Output Variable (y)', 'FontSize',14);
343 grid on

```

```

344
345 figure;
346 hold on
347 plot(X_trn, Y_trn, 'ob', 'markersize', 3);
348 plot(X_trn, Yappx_CS_RBF1, '-k', 'LineWidth', 2);
349 plot(X_trn, Yappx_CS1, '-r', 'LineWidth', 2);
350 plot(X_trn, Yappx_CS2, '-m', 'LineWidth', 2);
351 plot(X_trn, Yappx, '-g', 'LineWidth', 2);
352 title('Training data')
353 xlabel('X', 'FontSize', 14);
354 ylabel('Y=sin(X)', 'FontSize', 14);
355 legend('Exact', 'CS RBF1', 'CS1', 'CS2', 'Gaussian', 'Location',
        'SouthEast')
356 grid on
357
358 figure;
359 hold on
360 plot(X_vld, Y_vld, 'ob', 'markersize', 3);
361 plot(X_vld, Yvldapx_CS_RBF1, '-k', 'LineWidth', 2);
362 plot(X_vld, Yvldapx_CS1, '-r', 'LineWidth', 2);
363 plot(X_vld, Yvldapx_CS2, '-m', 'LineWidth', 2);
364 plot(X_vld, Yvldapx, '-g', 'LineWidth', 2);
365 title('Validation data')
366 xlabel('X', 'FontSize', 14);
367 ylabel('Y=sin(X)', 'FontSize', 14);
368 legend('Exact', 'CS RBF1', 'CS1', 'CS2', 'Gaussian', 'Location',
        'SouthEast')
369 grid on
370
371 %----- THIS IS THE END -----

```

A.1.3.2 Using different numbers of centres and RBFs for parabola function.

```

1 clc
2 clear all
3 close all
4
5 %*****
6 %----- Step 1: Generate training dataset -----
7 %*****
8 for i=1:100
9 X_trn(i)=2*pi*(i-1)/100;
10 End
11 Y_trn=awgn(sin(X_trn), 0.5, 'measured');
12 %Y_trn with Gaussian
13 for i=1:100
14 for j=1:100
15 XY_trn(i,1)=X_trn(i);
16 XY_trn(j,2)=Y_trn(j);
17 end
18 end
19
20 XY_trn;
21 N_tr = length(X_trn);
22
23 %*****
24 %----- Step 2: Normalizing both X_trn and Y_trn -----

```

```

25 %*****
26 x1max =max(X_trn);
27 X_trnN=(X_trn-min(X_trn))/(x1max);
28 %Normalized X_trn
29 Y_trnN=(Y_trn-min(Y_trn))/(max(Y_trn)-min(Y_trn));
30 %Normalized Y_trn
31
32 %*****
33 %-----Step 3:Choosing the shape parameter-----
34 %*****
35 shp = input('Enter the shape parameter = ');
36
37 %*****
38 %-----Step 4:Construct the interpolation matrix-----
39 %-----CS_RBF1, CS1, CS2, G-----
40 %*****
41 for i=1:N_tr
42 for j=1:N_tr
43 r(i,j)=abs(X_trnN(1,i)-X_trnN(1,j));
44 CS_RBF1(i,j)=(1/3)+r(i,j).^2-(4/3)*r(i,j).^3+2*(r(i,j).^2)*log(r(i,j));
45 CS1(i,j)=(112/45)*r(i,j).^(9/2)+(16/3)*r(i,j).^(7/2)-7*r(i,j).^4-(14/15)*r(i,j).^2+(1/9);
46 CS2(i,j)=(1/18)-r(i,j).^2+(4/9)*r(i,j).^3+0.5*r(i,j).^4-(4/3)*r(i,j).^3*log(r(i,j));
47 G(i,j)=exp(-(r(i,j)^2)/(2*(shp^2)));
48 if r(i,j)==0
49 CS_RBF1(i,j)=(1/3)+r(i,j).^2-(4/3)*r(i,j).^3;
50 CS2(i,j)=(1/18)-r(i,j).^2+(4/9)*r(i,j).^3+0.5*r(i,j).^4;
51 end
52 end
53 end
54
55 %*****
56 %-----Step 5:Using SVD to get the number of centres-----
57 %-----out of matrix CS_RBF1, CS1, CS2, G-----
58 %*****
59 delta = 0.01/100;
60
61 %-----Step 5.1:CS_RBF1-----
62 [U_CS_RBF1,S_CS_RBF1,V_CS_RBF1]=svd(CS_RBF1);
63 S11_CS_RBF1 = S_CS_RBF1(1,1);
64 %The firsts singular of singular value
65 S1_CS_RBF1 = S11_CS_RBF1*(delta);
66
67 for i=1:N_tr
68 Sii_CS_RBF1 = S_CS_RBF1(i,i);
69 if Sii_CS_RBF1 <= S1_CS_RBF1
70 M_CS_RBF1 = i-1;
71 break
72 end
73 i = i+1 ;
74 end
75
76 %-----Step 5.2:CS1-----
77 [U_CS1,S_CS1,V_CS1]=svd(CS1);
78 S11_CS1 = S_CS1(1,1); %The firsts singular of singular value
79 S1_CS1 = S11_CS1*(delta);
80
81 for i=1:N_tr
82 Sii_CS1 = S_CS1(i,i);

```

```

83 if Sii_CS1 <= S1_CS1
84 M_CS1 = i-1;
85 break
86 end
87 i = i+1 ;
88 end
89
90 %----- Step 5.3:CS2 -----
91 [U_CS2,S_CS2,V_CS2]=svd(CS2);
92 S11_CS2 =S_CS2(1,1); %The firsts singular of singular value
93 S1_CS2 = S11_CS2*(delta);
94
95 for i=1:N_tr
96 Sii_CS2 = S_CS2(i, i);
97 if Sii_CS2 <= S1_CS2
98 M_CS2 = i-1;
99 break
100 end
101 i = i+1 ;
102 end
103
104 %----- Step 5.4:Gaussian RBF -----
105 [U,S,V]=svd(G);
106 S11 = S(1,1);
107 S1 = S11*(delta);
108
109 for i=1:N_tr
110 Sii = S(i, i);
111 if Sii <= S1 ;
112 M = i-1
113 break
114 end
115 i = i+1 ;
116 end
117
118 %*****
119 %----- Step 6:Using QR to find the centres of basis function --
120 %----- and the location of centres -----
121 %*****
122 %----- Step 6.1:CS_RBF1 -----
123 V1_CS_RBF1 = -V_CS_RBF1;
124 V11_CS_RBF1=V1_CS_RBF1(1:M_CS_RBF1,1:M_CS_RBF1);
125 %partition matrix V
126 V21_CS_RBF1=V1_CS_RBF1(M_CS_RBF1+1:N_tr,1:M_CS_RBF1);V2_CS_RBF1 =
[V11_CS_RBF1' V21_CS_RBF1'];
127
128 [Q_CS_RBF1,R_CS_RBF1,P_CS_RBF1]=qr(V2_CS_RBF1);
129 mu_CS_RBF1 = X_trnN*P_CS_RBF1;
130 Xctr_CS_RBF1_ex =mu_CS_RBF1(1,1:M_CS_RBF1);
131 Xctr_CS_RBF1 = randsample(Xctr_CS_RBF1_ex,M)
132
133 %----- Step 6.2:CS1 -----
134 V1_CS1 = -V_CS1;
135 V11_CS1=V1_CS1(1:M_CS1,1:M_CS1); %partition matrix V
136 V21_CS1=V1_CS1(M_CS1+1:N_tr,1:M_CS1);
137 V2_CS1 = [V11_CS1' V21_CS1'];
138
139 [Q_CS1,R_CS1,P_CS1]=qr(V2_CS1);

```

```

140 mu_CS1 = X_trnN*P_CS1;
141 Xctr_CS1_ex = mu_CS1(1,1:M_CS1);
142
143 Xctr_CS1 = randsample(Xctr_CS1_ex,M)
144
145 %----- Step 6.3:CS2 -----
146 V1_CS2 = -V_CS2;
147 V11_CS2=V1_CS2(1:M_CS2,1:M_CS2);           %partition matrix V
148 V21_CS2=V1_CS2(M_CS2+1:N_tr,1:M_CS2);
149 V2_CS2 = [V11_CS2' V21_CS2'];
150
151 [Q_CS2,R_CS2,P_CS2]=qr(V2_CS2);
152 mu_CS2 = X_trnN*P_CS2;
153 Xctr_CS2_ex = mu_CS2(1,1:M_CS2);
154
155 Xctr_CS2 = randsample(Xctr_CS2_ex,M)
156
157 %----- Step 6.4:Gaussian RBF -----
158 V1 = -V;
159 V11=V1(1:M,1:M);           %partition matrix V
160 V21=V1(M+1:N_tr,1:M);
161 V2 = [V11' V21'];
162
163 [Q,R,P]=qr(V2);
164 mu = X_trnN*P;
165 Xctr = mu(1,1:M)
166
167 %*****
168 %----- Step 7:Construct the interpolation matrix -----
169 %*****
170 %----- Step 7.1:CS_RBF1 -----
171 for i=1:N_tr
172 for j=1:M
173 r1_CS_RBF1(i,j)=abs(X_trnN(1,i)-Xctr_CS_RBF1(1,j));
174 Phi_CS_RBF1(i,j)=(1/3)+r1_CS_RBF1(i,j).^2-
    (4/3)*r1_CS_RBF1(i,j).^3+2*(r1_CS_RBF1(i,j).^2)*log(r1_CS_RBF1(i,j));
175 if r1_CS_RBF1(i,j)== 0
176 Phi_CS_RBF1(i,j)=(1/3)+r1_CS_RBF1(i,j).^2-(4/3)*r1_CS_RBF1(i,j).^3;
177 end
178 end
179 end
180
181 %----- Step 7.2:CS1 -----
182 for i=1:N_tr
183 for j=1:M
184 r1_CS1(i,j)=abs(X_trnN(1,i)-Xctr_CS1(1,j));
185 Phi_CS1(i,j)=(112/45)*r1_CS1(i,j)^(9/2)+(16/3)*r1_CS1(i,j)^(7/2)-7*r1_CS1(i,j).^4-
    (14/15)*r1_CS1(i,j).^2+(1/9);
186 end
187 end
188
189 %----- Step 7.3:CS2 -----
190 for i=1:N_tr
191 for j=1:M
192 r1_CS2(i,j)=abs(X_trnN(1,i)-Xctr_CS2(1,j));
193 Phi_CS2(i,j)=(1/18)-r1_CS2(i,j).^2+(4/9)*r1_CS2(i,j).^3+0.5*r1_CS2(i,j).^4-
    (4/3)*r1_CS2(i,j).^3*log(r1_CS2(i,j));
194 if r1_CS2(i,j)== 0

```



```

195 Phi_CS2(i,j)=(1/18)*r1_CS2(i,j).^2+(4/9)*r1_CS2(i,j).^3+0.5*r1_CS2(i,j).^4;
196 end
197 end
198
199 %----- Step 7.4:Gaussian RBF-----
200 for i=1:N_tr
201 for j=1:M
202 r1(i,j)=abs(X_trnN(1,i)-Xctr(1,j));
203 Phi(i,j)=exp(-(r1(i,j)^2)/(2*(shp^2)));
204 end
205 end
206
207 %*****
208 %----- Step 8:Computing the weight 'w' -----
209 %*****
210 %Moore-Penrose Pseudoinverse of matrix
211 w_CS_RBF1 =pinv(Phi_CS_RBF1)*Y_trnN
212 w_CS1 = pinv(Phi_CS1)*Y_trnN
213 w_CS2 = pinv(Phi_CS2)*Y_trnN
214 w=pinv(Phi)*Y_trnN
215
216 %*****
217 %----- Step 9:Computing the approximation of training dataset -
218 %*****
219 %----- Step 9.1:CS_RBF1 -----
220 YappxN_CS_RBF1=Phi_CS_RBF1*w_CS_RBF1;
221 Yappx_CS_RBF1 = YappxN_CS_RBF1*(max(Y_trn)-min(Y_trn))+min(Y_trn);
222
223 %----- Step 9.2:CS1 -----
224 YappxN_CS1=Phi_CS1*w_CS1;
225 Yappx_CS1 = YappxN_CS1*(max(Y_trn)-min(Y_trn))+min(Y_trn);
226
227 %----- Step 9.3:CS2 -----
228 YappxN_CS2=Phi_CS2*w_CS2;
229 Yappx_CS2 = YappxN_CS2*(max(Y_trn)-min(Y_trn))+min(Y_trn);
230
231 %----- Step 9.4:Gaussian RBF-----
232 YappxN=Phi*w;
233 Yappx = YappxN*(max(Y_trn)-min(Y_trn))+min(Y_trn);
234
235 %*****
236 %----- Step 10:Computing the training error with MSE-----
237 %*****
238 Err_Trn_CS_RBF1=(1/N_tr)*sum((Y_trn-Yappx_CS_RBF1).^2);
239 Err_Trn_CS1=(1/N_tr)*sum((Y_trn-Yappx_CS1).^2);
240 Err_Trn_CS2=(1/N_tr)*sum((Y_trn-Yappx_CS2).^2);
241 Err_Trn=(1/N_tr)*sum((Y_trn-Yappx).^2);
242
243 T_Trn = table(Err_Trn_CS_RBF1,Err_Trn_CS1,Err_Trn_CS2,Err_Trn)
244
245 %*****
246 %----- Step 11:Generate validation dataset -----
247 %*****
248 %----//Generate a validation dataset of 1000 data points in ----//----
249 for i=1:1000
250 X_vld(i)=2*pi*(i-1)/1000);
251 End
252

```

```

253 Y_vld=awgn(sin(X_vld),0.5,'measured');
254 %Y_vld with Gaussian noise
255
256 for i=1:1000
257 for j=1:1000
258 XY_vld(i,1)=X_vld(i);
259 XY_vld(j,2)=Y_vld(j);
260 end
261 end
262 XY_vld;
263
264 x2max = max(X_vld);
265 X_vldN=(X_vld-min(X_vld))/(x2max);
266 %*****
267 %----- Step 12:Construct the interpolation matrix-----
268 %-----from X_vld to Xctr -----
269 %*****
270 %----- Step 12.1:CS_RBF1 -----
271 for i=1:1000
272 for j=1:M
273 r2_CS_RBF1(i,j)=abs(X_vldN(1,i)-Xctr_CS_RBF1(1,j));
274 Phi2_CS_RBF1(i,j)=(1/3)+r2_CS_RBF1(i,j)^2-
    (4/3)*r2_CS_RBF1(i,j)^3+2*(r2_CS_RBF1(i,j)^2)*log(r2_CS_RBF1(i,j));
275 if r2_CS_RBF1(i,j)== 0
276 Phi2_CS_RBF1(i,j)=(1/3)+r2_CS_RBF1(i,j)^2-(4/3)*r2_CS_RBF1(i,j)^3;
277 end
278 end
279 end
280
281 %----- Step 12.2:CS1 -----
282 for i=1:1000
283 for j=1:M
284 r2_CS1(i,j)=abs(X_vldN(1,i)-Xctr_CS1(1,j));
285 Phi2_CS1(i,j)=(112/45)*r2_CS1(i,j)^(9/2)+(16/3)*r2_CS1(i,j)^(7/2)-7*r2_CS1(i,j)^4-
    (14/15)*r2_CS1(i,j)^(1/9);
286 end
287 end
288
289 %----- Step 12.3:CS2 -----
290 for i=1:1000
291 for j=1:M
292 r2_CS2(i,j)=abs(X_vldN(1,i)-Xctr_CS2(1,j));
293 Phi2_CS2(i,j)=(1/18)*r2_CS2(i,j)^2+(4/9)*r2_CS2(i,j)^3+0.5*r2_CS2(i,j)^4-
    (4/3)*r2_CS2(i,j)^3*log(r2_CS2(i,j));
294 if r2_CS2(i,j)== 0
295 Phi2_CS2(i,j)=(1/18)*r2_CS2(i,j)^2+(4/9)*r2_CS2(i,j)^3+0.5*r2_CS2(i,j)^4;
296 end
297 end
298 end
299
300 %----- Step 12.4:Gaussian RBF-----
301 for i=1:1000
302 for j=1:M
303 r2(i,j)=abs(X_vldN(1,i)-Xctr(1,j));
304 Phi2(i,j)=exp(-(r2(i,j)^2)/(2*(shp^2)));
305 end
306 end
307

```

```

308 %*****
309 %-----Step 13:Construct the Y_vldapxN from Phi2 and weight 'w'
310 %*****
311 %----- Step 13.1:CS_RBF1 -----
312 Y_vldapxN_CS_RBF1=Phi2_CS_RBF1*w_CS_RBF1;
313 Y_vldapx_CS_RBF1 = Y_vldapxN_CS_RBF1.*(max(Y_vld)-min(Y_vld))+min(Y_vld);
314
315 %----- Step 13.2:CS1 -----
316 Y_vldapxN_CS1=Phi2_CS1*w_CS1;
317 Y_vldapx_CS1 = Y_vldapxN_CS1.*(max(Y_vld)-min(Y_vld))+min(Y_vld);
318
319 %----- Step 13.3:CS2 -----
320 Y_vldapxN_CS2=Phi2_CS2*w_CS2;
321 Y_vldapx_CS2 = Y_vldapxN_CS2.*(max(Y_vld)-min(Y_vld))+min(Y_vld);
322
323 %----- Step 13.4:Gaussian RBF -----
324 Y_vldapxN=Phi2*w;
325 Y_vldapx = Y_vldapxN.*(max(Y_vld)-min(Y_vld))+min(Y_vld);
326
327 %*****
328 %----- Step 14:Computing the validation error with MSE -----
329 %*****
330 Err_Vld_CS_RBF1=(1/1000)*sum((Y_vld-Y_vldapx_CS_RBF1).^2);
331 Err_Vld_CS1=(1/1000)*sum((Y_vld-Y_vldapx_CS1).^2);
332 Err_Vld_CS2=(1/1000)*sum((Y_vld-Y_vldapx_CS2).^2);
333 Err_Vld =(1/1000)*sum((Y_vld-Y_vldapx).^2);
334
335 T_Vld = table(Err_Vld_CS_RBF1,Err_Vld_CS1,Err_Vld_CS2,Err_Vld)
336
337 Y1 = sin(X_trn);
338
339 for i=1:100
340 Y3(i)= 20;
341 End
342
343 %---- Step 12 : Results Plotting -----
344 figure;
345 hold on
346 plot(X_trn,Y_trn,'ok','LineWidth',1);
347 plot(X_trn,Y3,'ok','LineWidth',1);
348 plot(X_trn,Y1,'k','LineWidth',1);
349 xlabel('x','FontSize',14);
350 ylabel('Y=sin(X)','FontSize',14);
351 grid on
352
353 figure;
354 hold on
355 plot(X_trn,Y_trn,'ok','markersize',3);
356 plot(X_trn,Yappx_CS_RBF1,'k','LineWidth',2);
357 plot(X_trn,Yappx_CS1,'-r','LineWidth',2);
358 plot(X_trn,Yappx_CS2,'-m','LineWidth',2);
359 plot(X_trn,Yappx,'-g','LineWidth',2);
360 title('Training data')
361 xlabel('X','FontSize',14);
362 ylabel('Y=sin(X)','FontSize',14);
363 legend('Exact','CS_RBF1','CS1','CS2','Gaussian','Location',
        'SouthEast')
364 grid on

```

```

365
366 figure;
367 hold on
368 plot(X_vld,Y_vld,'ok','markersize',3);
369 plot(X_vld,Y_vldapx_CS_RBF1,'-k','LineWidth',2);
370 plot(X_vld,Y_vldapx_CS1,'-r','LineWidth',2);
371 plot(X_vld,Y_vldapx_CS2,'-m','LineWidth',2);
372 plot(X_vld,Y_vldapx,'-g','LineWidth',2);
373 title('Validation data')
374 xlabel('X', 'FontSize',14);
375 ylabel('Y=sin(X)', 'FontSize',14);
376 legend('Exact', 'CS RBF1', 'CS1', 'CS2', 'Gaussian', 'Location',
        'SouthEast')
377 %----- THIS IS THE END -----

```

A.2 Main Code 2: Experiment 3 Selected Main Codes

```

1 clear all
2 close all
3
4 %-----
5 %----- Step 1:Generate training and testing dataset -----
6 %-----
7 %----- Step 1.1:Generate all dataset -----
8 x=linspace(0,1,61);
9 y=linspace(0,1,61);
10 L=length(x);
11
12 for i=1:L
13 for j=1:L
14 XO(j+(i-1)*L)=x(i);
15 YO(j+(i-1)*L)=y(j);
16 end
17 end
18
19 ZO=awgn(0.75*exp(((9*XO-2).^2)+((9*YO-2).^2))./(-4))+...
20 0.75*exp(((9*XO+1).^2)./(-4)-(9*YO+1)/10)+...
21 0.5*exp(((9*XO-7).^2)+((9*YO-3).^2))./(-4)-...
22 0.2*exp(-(9*XO-4).^2 -(9*YO-7).^2 ),15,'measured');
23 N = length(ZO);
24
25 for i=1:N
26 XYZO(i,1)=XO(i);
27 XYZO(i,2)=YO(i);
28 XYZO(i,3)=ZO(i);
29 end
30 XYZO;
31
32 %----- Step 1.2:Generate training dataset via choosing -----
33 %----- training from all dataset -----
34 xN=linspace(0,1,11);
35 yN=linspace(0,1,11);
36 LN=length(xN);
37

```

```

38 for i=1:LN
39 for j=1:LN
40 X_tr(j+(i-1)*LN)=xN(i);
41 Y_tr(j+(i-1)*LN)=yN(j);
42 end
43 end
44 N_tr = LN*LN;
45 %----- Step 1.3:Choose training from all dataset -----
46 for i=1:N_tr
47 for j=1:N
48 if X_tr(i)==XYZO(j,1)
49 if Y_tr(i)==XYZO(j,2)
50 Z_tr(i)=XYZO(j,3);
51 end
52 end
53 end
54 end
55
56 for i=1:N_tr
57 XYZ_tr(i,1)=X_tr(i);
58 XYZ_tr(i,2)=Y_tr(i);
59 XYZ_tr(i,3)=Z_tr(i);
60 End
61 XYZ_tr;
62
63 %----- Step 1.4:Select testing dataset other-----
64 %----- than the training dataset of the entire dataset -----
65 XYZ_vld = setdiff(XYZO, XYZ_tr, 'rows');
66
67 N_vld = N-N_tr;
68
69 for i=1:N_vld
70 X_vld(i)=XYZ_vld(i,1);
71 Y_vld(i)=XYZ_vld(i,2);
72 Z_vld(i)=XYZ_vld(i,3);
73 End
74
75 %-----
76 %----- Step 2:Choose a method to find the shape parameter -----
77 %-----
78 %----- Step 2.1:Choose Hardy method -----
79 for i=1:N_tr
80 for j=1:N_tr
81 H(i,j)=((X_tr(i)-X_tr(j))^2+(Y_tr(i)-Y_tr(j))^2)^(1/2);
82 if i==j
83 H(i,j)= 999999;
84 end
85 end
86 end
87
88 md = min(H)
89 d = sum(md)/(N_tr)
90 shp = 0.815*d;
91
92 %----- Step 2.2:Choose Franke method -----

```

```

93 % for i=1:N_tr
94 %   for j=1:N_tr
95 %     F(i,j)=(X_tr(i)-X_tr(j))^2+(Y_tr(i)-Y_tr(j))^2^(1/2);
96 %   end
97 % end
98 %
99 % fD = max(F)
100 %   D = max(fD)
101 %   shp = (1.25*D)/sqrt(N_tr);
102
103 %----- Step 2.3: Choose Carlson method -----
104 %   xN = (X_tr - min(X_tr))/(max(X_tr)-min(X_tr));
105 %   yN = (Y_tr - min(Y_tr))/(max(Y_tr)-min(Y_tr))
106 %   zN = (Z_tr - min(Z_tr))/(max(Z_tr)-min(Z_tr))
107 %
108 %   for i=1:N_tr
109 %     for j=1:N_tr
110 %       if j==1
111 %         P(i,j)=1;
112 %       end
113 %       if j==2
114 %         P(i,j)=xN(i);
115 %       end
116 %       if j==3
117 %         P(i,j)=yN(i);
118 %       end
119 %       if j==4
120 %         P(i,j)=xN(i)^2;
121 %       end
122 %       if j==5
123 %         P(i,j)=xN(i)*yN(i);
124 %       end
125 %       if j==6
126 %         P(i,j)=yN(i)^2;
127 %       end
128 %     end
129 %   end
130 %
131 %   c = inv(P' * P)*(P' * zN');
132 %   c' = pinv(P)* zN';
133 %   zApp = P*c;
134 %   V = sum((zN-zApp').^2 / N_tr)
135 %   shp = 1/(1+(120*V));
136
137 %--- Step 5 Using RC Algorithm -----
138 %--- Step 5.1 Construct the G matrix ---
139 %*****
140 %----- Step 3: Proceed with RC-Algorithm -----
141 %*****
142 for i=1:N_tr
143 for j=1:N_tr
144 r(i,j)=sqrt((X_tr(i)-X_tr(j))^2 + (Y_tr(i)-Y_tr(j))^2);
145 G(i,j)=exp(-r(i,j)^2/(2*(shp^2)));

```

```

146     end
147     end
148
149     delta = 0.01/100;
150
151     [U,S,V]=svd(G);
152     S11 = S(1,1);
153     S1 = S11*(delta);
154
155     for i=1:N_tr
156         Sii = S(i,i);
157         if Sii <= S1 ;
158             M = i-1
159             break
160         else
161             M=N_tr;
162             break
163         end
164         i = i+1 ;
165     end
166     V1 = V;
167     V11=V1(1:M, 1:M);
168     V21=V1(M+1:N_tr, 1:M);
169     V2 = [V11' V21'];
170     [Q,R,P]=qr(V2);
171     XY_tr = [X_tr', Y_tr'];
172     mu = XY_tr'*P;
173     Xctr = mu(:, 1:M)
174
175     %*****
176     %----- Step 4:Construct interpolation matrix -----
177     %*****
178     for i=1:N_tr
179         for j=1:M
180             r1(i,j)=sqrt((X_tr(1,i)-Xctr(1,j))^2 + (Y_tr(1,i)-Xctr(2,j))^2 );
181             Phi(i,j)=exp(-(r1(i,j)^2)/(2*(shp^2)));
182         end
183     end
184
185     %*****
186     %----- Step 5:Computing the weight 'w' -----
187     %*****
188     Z_tr = Z_tr';
189     w=pinv(Phi)*Z_tr;
190
191     %*****
192     %----- Step 6:Computing the approximation of -----
193     %-----training dataset -----
194     %*****
195     Zappx=Phi*w;
196
197     %*****
198     %----- Step 7:Computing the training error-----
199     %*****
200     Err_Trn = (1/N_tr)*sum((Z_tr-Zappx).^2)

```

```

201
202 %*****
203 %----- Step 8:Construct the interpolation matrix -----
204 %-----from Xvld to Xctr -----
205 %*****
206 for i=1:N_vld
207 for j=1:M
208 r2(i,j)=sqrt((X_vld(1,i)-Xctr(1,j)).^2+(Y_vld(1,i)-Xctr(2,j)).^2);
209 Phi2(i,j)=exp(-r2(i,j)^2/(2*(shp^2)));
210 end
211 end
212
213 %*****
214 %----- Step 9:Construct the Zvldapx from Phi2-----
215 %-----and weight 'w' -----
216 %*****
217 Zvldapx=Phi2*w;
218
219 %*****
220 %----- Step 10:Computing the test error with MSE -----
221 %*****
222 Z_vld = Z_vld';
223 Err_vld =(1/N_vld)*sum((Z_vld-Zvldapx).^2)
224
225 %*****
226 %----- Step 11:Results Plotting -----
227 %*****
228 for i=1:N
229 Solu(i,1)=XYZO(i,1);
230 Solu(i,2)=XYZO(i,2);
231 Solu(i,3)=XYZO(i,3);
232 End
233
234 for i=1 :N_tr
235 Solu_tr(i,1)=XYZ_tr(i,1);
236 Solu_tr(i,2)=XYZ_tr(i,2);
237 Solu_tr(i,3)=XYZ_tr(i,3);
238 Solu_tr(i,4)=Zappx(i,1);
239 End
240
241 for i=1 :N_vld
242 Solu_vld(i,1)=XYZ_vld(i,1);
243 Solu_vld(i,2)=XYZ_vld(i,2);
244 Solu_vld(i,3)=XYZ_vld(i,3);
245 Solu_vld(i,4)=Zvldapx(i,1);
246 End
247
248 figure;
249 hold on
250 plot3(Solu_tr(:,1),Solu_tr(:,2),Solu_tr(:,3),'ro','markersize',3,'Line
Width',2)
251 plot3(Solu_tr(:,1),Solu_tr(:,2),Solu_tr(:,4),'ko','markersize',4,'Line
Width',2)
252 title('Data set')

```



```

253     xlabel('Input Variable (X)', 'FontSize',14);
254     ylabel('Input Variable (Y)', 'FontSize',14);
255     zlabel('Output Variable (Z)', 'FontSize',14);
256     legend({'Approximate','Exact'});
257     hold off
258     grid on
259
260     figure;
261     hold on
262     plot3(Solu_vld(:,1),Solu_vld(:,2),Solu_vld(:,3),'ro','markersize',3,'L
ineWidth',2)
263     plot3(Solu_vld(:,1),Solu_vld(:,2),Solu_vld(:,4),'ko','markersize',4,'L
ineWidth',2)
264     title('Data set')
265     xlabel('Input Variable (X)', 'FontSize',14);
266     ylabel('Input Variable (Y)', 'FontSize',14);
267     zlabel('Output Variable (Z)', 'FontSize',14);
268     legend({'Approximate','Exact'});
269     hold off
270     grid on
271     %----- THIS IS THE END -----

```

A.3 Main Code 3: The Main Numerical Experiment

A.3.1 Experiment 1: Franke's function

```

1 clc
2 clear all
3 close all
4
5 %-----
6 %----- Step 1:Generate training and testing dataset -----
7 %-----
8 %----- Step 1.1: Define the input data -----
9 x=linspace(0,1,50);
10 y=linspace(0,1,50);
11 N_O=length(x);
12 for i=1:N_O
13 for j=1:N_O
14 X_trn(j+(i-1)*N_O)=x(i);
15 Y_trn(j+(i-1)*N_O)=y(j);
16 end
17 end
18 N_trn=length(X_trn);
19 XY_trn=[X_trn' Y_trn'];
20
21 %----- Step 1.2: Define the test function with noise -----
22 %----- 1.2.1:Define performance at snr=30-----
23 Z_trn = awgn(0.75*exp(((9*X_trn-2).^2)+(9*Y_trn-2).^2)/(-4)) + 0.75*exp(((9*X_trn+1).^2)/(-49)-
(9*Y_trn+1)/10) + 0.5*exp(((9*X_trn-7).^2)+(9*Y_trn-3).^2)/(-4)) - 0.2*exp(-(9*X_trn-4).^2 -
(9*Y_trn-7).^2,30,'measured');
24 %----- 1.2.2:Define performance at snr=15-----
25 Z_trn = awgn(0.75*exp(((9*X_trn-2).^2)+(9*Y_trn-2).^2)/(-4)) + 0.75*exp(((9*X_trn+1).^2)/(-49)-
(9*Y_trn+1)/10) + 0.5*exp(((9*X_trn-7).^2)+(9*Y_trn-3).^2)/(-4)) - 0.2*exp(-(9*X_trn-4).^2 -
(9*Y_trn-7).^2,15,'measured');

```

```

26
27 XYZ_trn=[XY_trn Z_trn];
28
29 %----- Step 1.3: Define the testing dataset by using -----
30 %----- the 3 different dataset which is 10000(100x100), -----
31 %----- 20164(142x142) and 30276(174x174) in this step -----
32 %----- 1.3.1 For 10000(100x100) nodes -----
33 X_t=linspace(0,1,100);
34 Y_t=linspace(0,1,100);
35 N_t=length(X_t);
36
37 %----- 1.3.2 For 20164(142x142) nodes -----
38 X_t=linspace(0,1,142);
39 Y_t=linspace(0,1,142);
40 N_t=length(X_t);
41
42 %----- 1.3.3 For 30276(174x174) nodes -----
43 X_t=linspace(0,1,174);
44 Y_t=linspace(0,1,174);
45 N_t=length(X_t);
46
47 for i=1:N_t
48 for j=1:N_t
49 XY_vld(j+(i-1)*N_t,1)=X_t(i);
50 XY_vld(j+(i-1)*N_t,2)=Y_t(j);
51 end
52 end
53 N_vld=length(XY_vld);
54
55 for i=1:N_vld
56 X_vld(i)= XY_vld(i,1);
57 Y_vld(i)= XY_vld(i,2);
58 End
59
60 Z_vld = 0.75*exp(((9*X_vld-2).^2)+((9*Y_vld-2).^2))/(-4) + 0.75*exp(((9*X_vld+1).^2)/(-4)-
(9*Y_vld+1)/10) + 0.5*exp(((9*X_vld-7).^2)+((9*Y_vld-3).^2))/(-4) - 0.2*exp(- (9*X_vld-4).^2 -
(9*Y_vld-7).^2 );
61
62 XYZ_vld=[XY_vld Z_vld'];
63
64 tic;
65 %*****
66 %----- Step 2: Construct the interpolation matrix -----
67 %*****
68 %----- 2.1 For MQ + Carlson RBF -----
69 xN =(X_trn -min(X_trn))/(max(X_trn)-min(X_trn));
70 yN =(Y_trn -min(Y_trn))/(max(Y_trn)-min(Y_trn));
71 zN =(Z_trn -min(Z_trn))/(max(Z_trn)-min(Z_trn));
72 zN = zN';
73
74 for i=1:N_trn
75 for j=1:N_trn
76 if j==1
77 P(i,j)=1;
78 end
79 if j==2
80 P(i,j)=xN(i);
81 end

```

```

82 if j==3
83 P(i,j)=yN(i);
84 end
85 if j==4
86 P(i,j)=xN(i)^2;
87 end
88 if j==5
89 P(i,j)=xN(i)*yN(i);
90 end
91 if j==6
92 P(i,j)=yN(i)^2;
93 end
94 end
95 end
96
97 c = pinv(P)*zN';
98 zApp = P*c;
99 V = sum((zN-zApp')^2 / N_trn);
100 shp = 1/(1+(120*V));

101 for i=1:N_trn
102 for j=1:N_trn
103 r(i,j)=sqrt((X_trn(i)-X_trn(j))^2 +(Y_trn(i)-Y_trn(j))^2);
104 G(i,j)=sqrt(r(i,j)^2 + shp^2);
105 end
106 end
107 %----- 2.2 For PS RBF-----
108 for i=1:N_trn
109 for j=1:N_trn
110 r(i,j)=sqrt((X_trn(i)-X_trn(j))^2 +(Y_trn(i)-Y_trn(j))^2);
111 if 0<=r(i,j) & r(i,j)<=1
112 G(i,j)=r(i,j)^((2*k)-1);
113 Else
114 G(i,j)=0;
115 end
116 end
117 end
118
119 %----- 2.3 For TPS RBF-----
120 for i=1:N_trn
121 for j=1:N_trn
122 r(i,j)=sqrt((X_trn(i)-X_trn(j))^2 +(Y_trn(i)-Y_trn(j))^2);
123 if 0<=r(i,j) & r(i,j)<=1 & r(i,j)~= 0
124 G(i,j)=(r(i,j)^2)*log(r(i,j));
125 Else
126 G(i,j)=0;
127 end
128 end
129 end
130
131 %----- 2.4 For WU1 RBF-----
132 for i=1:N_trn
133 for j=1:N_trn
134 r(i,j)=sqrt((X_trn(i)-X_trn(j))^2 +(Y_trn(i)-Y_trn(j))^2);
135 if 0<=r(i,j) & r(i,j)<=1
136 G(i,j)=(1-
           r(i,j)^7)*(5*r(i,j)^6+(35*r(i,j)^5)+(101*r(i,j)^4)+(147*r(i,j)^3)+(101*r(i,j)^2)+35*r(i,j)+
           5);
137 Else

```

```

138 G(i,j)=0;
139 end
140 end
141 end
142
143 %----- 2.5 For WU2 RBF-----
144 for i=1:N_trn
145 for j=1:N_trn
146 r(i,j)=sqrt((X_trn(i)-X_trn(j)).^2 +(Y_trn(i)-Y_trn(j)).^2);
147 if 0<=r(i,j) & r(i,j)<=1
148 G(i,j)=((1-r(i,j))^6)*((6*r(i,j))^5+(30*r(i,j))^4+(72*r(i,j))^3+(82*r(i,j))^2+36*r(i,j)+6);
149 Else
150 G(i,j)=0;
151 end
152 end
153 end
154
155 %----- 2.6 For WU3 RBF-----
156 for i=1:N_trn
157 for j=1:N_trn
158 r(i,j)=sqrt((X_trn(i)-X_trn(j)).^2 +(Y_trn(i)-Y_trn(j)).^2);
159 if 0<=r(i,j) & r(i,j)<=1
160 G(i,j)=((1-r(i,j))^5)*((5*r(i,j))^4+(25*r(i,j))^3+(48*r(i,j))^2+40*r(i,j)+8);
161 Else
162 G(i,j)=0;
163 end
164 end
165 end
166
167 %----- 2.7 For WU4 RBF-----
168 for i=1:N_trn
169 for j=1:N_trn
170 r(i,j)=sqrt((X_trn(i)-X_trn(j)).^2 +(Y_trn(i)-Y_trn(j)).^2);
171 if 0<=r(i,j) & r(i,j)<=1
172 G(i,j)=((1-r(i,j))^4)*((5*r(i,j))^3+(20*r(i,j))^2+29*r(i,j)+16);
173 Else
174 G(i,j)=0;
175 end
176 end
177 end
178
179 %----- 2.8 For WL1 RBF-----
180 for i=1:N_trn
181 for j=1:N_trn
182 r(i,j)=sqrt((X_trn(i)-X_trn(j)).^2 +(Y_trn(i)-Y_trn(j)).^2);
183 if 0<=r(i,j) & r(i,j)<=1
184 G(i,j)=(1-r(i,j));
185 Else
186 G(i,j)=0;
187 end
188 end
189 end
190
191 %----- 2.9 For WL2 RBF-----
192 for i=1:N_trn
193 for j=1:N_trn
194 r(i,j)=sqrt((X_trn(i)-X_trn(j)).^2 +(Y_trn(i)-Y_trn(j)).^2);
195 if 0<=r(i,j) & r(i,j)<=1
196 G(i,j)=((1-r(i,j))^3)*(3*r(i,j)+1);

```

```

197 Else
198 G(i,j)=0;
199 end
200 end
201 end
202
203 %----- 2.10 For WL3 RBF-----
204 for i=1:N_trn
205 for j=1:N_trn
206 r(i,j)=sqrt((X_trn(i)-X_trn(j)).^2 +(Y_trn(i)-Y_trn(j)).^2);
207 if 0<=r(i,j) & r(i,j)<=1
208 G(i,j)=((1-r(i,j))^5)*((8*r(i,j)^2)+5*r(i,j)+1);
209 Else
210 G(i,j)=0;
211 end
212 end
213 end
214
215 %----- 2.11 For WL4 RBF-----
216 for i=1:N_trn
217 for j=1:N_trn
218 r(i,j)=sqrt((X_trn(i)-X_trn(j)).^2 +(Y_trn(i)-Y_trn(j)).^2);
219 if 0<=r(i,j) & r(i,j)<=1
220 G(i,j)=((1-r(i,j))^2);
221 Else
222 G(i,j)=0;
223 end
224 end
225 end
226 %----- 2.12 For WL5 RBF-----
227 for i=1:N_trn
228 for j=1:N_trn
229 r(i,j)=sqrt((X_trn(i)-X_trn(j)).^2 +(Y_trn(i)-Y_trn(j)).^2);
230 if 0<=r(i,j) & r(i,j)<=1
231 G(i,j)=((1-r(i,j))^4)*(4*r(i,j)+1);
232 Else
233 G(i,j)=0;
234 end
235 end
236 end
237 %----- 2.13 For WL6 RBF-----
238 for i=1:N_trn
239 for j=1:N_trn
240 r(i,j)=sqrt((X_trn(i)-X_trn(j)).^2 +(Y_trn(i)-Y_trn(j)).^2);
241 if 0<=r(i,j) & r(i,j)<=1
242 G(i,j)=((1-r(i,j))^6)*((35*r(i,j)^2)+18*r(i,j)+3);
243 Else
244 G(i,j)=0;
245 end
246 end
247 end
248
249 %----- 2.14 For WL7 RBF-----
250 for i=1:N_trn
251 for j=1:N_trn
252 r(i,j)=sqrt((X_trn(i)-X_trn(j)).^2 +(Y_trn(i)-Y_trn(j)).^2);
253 if 0<=r(i,j) & r(i,j)<=1
254 G(i,j)=((1-r(i,j))^8)*((32*r(i,j)^3)+(25*r(i,j)^2)+8*r(i,j)+1);
255 Else

```

```

256 G(i,j)=0;
257 end
258 end
259 end
260
261 %----- 2.15 For BUH1 RBF-----
262 for i=1:N_trn
263 for j=1:N_trn
264 r(i,j)=sqrt((X_trn(i)-X_trn(j)).^2 +(Y_trn(i)-Y_trn(j)).^2);
265 G(i,j)=(1/6)*(2*r(i,j).^2)+(16/3)*r(i,j).^3 -(7/2)*r(i,j).^4 + 2*(r(i,j).^4)*log(r(i,j));
266 if r(i,j)== 0
267 G(i,j)=(1/6)*(2*r(i,j).^2)+(16/3)*r(i,j).^3 -(7/2)*r(i,j).^4;
268 end
269 end
270 end
271
272 %----- 2.16 For BUH2 RBF-----
273 for i=1:N_trn
274 for j=1:N_trn
275 r(i,j)=sqrt((X_trn(i)-X_trn(j)).^2 +(Y_trn(i)-Y_trn(j)).^2);
276 if 0<=r(i,j) & r(i,j)<=1
277 G(i,j)=(112/45)*r(i,j).^(9/2)+(16/3)*r(i,j).^(7/2)-7*r(i,j).^4-(14/15)*r(i,j).^2+(1/9);
278 Else
279 G(i,j)=0;
280 end
281 end
282 end
283 %----- 2.17 For BUH3 RBF-----
284 for i=1:N_trn
285 for j=1:N_trn
286 r(i,j)=sqrt((X_trn(i)-X_trn(j)).^2 +(Y_trn(i)-Y_trn(j)).^2);
287 G(i,j)=(1/18)*r(i,j).^2+(4/9)*r(i,j).^3+0.5*r(i,j).^4-(4/3)*r(i,j).^3*log(r(i,j));
288 if r(i,j)== 0
289 G(i,j)=(1/18)*r(i,j).^2+(4/9)*r(i,j).^3+0.5*r(i,j).^4;
290 end
291 end
292 end
293
294 %*****
295 %-----Step 3:Using SVD to get the number of centres-----
296 %*****
297 delta = 0.01/100;
298 [U,S,V]=svd(G);
299 S11 = S(1,1);
300 S1 = S11*delta);
301
302 for i=1:N_trn
303 Sii = S(i,i);
304 if Sii <= S1 ;
305 M = i-1
306 break
307 end
308 i = i+1 ;
309 end
310
311 %*****
312 %-----Step 4:Using QR to find the centres of basis function --
313 %-----and the location of centres -----

```

```

314 %*****
315 V1 = V;
316 V11=V1(1:M, 1:M);           %partition matrix V
317 V21=V1(M+1:N_trn, 1:M);
318 V2 = [V11' V21'];
319 [Q, R, P] = qr(V2);
320 XY_tr = [X_trn', Y_trn'];
321 mu = XY_trn'*P;
322 Xctr = mu(:, 1:M);
323
324 %*****
325 %----- Step 5: Construct the new interpolation matrix -----
326 %*****
327 for i=1:N_trn
328 for j=1:M
329 r1(i, j)=sqrt((X_trn(1, i)-Xctr(1, j))^2 + (Y_trn(1, i)-Xctr(2, j))^2 );
330 if 0<=r1(i, j) & r1(i, j)<=1
331 Phi(i, j)=((1-r1(i, j))^4)*(5*r1(i, j)^3)+(20*r1(i, j)^2)+29*r1(i, j)+16);
332 Else
333 Phi(i, j)=0;
334 end
335 end
336 end
337
338 %*****
339 %----- Step 6: Computing the weight 'w' -----
340 %*****
341 w=pinv(Phi)*Z_trn;
342
343 %*****
344 %----- Step 7: Computing the approximation of training dataset --
345 %*****
346 Zappx=Phi*w;
347
348 %*****
349 %----- Step 8: Computing the training error -----
350 %*****
351 Err_max_trn = max(abs(Z_trn-Zappx))
352 Err_RMSE_trn =sqrt((1/N_trn)*sum((Z_trn-Zappx).^2))
353
354 %*****
355 %----- Step 9: Construct the interpolation matrix -----
356 %----- from Xvld to Xctr -----
357 %*****
358 %----- 9.1 For MQ +Carlson RBF -----
359 for i=1:N_vld
360 for j=1:M
361 r2(i, j)=sqrt((X_vld(1, i)-Xctr(1, j))^2 + (Y_vld(1, i)-Xctr(2, j))^2 );
362 Phi2(i, j)= sqrt(r2(i, j)^2 + shp^2);
363 end
364 end
365
366 %----- 9.2 For PS RBF -----
367 for i=1:N_vld
368 for j=1:M
369 r2(i, j)=sqrt((X_vld(1, i)-Xctr(1, j))^2 + (Y_vld(1, i)-Xctr(2, j))^2 );
370 if 0<=r2(i, j) & r2(i, j)<=1

```

```

371 Phi2(i,j)=r2(i,j)^((2*k)-1);
372 else
373 Phi2(i,j)=0;
374 end
375 end
376 end
377
378 %----- 9.3 For TPS RBF-----
379 for i=1:N_vld
380 for j=1:M
381 r2(i,j)=sqrt((X_vld(1,i)-Xctr(1,j))^2 + (Y_vld(1,i)-Xctr(2,j))^2 );
382 if 0<=r2(i,j) & r2(i,j)<=1 & r2(i,j)~=0
383 Phi2(i,j)=(r2(i,j)^2)*log(r2(i,j));
384 else
385 Phi2(i,j)=0;
386 end
387 end
388 end
389
390 %----- 9.4 For WU1 RBF-----
391 for i=1:N_vld
392 for j=1:M
393 r2(i,j)=sqrt((X_vld(1,i)-Xctr(1,j))^2 + (Y_vld(1,i)-Xctr(2,j))^2 );
394 if 0<=r2(i,j) & r2(i,j)<=1
395 Phi2(i,j)=(1-
    r2(i,j)^7)*(5*r2(i,j)^6+(35*r2(i,j)^5)+(101*r2(i,j)^4)+(147*r2(i,j)^3)+(101*r2(i,j)^2)+35
    *r2(i,j)+5);
396 else
397 Phi2(i,j)=0;
398 end
399 end
400 end
401
402 %----- 9.5 For WU2 RBF-----
403 for i=1:N_vld
404 for j=1:M
405 r2(i,j)=sqrt((X_vld(1,i)-Xctr(1,j))^2 + (Y_vld(1,i)-Xctr(2,j))^2 );
406 if 0<=r2(i,j) & r2(i,j)<=1
407 Phi2(i,j)=(1-
    r2(i,j)^6)*(6*r2(i,j)^5+(30*r2(i,j)^4)+(72*r2(i,j)^3)+(82*r2(i,j)^2)+36*r2(i,j)+6);
408 else
409 Phi2(i,j)=0;
410 end
411 end
412 end
413
414 %----- 9.6 For WU3 RBF-----
415 for i=1:N_vld
416 for j=1:M
417 r2(i,j)=sqrt((X_vld(1,i)-Xctr(1,j))^2 + (Y_vld(1,i)-Xctr(2,j))^2 );
418 if 0<=r2(i,j) & r2(i,j)<=1
419 Phi2(i,j)=(1-r2(i,j))^5*(5*r2(i,j)^4+(25*r2(i,j)^3)+(48*r2(i,j)^2)+40*r2(i,j)+8);
420 else
421 Phi2(i,j)=0;
422 end
423 end
424 end
425
426 %----- 9.7 For WU4 RBF-----

```



```

427 for i=1:N_vld
428 for j=1:M
429 r2(i,j)=sqrt((X_vld(1,i)-Xctr(1,j))^2 + (Y_vld(1,i)-Xctr(2,j))^2 );
430 if 0<=r2(i,j) & r2(i,j)<=1
431 Phi2(i,j)=((1-r2(i,j))^4)*((5*r2(i,j)^3)+(20*r2(i,j)^2)+29*r2(i,j)+16);
432 else
433 Phi2(i,j)=0;
434 end
435 end
436 end
437
438 %----- 9.8 For WL1 RBF-----
439 for i=1:N_vld
440 for j=1:M
441 r2(i,j)=sqrt((X_vld(1,i)-Xctr(1,j))^2 + (Y_vld(1,i)-Xctr(2,j))^2 );
442 if 0<=r2(i,j) & r2(i,j)<=1
443 Phi2(i,j)=((1-r2(i,j)));
444 else
445 Phi2(i,j)=0;
446 end
447 end
448 end
449
450 %----- 9.9 For WL2 RBF-----
451 for i=1:N_vld
452 for j=1:M
453 r2(i,j)=sqrt((X_vld(1,i)-Xctr(1,j))^2 + (Y_vld(1,i)-Xctr(2,j))^2 );
454 if 0<=r2(i,j) & r2(i,j)<=1
455 Phi2(i,j)=((1-r2(i,j))^3)*(3*r2(i,j)+1);
456 else
457 Phi2(i,j)=0;
458 end
459 end
460 end
461
462 %----- 9.10 For WL3 RBF-----
463 for i=1:N_vld
464 for j=1:M
465 r2(i,j)=sqrt((X_vld(1,i)-Xctr(1,j))^2 + (Y_vld(1,i)-Xctr(2,j))^2 );
466 if 0<=r2(i,j) & r2(i,j)<=1
467 Phi2(i,j)=((1-r2(i,j))^5)*((8*r2(i,j)^2)+5*r2(i,j)+1);
468 else
469 Phi2(i,j)=0;
470 end
471 end
472 end
473
474 %----- 9.11 For WL4 RBF-----
475 for i=1:N_vld
476 for j=1:M
477 r2(i,j)=sqrt((X_vld(1,i)-Xctr(1,j))^2 + (Y_vld(1,i)-Xctr(2,j))^2 );
478 if 0<=r2(i,j) & r2(i,j)<=1
479 Phi2(i,j)=((1-r2(i,j))^2);
480 else
481 Phi2(i,j)=0;
482 end
483 end
484 end
485

```

```

486 %----- 9.12 For WL5 RBF-----
487 for i=1:N_vld
488 for j=1:M
489 r2(i,j)=sqrt((X_vld(1,i)-Xctr(1,j))^2 + (Y_vld(1,i)-Xctr(2,j))^2 );
490 if 0<=r2(i,j) & r2(i,j)<=1
491 Phi2(i,j)=(1-r2(i,j))^4*(4*r2(i,j)+1);
492 else
493 Phi2(i,j)=0;
494 end
495 end
496 end
497
498 %----- 9.13 For WL6 RBF-----
499 for i=1:N_vld
500 for j=1:M
501 r2(i,j)=sqrt((X_vld(1,i)-Xctr(1,j))^2 + (Y_vld(1,i)-Xctr(2,j))^2 );
502 if 0<=r2(i,j) & r2(i,j)<=1
503 Phi2(i,j)=(1-r2(i,j))^6*(35*r2(i,j)^2+18*r2(i,j)+3);
504 else
505 Phi2(i,j)=0;
506 end
507 end
508 end
509
510 %----- 9.14 For WL7 RBF-----
511 for i=1:N_vld
512 for j=1:M
513 r2(i,j)=sqrt((X_vld(1,i)-Xctr(1,j))^2 + (Y_vld(1,i)-Xctr(2,j))^2 );
514 if 0<=r2(i,j) & r2(i,j)<=1
515 Phi2(i,j)=(1-r2(i,j))^8*(32*r2(i,j)^3+(25*r2(i,j)^2)+8*r2(i,j)+1);
516 else
517 Phi2(i,j)=0;
518 end
519 end
520 end
521
522 %----- 9.15 For BUH1 RBF-----
523 for i=1:N_vld
524 for j=1:M
525 r2(i,j)=sqrt((X_vld(1,i)-Xctr(1,j))^2 + (Y_vld(1,i)-Xctr(2,j))^2 );
526 Phi2(i,j)=(1/6)*(2*r2(i,j)^2+(1/3)*r2(i,j)^3 -(7/2)*r2(i,j)^4 +
2*r2(i,j)^4*log(r2(i,j)));
527 if r2(i,j)==0
528 Phi2(i,j)=(1/6)*(2*r2(i,j)^2+(1/3)*r2(i,j)^3 -(7/2)*r2(i,j)^4);
529 end
530 end
531 end
532
533 %----- 9.16 For BUH2 RBF-----
534 for i=1:N_vld
535 for j=1:M
536 r2(i,j)=sqrt((X_vld(1,i)-Xctr(1,j))^2 + (Y_vld(1,i)-Xctr(2,j))^2 );
537 if 0<=r2(i,j) & r2(i,j)<=1
538 Phi2(i,j)=(112/45)*r2(i,j)^(9/2)+(1/3)*r2(i,j)^(7/2)-7*r2(i,j)^4-(14/15)*r2(i,j)^(2+1/9);
539 else
540 Phi2(i,j)=0;
541 end
542 end
543 end

```

```

544
545 %----- 9.17 For BUH3 RBF-----
546 for i=1:N_vld
547 for j=1:M
548 r2(i,j)=sqrt((X_vld(1,i)-Xctr(1,j)).^2 + (Y_vld(1,i)-Xctr(2,j)).^2 );
549 Phi2(i,j)=(1/18)*r2(i,j).^2+(4/9)*r2(i,j).^3+0.5*r2(i,j).^4-(4/3)*r2(i,j).^3*log(r2(i,j));
550 if r2(i,j)== 0
551 Phi2(i,j)=(1/18)*r2(i,j).^2+(4/9)*r2(i,j).^3+0.5*r2(i,j).^4;
552 end
553 end
554 end
555
556 %*****
557 %----- Step 10:Construct the Zvldapx from Phi2 and weight 'w' --
558 %*****
559 Zvldapx=Phi2*w;
560
561 %*****
562 %----- Step 11:Computing the test error with MSE -----
563 %*****
564 Z_vld = Z_vld';
565 Err_max_vld =max(abs(Z_vld-Zvldapx))
566 Err_RMSE_vld =sqrt((1/N_vld)*sum((Z_vld-Zvldapx).^2))
567 toc;
568 %*****
569 %----- Step 12:Find the condition number-----
570 %*****
571 con_G=cond(G)
572 con_Phi = cond(Phi)
573
574 %*****
575 %----- Step 13:Results Plotting -----
576 %*****
577 for i=1 :N_trn
578 Solu_tr(i,1)=XYZ_trn(i,1);
579 Solu_tr(i,2)=XYZ_trn(i,2);
580 Solu_tr(i,3)=XYZ_trn(i,3);
581 Solu_tr(i,4)=Zappx(i,1);
582 End
583
584 for i=1 :N_vld
585 Solu_vld(i,1)=XYZ_vld(i,1);
586 Solu_vld(i,2)=XYZ_vld(i,2);
587 Solu_vld(i,3)=XYZ_vld(i,3);
588 Solu_vld(i,4)=Zvldapx(i,1);
589 End
590
591 figure;
592 hold on
593 plot3(Solu_tr(:,1),Solu_tr(:,2),Solu_tr(:,3),'ro','markersize',3,'LineWidth',
2)
594 plot3(Solu_tr(:,1),Solu_tr(:,2),Solu_tr(:,4),'ko','markersize',4,'LineWidth',
2)
595 title('Data set')
596 xlabel('Input Variable (X)', 'FontSize',14);
597 ylabel('Input Variable (Y)', 'FontSize',14);
598 zlabel('Output Variable (Z)', 'FontSize',14);
599 legend({'Exact', 'Approximate'});

```

```

600 hold off
601 grid on
602
603 figure;
604 hold on
605 plot3(Solu_vld(:,1),Solu_vld(:,2),Solu_vld(:,3),'ro','markersize',3,'LineWidth
    h',2)
606 plot3(Solu_vld(:,1),Solu_vld(:,2),Solu_vld(:,4),'ko','markersize',4,'LineWidth
    h',2)
607 title('Data set')
608 xlabel('Input Variable (X)', 'FontSize',14);
609 ylabel('Input Variable (Y)', 'FontSize',14);
610 zlabel('Output Variable (Z)', 'FontSize',14);
611 legend({'Exact','Approximate'});
612 hold off
613 grid on
614 %----- THIS IS THE END -----

```

A.3.2 Experiment 2: F7

```

1 clc
2 clear all
3 close all
4
5 %-----
6 %----- Step 1:Generate training and testing dataset -----
7 %-----
8 %----- Step 1.1: Define the input data -----
9 x=linspace(0,1,50);
10 y=linspace(0,1,50);
11 N_O=length(x);
12 for i=1:N_O
13 for j=1:N_O
14 X_trn(j+(i-1)*N_O)=x(i);
15 Y_trn(j+(i-1)*N_O)=y(j);
16 end
17 end
18 N_trn=length(X_trn);
19 XY_trn=[X_trn' Y_trn'];
20
21 %----- Step 1.2: Define the test function with noise -----
22 %----- 1.2.1:Define performance at snr=30 -----
23 Z_trn = awgn(2*cos(10.* X_trn)*sin(10.*Y_trn)+sin(10.*
    X_trn.*Y_trn,30,'measured');
24
25 %----- 1.2.2:Define performance at snr=15 -----
26 Z_trn = awgn(2*cos(10.* X_trn)*sin(10.*Y_trn)+sin(10.*
    X_trn.*Y_trn,15,'measured');
27
28 XYZ_trn=[XY_trn Z_trn];
29
30 %----- Step 1.3: Define the testing dataset by using -----
31 %----- the 3 different dataset which is 10000(100x100), -----
32 %----- 20164(142x142) and 30276(174x174) in this step -----
33 %----- 1.3.1 For 10000(100x100) nodes -----

```

```

34 X_t=linspace(0,1,100);
35 Y_t=linspace(0,1,100);
36 N_t=length(X_t);
37
38 %----- 1.3.2 For 20164 (142x142) nodes-----
39 X_t=linspace(0,1,142);
40 Y_t=linspace(0,1,142);
41 N_t=length(X_t);
42
43 %----- 1.3.3 For 30276 (174x174) nodes-----
44 X_t=linspace(0,1,174);
45 Y_t=linspace(0,1,174);
46 N_t=length(X_t);
47
48 for i=1:N_t
49 for j=1:N_t
50 XY_vld(j+(i-1)*N_t,1)=X_t(i);
51 XY_vld(j+(i-1)*N_t,2)=Y_t(j);
52 end
53 end
54 N_vld=length(XY_vld);
55
56 for i=1:N_vld
57 X_vld(i)= XY_vld(i,1);
58 Y_vld(i)= XY_vld(i,2);
59 End
60
61 Z_vld = 2*cos(10*X_vld)*sin(10*Y_vld)+sin(10*X_vld*Y_vld);
62
63
64 XYZ_vld=[XY_vld Z_vld'];
65
66 tic;
67 %*****
68 %----- Step 2: Construct the interpolation matrix-----
69 %*****
70 %----- 2.1 For MQ +Carlson RBF-----
71 xN =(X_trn -min(X_trn))/(max(X_trn)-min(X_trn));
72 yN =(Y_trn -min(Y_trn))/(max(Y_trn)-min(Y_trn));
73 zN =(Z_trn -min(Z_trn))/(max(Z_trn)-min(Z_trn));
74 zN =zN';
75
76 for i=1:N_trn
77 for j=1:N_trn
78 if j==1
79 P(i,j)=1;
80 end
81 if j==2
82 P(i,j)=xN(i);
83 end
84 if j==3
85 P(i,j)=yN(i);
86 end
87 if j==4
88 P(i,j)=xN(i)^2;
89 end
90 if j==5
91 P(i,j)=xN(i)*yN(i);

```

```

92 end
93 if j==6
94 P(i,j)=yN(i)^2;
95 end
96 end
97 end
98
99 c = pinv(P)*zN';
100 zApp = P*c;
101 V = sum((zN-zApp')^2 /N_trn);
102 shp = 1/(1+(120*V));
103
104 for i=1:N_trn
105 for j=1:N_trn
106 r(i,j)=sqrt((X_trn(i)-X_trn(j))^2 +(Y_trn(i)-Y_trn(j))^2);
107 G(i,j)=sqrt(r(i,j)^2 + shp^2);
108 end
109 end
110 %----- 2.2 For PS RBF-----
111 for i=1:N_trn
112 for j=1:N_trn
113 r(i,j)=sqrt((X_trn(i)-X_trn(j))^2 +(Y_trn(i)-Y_trn(j))^2);
114 if 0<=r(i,j) & r(i,j)<=1
115 G(i,j) = r(i,j)^((2*k)-1);
116 Else
117 G(i,j)=0;
118 end
119 end
120 end
121
122 %----- 2.3 For TPS RBF-----
123 for i=1:N_trn
124 for j=1:N_trn
125 r(i,j)=sqrt((X_trn(i)-X_trn(j))^2 +(Y_trn(i)-Y_trn(j))^2);
126 if 0<=r(i,j) & r(i,j)<=1 & r(i,j)~=0
127 G(i,j)=(r(i,j)^2)*log(r(i,j));
128 Else
129 G(i,j)=0;
130 end
131 end
132 end
133
134 %----- 2.4 For WU1 RBF-----
135 for i=1:N_trn
136 for j=1:N_trn
137 r(i,j)=sqrt((X_trn(i)-X_trn(j))^2 +(Y_trn(i)-Y_trn(j))^2);
138 if 0<=r(i,j) & r(i,j)<=1
139 G(i,j)=(1-
    r(i,j)^7)*(5*r(i,j)^6+(35*r(i,j)^5)+(101*r(i,j)^4)+(147*r(i,j)^3)+(101*r(i,j)^2)+35*r(i,j)+
    5);
140 Else
141 G(i,j)=0;
142 end
143 end
144 end
145
146 %----- 2.5 For WU2 RBF-----
147 for i=1:N_trn
148 for j=1:N_trn

```

```

149 r(i,j)=sqrt((X_trn(i)-X_trn(j)).^2 +(Y_trn(i)-Y_trn(j)).^2);
150 if 0<=r(i,j) & r(i,j)<=1
151 G(i,j)=((1-r(i,j))^6)*((6*r(i,j)^5)+(30*r(i,j)^4)+(72*r(i,j)^3)+(82*r(i,j)^2)+36*r(i,j)+6);
152 Else
153 G(i,j)=0;
154 end
155 end
156 end
157
158 %----- 2.6 For WU3 RBF-----
159 for i=1:N_trn
160 for j=1:N_trn
161 r(i,j)=sqrt((X_trn(i)-X_trn(j)).^2 +(Y_trn(i)-Y_trn(j)).^2);
162 if 0<=r(i,j) & r(i,j)<=1
163 G(i,j)=((1-r(i,j))^5)*((5*r(i,j)^4)+(25*r(i,j)^3)+(48*r(i,j)^2)+40*r(i,j)+8);
164 Else
165 G(i,j)=0;
166 end
167 end
168 end
169
170 %----- 2.7 For WU4 RBF-----
171 for i=1:N_trn
172 for j=1:N_trn
173 r(i,j)=sqrt((X_trn(i)-X_trn(j)).^2 +(Y_trn(i)-Y_trn(j)).^2);
174 if 0<=r(i,j) & r(i,j)<=1
175 G(i,j)=((1-r(i,j))^4)*((5*r(i,j)^3)+(20*r(i,j)^2)+29*r(i,j)+16);
176 Else
177 G(i,j)=0;
178 end
179 end
180 end
181
182 %----- 2.8 For WL1 RBF-----
183 for i=1:N_trn
184 for j=1:N_trn
185 r(i,j)=sqrt((X_trn(i)-X_trn(j)).^2 +(Y_trn(i)-Y_trn(j)).^2);
186 if 0<=r(i,j) & r(i,j)<=1
187 G(i,j)=((1-r(i,j)));
188 Else
189 G(i,j)=0;
190 end
191 end
192 end
193
194 %----- 2.9 For WL2 RBF-----
195 for i=1:N_trn
196 for j=1:N_trn
197 r(i,j)=sqrt((X_trn(i)-X_trn(j)).^2 +(Y_trn(i)-Y_trn(j)).^2);
198 if 0<=r(i,j) & r(i,j)<=1
199 G(i,j)=((1-r(i,j))^3)*(3*r(i,j)+1);
200 Else
201 G(i,j)=0;
202 end
203 end
204 end
205
206 %----- 2.10 For WL3 RBF-----
207 for i=1:N_trn

```

```

208 for j=1:N_trn
209 r(i,j)=sqrt((X_trn(i)-X_trn(j)).^2 +(Y_trn(i)-Y_trn(j)).^2);
210 if 0<=r(i,j) & r(i,j)<=1
211 G(i,j)=((1-r(i,j))^5)*((8*r(i,j)^2)+5*r(i,j)+1);
212 Else
213 G(i,j)=0;
214 end
215 end
216 end
217
218 %----- 2.11 For WL4 RBF-----
219 for i=1:N_trn
220 for j=1:N_trn
221 r(i,j)=sqrt((X_trn(i)-X_trn(j)).^2 +(Y_trn(i)-Y_trn(j)).^2);
222 if 0<=r(i,j) & r(i,j)<=1
223 G(i,j)=((1-r(i,j))^2);
224 Else
225 G(i,j)=0;
226 end
227 end
228 end
229
230 %----- 2.12 For WL5 RBF-----
231 for i=1:N_trn
232 for j=1:N_trn
233 r(i,j)=sqrt((X_trn(i)-X_trn(j)).^2 +(Y_trn(i)-Y_trn(j)).^2);
234 if 0<=r(i,j) & r(i,j)<=1
235 G(i,j)=((1-r(i,j))^4)*(4*r(i,j)+1);
236 Else
237 G(i,j)=0;
238 end
239 end
240 end
241
242 %----- 2.13 For WL6 RBF-----
243 for i=1:N_trn
244 for j=1:N_trn
245 r(i,j)=sqrt((X_trn(i)-X_trn(j)).^2 +(Y_trn(i)-Y_trn(j)).^2);
246 if 0<=r(i,j) & r(i,j)<=1
247 G(i,j)=((1-r(i,j))^6)*((35*r(i,j)^2)+18*r(i,j)+3);
248 Else
249 G(i,j)=0;
250 end
251 end
252 end
253
254 %----- 2.14 For WL7 RBF-----
255 for i=1:N_trn
256 for j=1:N_trn
257 r(i,j)=sqrt((X_trn(i)-X_trn(j)).^2 +(Y_trn(i)-Y_trn(j)).^2);
258 if 0<=r(i,j) & r(i,j)<=1
259 G(i,j)=((1-r(i,j))^8)*((32*r(i,j)^3)+(25*r(i,j)^2)+8*r(i,j)+1);
260 Else
261 G(i,j)=0;
262 end
263 end
264 end
265
266 %----- 2.15 For BUH1 RBF-----

```



```

267 for i=1:N_trn
268 for j=1:N_trn
269 r(i,j)=sqrt((X_trn(i)-X_trn(j)).^2 +(Y_trn(i)-Y_trn(j)).^2);
270 G(i,j)=(1/6)*(2*r(i,j).^2)+(16/3)*r(i,j).^3 -(7/2)*r(i,j).^4 + 2*(r(i,j).^4)*log(r(i,j));
271 if r(i,j)== 0
272 G(i,j)=(1/6)*(2*r(i,j).^2)+(16/3)*r(i,j).^3 -(7/2)*r(i,j).^4;
273 end
274 end
275 end
276
277 %----- 2.16 For BUH2 RBF-----
278 for i=1:N_trn
279 for j=1:N_trn
280 r(i,j)=sqrt((X_trn(i)-X_trn(j)).^2 +(Y_trn(i)-Y_trn(j)).^2);
281 if 0<=r(i,j) & r(i,j)<=1
282 G(i,j)=(112/45)*r(i,j).^(9/2)+(16/3)*r(i,j).^(7/2)-7*r(i,j).^4-(14/15)*r(i,j).^2+(1/9);
283 Else
284 G(i,j)=0;
285 end
286 end
287 end
288
289 %----- 2.17 For BUH3 RBF-----
290 for i=1:N_trn
291 for j=1:N_trn
292 r(i,j)=sqrt((X_trn(i)-X_trn(j)).^2 +(Y_trn(i)-Y_trn(j)).^2);
293 G(i,j)=(1/18)*r(i,j).^2+(4/9)*r(i,j).^3+0.5*r(i,j).^4-(4/3)*r(i,j).^3*log(r(i,j));
294 if r(i,j)== 0
295 G(i,j)=(1/18)*r(i,j).^2+(4/9)*r(i,j).^3+0.5*r(i,j).^4;
296 end
297 end
298 end
299
300 %*****
301 %----- Step 3:Using SVD to get the number of centres-----
302 %*****
303 delta = 0.01/100;
304 [U, S, V]= svd(G);
305 S11 = S(1,1);
306 S1 = S11*(delta);
307
308 for i=1:N_trn
309 Sii = S(i,i);
310 if Sii <= S1 ;
311 M = i-1
312 break
313 end
314 i = i+1 ;
315 end
316
317 %*****
318 %----- Step 4:Using QR to find the centres of basis function --
319 %----- and the location of centres -----
320 %*****
321 V1 = V;
322 V11=V1(1:M, 1:M); %partition matrix V
323 V21=V1(M+1:N_trn, 1:M);
324 V2 = [V11' V21'];

```

```

325 [Q, R, P] = qr(V2);
326 XY_tr = [X_trn', Y_trn'];
327 mu = XY_trn'*P;
328 Xctr = mu(:, 1:M);
329
330 %*****
331 %----- Step 5: Construct the new interpolation matrix-----
332 %*****
333 for i=1:N_trn
334 for j=1:M
335 r1(i, j)=sqrt((X_trn(1, i)-Xctr(1, j)).^2 + (Y_trn(1, i)-Xctr(2, j)).^2 );
336 if 0<=r1(i, j) & r1(i, j)<=1
337 Phi(i, j)=((1-r1(i, j))^4)*(5*r1(i, j)^3)+(20*r1(i, j)^2)+29*r1(i, j)+16);
338 Else
339 Phi(i, j)=0;
340 end
341 end
342 end
343
344 %*****
345 %----- Step 6: Computing the weight 'w' -----
346 %*****
347 w=pinv(Phi)*Z_trn;
348
349 %*****
350 %----- Step 7: Computing the approximation of training dataset --
351 %*****
352 Zappx=Phi*w;
353
354 %*****
355 %----- Step 8: Computing the training error-----
356 %*****
357 Err_max_trn = max(abs(Z_trn-Zappx))
358 Err_RMSE_trn =sqrt((1/N_trn)*sum((Z_trn-Zappx).^2))
359
360 %*****
361 %----- Step 9: Construct the interpolation matrix -----
362 %----- from Xvld to Xctr -----
363 %*****
364 %----- 9.1 For MQ + Carlson RBF-----
365 for i=1:N_vld
366 for j=1:M
367 r2(i, j)=sqrt((X_vld(1, i)-Xctr(1, j)).^2 + (Y_vld(1, i)-Xctr(2, j)).^2 );
368 Phi2(i, j)= sqrt(r2(i, j)^2 + shp^2);
369 end
370 end
371
372 %----- 9.2 For PS RBF-----
373 for i=1:N_vld
374 for j=1:M
375 r2(i, j)=sqrt((X_vld(1, i)-Xctr(1, j)).^2 + (Y_vld(1, i)-Xctr(2, j)).^2 );
376 if 0<=r2(i, j) & r2(i, j)<=1
377 Phi2(i, j)=r2(i, j)^((2*k)-1);
378 else
379 Phi2(i, j)=0;
380 end
381 end
382 end

```

```

383
384 %----- 9.3 For TPS RBF-----
385 for i=1:N_vld
386 for j=1:M
387 r2(i,j)=sqrt((X_vld(1,i)-Xctr(1,j)).^2 + (Y_vld(1,i)-Xctr(2,j)).^2 );
388 if 0<=r2(i,j) & r2(i,j)<=1 & r2(i,j)~=0
389 Phi2(i,j)=(r2(i,j)^2)*log(r2(i,j));
390 else
391 Phi2(i,j)=0;
392 end
393 end
394 end
395
396 %----- 9.4 For WU1 RBF-----
397 for i=1:N_vld
398 for j=1:M
399 r2(i,j)=sqrt((X_vld(1,i)-Xctr(1,j)).^2 + (Y_vld(1,i)-Xctr(2,j)).^2 );
400 if 0<=r2(i,j) & r2(i,j)<=1
401 Phi2(i,j)=(1-
      r2(i,j))^7*(5*r2(i,j)^6+(35*r2(i,j)^5+(101*r2(i,j)^4+(147*r2(i,j)^3+(101*r2(i,j)^2)+35
      *r2(i,j)+5);
402 else
403 Phi2(i,j)=0;
404 end
405 end
406 end
407
408 %----- 9.5 For WU2 RBF-----
409 for i=1:N_vld
410 for j=1:M
411 r2(i,j)=sqrt((X_vld(1,i)-Xctr(1,j)).^2 + (Y_vld(1,i)-Xctr(2,j)).^2 );
412 if 0<=r2(i,j) & r2(i,j)<=1
413 Phi2(i,j)=(1-
      r2(i,j))^6*(6*r2(i,j)^5+(30*r2(i,j)^4+(72*r2(i,j)^3+(82*r2(i,j)^2)+36*r2(i,j)+6);
414 else
415 Phi2(i,j)=0;
416 end
417 end
418 end
419
420 %----- 9.6 For WU3 RBF-----
421 for i=1:N_vld
422 for j=1:M
423 r2(i,j)=sqrt((X_vld(1,i)-Xctr(1,j)).^2 + (Y_vld(1,i)-Xctr(2,j)).^2 );
424 if 0<=r2(i,j) & r2(i,j)<=1
425 Phi2(i,j)=(1-r2(i,j))^5*(5*r2(i,j)^4+(25*r2(i,j)^3+(48*r2(i,j)^2)+40*r2(i,j)+8);
426 else
427 Phi2(i,j)=0;
428 end
429 end
430 end
431
432 %----- 9.7 For WU4 RBF-----
433 for i=1:N_vld
434 for j=1:M
435 r2(i,j)=sqrt((X_vld(1,i)-Xctr(1,j)).^2 + (Y_vld(1,i)-Xctr(2,j)).^2 );
436 if 0<=r2(i,j) & r2(i,j)<=1
437 Phi2(i,j)=(1-r2(i,j))^4*(5*r2(i,j)^3+(20*r2(i,j)^2)+29*r2(i,j)+16);
438 else

```

```

439 Phi2(i,j)=0;
440 end
441 end
442 end
443
444 %----- 9.8 For WL1 RBF-----
445 for i=1:N_vld
446 for j=1:M
447 r2(i,j)=sqrt((X_vld(1,i)-Xctr(1,j))^2 + (Y_vld(1,i)-Xctr(2,j))^2 );
448 if 0<=r2(i,j) & r2(i,j)<=1
449 Phi2(i,j)=((1-r2(i,j)));
450 else
451 Phi2(i,j)=0;
452 end
453 end
454 end
455
456 %----- 9.9 For WL2 RBF-----
457 for i=1:N_vld
458 for j=1:M
459 r2(i,j)=sqrt((X_vld(1,i)-Xctr(1,j))^2 + (Y_vld(1,i)-Xctr(2,j))^2 );
460 if 0<=r2(i,j) & r2(i,j)<=1
461 Phi2(i,j)=((1-r2(i,j))^3)*(3*r2(i,j)+1);
462 else
463 Phi2(i,j)=0;
464 end
465 end
466 end
467
468 %----- 9.10 For WL3 RBF-----
469 for i=1:N_vld
470 for j=1:M
471 r2(i,j)=sqrt((X_vld(1,i)-Xctr(1,j))^2 + (Y_vld(1,i)-Xctr(2,j))^2 );
472 if 0<=r2(i,j) & r2(i,j)<=1
473 Phi2(i,j)=((1-r2(i,j))^5)*((8*r2(i,j)^2)+5*r2(i,j)+1);
474 else
475 Phi2(i,j)=0;
476 end
477 end
478 end
479
480 %----- 9.11 For WL4 RBF-----
481 for i=1:N_vld
482 for j=1:M
483 r2(i,j)=sqrt((X_vld(1,i)-Xctr(1,j))^2 + (Y_vld(1,i)-Xctr(2,j))^2 );
484 if 0<=r2(i,j) & r2(i,j)<=1
485 Phi2(i,j)=((1-r2(i,j))^2);
486 else
487 Phi2(i,j)=0;
488 end
489 end
490 end
491
492 %----- 9.12 For WL5 RBF-----
493 for i=1:N_vld
494 for j=1:M
495 r2(i,j)=sqrt((X_vld(1,i)-Xctr(1,j))^2 + (Y_vld(1,i)-Xctr(2,j))^2 );
496 if 0<=r2(i,j) & r2(i,j)<=1
497 Phi2(i,j)=((1-r2(i,j))^4)*(4*r2(i,j)+1);

```

```

498 else
499 Phi2(i,j)=0;
500 end
501 end
502 end
503
504 %----- 9.13 For WL6 RBF-----
505 for i=1:N_vld
506 for j=1:M
507 r2(i,j)=sqrt((X_vld(1,i)-Xctr(1,j))^2 + (Y_vld(1,i)-Xctr(2,j))^2 );
508 if 0<=r2(i,j) & r2(i,j)<=1
509 Phi2(i,j)=((1-r2(i,j))^6)*(35*r2(i,j)^2+18*r2(i,j)+3);
510 else
511 Phi2(i,j)=0;
512 end
513 end
514 end
515
516 %----- 9.14 For WL7 RBF-----
517 for i=1:N_vld
518 for j=1:M
519 r2(i,j)=sqrt((X_vld(1,i)-Xctr(1,j))^2 + (Y_vld(1,i)-Xctr(2,j))^2 );
520 if 0<=r2(i,j) & r2(i,j)<=1
521 Phi2(i,j)=((1-r2(i,j))^8)*(32*r2(i,j)^3+(25*r2(i,j)^2)+8*r2(i,j)+1);
522 else
523 Phi2(i,j)=0;
524 end
525 end
526 end
527
528 %----- 9.15 For BUH1 RBF-----
529 for i=1:N_vld
530 for j=1:M
531 r2(i,j)=sqrt((X_vld(1,i)-Xctr(1,j))^2 + (Y_vld(1,i)-Xctr(2,j))^2 );
532 Phi2(i,j)=(1/6)-(2*r2(i,j)^2)+(1/3)*r2(i,j)^3 -(7/2)*r2(i,j)^4 +
2*(r2(i,j)^4)*log(r2(i,j));
533 if r2(i,j)==0
534 Phi2(i,j)=(1/6)-(2*r2(i,j)^2)+(1/3)*r2(i,j)^3 -(7/2)*r2(i,j)^4;
535 end
536 end
537 end
538
539 %----- 9.16 For BUH2 RBF-----
540 for i=1:N_vld
541 for j=1:M
542 r2(i,j)=sqrt((X_vld(1,i)-Xctr(1,j))^2 + (Y_vld(1,i)-Xctr(2,j))^2 );
543 if 0<=r2(i,j) & r2(i,j)<=1
544 Phi2(i,j)=(112/45)*r2(i,j)^(9/2)+(16/3)*r2(i,j)^(7/2)-7*r2(i,j)^4-(14/15)*r2(i,j)^(2+(1/9));
545 else
546 Phi2(i,j)=0;
547 end
548 end
549 end
550
551 %----- 9.17 For BUH3 RBF-----
552 for i=1:N_vld
553 for j=1:M
554 r2(i,j)=sqrt((X_vld(1,i)-Xctr(1,j))^2 + (Y_vld(1,i)-Xctr(2,j))^2 );
555 Phi2(i,j)=(1/18)*r2(i,j)^2+(4/9)*r2(i,j)^3+0.5*r2(i,j)^4-(4/3)*r2(i,j)^3*log(r2(i,j));

```

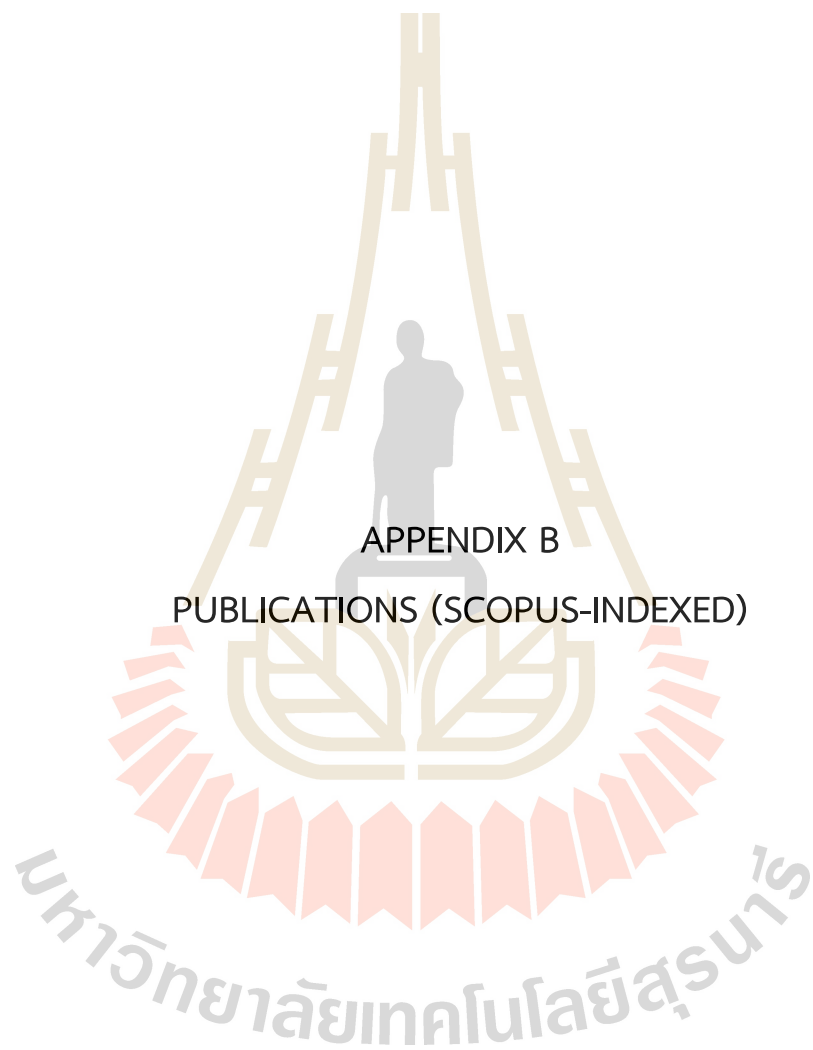
```

556 if r2(i,j)== 0
557 Phi2(i,j)=(1/18)*r2(i,j).^2+(4/9)*r2(i,j).^3+0.5*r2(i,j).^4;
558 end
559 end
560 end
561
562 %*****
563 %----- Step 10: Construct the Zvldapx from Phi2 and weight 'w' --
564 %*****
565 Zvldapx=Phi2*w;
566
567 %*****
568 %----- Step 11: Computing the test error with MSE -----
569 %*****
570 Z_vld = Z_vld';
571 Err_max_vld =max(abs(Z_vld-Zvldapx))
572 Err_RMSE_vld =sqrt((1/N_vld)*sum((Z_vld-Zvldapx).^2))
573 toc;
574 %*****
575 %----- Step 12: Find the condition number-----
576 %*****
577 con_G=cond(G)
578 con_Phi = cond(Phi)
579
580 %*****
581 %----- Step 13: Results Plotting -----
582 %*****
583 for i=1 :N_trn
584 Solu_tr(i,1)=XYZ_trn(i,1);
585 Solu_tr(i,2)=XYZ_trn(i,2);
586 Solu_tr(i,3)=XYZ_trn(i,3);
587 Solu_tr(i,4)=Zappx(i,1);
588 End
589
590 for i=1 :N_vld
591 Solu_vld(i,1)=XYZ_vld(i,1);
592 Solu_vld(i,2)=XYZ_vld(i,2);
593 Solu_vld(i,3)=XYZ_vld(i,3);
594 Solu_vld(i,4)=Zvldapx(i,1);
595 End
596
597 figure;
598 hold on
599 plot3(Solu_tr(:,1),Solu_tr(:,2),Solu_tr(:,3),'ro','markersize',3,'LineWidth',
    2)
600 plot3(Solu_tr(:,1),Solu_tr(:,2),Solu_tr(:,4),'ko','markersize',4,'LineWidth',
    2)
601 title('Data set')
602 xlabel('Input Variable (X)', 'FontSize',14);
603 ylabel('Input Variable (Y)', 'FontSize',14);
604 zlabel('Output Variable (Z)', 'FontSize',14);
605 legend({'Exact', 'Approximate'});
606 hold off
607 grid on
608
609 figure;
610 hold on

```

```
611 plot3(Solu_vld(:,1),Solu_vld(:,2),Solu_vld(:,3),'ro','markersize',3,'LineWidt
h',2)
612 plot3(Solu_vld(:,1),Solu_vld(:,2),Solu_vld(:,4),'ko','markersize',4,'LineWidt
h',2)
613 title('Data set')
614 xlabel('Input Variable (X)', 'FontSize',14);
615 ylabel('Input Variable (Y)', 'FontSize',14);
616 zlabel('Output Variable (Z)', 'FontSize',14);
617 legend({'Exact','Approximate'});
618 hold off
619 grid on
620 %-----THIS IS THE END -----
memory
```





APPENDIX B

PUBLICATIONS (SCOPUS-INDEXED)

B.1 Experiment 1

5th International Conference on Mathematical Applications in Engineering IOP Publishing
 IOP Conf. Series: Journal of Physics: Conf. Series **1489** (2020) 012020 doi:10.1088/1742-6596/1489/1/012020

A Numerical Study of a Compactly-Supported Radial Basis Function Applied with a Collocation Meshfree Scheme for Solving PDEs

S Tavaen¹, K Chanthawara² and S Kaennakham^{3,*}

^{1,3}School of Mathematics, Institute of Science, Suranaree University of Technology, Nakhon Ratchasima 30000, Thailand
² Program of Mathematics, Faculty of Science, Ubon Ratchathani Rajabhat University, Mueang Ubon Ratchathani, Ubon Ratchathani 34000, Thailand
^{*}Centre of Excellence in Mathematics, Bangkok 10400, Thailand

E-mail: *sayan_kk@g.sut.ac.th

Abstract. It is known that all Radial Basis Function-based meshfree methods suffer from a lack of reliable judgement on the choice of shape parameter, appearing in most of the RBFs. While the popularity of meshfree/meshless numerical methods is growing fast over the past decade, the great challenge is still to find an optimal RBF form with its optimal shape parameter. In this work, the main focus is on one type of RBF namely 'Compactly-Supported (CS-RBF)' that contains no parameter, and yet has not been explored numerically as much in the past, particularly under the context of data interpolation/approximation and solving partial differential equations (PDEs). To compare the potential advantages of CS-RBF, two most popular choices of RBF widely used; Multiquadric (MQ), and Gaussian (GA) were studied parallelly. The information gathered and presented in this work shall be useful for the future users in making decision on RBF.

1. Introduction

Amongst the well-known numerical schemes; finite volume, finite difference, and finite element method that have been invented, developed, and applied in a wide range of science and engineering problems, a rather young idea was discovered and has been categorized as 'meshless/meshfree' methods [1, 2]. The methods under this category have recently become promising alternative tools for numerically solving variety of science and engineering problems. Generally, these meshless schemes can be grouped into two main classes [3];

- Strong forms ; The finite point method [4], The hp-meshless cloud method [5], the collocation method [6], and references therein.
- Weak forms ; The diffuse element method [7], The element-free Galerkin method (EFGM; [8], The point interpolation method [9], and references therein.

Each of these has its own advantages/disadvantages depending on several factors involved; domain geometry, governing equations, boundary/initial conditions, computer arithmetic, etc. Amongst those being proposed and developed nowadays, one of the well-known meshfree method is that called 'RBF-collocation' or sometimes called 'Kansa's method', where it uses a set of global approximation function

 Content from this work may be used under the terms of the [Creative Commons Attribution 3.0 licence](https://creativecommons.org/licenses/by/3.0/). Any further distribution of this work must maintain attribution to the author(s) and the title of the work, journal citation and DOI.
 Published under licence by IOP Publishing Ltd 1

Figure B.1 A Numerical Study of a Compactly-Supported Radial Basis Function Applied with a Collocation Meshfree Scheme for Solving PDEs.

B.2 Experiment 2

First International Conference on Advances in Physical Sciences and Materials
Journal of Physics: Conference Series
IOP Publishing
1706 (2020) 012165 doi:10.1088/1742-6596/1706/1/012165

Performances of non-parameterised radial basis functions in pattern recognition applications

S Tavaen^{1,*}, R Viriyapong² and S Kaennakham^{1,3}

¹School of Mathematics, Institute of Science, Suranaree University of Technology, Nakhon Ratchasima, 30000, Thailand.
²Department of Mathematics, Faculty of Science, Naresuan University, Phitsanulok, 65000, Thailand.
³Centre of Excellence in Mathematics, Bangkok, 10400, Thailand.

*E-mail: sunisat58@nu.ac.th

Abstract. Pattern recognition appears in many applications with most popular scheme are those involved the so-called 'Radial Basis Function (RBF)'. It is known that the shape parameter contained in some RBFs used has great influence on the final quality of prediction. This study focusses on RBFs which contains no parameters where three data patterns are used for performance validation. With a good choice of number of centres, it is clearly possible to obtain satisfactory results with no burden on choosing the suitable or optimal shape. This can well shed more light into applications with more complexity with less user's judgment and be more automatic in the process.

1. Introduction
 Pattern recognition is the process of differentiating and dividing the data according to certain criteria or by general components, which are performed by special algorithms. Because pattern recognition helps to classification and prediction, it is one of the important components of machine learning technology [1]. Pattern recognition is applied to image processing [2], industry [3], and medical [4] (see references therein).
 The task of pattern recognition is to construct the model with unknown input-output mapping pattern. It is to construct the best model, if any, from the train data with some mapping functions and expect this model to best represent the rest of the data, called 'training data'. Both sets of the data can be of the following form;

$$D = \{(\mathbf{x}_i, y_i) \mid \mathbf{x}_i \in \mathbb{R}^d, y_i \in \mathbb{R}, i = 1, 2, \dots, n\} \quad (1)$$

where \mathbf{x}_i are inputs with the corresponding y_i are outputs. The main task is to find a mapping D from the d -dimensional input space to 1-dimensional output space. Over the decade, there have been several models designed to tackle the problem and some are statistical model, structural model, template matching model, neural network based model, fuzzy based model, and hybrid model. Amongst these, very often that radial basis functions (RBF) are involved where the crucial factor is the shape parameter, mostly contained within the RBF used. The most popular choice for RBF is the famous Gaussian type and its performance is certainly determined by its shape parameter. Therefore, the main objective of this

 Content from this work may be used under the terms of the [Creative Commons Attribution 3.0 licence](https://creativecommons.org/licenses/by/3.0/). Any further distribution of this work must maintain attribution to the author(s) and the title of the work, journal citation and DOI.
 Published under licence by IOP Publishing Ltd

Figure B.2 Performances of Non-Parameterised Radial Basis Functions in Pattern Recognition Applications.

B.3 Experiment 3

ICASSCT 2021
IOP Publishing

Journal of Physics: Conference Series
1921 (2021) 012124
doi:10.1088/1742-6596/1921/1/012124

A Comparison Study on Shape Parameter Selection in Pattern Recognition by Radial Basis Function Neural Networks

S Tavaen^{1*} and S Kaennakham^{1,2}

¹School of Mathematics, Institute of Science, Suranaree University of Technology, Nakhon Ratchasima, 30000, Thailand.

²Centre of Excellence in Mathematics, Bangkok 10400, Thailand.

*Corresponding Author: Sunisa Tavaen. Email: sunisat58@email.nu.ac.th

Abstract. This study investigates three choices of shape parameter selection when the so-called Radial Basis Function (RBF) is used. Under the problem of pattern recognition via RBF-Neural Network using RC-algorithm, three RBFs are focussed on; Gaussian (GA), Multiquadric (MQ), and Compactly-Supported (CS1). Two pattern recognition cases are tested and the best choice of shape parameter is validated using Model-Selection Criteria (MSC).

Keywords. Pattern Recognition, Radial Basis Function, Neural Networks, Gaussian, Multiquadric

1. Introduction

Over the past decades it has been noticeable that Radial Basis Function neural networks (RBFNs) have been slowly replacing the traditional Multilayer Perceptron (MLP) neural networks particularly in the applications of supervised learning concept. The main attractive feature is having the single hidden layer making the training process comparatively faster. RBFNs were introduced in 1987 by Powell M.J.D. [1] and have been developed by many researches and applied to many science and engineering problems. Some nice applications involve the process of interference cancellation [2], the diagnosis of damage of radial gate [3], on complex-valued Radial Basis Function Network in signal processing process [4], and the classification of incomplete feature vectors in pattern recognition [5] (see also the references therein).

Radial Basis Functions (RBF), φ , are commonly found as multivariate functions whose values are dependent only on the distance from the origin. This means that $\varphi(\mathbf{x}) = \varphi(r) \in \mathbb{R}$ with $\mathbf{x} \in \mathbb{R}^n$ and $r \in \mathbb{R}$; or, in other words, on the distance from a point of a given set $\{\mathbf{x}_j\}$, and $\varphi(\mathbf{x} - \mathbf{x}_j) = \varphi(r_j) \in \mathbb{R}$. Here, $r_j = \|\mathbf{x} - \mathbf{x}^j\|_2$ is the Euclidean distance expressed in n -dimensional space as;

$$r_j = \|\mathbf{x} - \mathbf{x}^j\|_2 = \sqrt{(x_1 - x_1^j)^2 + (x_2 - x_2^j)^2 + \dots + (x_n - x_n^j)^2} \quad (1)$$

and any function φ satisfying $\varphi(\mathbf{x}) = \varphi(\|\mathbf{x}\|_2)$ is a radial function.

Despite of their great features one can benefit from using RBFNs, the key of success is still the choice of RBF to use. Many forms of popular RBFs contain the so-called 'shape parameter' and it is known to determine the quality of the whole model where the optimal choice is still problematic, one often needs to make somewhat an 'ad-hoc' decision'. Figure 1 displays the clear influence on the function surface caused

Content from this work may be used under the terms of the [Creative Commons Attribution 3.0 licence](https://creativecommons.org/licenses/by/3.0/). Any further distribution of this work must maintain attribution to the author(s) and the title of the work, journal citation and DOI.

1

Published under licence by IOP Publishing Ltd

Figure B.3 A Comparison Study on Shape Parameter Selection in Pattern Recognition by Radial Basis Function Neural Networks.

B.4 Experiment 4

77

Fuzzy Systems and Data Mining VII
A.J. Tallón-Ballesteros (Ed.)
 © 2021 The authors and IOS Press.
 This article is published online with Open Access by IOS Press and distributed under the terms
 of the Creative Commons Attribution Non-Commercial License 4.0 (CC BY-NC 4.0).
 doi:10.3233/FAIM210178

Generalized-Multiquadric Radial Basis Function Neural Networks (RBFNs) with Variable Shape Parameters for Function Recovery

Sayan Kaennakham^{a,1}, Pichapop Paewpolsong^a, Natdanai Sriapai^a and Sunisa Tavaen^a
^a*School of Mathematics, Institute of Science, Suranaree University of Technology,
 Nakhon Ratchasima, Thailand*

Abstract. After being introduced to approximate two-dimensional geographical surfaces in 1971, the multivariate radial basis functions (RBFs) have been receiving a great amount of attention from scientists and engineers. In 1987 the idea was extended into the construction of neural networks corresponding to the beginning of the era of artificial intelligence, forming what is now called 'Radial Basis Function Neural Networks (RBFNs)'. Ever since, RBFNs have been developed and applied to a wide variety of problems; approximation, interpolation, classification, prediction, in nowadays science, engineering, and medicine. This also includes numerically solving partial differential equations (PDEs), another essential branch of RBFNs under the name of the 'Meshfree/Meshless' method. Amongst many, the so-called 'Multiquadric (MQ)' is known as one of the mostly-used forms of RBFs and yet only a couple of its versions have been extensively studied. This study aims to extend the idea toward more general forms of MQ. At the same time, the key factor playing a very crucial role for MQ called 'shape parameter' (where selecting a reliable one remains an open problem until now) is also under investigation. The scheme was applied to tackle the problem of function recovery as well as an approximation of its derivatives using six forms of MQ with two choices of the variable shape parameter. The numerical results obtained in this study shall provide useful information on selecting both a suitable form of MQ and a reliable choice of MQ-shape for further applications in general.

Keywords. Generalized-Multiquadric, Radial Basis Function Neural Networks (RBFNs), Variable Shape Parameters, Function Recovery

1. Introduction

Radial Basis Functions (RBFs), φ , are commonly found as multivariate functions whose values are dependent only on the distance from the origin. This means that $\varphi(\mathbf{x}) = \varphi(r) \in \mathbb{R}$ with $\mathbf{x} \in \mathbb{R}^n$ and $r \in \mathbb{R}$, or, in other words, on the distance from a point of a given set $\{\mathbf{x}_j\}$, and $\varphi(\mathbf{x} - \mathbf{x}_j) = \varphi(r_j) \in \mathbb{R}$. Here, r_j is the Euclidean distance. As illustrated in Figure 1, RBF networks (RBFNs) broadly consist of three layers; 1) *Input*

¹ Corresponding Author, Sayan Kaennakham, School of Mathematics, Institute of Science, Suranaree University of Technology, Nakhon Ratchasima, Thailand; E-mail: sayan_kk@g.sut.ac.th.

Figure B.4 Generalized-Multiquadric Radial Basis Function Neural Networks (RBFNs) with Variable Shape Parameters for Function Recovery.

CURRICULUM VITAE

NAME : Sunisa Tavaen

GENDER : Female

EDUCATION BACKGROUND:

- Bachelor of Science Program in Mathematics, Naresuan University, Thailand, 2019

SCHOLARSHIP:

- Development and Promotion of Science and Technology Talents Project, Thai government scholarship

SELECTED PUBLICATIONS:

- **Sunisa Tavaen**, Krittidej Chanthawara and Sayan Kaennakham (2020) A Numerical Study of a Compactly-Supported Radial Basis Function Applied with a Collocation Meshfree Scheme for Solving PDEs, "Journal of Physics Conference Series", vol. 1489, no.1. doi: 10.1088/1742-6596/1489/1/012020.

- **Sunisa Tavaen**, Ratchada Viriyapong and Sayan Kaennakham (2020) Performances of non-parameterised radial basis functions in pattern recognition applications, "Journal of Physics Conference Series", vol. 1706, no.1. doi: 10.1088/1742-6596/1706/1/012165.

- **Sunisa Tavaen** and Sayan Kaennakham (2021) A Comparison Study on Shape Parameter Selection in Pattern Recognition by Radial Basis Function Neural Networks, "Journal of Physics: Conference Series: in First International Conference on Advances in Smart Sensor, Signal Processing and Communication Technology (ICASSCT 2021), 19-20, March 2021, Goa, India", vol. 1921.

- Sayan Kaennakham, Pichapop Paewpolsong, Natdanai Sriapai and **Sunisa Tavaen** (2021) Generalized-Multiquadric Radial Basis Function Neural Networks (RBFNs) with Variable Shape Parameters for Function Recovery. "Fuzzy Systems and Data Mining VII", vol. 340. pp. 77 - 85. doi: 10.3233/FAIA210178.

- Dusita Ritthison, **Sunisa Tavaen** and Sayan Kaennakham (2022) A Modified Local Distance-weighted (MLD) Method of Interpolation and Its Numerical Performances for Large Scattered Datasets. "Current Applied Science and Technology", vol. 22, no. 6.

- **Sunisa Tavaen** and Sayan Kaennakham (202x) Numerical Comparison of Shapeless Radial Basis Function Networks in Pattern Recognition. "Computers, Materials & Continua", vol. x. doi:10.32604/cmc.202x.xxxxxx. (Accepted)